Sensitivity Analysis of Oscillating Dynamical Systems with Applications to the Mammalian Circadian Clock

by

Anna Katharina Wilkins

Submitted to the Department of Chemical Engineering
in partial fulfillment of the requirements for the degree of

Doctor of Philosophy in Chemical Engineering

at the

MASSACHUSETTS INSTITUTE OF TECHNOLOGY

May 2008

Author .....
Department of Chemical Engineering
May 20, 2008

Certified by .....
Paul I. Barton
Lammot du Pont Professor of Chemical Engineering
Thesis Supervisor

Certified by .....
Bruce Tidor
Professor of Biological Engineering and Computer Science
Thesis Supervisor

Accepted by .....
William M. Deen
Professor of Chemical Engineering
Chairman, Committee for Graduate Students

Sensitivity Analysis of Oscillating Dynamical Systems with Applications to the Mammalian Circadian Clock

by

Anna Katharina Wilkins

Submitted to the Department of Chemical Engineering
on May 20, 2008, in partial fulfillment of the
requirements for the degree of
Doctor of Philosophy in Chemical Engineering

Abstract

The work presented in this thesis consists of two major parts. In Chapter 2, the theory for sensitivity analysis of oscillatory systems is developed and discussed. Several contributions are made, in particular in the precise definition of phase sensitivities and in the generalization of the theory to all types of autonomous oscillators. All methods rely on the solution of a boundary value problem, which identifies the periodic orbit. The choice of initial condition on the limit cycle has important consequences for phase sensitivity analysis, and its influence is quantified and discussed in detail. The results are exact and efficient to compute compared to existing partial methods.

The theory is then applied to different models of the mammalian circadian clock system in the following chapters. First, different types of sensitivities in a pair of smaller models are analyzed. The models have slightly different architectures, with one having an additonal negative feedback loop compared to the other. The differences in their behavior with respect to phases, the period and amplitude are discussed in the context of their network architecture. It is found that, contrary to previous assumptions in the literature, the additional negative feedback loop makes the model less "flexible" in at least one sense that was studied here.

The theory was also applied to larger, more detailed models of the mammalian circadian clock, based on the original model of Forger and Peskin. Between the original model's publication in 2003 and the present time, several key advances were made in understanding the mechanistic detail of the mammalian circadian clock, and at least one additional clock gene was identified. These advances are incorporated in an extended model, which is then studied using sensitivity analysis. Period sensitivity analysis is performed first and it was found that only one negative feedback loop dominates the setting of the period. This was an interesting one-to-one correlation between one topological feature of the network and a single metric of network performance. This led to the question of whether the network architecture is modular, in the sense that each of the several feedback loops might be responsible for a separate network function. A function of particular interest is the ability to separately track "dawn" and "dusk", which is reported to be present in the circadian clock. The ability of the mammalian circadian clock to modify different relative phases — defined by different molecular events — independently of the period was analyzed. If the model can maintain a perceived day — defined by the time difference between two phases — of different lengths, it can be argued that the model can track dawn and dusk separately. This capability is found in all mammalian clock models that were studied in this work, and

furthermore, that a network-wide effort is needed to do so. Unlike in the case of the period sensitivities, relative phase sensitivities are distributed throughout several feedback loops. Interestingly, a small number of "key parameters" could be identified in the detailed models that consistently play important roles in the setting of period, amplitude and phases. It appears that most circadian clock features are under shared control by local parameters and by the more global "key parameters".

Lastly, it is shown that sensitivity analysis, in particular period sensitivity analysis, can be very useful in parameter estimation for oscillatory systems biology models. In an approach termed "feature-based parameter fitting", the model's parameter values are selected based on their impact on the "features" of an oscillation (period, phases, amplitudes) rather than concentration data points. It is discussed how this approach changes the cost function during the parameter estimation optimization, and when it can be beneficial. A minimal model system from circadian biology, the Goodwin oscillator, is taken as an example.

Overall, in this thesis it is shown that the contributions made to the theoretical understanding of sensitivities in oscillatory systems are relevant and useful in trying to answer questions that are currently open in circadian biology. In some cases, the theory could indicate exactly which experiments or detailed mechanistic studies are needed in order to perform meaningful mathematical analysis of the system as a whole. It is shown that, provided the biologically relevant quantities are analyzed, a network-wide understanding of the interplay between network function and topology can be gained and differences in performance between models of different size or topology can be quantified.

Thesis Supervisor: Paul I. Barton
Title: Lammot du Pont Professor of Chemical Engineering

Thesis Supervisor: Bruce Tidor
Title: Professor of Biological Engineering and Computer Science

Acknowledgments

There are many people in my life to whom I am deeply grateful. My parents Elisabeth and Udo Schampel and siblings Johannes and Christina have shown me their support throughout my life, and have always inspired me to strive to give my all to whatever I was doing.

My advisors, Dr. Paul Barton and Dr. Bruce Tidor, have often expressed their confidence in my abilities, even when I wasn't so sure at all. Bruce provided me with valuable instruction in the scientific thought process and writing. He also makes sure the Tidor lab is a hospitable place, with ample stocks of all office and computer supplies, but more importanly, tea, coffee, milk and snacks, which was greatly appreciated. I could not have done my work without the enthusiasm that Paul brought to the table during the long time it took me to understand the mathematical aspects of my work. His involvement and attention to detail along with his profound knowledge were an inspiration to me, and his sense of humor and patience often made what could have been a frustrating experience seem like a fun challenge.

I want to thank my committee members, Dr. Douglas Lauffenburger and Dr. Jacob White, who have been encouraging and positive throughout the years. Jacob met with me repeatedly and with great patience helped me understand details that proved crucial to the success of my work.

There have been a series of teachers and mentors in my life who have all influenced me and helped me chose my path in life and in science. Dr. Balewski was my high-school chemistry teacher, who besides being an excellent teacher, openly discussed the challenges and benefits of being a working mother and of being a woman in science. As an undergrad at Karlsruhe Technical University, I was fortunate to be able to work in the laboratory of Professor Clemens Posten. It was my first step towards biology and the positive experience led me to take this interest further. During my Diplom-thesis, I worked under Dr. Jack Benner at New England Biolabs, Inc. Jack has been a source of inspiration and encouragement, and of a vaste amount of scientific facts and stories that he told with great zeal. Besides Jack, several people at NEB encouraged and helped me with my applications for graduate school, I want to mention in particular Dr. Ron Chong and Dr. Chris Noren.

My labmates, present and past, were a source of moral support as well as scientific in-

spiration, help and instruction: Dr. Adam Singer, Dr. Cha Kun Lee, Dr. Benoit Chachuat, Dr. Alexander Mitsos and Dr. Bambang Adiwijaya have all helped me in my first years at MIT and have provided valuable insights in getting adjusted to graduate student life and getting my project off the ground. Dr. Caitlin Bever and Joshua Apgar have helped immensely in the second half of my project, with their insights, opinions, detailed knowledge of systems biology, and last, but not least, their good humor and friendship.

I want to thank Dr. Kristin Mattern, Michelle and Andy Miller, Sanjoy Sircar, Theis Clarke, Ben Wang, Dr. Jane Rempel and Dr. Kris Wood for their friendship and for many interesting lunch-table converstaions, and in particular Kristin, Michelle and Andy for all the hours we spent studying for quals.

My mother-in-law, Marcia Wilkins, deserves a special note. She was my fiercest supporter in the decision to attend MIT for graduate school, and seems to have an enormous amount of confidence in me. She had the positive outlook that it will all be worth it in the end, which she repeatedly told me when I was frustrated.

Last but certainly not least, I want to thank my family. My husband Paul is an unwavering source of support and an amazing, hands-on father to our daughter Nadia. In times of late nights, stress and deadlines, he took over my chores without comment, and often provided technical support for all things Linux. It can't have been easy and I am deeply thankful for it.

Contents

List of Figures

List of Tables

Chapter 1

Introduction

1.1 Sensitivity Analysis of Oscillatory Systems

Sensitivity analysis of dynamic systems is a well established area of numerical analysis. This mathematical technique evaluates how infinitesimal parameter perturbations change the output of a given mathematical model. Much has been written on its numerical implementation for different types of dynamic systems (e.g., [28, 72]) as well as its application to many areas, including optimization, parameter estimation, observability analysis, controlability analysis, model reduction, parameter identifiability and systems biology.

The study of the sensitivity analysis of oscillatory systems of ordinary differential equations (ODEs) has been an area of active research for a considerable time [18, 89, 56, 64]. However, several challenges had not been overcome prior to the work presented in this thesis. In particular, the analysis of limit-cycle oscillators (LCOs) brings with it a specific set of challenges. An LCO is a system where, from any initial condition within a region of attraction, a periodic orbit is approached asymptotically. The presence of transients for initial conditions that are not exactly on the periodic orbit represents an obstacle. Because the periodic orbit itself is independent of the initial conditions, but is determined by the system parameters, any inital condition specifically on the periodic orbit must be an implicit function of the system parameters. For the sensitivity analysis of oscillatory systems, one has few choices. A first approach involves identifying a starting point on the limit cycle, where the initial condition sensitivities were assumed to be zero. This approach can be used to identify the period and amplitude sensitivities of LCOs [48, 64, 56]. Rosenwasser and Bure showed in 1974 [18, 89], however, that an error is introduced that does not decay to

zero but rather undergoes a transient to finally yield a periodic contribution to the overall sensitivities. It is impossible to quantify the magnitude of this error, and thus only the sensitivity values at certain points, namely the stationary points of each variable, can be evaluated correctly and only after the transients have passed. While this approach does allow the identification of period and amplitude sensitivities, it is not exact in the sense that the numerical procedure involves truncating a limit. It is also important to realize that certain points on the limit cycle need to be avoided when evaluating period sensitivities because the formulation requires division by a term that can evaluate to zero [63]. The need to integrate a potentially large system over many periods to wait for the error to approach a periodic contribution makes this method numerically inefficient. It is still widely used and referenced in the literature [37, 56, 48, 10, 111] and also forms the basis for an alternative method for the computation of period sensitivities based on singular value decomposition of the dominant (unbounded) term of the state sensitivities [111].

A better approach was proposed by Rosenwasser and Yusupov [89] and involves the formulation of a boundary value problem (BVP) which allows the simultaneous solution for the period sensitivities and for initial condition sensitivities. The starting point from which the initial condition sensitivities are computed is defined by fixing one of the state variables to its starting value, which is necessary because the BVP would otherwise be underdetermined. This approach leads to exact sensitivity trajectories that can, from the start, be decomposed into an unbounded part containing the period sensitivities and a periodic part containing the sensitivities of amplitudes (shape) and phase. The influence of the definition of the starting point is not further discussed in reference [89], however, it forms the basis for the contributions made in the theoretical part of this thesis. In the dynamical systems literature, the definition of a point on the limit cycle is called a phase locking condition (PLC) [92]. We examine closely the impact that the choice of PLC has on the overall structure of the solution of the sensitivity system. It is shown that the PLC lends a definition of time zero to the system, which is itself dependent on the parameters. The only previous mention of the need to define a time reference for the sensitivity analysis of oscillatory systems was found in reference [99], which reports a need to "have the zero of the perturbed and unperturbed motion coincide." However, it was not considered in this formulation that the influence of the PLC might not be constant throughout the cycle. None of the later works on the decomposition of the sensitivities [56, 48, 89, 63] or on phase

sensitivities [37, 38, 56, 10] have picked up this remark and included it in their own analyses.

In the theoretical part of this work, given in Chapter 2, it is shown that the contribution of the PLC to the sensitivity solution is not constant, but rather periodic. It is possible to decompose the state sensitivity trajectories further and separate the periodic part into the periodic effects of shape (amplitude) change and those of phase change (which contains the influence of the PLC). The latter then forms the basis of performing relative phase sensitivity analysis. Previous attempts to compute relative phase sensitivities were hampered by this missing piece, and in fact, a numerical comparison shows that it is exactly the contribution from the PLC that is missing in order to match the numerical results of reference [37] to a finite-difference approximation.

Besides LCOs, there exist other mathematical types of oscillators, which are defined in Chapter 2 and to which the methods developed for LCOs are extended. Previously, the period sensitivity analysis for non-limit-cycle oscillators (NLCOs) was presented using the example of the Oregonator, modeling an oscillating chemical reaction mechanism [27]. The separation of what was called "secular" and "cleaned out" terms for NLCOs (i.e., the unbounded and periodic parts of the sensitivity solution, respectively stemming from the period sensitivities and the combined matrix of amplitude and phase sensitivities), was presented by Larter in 1983 [63], based on ideas by Tomovic and Vukobratovic [99]. The initial values of the state sensitivities are zero in the case of an NLCO, and the resulting sensitivity trajectories as well as period sensitivities are exact.

This thesis develops a general formulation for the sensitivity analysis for any type of autonomously oscillating ODE system and provides insight for how the choice of initial condition(s) or PLC(s) affects the solution of the sensitivity equations. Exact period, amplitude and relative phase sensitivities can be computed for all parameters and initial conditions.

1.2 The Mammalian Circadian Clock

Measuring time is a skill that all eukaryotes possess almost without exception, as well as simpler species. In fact, the ability to do so gives organisms yet another dimension in which to compete — time can be considered a subtle biological niche. In the idiom "The early bird catches the worm," the need for timekeeping is expressed in intuitive terms. If a bird's diet consists mainly of worms, it is necessary that its waking hours coincide with the times

at which its prey is active and easy to catch.

The mechanism that enables timekeeping is called the "biological clock", "internal clock" or "circadian clock". In particular the latter two terms reveal two central concepts associated with its study. The word "internal" indicates that the rhythm that is generated is not merely a reaction to external stimuli (exogenous rhythms) but rather an intrinsic mechanism that keeps time endogenously. In fact, experiments have shown that the clock keeps ticking even if all outside stimuli are removed. The term "circadian" comes from the latin words *circa*, meaning "approximately", and *diem*, meaning "day". This term was chosen because the rhythm in the absence of outside stimuli maintains a period of close to, but not exactly 24 hours.

In human beings the influence of the internal clock can be traced throughout many physiological processes. Renal and metabolic activity, the secretion of different hormones, the heart rate and blood pressure, the times of high mental performance and alertness as well as the body temperature underlie control by the internal clock [26, 42]. As a consequence, some acute medical conditions, such as strokes and heart attacks, asthma attacks, and even death show statistically significant circadian rhythms in their onsets [26, 79]. More recently, it has come to scientists' and physicians' attention that the timing at which medication is administered can have a pronounced effect on the therapeutic outcome [110]. To mention but one example, in reference [79] a study on the effects of circadian timing of chemotherapy in children diagnosed with acute leukemia is discussed. A threefold increase in survival was observed in patients who received the same dose of medication in the evening rather than in the morning. Similar effects had been observed in mouse studies, and the reason is likely a different peak time in cell division between tumor cells and normal cells, as has been observed in ovarian cancer in humans.

Beyond the chronopharmaceutical effects caused by the internal clock, there are certain conditions that are caused directly by its malfunctioning. Individuals afflicted with Familial Advanced Sleep Phase Syndrome (FASPS) are unable to stay awake late in the day, and rise from their night sleep very early [26, 74]. The mirror of FASPS is the Delayed Sleep Phase Syndrome (DSPS), which causes individuals to stay up very late and to be unable to awake at a morning hour that is considered normal by much of society [26, 74]. The mood disorder SAD (Seasonal Affective Disorder) has been found to have a circadian component as well, a revelation that may help design better treatments [70, 74].

A third aspect of the circadian clock and its influence on the lives of humans is its functioning in the face of modern day realities. Shift work is a reality for many professions, from highly skilled surgeons to truck drivers, and is possibly most pronounced in the Armed Forces, where multi-day missions present a challenge to alertness and decision-making in the face of sleep-deprivation and fatigue. It is telling that decision-making at hours that are not ideally suited for this task can have drastic consequences. The malfunctioning of the Chernobyl reactor was inadvertantly initiated at 1:23 a.m. by fatigued operators [26]. The Titanic ran into an iceberg at 11:40 p.m. The Exxon Valdez ran aground shortly after midnight. Less dramatic but much more common is the incidence of traffic accidents. Fatigue-related accidents are reported to peak at 2 a.m., at which time accidents are reported at a 5.5 times higher rate than at 6 p.m. [26]. Furthermore, it was reported that rotating shift workers incur an elevated risk of developing cancer as well as hypertension and gastrointestinal problems [42].

The effects of proper and improper functioning of the internal clock indicate the need to understand how it affects other systems in the human body, with the goal of being able to intervene and create beneficial effects.

The advent of molecular biology and genetics has contributed a great deal towards this goal. Many of the molecular components of the mammalian circadian clock are now well understood, and the molecular basis for some circadian disorders is known [97]. A detailed account of the current knowlege in mammalian circadian molecular biology is given in Chapter 4. Treatments using light or substances such as melatonin have recently become available for some of the circadian diseases, sleep and mood disorders, but are still in their infancy [26]. It is hoped that with increased system-wide understanding of the circadian clock, these treatment and intervention options will continue to improve. The analysis of the circadian clock mechanism is discussed in the next section.

1.2.1 Analyzing the Circadian Clock

Efforts to understand the circadian clock in a system-wide fashion can be separated into two areas. First, the study of exogenous effects and components is a field rich in history and relevance. The pioneering works by Colin Pittendrigh as well as by Jürgen Aschoff set the stage and provided much of the understanding of the clock that forms the basis for today's active research. A central aspect of both researchers' work focussed on the

effects that outside stimuli had on the clock. One of the key features of the circadian clock is its ability to entrain to a periodic stimulus. The most obvious stimulus is light, but entrainment to temperature and other signals has also been reported. The entrainment properties of the clock were studied in detail and with different underlying hyotheses [26]. Experimental studies, often on rodents, revealed minimal light-dark schedules that allow for stable entrainment and showed that the circadian clock has different phase-change responses if exposed to a light pulse, depending on the timing of the pulse.

A second, complementary area, is the study of the endogenous component of the clock, in other words, the study of the clock in the absence of any outside influence. The amazing stability of the free running period (FRP) of the circadian clock is one of the properties that was postulated by Pittendrigh and Daan in 1976 [82]. This property is the ability of the clock to continue to run with near-24-hour period for an extended time after all outside stimuli were removed. A second, related property of the clock is called "temperature compensation". This property was discovered when the circadian rhythm of *Drosophila* hatching was studied — while changes in the ambient temperature could induce temporary transients, the period of oscillation was nearly unchanged after the rhythm had stabilized again [26]. While this effect appears more relevant for plants and poikilotherms, such as insects, even homeothermic animals have temperature-compensated clocks. The compensation mechanism might thus be an integral part of the circadian clock mechanism that was conserved throughout evolution [26].

From a mathematical standpoint, it was argued that an LCO can represent some of the clock properties rather well [26]. In particular, LCOs have a built-in robustness against perturbations. Any change in concentrations will not permanently change the periodic orbit or any of its properties (it might however induce a phase shift). This behavior matches both the stability of the 24-hour period as well as the ability of the clock to entrain. Depending on the magnitude and kind of stimulus, different phase resetting mechanisms can be explained as well as transitions to non-oscillatory regions (if a bifurcation point is crossed). It is known that simple LCOs can be constructed using negative feedback loops, such as the one represented in the Goodwin oscillator [90]. In fact, all circadian clocks known in nature have negative feedback loops in the structure of their molecular network. Progress in molecular circadian biology coupled with developments in mathematical aspects of the problem have led to an active field of research, one particular aspect of which is discussed next.

1.2.2 Sensitivity Analysis of the Circadian Clock

Sensitivity analysis was successfully used by many computational systems biologists with an interest in the circadian clock. Examples range from applications to very simple models [90] to more detailed ones [35, 66, 29]. In the following, the study of the endogenous behavior of the circadian clock at constant darkness using sensitivity analysis is summarized briefly. Studies on entrained (forced) models are new, scarce, and beyond the scope of this work [38, 76].

The property of temperature compensation was analyzed using period sensitivities, and a relationship between the period sensitivities of individual rate constants, and the temperature compensation of the entire system could be established [90, 66, 44, 59]. The basic idea was that overall, positive and negative effects of temperature changes need to balance each other out in a sense that the associated parameter sensitivities need to add up to zero [90]. Later studies have added specific details on the biophysical properties of some pathways [59] or hypotheses on how a system with temperature compensation can be robust to mutation at the same time [44].

Furthermore, period sensitivity analysis was used to study the overall stability of the oscillations under perturbations [111], and of the robustness of circadian rhythms in comparison to other cellular rhythms (glycolysis, calcium oscillations) [108]. In their 2004 study, Stelling *et al.* find that phosphorylation reactions carry high sensitivities towards perturbations, in two medium-scale models of the *Drosophila* circadian clock [35, 67]. Leloup and Goldbeter studied the bifurcation behavior and potential existence of multiple oscillatory mechanisms within their model using sensitivity analysis [69], where the sensitivities were computed with respect to finite parameter variations.

Phase sensitivity analysis was performed less frequently, likely due to the lack of an appropriate mathematical foundation for their computation. Rand *et al.* [85] computed a phase sensitivity (similar to the shortcut formulation in Chapter 2) in order to evaluate the flexibility of the network as a function of the number of feedback loops. Gunawan and Doyle reported on an isochron-based phase sensitivity [37] which was performed on two *Drosophila* models [67, 100] using finite parameter perturbations, finding overlapping control mechanisms for period and phase control. Similarly, Bagheri *et al.* [10] find that similarity between certain performance metrics, such as relative phase and period sensitivities found

by finite parameter variation, can be found in *Drosophila* [67] and mouse [68] models, while others might be less correlated with each other.

In this thesis, the theory developed in Chapter 2 is first applied to a pair of small models of the mammalian circadian clock [12, 13], where the period, amplitude, and phase sensitivities are computed and compared between the two slightly different network architectures. In Chapter 4, the current state of molecular circadian biology is presented and several aspects of it are incorporated into a model that extends the current, most detailed model of the mammalian circadian clock [29]. Chapter 5 presents a detailed period sensitivity analysis of this mechanistic, predictive model [29] and shows results that span from the molecular to the systems level. The analyis identifies the relative importance of individual reactions in setting the period; interestingly, these reactions are localized to a particular part of the molecular network. The results agree with recent experimental reports that have identified the molecular cause for the FRP-abnormality found in individuals with FASPS [97]. In Chapter 6, both the original model and its extended version developed in Chapter 4 are subjected to detailed phase sensitivity analysis using the exact methods developed in Chapter 2. Here the endogenous phase control mechanisms were studied for multiple phases, both with respect to infinitesimal as well as finite parameter changes. Commonalities between period, amplitude and phase control are found and analyzed.

In the final Chapter 7, the use of "feature sensitivities", or sensitivities of oscillation-specific outputs of dynamic systems, is discussed in the context of parameter estimation. It is shown that the parameter estimation for oscillatory systems has different challenges and benefits from different methods than that of other dynamic systems.

Chapter 2

Sensitivity Analysis for Oscillating Dynamical Systems

Abstract

Boundary value formulations are presented for exact and efficient sensitivity analysis, with respect to model parameters and initial conditions, of different classes of oscillating systems. Methods for the computation of sensitivities of derived quantities of oscillations such as period, amplitude and different types of phases are first developed for limit-cycle oscillators. In particular, a novel decomposition of the state sensitivities into three parts is proposed which provides an intuitive classification of the influence of parameter changes on period, amplitude and relative phase. The importance of the choice of time reference, i.e., the phase locking condition, is demonstrated and discussed, and its influence on the sensitivity solution is quantified. The methods are then extended to other classes of oscillatory systems in a general formulation. Numerical techniques are presented to facilitate the solution of the boundary value problem, and the computation of different types of sensitivities. Numerical results compare favorably to finite difference approximations and are superior both in computational efficiency and in numerical precision to existing partial methods.

2.1 Introduction

Sensitivity analysis is a useful tool for the analysis of dynamic systems. It can be used to give local information on the impact of an infinitesimal parameter change on the behavior of the system, including derived functions of its output. As such, sensitivity analysis can be applied in model reduction, stability analysis, or in the analysis of biochemical pathways, to name a few [104]. While there are higher-order sensitivities, and different methods to compute "global" sensitivities, the sensitivities discussed in this article are local, first-order sensitivities, defined as

$$s_{ij}(t,\boldsymbol{\phi}) \equiv \left.\frac{\partial y_i}{\partial \phi_j}\right|_{t,\boldsymbol{\phi}} = \lim_{\epsilon \to 0} \frac{y_i(t,\boldsymbol{\phi}+\epsilon \mathbf{e}_j) - y_i(t,\boldsymbol{\phi})}{\epsilon}$$

where $\mathbf{e}_j$ is the jth unit vector and y_i is the ith component of $\mathbf{y}(t,\boldsymbol{\phi})$, a scalar or vector of state variables which change in time according to a dynamic system

$$\frac{d}{dt} y(t,\phi) = f(y(t,\phi),t,\phi).$$

The vector or scalar valued quantity ϕ can be either a model parameter, or an initial condition of the dynamic system, or a combination of both.

The efficient and accurate calculation of sensitivity information in dynamic systems is well understood, and can be performed easily in such numerical software packages as Jacobian [1].

This paper reports on methods that were specifically developed to enable the calculation of sensitivity information for oscillating dynamic systems. Different classes of such systems are distinguished and their respective treatment is detailed. Where applicable, previous work is built upon in order to present a comprehensive guide to sensitivity analysis of oscillating systems. Due to the exact and intuitive nature of the equations and methods in this work, the quantities that are computed relate to well defined derived functions of the dynamic systems, in particular period, amplitude and different kinds of phases.

2.1.1 Limit-Cycle Oscillators and Non-Limit-Cycle Oscillators

This ma-nuscript covers the sensitivity analysis of different classes of oscillating dynamical systems, all of which are described by systems of ordinary differential equations (ODEs). Before beginning the discussion, a general distinction needs to be made between the different classes: non-limit-cycle oscillators, limit-cycle oscillators and intermediate-type oscillators.

In this work, the term *non-limit-cycle oscillator* (NLCO) is used to describe any autonomous oscillating system in which any initial condition repeats periodically. In other words, their periodic orbits are not isolated and they do not exhibit transient behavior. The initial conditions and parameters both determine the trajectory of oscillation. Prominent examples of such systems are most predator-prey models such as the Lotka-Volterra system [63].

In *limit-cycle oscillators* (LCOs), on the other hand, the periodic orbit is isolated and

closed [96], meaning it is determined solely by the parameters of the system, and the shape and position of the limit cycle in phase space is independent of the initial conditions as long as the initial conditions lie within the region of attraction of the periodic orbit. Stable limit cycles, which are the focus of the present work, are approached in an asymptotic fashion from any initial condition within this region of attraction, unless the initial conditions lie exactly on the limit-cycle trajectory. LCOs are always governed by nonlinear ODE systems [96]. Many oscillatory biological systems have been modeled as LCOs, such as the circadian clock [29, 90] which will be examined in detail later. An intrinsic property of LCOs is the capability to return to the original oscillation (albeit phase shifted) after a perturbation in one or several state variables. This property makes LCOs an intuitive choice for the modeling of the biological oscillators in the circadian clock mechanism that show robustness to such perturbations with respect to amplitude and period, yet are entrainable to a specific phase of oscillation by outside signals [26].

Since these two classes of oscillators show different parameter and initial condition dependencies, their sensitivity analysis was formulated separately and is discussed in the following sections. Due to their more interesting and challenging nature, the majority of the present work focuses on LCOs and the theory necessary for their treatment is developed first. The extension to NLCOs is then easily shown.

Intermediate-type oscillators are systems that can show behaviors previously attributed to both other types, in that their periodic orbits are not isolated, but transients can still be found at least in some manifold. It is shown how these intermediate-type oscillators relate mathematically to both other classes, and a general formulation is presented in this paper which covers all classes of oscillators.

2.2 Sensitivity Analysis of Limit-Cycle Oscillators

In the context of this manuscript, a LCO is defined as a dynamic system with periodic orbit of period T whose monodromy matrix $\mathbf{M}$ (Section 2.2.2) has exactly one eigenvalue equal to one, and as a consequence the matrix $[(\mathbf{M}-\mathbf{I}) \quad \dot{\mathbf{y}}(T)]$ has rank n_y (see Corollary 2).

2.2.1 The Boundary Value Problem

Sensitivity analysis of stable LCO systems is challenging due to several of their characteristics. First, the system asymptotically approaches the limit-cycle trajectory, but never exactly reaches it, unless the initial conditions lie on the limit cycle. Consequently, if the aim is to analyze the limit-cycle trajectory, initial conditions on the periodic orbit must be identified. Clearly, those initial conditions are not independent of the parameter values, which determine the shape and location of the limit-cycle trajectory. Therefore, the initial conditions for the parametric sensitivities cannot be set to zero, as is usually done for dynamic systems when the initial conditions are independent of the parameters.

A boundary value problem (BVP) is formulated for $\mathbf{y}_0(\mathbf{p})$ and $T(\mathbf{p})$ subject to

$$\mathbf{y}(T(\mathbf{p}), \mathbf{p}; \mathbf{y}_0(\mathbf{p})) - \mathbf{y}_0(\mathbf{p}) = \mathbf{0} \tag{2.1}$$

$$\dot{y}_i(0, \mathbf{p}; \mathbf{y}_0(\mathbf{p})) = 0 \tag{2.2}$$

for some arbitrary $i \in \{1, ..., n_y\}$, with $\mathbf{y}(t, \mathbf{p}; \mathbf{y}_0(\mathbf{p}))$ given by the solution of

$$\frac{d}{dt}\mathbf{y}(t, \mathbf{p}; \mathbf{y}_0(\mathbf{p})) = \mathbf{f}(\mathbf{y}(t, \mathbf{p}; \mathbf{y}_0(\mathbf{p})), \mathbf{p}), \tag{2.3}$$

$$\mathbf{y}(0, \mathbf{p}; \mathbf{y}_0(\mathbf{p})) = \mathbf{y}_0(\mathbf{p}) \tag{2.4}$$

where $\mathbf{y}(t, \mathbf{p}; \mathbf{y}_0(\mathbf{p})) \in \mathbb{R}^{n_y}$ are the state variables and $\mathbf{p} \in \mathbb{R}^{n_p}$ are the parameters. By solving this BVP for given values for $\mathbf{p}$, initial conditions for the state variables that lie on the limit cycle are obtained as well as the period of oscillation, $T(\mathbf{p})$.

If only Eq. (2.1) were used, this BVP would have infinitely many solutions. The (n_y+1)st condition in Eq. (2.2) is one possible example of a *phase locking condition* (PLC), which fixes the solution to a isolated point on the limit cycle. In this example, this is the point where the state variable y_i is stationary. From the fact that (2.3) describes an oscillating system, at least one such point exists. Any arbitrary state variable can be chosen for this constraint, as long as a valid PLC is formulated. A PLC is valid if it defines an isolated point on the periodic orbit (this restriction excludes, e.g., stationary points in flat regions of the trajectory of y_i from being used in Eq. (2.2)) and it yields a solution that is unique and smooth in a neighborhood of $\mathbf{p}$ (this restriction excludes, for example, points where both $\dot{y}_i(0, \mathbf{p}; \mathbf{y}_0(\mathbf{p})) = 0$ and $\ddot{y}_i(0, \mathbf{p}; \mathbf{y}_0(\mathbf{p})) = 0$, as will be discussed in Sections 2.2.7

and 2.2.7). The choice of PLC presented here is useful for computing derived quantities, such as the peak-to-peak sensitivities presented in Section 2.2.7, and will be used for all examples unless otherwise mentioned.

Notice that $\mathbf{y}_0(\mathbf{p})$ and $T(\mathbf{p})$ calculated in this manner are functions of $\mathbf{p}$.

2.2.2 Floquet Theory

The Monodromy Matrix

Given a $\mathbf{y}(t)$ which satisfies Eqs. (2.1) and (2.3), then $\mathbf{A} \equiv \frac{\partial \mathbf{f}}{\partial \mathbf{y}}$ will be a matrix with periodic coefficients. Let $\mathbf{H}(t)$ be the solution to the linear system with periodically time-varying coefficients

$$\dot{\mathbf{H}}(t) = \mathbf{A}(t)\mathbf{H}(t) \tag{2.5}$$

with $\mathbf{H}(0) = \mathbf{I}$. The matrix $\mathbf{H}$ can be interpreted as the partial derivatives of the state variables $\mathbf{y}$ of the LCO with respect to the initial conditions, $h_{ij} \equiv \frac{\partial y_i}{\partial y_{0j}}$.

The monodromy matrix $\mathbf{M}$ of this system is defined as $\mathbf{M} \equiv \mathbf{H}(T)$ and has the property

$$\mathbf{H}(t+T) = \mathbf{H}(t)\mathbf{M}. \tag{2.6}$$

The eigenvalues ρ of $\mathbf{M}$ are called multipliers [89] (or characteristic roots [41]) of Equation (2.5). The characteristic exponents of Eq. (2.5) are then $\lambda_i = \frac{1}{T}\ln\rho_i$. The multipliers or exponents can be used to determine whether a solution of Eqs. (2.1) and (2.3) is stable. A solution to Eqs. (2.1) and (2.3) is orbitally stable if one multiplier is equal to 1, and all others lie inside the unit circle [5]. The eigenvalues and eigenvectors of $\mathbf{M}$ provide information on bifurcation behavior [24] and phase noise [53, 21, 22]. Throughout this section of the paper, it is assumed that the solution of Equation (2.3) is Lyapunov stable, that one multiplier is equal to 1, and all others lie inside the unit circle.

General Properties of the Matrix H

Given a general periodically time-varying linear system,

$$\dot{\mathbf{X}}(t) = \mathbf{A}(t)\mathbf{X}(t), \tag{2.7}$$

the state transition matrix relates $\mathbf{X}(s)$ to $\mathbf{X}(t)$ as in

$$\mathbf{X}(t) = \mathbf{H}(t,s)\mathbf{X}(s). \tag{2.8}$$

It is assumed that the state transition matrix $\mathbf{H}(t,s)$ of the linear system in Eq. (2.5) can be factored so that it takes the form [23]

$$\mathbf{H}(t,s) = \mathbf{U}(t)\mathbf{D}(t-s)\mathbf{V}(s).$$

If $\mathbf{H}(t,s)$ is diagonalizable, then $\mathbf{D}(t)$ is of the form

$$\mathbf{D}(t) = \begin{bmatrix} 1 & 0 & 0 & ... \\ 0 & e^{t\lambda_2} & 0 & ... \\ 0 & 0 & ... & ... \\ 0 & ... & & e^{t\lambda_{n_y}} \end{bmatrix}$$

where λ_i are the characteristic exponents of system (2.3) and where $\mathbf{U}(t) \in \mathbb{R}^{n_y \times n_y}$ and $\mathbf{V}(t) \in \mathbb{R}^{n_y \times n_y}$ are both T-periodic and nonsingular for all t, and satisfy

$$\mathbf{U}(t) = \mathbf{V}^{-1}(t).$$

If $\mathbf{H}(t,s)$ is not diagonalizable, then $\mathbf{D}(t)$ takes a block-diagonal form [95], with as many blocks $\mathbf{D}_i$ as there are linearly independent eigenvectors, with each block of size $n_i \times n_i$ taking the form

$$\mathbf{D}_i(t) = \begin{bmatrix} e^{\lambda_i(t)} & te^{t\lambda_i} & ... & \frac{1}{(n_i-1)!}t^{(n_i-1)}e^{t\lambda_i} \\ 0 & e^{t\lambda_i} & .. & \frac{1}{(n_i-2)!}t^{(n_i-2)}e^{t\lambda_i} \\ 0 & 0 & \ddots & \vdots \\ 0 & 0 & ... & e^{t\lambda_i} \end{bmatrix}. \tag{2.9}$$

The first row and column of $\mathbf{D}(t)$ is the same in both cases, as by definition the system has exactly one multiplier equal to one. For $s = 0$, $\mathbf{H}(t,s)$ becomes $\mathbf{H}(t)$ in Eq. (2.5) and it follows that $\mathbf{H}(t)$ can be written as $\mathbf{H}(t) = \mathbf{H}_1(t) + \mathbf{H}_2(t)$, where $\mathbf{H}_1(t)$ and $\mathbf{H}_2(t)$ are both

solutions to Eq. (2.5) and given by

$$\mathbf{H}_1(t) = [\dot{\mathbf{y}}(t) \quad \mathbf{O}_{n_y,n_y-1}]\mathbf{V}(0) \tag{2.10}$$
$$\mathbf{H}_2(t) = [\mathbf{O}_{n_y,1} \quad \mathbf{G}(t)]\mathbf{V}(0)$$

with $\mathbf{O}_{i,k}$ being the zero matrix with i rows and k columns [89, 18]. Furthermore, since all characteristic exponents λ_i have negative real parts for $i > 1$, the matrix $\mathbf{H}_2(t)$ decays for large times t, so that $\mathbf{H}(t) \to \mathbf{H}_1(t)$, and $\mathbf{H}_1(t)$ is T-periodic.

2.2.3 Parametric Sensitivity Analysis

Suppose a dynamic system is described by Eq. (2.3). Then, the matrix of parametric sensitivities $s_{ij} \equiv \frac{\partial y_i}{\partial p_j}$ satisfy the following differential equation:

$$\frac{d}{dt}\mathbf{S}(t,\mathbf{p}) = \mathbf{A}(t,\mathbf{p})\mathbf{S}(t,\mathbf{p}) + \mathbf{B}(t,\mathbf{p}), \tag{2.11}$$

where $\mathbf{A}(t,\mathbf{p}) = \left.\frac{\partial \mathbf{f}}{\partial \mathbf{y}}\right|_{\mathbf{y}(t,\mathbf{p}),\mathbf{p}}$, $\mathbf{B}(t,\mathbf{p}) = \left.\frac{\partial \mathbf{f}}{\partial \mathbf{p}}\right|_{\mathbf{y}(t,\mathbf{p}),\mathbf{p}}$ and $\mathbf{S}(t,\mathbf{p}) \in \mathbb{R}^{n_y \times n_p}$.

In the analysis of oscillatory systems, the family of periodic solutions $\mathbf{y}(t,\mathbf{p})$ of Eq. (2.3) is of interest. These solutions describe an oscillation with period $T(\mathbf{p})$, and therefore satisfy Eq. (2.1). As a consequence, $\mathbf{f}(\mathbf{y}(t,\mathbf{p}),\mathbf{p};\mathbf{y}_0(\mathbf{p}))$, $\mathbf{A}(t,\mathbf{p})$ and $\mathbf{B}(t,\mathbf{p})$ are periodic in time as well (for the remainder of this section, only the periodic solution is analyzed, unless otherwise mentioned). It was previously shown [89] that the general solution of Eq. (2.11) is

$$\mathbf{S}(t,\mathbf{p}) = \mathbf{H}(t,\mathbf{p})(\mathbf{S}_0 - \mathbf{Z}(0,\mathbf{p})) + t\mathbf{R}(t,\mathbf{p}) + \mathbf{Z}(t,\mathbf{p}) \tag{2.12}$$

where $\mathbf{R}(t,\mathbf{p})$ and $\mathbf{Z}(t,\mathbf{p})$ are also periodic in time with period $T(\mathbf{p})$, and where $\mathbf{S}_0 \equiv \mathbf{S}(0,\mathbf{p})$. The first term of this equation takes into account the influence of the initial conditions for the sensitivities, $\mathbf{S}_0 \equiv \frac{\partial \mathbf{y}_0}{\partial \mathbf{p}}$, which for many dynamical systems would be the zero matrix (i.e., the initial condition is not influenced by the parameters). The situation for limit-cycle oscillators is different, however. As shown in the previous section, $\mathbf{H}(t,\mathbf{p})$ does not decay, and therefore if the initial conditions $\mathbf{S}_0$ are not equal to $\mathbf{Z}(0,\mathbf{p})$, this term does not decay. The underlying cause is that, in fact, the $\mathbf{y}_0$ that satisfies Eqs. (2.1-2.3) does depend on the parameters $\mathbf{p}$.

If this influence of the initial conditions is to be captured in the total sensitivity, one

effectively wants to compute the quantity

$$\mathbf{S}\left(\cdot,\cdot;\frac{\partial \mathbf{y}_0}{\partial \mathbf{p}}\right) \equiv \frac{\partial \mathbf{y}}{\partial \mathbf{y}_0}\frac{\partial \mathbf{y}_0}{\partial \mathbf{p}} + \left(\frac{\partial \mathbf{y}}{\partial \mathbf{p}}\right)_{\mathbf{y}_0=const.}$$

where $\left(\frac{\partial \mathbf{y}}{\partial \mathbf{p}}\right)_{\mathbf{y}_0=const.} = \mathbf{S}(\cdot,\cdot;\mathbf{0})$ are the sensitivities at constant initial conditions. In other words, the nonzero sensitivity initial conditions $\mathbf{S}_0$ need to be determined. It was previously shown [89] that the solution of Eq. (2.11) then takes the form

$$\mathbf{S}(t,\mathbf{p};\mathbf{S}_0(\mathbf{p})) = t\mathbf{R}(t,\mathbf{p}) + \mathbf{Z}(t,\mathbf{p};\mathbf{S}_0(\mathbf{p})), \tag{2.13}$$

where $\mathbf{Z}(0,\mathbf{p};\mathbf{S}_0(\mathbf{p})) = \mathbf{S}_0(\mathbf{p})$.

Several characteristics of the sensitivity trajectories become apparent. As Eq. (2.13) shows, the parametric sensitivities of a periodic system are composed of two parts. The periodic part

$$\mathbf{Z} = \left(\frac{\partial \mathbf{y}}{\partial \mathbf{p}}\right)_{T(\mathbf{p})=const.}$$

corresponds to the partial derivative of the state variables with respect to the parameters, with the period kept constant. This quantity can be further decomposed to distinguish amplitude from phase contributions, which will be discussed in more detail in Section 2.2.5. It was sometimes referred to as the "cleaned out" sensitivity coefficients in previous publications [99].

The unbounded part $t\mathbf{R}(t,\mathbf{p})$ contains information on the influence of the parameters on the period of the oscillation. In fact, [89] shows that

$$\mathbf{R}(t,\mathbf{p}) = -\frac{\dot{\mathbf{y}}(t,\mathbf{p};\mathbf{y}_0(\mathbf{p}))}{T(\mathbf{p})}\left.\frac{\partial T}{\partial \mathbf{p}}\right|_{\mathbf{p}}, \tag{2.14}$$

where $\dot{\mathbf{y}}(t,\mathbf{p};\mathbf{y}_0(\mathbf{p}))$ is a column vector of length n_y and $\frac{\partial T}{\partial \mathbf{p}}$ is a row vector of length n_p. The unboundedness of this part caused concern in some previous work, and it was proposed to scale the time t to obtain a "cyclic time" to avoid the problem [99]. However, it is crucial to notice that even if the unboundedness of this part is eliminated, another source of error and transients in the general solution remains. This is the error caused by inappropriate initial conditions for $\mathbf{S}$, which leads both to a transient of unknown magnitude as well as a persistent, periodic contribution as time goes to infinity, as can be seen in Eq. (2.12)

and Section 2.2.2. In order to calculate meaningful sensitivities $\mathbf{S}(t, \mathbf{p}; \mathbf{S}_0(\mathbf{p}))$ as well as $\mathbf{Z}(t, \mathbf{p})$ and $\mathbf{R}(t, \mathbf{p})$ for any given time t, correct initial conditions $\mathbf{S}_0$ need to be determined. Methods to compute the exact initial conditions and the various parts of the sensitivity for both LCOs and NLCOs are detailed next.

2.2.4 Boundary Value Formulation for the Period Sensitivities

Eqs. (2.1–2.2) can be differentiated with respect to the parameters $\mathbf{p}$, yielding the following expressions:

$$\begin{aligned} \left.\frac{d\mathbf{y}}{dt}\right|_{T,\mathbf{p},\mathbf{y}_0} \left.\frac{\partial T}{\partial \mathbf{p}}\right|_{\mathbf{p}} + \left(\left.\frac{\partial \mathbf{y}}{\partial \mathbf{p}}\right|_{T,\mathbf{p},\mathbf{y}_0}\right)_{\mathbf{y}(0)=const.} + \left.\frac{\partial \mathbf{y}}{\partial \mathbf{y}_0}\right|_{T,\mathbf{p},\mathbf{y}_0} \left.\frac{\partial \mathbf{y}_0}{\partial \mathbf{p}}\right|_{\mathbf{p}} \\ - \left.\frac{\partial \mathbf{y}}{\partial \mathbf{y}_0}\right|_{0,\mathbf{p},\mathbf{y}_0} \left.\frac{\partial \mathbf{y}_0}{\partial \mathbf{p}}\right|_{\mathbf{p}} = \mathbf{0} \end{aligned} \tag{2.15}$$

$$\left.\frac{\partial f_i}{\partial \mathbf{y}}\right|_{\mathbf{y}_0,\mathbf{p}} \left.\frac{\partial \mathbf{y}_0}{\partial \mathbf{p}}\right|_{\mathbf{p}} + \left.\frac{\partial f_i}{\partial \mathbf{p}}\right|_{\mathbf{y}_0,\mathbf{p}} = \mathbf{0}. \tag{2.16}$$

This set of equations can then be rewritten in matrix form as

$$\begin{bmatrix} (\mathbf{M}(\mathbf{p}) - \mathbf{I}) & \dot{\mathbf{y}}(T, \mathbf{p}; \mathbf{y}_0(\mathbf{p})) \\ \left.\frac{\partial f_i}{\partial \mathbf{y}}\right|_{\mathbf{y}_0,\mathbf{p}} & 0 \end{bmatrix} \begin{bmatrix} \mathbf{S}_0(\mathbf{p}) \\ \left.\frac{\partial T}{\partial \mathbf{p}}\right|_{\mathbf{p}} \end{bmatrix} = \begin{bmatrix} -\mathbf{S}(T, \mathbf{p}; \mathbf{0}) \\ -\left.\frac{\partial f_i}{\partial \mathbf{p}}\right|_{\mathbf{y}_0,\mathbf{p}} \end{bmatrix} \tag{2.17}$$

where $\mathbf{I}$ is the $n_y \times n_y$ identity matrix, $\mathbf{M}(\mathbf{p})$ is the monodromy matrix of the sensitivity system $\left.\frac{\partial \mathbf{y}}{\partial \mathbf{y}_0}\right|_{T,\mathbf{p},\mathbf{y}_0}$, and $\mathbf{S}(T, \mathbf{p}; \mathbf{0})$ is the solution of sensitivity equation (2.11) for zero initial conditions at time T, $\left(\left.\frac{\partial \mathbf{y}}{\partial \mathbf{p}}\right|_{T,\mathbf{p},\mathbf{y}_0}\right)_{\mathbf{y}(0)=const.}$. This equation can be solved for the matrix of unknowns,

$$\begin{bmatrix} \mathbf{S}_0(\mathbf{p}) \\ \left.\frac{\partial T}{\partial \mathbf{p}}\right|_{\mathbf{p}} \end{bmatrix},$$

obtaining a set of initial conditions for the sensitivities $\mathbf{S}_0(\mathbf{p})$ and the period sensitivities.

Using these quantities, it will be shown that all the various parts of the sensitivites can be computed exactly, without using iterative processes or approximations.

There have been several previous approaches to calculate the period sensitivities in LCOs. Typically, the fact that the unbounded term will dominate at large times is used to

estimate the period sensitivity in an iterative procedure [18, 56, 64, 48]. Another approach uses a method based on singular value decomposition [111]. A third method involves the computation of relative phase sensitivities [56, 37]. All these methods have in common that at some point during the numerical procedure, estimations are made, typically where the exact mathematical quantity involves a limit that is estimated by truncating the sequence finitely.

Rosenwasser and Yusupov [89] describe a very similar BVP-based method for LCOs that allows the calculation of the period sensitivities in the same way as presented here, and that is exact (i.e., the only source of error is the numerical tolerance to which the BVP is solved). Because a different type of PLC is used, the solution for the sensitivity initial conditions is different. The possible multiplicity of such solutions is not discussed. The work presented here shows how the choice of PLC influences the solution of the sensitivity trajectories (Section 2.2.5) and the fact that the choice of PLC matters in performing relative phase sensitivity (Section 2.2.7). While reference [89] shows a decomposition of the sensitivity solution that separates out the influence of the period (Section 2.2.3), this work introduces a meaningful decomposition into three parts, where the influence of relative phase and is separated from that of the amplitudes (Section 2.2.5). Furthermore, this work extends all theory to oscillator types other than LCOs in Section 2.4.

2.2.5 Many Sensitivity Systems for Limit-Cycle Oscillators

Instead of Eq. (2.2), other PLCs can be used, as long as the resulting system is well-posed [62]. An example [89] is to choose a suitable value a for one of the state variables y_j, such that $y_j(0, \mathbf{p}) = a$ forms the $(n_y + 1)$st equation of the BVP. This change will only affect the last row of the matrix equation (2.17) and yields the same period sensitivities $\frac{\partial T}{\partial \mathbf{p}}$, as will become evident after the following analysis.

The matrix $(\mathbf{M}(\mathbf{p}) - \mathbf{I})$ is singular with a rank of $(n_y - 1)$, since it has been assumed that $\mathbf{M}$ has exactly one eigenvalue equal to one, and therefore $(\mathbf{M}(\mathbf{p}) - \mathbf{I})$ has exactly one eigenvalue equal to zero. The partial system

$$\begin{bmatrix} (\mathbf{M}(\mathbf{p}) - \mathbf{I}) & \dot{\mathbf{y}}(T, \mathbf{p}; \mathbf{y}_0(\mathbf{p})) \end{bmatrix} \begin{bmatrix} \mathbf{S}_0(\mathbf{p}) \\ \frac{\partial T}{\partial \mathbf{p}}\Big|_{\mathbf{p}} \end{bmatrix} = \begin{bmatrix} -\mathbf{S}(T, \mathbf{p}; \mathbf{0}) \end{bmatrix} \tag{2.18}$$

of Eq. (2.17) does not have a unique solution, but $\frac{\partial T}{\partial \mathbf{p}}$ is still uniquely determined by this system.

What follows is that if $\mathbf{S}_0^*$ is a solution of Eq. (2.18) then $\hat{\mathbf{S}}_0 = \mathbf{S}_0^* + \dot{\mathbf{y}}(0)\boldsymbol{\delta}(0)$ is also a solution. $\boldsymbol{\delta}(0)$ is any row vector of size n_p. The vector $\dot{\mathbf{y}}(0, \mathbf{p}; \mathbf{y}_0(\mathbf{p})) = \dot{\mathbf{y}}(T, \mathbf{p}; \mathbf{y}_0(\mathbf{p}))$ is a right eigenvector of $(\mathbf{M}-\mathbf{I})$ associated with the zero eigenvalue since it is a right eigenvector of the monodromy matrix $\mathbf{M}$, associated with the multiplier equal to one [21].

Theorem 1. *Suppose that at a solution of equations (2.1–2.2) the Jacobian matrix on the left-hand side of Eq. (2.17) with respect to* $\mathbf{y}_0(\mathbf{p})$ *and* $T(\mathbf{p})$ *is nonsingular. Then:*

1. $\left.\frac{\partial T}{\partial \mathbf{p}}\right|_{\mathbf{p}}$ *is determined uniquely by Eq. (2.18), i.e., independent of the choice of PLC.*
2. *Any solution of Eq. (2.11) for* T*–periodic* $\mathbf{A}$ *and* $\mathbf{B}$ *has the form*

$$\mathbf{S}(t) = -\frac{t}{T}\dot{\mathbf{y}}(t)\frac{\partial T}{\partial \mathbf{p}} + \mathbf{Q}(t). \tag{2.19}$$

3. *If* $\mathbf{S}$ *is a solution of Eq. (2.11) then*

$$\hat{\mathbf{S}}(t) = -\frac{t}{T}\dot{\mathbf{y}}(t)\frac{\partial T}{\partial \mathbf{p}} + \hat{\mathbf{Q}}(t)$$

is also a solution of Eq. (2.11) (e.g., for another PLC) where

$$\hat{\mathbf{Q}}(t) \equiv \mathbf{Q}(t) + \dot{\mathbf{y}}(t)\boldsymbol{\gamma}$$

and $\boldsymbol{\gamma} \equiv [\gamma_1, \gamma_2, \ldots, \gamma_{n_p}]$ *is any time invariant row vector.*

4. *Any initial condition* $\mathbf{S}_0$ *for Eq. (2.11) that satisfies Eq. (2.18) yields a solution* $\mathbf{S}$ *with a* T*-periodic* $\mathbf{Q}$ *in* (2.19)*.*

Proof. 1. By hypothesis Eq. (2.17) has a unique solution. In other words, the square matrix is of rank (n_y+1) and therefore the partial system in Eq. (2.18) must be of full rank (n_y) (since one extra row can only increase the rank by one). Since $[\mathbf{M}(\mathbf{p})-\mathbf{I}]$ is of rank $n_y - 1$, the partial system Eq. (2.18) can be put in the following row echelon

form:

$$\left[\begin{array}{ccccc|c} * & * & ... & * & * & * \\ 0 & * & ... & * & * & * \\ \vdots & \vdots & \ddots & \vdots & \vdots & \vdots \\ 0 & 0 & ... & * & * & * \\ 0 & 0 & .... & 0 & 0 & * \end{array}\right] \left[\begin{array}{c} \mathbf{S}_0(\mathbf{p}) \\ \left.\frac{\partial T}{\partial \mathbf{p}}\right|_{\mathbf{p}} \end{array}\right] = \left[\begin{array}{c} -\mathbf{\Psi}\mathbf{S}(T, \mathbf{p}; \mathbf{0}) \end{array}\right]$$

where $\mathbf{\Psi}$ is a matrix representing the elementary row operations performed to obtain row-echelon form. Since the $(n_y + 1)$st column must contribute a pivot to the system, $\frac{\partial T}{\partial \mathbf{p}}$ is uniquely determined.

2. The general solution of Eq. (2.11) is given by Eq. (2.12) and shows it can always be decomposed as Eq. (2.19), such that $\mathbf{Q}(t)$ is not necessarily periodic but contains the influence of the initial conditions and the periodic part $\mathbf{Z}(t)$.

3. Take a solution $\mathbf{S}$ to Eq. (2.11) of the form (2.19). Then, if $\dot{\mathbf{y}}\boldsymbol{\gamma}$ is added to $\mathbf{S}$,

$$\dot{\mathbf{S}} + \ddot{\mathbf{y}}\boldsymbol{\gamma} = \mathbf{A}(\mathbf{S} + \dot{\mathbf{y}}\boldsymbol{\gamma}) + \mathbf{B} \tag{2.20}$$

which solves Eq. (2.11) because

$$\ddot{\mathbf{y}} = \mathbf{A}\dot{\mathbf{y}}.$$

Furthermore, all solutions $\hat{\mathbf{S}}(t)$ can be decomposed as in Eq. (2.19) because

$$\mathbf{S} + \dot{\mathbf{y}}\boldsymbol{\gamma} = t\mathbf{R} + \mathbf{Q} + \dot{\mathbf{y}}\boldsymbol{\gamma}$$

where $\mathbf{R} = -\frac{\dot{\mathbf{y}}}{T}\frac{\partial T}{\partial \mathbf{p}}$, and $\frac{\partial T}{\partial \mathbf{p}}$ is uniquely determined by Eq. (2.18), so that $\hat{\mathbf{R}} = \mathbf{R}$. Then

$$\hat{\mathbf{S}} = t\mathbf{R} + \hat{\mathbf{Q}}$$

where $\hat{\mathbf{Q}} \equiv \mathbf{Q} + \dot{\mathbf{y}}\boldsymbol{\gamma}$.

4. Substitute Eq. (2.12) into Eq. (2.18) to obtain

$$(\mathbf{M} - \mathbf{I})(\mathbf{S}_0 - \mathbf{Z}(0)) = \mathbf{0}.$$

$\mathbf{Q}(t + T) - \mathbf{Q}(t) = \mathbf{S}(t + T) - \mathbf{S}(t) + \dot{\mathbf{y}}(t)\frac{\partial T}{\partial \mathbf{p}}$, so by using Eq. (2.12) together with

Eq. (2.6) to obtain

$$\mathbf{Q}(t+T) - \mathbf{Q}(t) = \mathbf{H}(t)(\mathbf{M} - \mathbf{I})(\mathbf{S}_0 - \mathbf{Z}(0)) = \mathbf{0}$$

and therefore $\mathbf{Q}$ is T periodic.

□

It is important to notice that once a solution for the BVP in Eq. (2.1) is found (using any PLC), it is irrelevant which PLC is used to compute the sensitivity matrices (as long as it is consistent with the initial conditions found from the solution of the BVP). This is due to the fact that the influence of the initial conditions is only implicit in the matrices $\mathbf{A}$ and $\mathbf{B}$ and it was shown that all solutions are consistent with those.

Decomposition of the Periodic $\mathbf{Z}(t)$ Matrix

It was suggested in reference [64] that the periodic matrix $\mathbf{Z}(t)$ contains information on how the shape of the limit cycle depends on the parameters of the system, where the influence of the period change is eliminated. Furthermore, this matrix is thought to contain information on phase behavior of the limit cycle [56]. Presumably, if any information on the shape of the limit cycle is to be found, one would like to eliminate all components that encode phase information, or in other words, that are in the $\dot{\mathbf{y}}(t)$ direction. The matrix $\mathbf{Z}(t)$ can then be written as a sum of two contributions:

$$\mathbf{Z}(t) = \mathbf{W}(t) + \dot{\mathbf{y}}(t)\boldsymbol{\delta}(t)$$

The initial condition from a solution of Eq. (2.18) that is orthogonal to the null space of $(\mathbf{M} - \mathbf{I})$ will be termed $\mathbf{W}(0)$.

Since $\dot{\mathbf{y}}(T)$ spans the null space of $(\mathbf{M}(\mathbf{p}) - \mathbf{I})$, $\mathbf{W}(0)$ can be computed by augmenting Eq. (2.18) with this eigenvector (corresponding to the zero eigenvalue) as the $(n_y + 1)$st row. The resulting system of equations is

$$\begin{bmatrix} (\mathbf{M}(\mathbf{p}) - \mathbf{I}) & \dot{\mathbf{y}}(T, \mathbf{p}; \mathbf{y}_0(\mathbf{p})) \\ \dot{\mathbf{y}}^{\mathrm{T}}(T, \mathbf{p}; \mathbf{y}_0(\mathbf{p})) & 0 \end{bmatrix} \begin{bmatrix} \mathbf{W}(0, \mathbf{p}) \\ \left.\frac{\partial T}{\partial \mathbf{p}}\right|_{\mathbf{p}} \end{bmatrix} = \begin{bmatrix} -\mathbf{S}(T, \mathbf{p}; \mathbf{0}) \\ \mathbf{0} \end{bmatrix}. \tag{2.21}$$

The $(n_y + 1)$st row in this situation does not represent a PLC, and can thus be added for any solution of the BVP in Eq. (2.1).

However, this method only provides an initial condition. The matrix $\mathbf{W}(t)$ is constructed from any matrix $\mathbf{Z}(t)$ (or from $\mathbf{S}(t)$, in the exact same manner) using the projection

$$\mathbf{W}(t) = \left(\mathbf{I} - \frac{\dot{\mathbf{y}}(t)\,\dot{\mathbf{y}}(t)^{\mathrm{T}}}{||\dot{\mathbf{y}}(t)||^2}\right)\mathbf{Z}(t). \tag{2.22}$$

It is known that $\mathbf{Z}(t+T) = \mathbf{Z}(t)$ as well as $\dot{\mathbf{y}}(t+T) = \dot{\mathbf{y}}(t)$, so it is clear that $\mathbf{W}(t+T) = \mathbf{W}(t)$ is periodic also. Using the same argument, the contribution in the $\dot{\mathbf{y}}(t)$ direction

$$\boldsymbol{\delta}(t) = \frac{1}{||\dot{\mathbf{y}}(t)||^2}\,[\dot{\mathbf{y}}(t)^{\mathrm{T}}\mathbf{Z}(t)]$$

is also T periodic.

In summary, this decomposition of the matrix $\mathbf{Z}(t)$ leads to a three part decomposition of the overall sensitivities, yielding

$$\mathbf{S}(t) = -\frac{t}{T}\dot{\mathbf{y}}(t)\frac{\partial T}{\partial \mathbf{p}} + \mathbf{W}(t) + \dot{\mathbf{y}}(t)\boldsymbol{\delta}(t).$$

The interpretation of the latter two parts as containing shape and phase information, respectively, is justified in the following text.

2.2.6 Amplitude Sensitivities

Define the amplitude of y_i as

$$\Omega_i(\mathbf{p}) \equiv y_i(t_{i,max}(\mathbf{p}), \mathbf{p}; \mathbf{y}_0(\mathbf{p})) - y_i(t_{i,min}(\mathbf{p}), \mathbf{p}; \mathbf{y}_0(\mathbf{p}))$$

where $t_{i,max}$ and $t_{i,min}$ are times at which y_i attains its maximum and minimum value, respectively, and differentiate with respect to $\mathbf{p}$ to obtain

$$\begin{aligned}\left.\frac{\partial \Omega_i}{\partial \mathbf{p}}\right|_{\mathbf{p}} &= \mathbf{s}_i(t_{i,max}(\mathbf{p}), \mathbf{p}; \mathbf{S}_0(\mathbf{p})) + \dot{y}_i(t_{i,max}(\mathbf{p}), \mathbf{p}; \mathbf{y}_0(\mathbf{p}))\left.\frac{\partial t_{i,max}}{\partial \mathbf{p}}\right|_{\mathbf{p}} \\ &\quad -\mathbf{s}_i(t_{i,min}(\mathbf{p}), \mathbf{p}; \mathbf{S}_0(\mathbf{p})) - \dot{y}_i(t_{i,min}(\mathbf{p}), \mathbf{p}; \mathbf{y}_0(\mathbf{p}))\left.\frac{\partial t_{i,min}}{\partial \mathbf{p}}\right|_{\mathbf{p}}\end{aligned}$$

where $\mathbf{s}_i$ represents the ith row of the full sensitivity matrix. The amplitude of oscillation is

thus a derived quantity specific to each state variable and because $\mathbf{y}(t)$ is a smooth function, the terms multiplied by $\dot{y}_i(t_{i,max}(\mathbf{p}), \mathbf{p}; \mathbf{y}_0(\mathbf{p}))$ and by $\dot{y}_i(t_{i,min}(\mathbf{p}), \mathbf{p}; \mathbf{y}_0(\mathbf{p}))$ vanish, the amplitude sensitivity is the difference between the sensitivities at the maximum and the minimum of this state variable, as shown in references [18, 56]. Furthermore, the sensitivity of the amplitude of y_i can be calculated directly from any of the sensitivities $\mathbf{S}$, $\mathbf{Z}$ or $\mathbf{W}$. From the fact that $\dot{y}_i(t_{i,max}) = 0$ it follows that $\mathbf{s}_i(t_{i,max}) = \mathbf{z}_i(t_{i,max}) = \mathbf{w}_i(t_{i,max})$. This illustrates the fact that $\mathbf{W}$ contains information on the shape of the limit cycle.

Theorem 2. *For a LCO, the matrix $\mathbf{W}(t)$ is uniquely defined by $\mathbf{y}(t)$ for each point on the limit cycle.*

Proof. Take two sensitivity solutions $\mathbf{S}_1(t, \mathbf{p}; \mathbf{S}_{0,1}(\mathbf{p}))$ and $\mathbf{S}_2(s, \mathbf{p}; \mathbf{S}_{0,2}(\mathbf{p}))$, constructed using PLC_1 and PLC_2, respectively. The two PLCs define time references such that at some point on the limit cycle, $\mathbf{y}(t = \alpha) = \mathbf{y}(s = \beta)$. Differentiate with respect to the parameters to obtain

$$\mathbf{S}_1(t = \alpha) + \dot{\mathbf{y}}(t = \alpha)\frac{\partial \alpha}{\partial \mathbf{p}} = \mathbf{S}_2(s = \beta) + \dot{\mathbf{y}}(s = \beta)\frac{\partial \beta}{\partial \mathbf{p}}$$

showing that solutions satisfying Eq. (2.18) differ only in their contributions in the direction $\dot{\mathbf{y}}(t)$, and this difference is eliminated by using the projection described in Eq. (2.22) to construct $\mathbf{W}(t)$. □

Corollary 1. *The only difference between any two sensitivity solutions for the same $\mathbf{y}_0(\mathbf{p})$ is $\boldsymbol{\delta}(t)$.*

2.2.7 Phase Sensitivities

The Relative Phase Sensitivities $\boldsymbol{\delta}(t)$

This section will show that there is an intuitive interpretation of $\boldsymbol{\delta}(t)$ as a quantification of how the timing of an event defined by a PLC depends on the parameters of the system. In other words, the quantity $\boldsymbol{\delta}(t)$ is a relative phase sensitivity, where "relative phase" is defined as a time difference $(\beta - \alpha)$ between two events, described by two different PLCs.

Take $\mathbf{y}^*(t, \mathbf{p}; \mathbf{y}_0^*(\mathbf{p}))$ to be the solution of the BVP using PLC_1, leading to a sensitivity solution

$$\mathbf{S}^*(t) = t\mathbf{R}^*(t) + \mathbf{W}^*(t) + \dot{\mathbf{y}}^*(t)\boldsymbol{\delta}^*(t), \tag{2.23}$$

and $\mathbf{y}^{**}(s, \mathbf{p}; \mathbf{y}_0^{**}(\mathbf{p}))$ to be the solution of the BVP using PLC_2, leading to a sensitivity solution

$$\mathbf{S}^{**}(s) = s\mathbf{R}^{**}(s) + \mathbf{W}^{**}(s) + \dot{\mathbf{y}}^{**}(s)\boldsymbol{\delta}^{**}(s). \tag{2.24}$$

Define a pair (α, β) by

$$\mathbf{y}^{*}(t = \beta, \mathbf{p}; \mathbf{y}_0^{*}(\mathbf{p})) = \mathbf{y}^{**}(s = \alpha, \mathbf{p}; \mathbf{y}_0^{**}(\mathbf{p})) \tag{2.25}$$

and thus also $\dot{\mathbf{y}}^{*}(\beta, \mathbf{p}; \mathbf{y}_0^{*}(\mathbf{p})) = \dot{\mathbf{y}}^{**}(\alpha, \mathbf{p}; \mathbf{y}_0^{**}(\mathbf{p}))$. Differentiate Eq. (2.25) with respect to $\mathbf{p}$ to obtain

$$\mathbf{S}^{*}(\beta) + \dot{\mathbf{y}}^{*}(\beta)\frac{\partial \beta}{\partial \mathbf{p}} = \mathbf{S}^{**}(\alpha) + \dot{\mathbf{y}}^{**}(\alpha)\frac{\partial \alpha}{\partial \mathbf{p}}.$$

Eqns. (2.23–2.24) can be used to cancel identical terms:

$$\mathbf{W}^{*}(\beta) + \dot{\mathbf{y}}^{*}(\beta)\left(-\frac{\beta}{T}\frac{\partial T}{\partial \mathbf{p}} + \frac{\alpha}{T}\frac{\partial T}{\partial \mathbf{p}} + \boldsymbol{\delta}^{*}(\beta) + \frac{\partial \beta}{\partial \mathbf{p}} - \frac{\partial \alpha}{\partial \mathbf{p}} - \boldsymbol{\delta}^{**}(\alpha)\right) = \mathbf{W}^{**}(\alpha).$$

By Theorem 2 $\mathbf{W}^{*}(\beta) = \mathbf{W}^{**}(\alpha)$ and $\dot{\mathbf{y}}^{*}(\beta) \neq \mathbf{0}$ so that

$$\frac{\partial(\alpha - \beta)}{\partial \mathbf{p}} = \frac{(\alpha - \beta)}{T}\frac{\partial T}{\partial \mathbf{p}} + \boldsymbol{\delta}^{*}(\beta) - \boldsymbol{\delta}^{**}(\alpha) \tag{2.26}$$

This result is interesting because it enables two effects to be distinguished. The first term is the overall contribution of the period sensitivity to the sensitivity of the phase, whereas the following two terms describe the flexibility of the limit cycle in the sense that phase variation can occur independently of period variation.

Notice that if PLC_1 and PLC_2 had been chosen in such a way that they locked the phase at the same point, but using different PLCs, then $\beta = \alpha$ and the influence of different PLCs on the sensitivity solution is entirely quantified by the different $\boldsymbol{\delta}$s. This effect is illustrated in Figure 2-1 and it makes clear the need for a precise definition of "phase" when analyzing oscillatory dynamical systems. Care must be taken to use only PLCs that are valid. An example of an invalid PLC would be to use $y_i(0) = \xi$ at an extremum of y_i, because in this scenario the point $y_i(0) = \xi$ might no longer exist after an infinitesimal parameter change, i.e. the phase sensitivity is not defined.

Notice furthermore that if $\alpha = 0$, the measure $-\frac{\partial(\alpha-\beta)}{\partial \mathbf{p}}$ describes the sensitivity of the timing of the event $\mathbf{y}^{*}(t = \beta)$ with reference to the time scale defined by PLC_1.

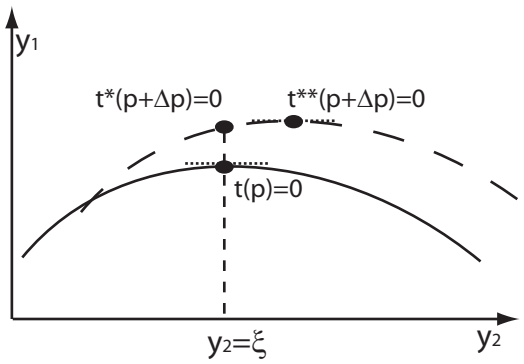

Figure 2-1: Illustration of the effect of the PLC on the sensitivity solution. A finite perturbation of the parameters from $\mathbf{p}$ to $(\mathbf{p}+\Delta\mathbf{p})$ causes a shift of the limit cycle from the solid line to the dashed line. The PLC $\dot{y}_1(0) = 0$ results in a new time reference shown as t^{**}, the PLC $y_2(0) = \xi$ results in the time t^*.

Peak-to-Peak Phase Sensitivities

The peak-to-peak sensitivities defined here are one particular kind of relative phase sensitivities, where the relative phase of interest is the time difference between extrema in different state variables. While the formulation presented above can be used, the structure of the problem lends itself to a short-cut which will be described briefly.

Suppose the time scale is defined using the PLC

$$\dot{y}_1(0, \mathbf{p}; \mathbf{y}_0(\mathbf{p})) = 0. \tag{2.27}$$

Then define $\beta(\mathbf{p})$ from the equation

$$\dot{y}_j(\beta(\mathbf{p}), \mathbf{p}; \mathbf{y}_0(\mathbf{p})) = 0 \tag{2.28}$$

i.e., β is the time of the extremum in y_j relative to the extremum in y_1. This can also be written as

$$f_j(\mathbf{y}(\beta(\mathbf{p}), \mathbf{p}; \mathbf{y}_0(\mathbf{p})), \mathbf{p}) = 0 \tag{2.29}$$

and differentiated with respect to $\mathbf{p}$ to yield

$$\left.\frac{\partial f_j}{\partial \mathbf{y}}\right|_{\mathbf{y}(\beta(\mathbf{p}),\mathbf{p};\mathbf{y}_0(\mathbf{p})),\mathbf{p}} \left(\dot{\mathbf{y}}(\beta(\mathbf{p}),\mathbf{p};\mathbf{y}_0(\mathbf{p})) \left.\frac{\partial \beta}{\partial \mathbf{p}}\right|_{\mathbf{p}} + \mathbf{S}\left(\beta(\mathbf{p}),\mathbf{p};\left.\frac{\partial \mathbf{y}_0}{\partial \mathbf{p}}\right|_{\mathbf{p}}\right)\right) + \left.\frac{\partial f_j}{\partial \mathbf{p}}\right|_{\mathbf{y}(\beta(\mathbf{p}),\mathbf{p};\mathbf{y}_0(\mathbf{p})),\mathbf{p}} = \mathbf{0}, \tag{2.30}$$

which can be solved directly for $\left.\frac{\partial \beta}{\partial \mathbf{p}}\right|_{\mathbf{p}}$, providing the peak-to-peak sensitivity without the calculation of $\boldsymbol{\delta}$s. Again, close attention should be paid to the validity of the PLC for the point chosen. If in this case, $\left.\frac{\partial f_j}{\partial \mathbf{y}}\right|_{\mathbf{y}(\beta(\mathbf{p}),\mathbf{p};\mathbf{y}_0(\mathbf{p})),\mathbf{p}} \dot{\mathbf{y}}(\beta(\mathbf{p}),\mathbf{p};\mathbf{y}_0(\mathbf{p})) = 0$ in Eq. (2.30), or in other words $\ddot{\mathbf{y}}(\beta(\mathbf{p}),\mathbf{p};\mathbf{y}_0(\mathbf{p})) = 0$, the PLC is not valid and this equation cannot be used to determine a unique $\frac{\partial \beta}{\partial \mathbf{p}}$ (an intuitive example here is the case of a saddle point in y_j, where an infinitesimal parameter change might remove the stationary point and turn the saddle point into an inflexion point instead). In this case, it may be possible to use higher-order derivatives of the PLC with respect to the parameters to determine a unique $\frac{\partial \beta}{\partial \mathbf{p}}$. However, this analysis is not detailed here.

This simplified method yields the same result as the more general method from the previous section, as evident after the following exercise. Take Eq. (2.27) as PLC_1, yielding the time reference $\mathbf{y}(t)$. Use Eq. (2.28) as the second PLC, with the time reference $\mathbf{y}^{**}(s)$ and $\alpha = 0$, so that $\mathbf{y}(\beta) = \mathbf{y}^{**}(0)$. Then Eq. (2.30) can be written as

$$\left.\frac{\partial f_j}{\partial \mathbf{y}}\right|_{\mathbf{y}(\beta,\mathbf{p}),\mathbf{p}} \left(\dot{\mathbf{y}}(\beta,\mathbf{p}) \left(\left.\frac{\partial \beta}{\partial \mathbf{p}}\right|_{\mathbf{p}} - \frac{\beta}{T}\frac{\partial T}{\partial \mathbf{p}} + \boldsymbol{\delta}(\beta) \right) + \mathbf{W}(\beta,\mathbf{p}) \right) + \left.\frac{\partial f_j}{\partial \mathbf{p}}\right|_{\mathbf{y}(\beta,\mathbf{p}),\mathbf{p}} = \mathbf{0}. \tag{2.31}$$

From the second PLC it is known that

$$\left.\frac{\partial f_j}{\partial \mathbf{y}}\right|_{\mathbf{y}^{**}(0,\mathbf{p}),\mathbf{p}} (\mathbf{W}^{**}(0) + \dot{\mathbf{y}}^{**}(0,\mathbf{p})\boldsymbol{\delta}^{**}(0)) + \left.\frac{\partial f_j}{\partial \mathbf{p}}\right|_{\mathbf{y}^{**}(0,\mathbf{p}),\mathbf{p}} = \mathbf{0}, \tag{2.32}$$

where as shown in Theorem 2, $\mathbf{W}^{**}(0) = \mathbf{W}(\beta)$, and thus Eq. (2.32) can be substituted into Eq. (2.31) to obtain

$$\left.\frac{\partial f_j}{\partial \mathbf{y}}\right|_{\mathbf{y}(\beta,\mathbf{p}),\mathbf{p}} \dot{\mathbf{y}}(\beta,\mathbf{p}) \left(\left.\frac{\partial \beta}{\partial \mathbf{p}}\right|_{\mathbf{p}} - \frac{\beta}{T}\frac{\partial T}{\partial \mathbf{p}} + \boldsymbol{\delta}(\beta) - \boldsymbol{\delta}^{**}(0) \right) = \mathbf{0}. \tag{2.33}$$

which is consistent with Eq. (2.26). In fact, this simpler method can be used for any type of PLC for the zero time reference, as long as the time β is defined by an extremum in $y_j(t)$.

Notice that this type of sensitivity again reduces to Eq. (2.18) if one considers the special case of

$$f_1(\mathbf{y}(T(\mathbf{p});\mathbf{p},\mathbf{y}_0(\mathbf{p})),\mathbf{p}) = 0.$$

After differentiation, this leads to

$$\left.\frac{\partial f_1}{\partial \mathbf{y}}\right|_{\mathbf{y}(T(\mathbf{p}),\mathbf{p};\mathbf{y}_0(\mathbf{p})),\mathbf{p}} \left(\dot{\mathbf{y}}(T(\mathbf{p}),\mathbf{p};\mathbf{y}_0(\mathbf{p})) \left.\frac{\partial T}{\partial \mathbf{p}}\right|_{\mathbf{p}} + \mathbf{S}\left(T(\mathbf{p}),\mathbf{p};\left.\frac{\partial \mathbf{y}_0}{\partial \mathbf{p}}\right|_{\mathbf{p}}\right)\right) + \left.\frac{\partial f_1}{\partial \mathbf{p}}\right|_{\mathbf{y}(T(\mathbf{p}),\mathbf{p};\mathbf{y}_0(\mathbf{p})),\mathbf{p}} = \mathbf{0}.$$

Using Eq. (2.15) it is known that

$$\left.\frac{\partial \mathbf{y}_0}{\partial \mathbf{p}}\right|_{\mathbf{p}} = \dot{\mathbf{y}}(T(\mathbf{p});\mathbf{p},\mathbf{y}_0(\mathbf{p})) \left.\frac{\partial T}{\partial \mathbf{p}}\right|_{\mathbf{p}} + \mathbf{S}\left(T(\mathbf{p}),\mathbf{p};\left.\frac{\partial \mathbf{y}_0}{\partial \mathbf{p}}\right|_{\mathbf{p}}\right).$$

Since the partial derivatives of f_1 are T periodic, it is shown that this Equation reduces to the PLC used in Eq. (2.16), making this peak-to-peak sensitivity consistent with the computation of the period sensitivities earlier. The period sensitivities can therefore be considered a special case of the peak-to-peak sensitivities, namely the time difference of a peak of one state variable to the next peak in the same state variable.

Phase Sensitivities with Respect to Initial Conditions

This section first defines a new phase sensitivity and then provides a partial proof that links together two previous results in the literature ([23] and [56]). The phase γ is defined as the permanent phase shift induced by a perturbation in the state variables away from the limit cycle compared to an unperturbed trajectory. It is assumed this perturbation happens at time zero.

The phase sensitivities computed here are a measure of how this phase shift depends on the perturbation of the initial conditions. The main difference between this analysis and the previous sections is that trajectories off the limit cycle are considered.

Take two different sets of initial conditions: $\mathbf{y}_0$ on, and $\mathbf{y}_1$ off the limit cycle, which are thus independent from each other. By the definition of an orbitally stable limit cycle ([41], Theorem 11.1), $\gamma(\mathbf{p}, \mathbf{y}_0, \mathbf{y}_1)$ can be defined by the relation

$$\lim_{t\to+\infty} \mathbf{y}(t + \gamma(\mathbf{p}, \mathbf{y}_0, \mathbf{y}_1), \mathbf{p}; \mathbf{y}_1) - \mathbf{y}(t, \mathbf{p}; \mathbf{y}_0(\mathbf{p})) = \mathbf{0}. \tag{2.34}$$

Note that γ does not depend on t. Also note that neither the limits

$$\lim_{t\to+\infty} \mathbf{y}(t + \gamma(\mathbf{p}, \mathbf{y}_0, \mathbf{y}_1), \mathbf{p}; \mathbf{y}_1) \quad \text{or} \quad \lim_{t\to+\infty} \mathbf{y}(t, \mathbf{p}; \mathbf{y}_0(\mathbf{p}))$$

exist (except for initial conditions that are equilibrium points) because the system is a LCO. However, the limit of the difference does exist.

Then differentiation with respect to the initial conditions yields

$$\frac{\partial}{\partial \mathbf{y}_0} \left(\lim_{t\to+\infty} \mathbf{y}(t + \gamma(\mathbf{p}, \mathbf{y}_0, \mathbf{y}_1), \mathbf{p}; \mathbf{y}_1) - \mathbf{y}(t, \mathbf{p}; \mathbf{y}_0(\mathbf{p})) \right) = \mathbf{0}.$$

If under appropriate assumption, the order of differentiation and limit-taking can be reversed, then

$$\begin{aligned} &\lim_{t\to+\infty} \frac{\partial}{\partial \mathbf{y}_0} \left(\mathbf{y}(t + \gamma(\mathbf{p}, \mathbf{y}_0, \mathbf{y}_1), \mathbf{p}; \mathbf{y}_1) - \mathbf{y}(t, \mathbf{p}; \mathbf{y}_0(\mathbf{p})) \right) = \\ &\frac{\partial}{\partial \mathbf{y}_0} \left(\lim_{t\to+\infty} \mathbf{y}(t + \gamma(\mathbf{p}, \mathbf{y}_0, \mathbf{y}_1), \mathbf{p}; \mathbf{y}_1) - \mathbf{y}(t, \mathbf{p}; \mathbf{y}_0(\mathbf{p})) \right). \end{aligned} \tag{2.35}$$

The derivative of $\mathbf{y}$ with respect to the initial condition $\mathbf{y}_0$ is given by the solution $\mathbf{H}(t)$ of the Eq. (2.5).

Formal differentiation with respect to $\mathbf{y}_0$ then yields

$$\lim_{t\to+\infty} \dot{\mathbf{y}}(t + \gamma(\mathbf{p}, \mathbf{y}_0, \mathbf{y}_1), \mathbf{p}; \mathbf{y}_1) \left. \frac{\partial \gamma}{\partial \mathbf{y}_0} \right|_{\mathbf{p}, \mathbf{y}_0(\mathbf{p}), \mathbf{y}_1} - \mathbf{H}(t) = \mathbf{0}.$$

As discussed in Section 2.2.2, $\mathbf{H}(t) = \mathbf{H}_1(t) + \mathbf{H}_2(t)$ where $\mathbf{H}_1(t)$ is a rank one matrix equal to $\dot{\mathbf{y}}(t, \mathbf{p}; \mathbf{y}_0(\mathbf{p}))\mathbf{v}_1^{\mathrm{T}}(\mathbf{y}_0(\mathbf{p}))$ where $\mathbf{v}_1^{\mathrm{T}}(\mathbf{y}_0(\mathbf{p}))$ is a constant vector corresponding to the first

row of $\mathbf{V}(0,\mathbf{p};(\mathbf{y}_0(\mathbf{p})))$ in Eq. (2.10) and $\lim_{t\to+\infty}\mathbf{H}_2(t)=\mathbf{0}$. This implies

$$\lim_{t\to+\infty}\dot{\mathbf{y}}(t+\gamma(\mathbf{p},\mathbf{y}_0,\mathbf{y}_1),\mathbf{p};\mathbf{y}_1)\left.\frac{\partial\gamma}{\partial\mathbf{y}_0}\right|_{\mathbf{p},\mathbf{y}_0(\mathbf{p}),\mathbf{y}_1}-\dot{\mathbf{y}}(t,\mathbf{p};\mathbf{y}_0(\mathbf{p}))\mathbf{v}_1^{\mathrm{T}}(\mathbf{y}_0(\mathbf{p}))=\mathbf{0}. \tag{2.36}$$

In addition we know that

$$\lim_{t\to+\infty}\dot{\mathbf{y}}(t+\gamma(\mathbf{p},\mathbf{y}_0,\mathbf{y}_1),\mathbf{p};\mathbf{y}_1)-\dot{\mathbf{y}}(t,\mathbf{p};\mathbf{y}_0(\mathbf{p}))=\mathbf{0}. \tag{2.37}$$

by a simple extension of Eq. (2.34). If Eq. (2.37) is multiplied by $\left.\frac{\partial\gamma}{\partial\mathbf{y}_0}\right|_{\mathbf{p},\mathbf{y}_0(\mathbf{p}),\mathbf{y}_1}$ and subtracted off Eq. (2.36), we obtain

$$\begin{aligned}\lim_{t\to+\infty}\dot{\mathbf{y}}(t+\gamma(\mathbf{p},\mathbf{y}_0,\mathbf{y}_1),\mathbf{p};\mathbf{y}_1)\left.\frac{\partial\gamma}{\partial\mathbf{y}_0}\right|_{\mathbf{p},\mathbf{y}_0(\mathbf{p}),\mathbf{y}_1}-\dot{\mathbf{y}}(t,\mathbf{p};\mathbf{y}_0(\mathbf{p}))\mathbf{v}_1^{\mathrm{T}}(\mathbf{y}_0(\mathbf{p}))\\ -\dot{\mathbf{y}}(t+\gamma(\mathbf{p},\mathbf{y}_0,\mathbf{y}_1),\mathbf{p};\mathbf{y}_1)\left.\frac{\partial\gamma}{\partial\mathbf{y}_0}\right|_{\mathbf{p},\mathbf{y}_0(\mathbf{p}),\mathbf{y}_1}+\dot{\mathbf{y}}(t,\mathbf{p};\mathbf{y}_0(\mathbf{p}))\left.\frac{\partial\gamma}{\partial\mathbf{y}_0}\right|_{\mathbf{p},\mathbf{y}_0(\mathbf{p}),\mathbf{y}_1}=\mathbf{0}\end{aligned}$$

and eventually

$$\lim_{t\to+\infty}-\dot{\mathbf{y}}(t,\mathbf{p};\mathbf{y}_0(\mathbf{p}))\mathbf{v}_1^{\mathrm{T}}(\mathbf{y}_0(\mathbf{p}))+\dot{\mathbf{y}}(t,\mathbf{p};\mathbf{y}_0(\mathbf{p}))\left.\frac{\partial\gamma}{\partial\mathbf{y}_0}\right|_{\mathbf{p},\mathbf{y}_0(\mathbf{p}),\mathbf{y}_1}=\mathbf{0}.$$

Since it is known that $\lim_{t\to+\infty}\dot{\mathbf{y}}(t,\mathbf{p};\mathbf{y}_0(\mathbf{p}))$ does not exist, we can conlude that

$$\left.\frac{\partial\gamma}{\partial\mathbf{y}_0}\right|_{\mathbf{p},\mathbf{y}_0(\mathbf{p}),\mathbf{y}_1}=\mathbf{v}_1^{\mathrm{T}}(\mathbf{y}_0(\mathbf{p})) \tag{2.38}$$

Let $\mathbf{y}_1$ tend to $\mathbf{y}_0(\mathbf{p})$ to obtain the phase sensitivity with respect to a perturbation in the states at $\mathbf{y}_0(\mathbf{p})$. Physical meaning was previously attributed to the first right eigenvector of the Monodromy matrix $\mathbf{v}_1^{\mathrm{T}}(\mathbf{y}_0(\mathbf{p}))$ in the context of phase noise in electrical oscillators [53, 23]. It corresponds to the quantity -Q(0) described in Reference [56] as

$$Q_j(0)=-\frac{\partial\gamma}{\partial y_{0j}}=-\lim_{t\to\infty}\frac{h_{ij}(t)}{\dot{y}_i(t)}$$

where y_{0j} is the jth initial condition,$h_{ij}(t)$ is the element in the ith row and jth column of $\mathbf{H}(t)$, and thus $\lim_{t\to\infty}\frac{h_{ij}}{\dot{y}_i}=v_j^{\mathrm{T}}(0)$ from Eq. (2.10).

Interestingly the result in Eq. (2.38) does not depend on $\mathbf{y}_1$ at all. This is astonishing at

first glance, however an intuitive explanation serves well to illustrate this fact. If the time span γ is defined by a 'start time' and an 'end time', then $\mathbf{y}_0(\mathbf{p})$ and $\mathbf{y}_1$, respectively, define those times. It is now easily seen that the change of γ as a result of a change in 'start time' is independent of the end time. A similar argument explains the sign difference between the result by Kramer et. al.[56] and in this work - it is a matter of which time reference is used to define the phase which sign the final result carries.

2.3 Sensitivity Analysis for Non-Limit-Cycle Oscillators

We define a NLCO as a dynamic system with periodic orbits in which the rank of the matrix (2.40) is equal to one. This implies that the monodromy matrices $\mathbf{M}$ have exactly n_y eigenvalues equal to one (see Corollary 3).

2.3.1 Sensitivity Analysis

For NLCOs, the initialization of the parametric sensitivities is straightforward. The parametric sensitivities at time $t = 0$ are zero, since the initial conditions do not depend on the parameter values. As a consequence, the sensitivities $\mathbf{S}$ can easily be determined by integration of Eq. (2.11) with $\mathbf{S}_0 = \mathbf{0}$. The full sensitivities can be decomposed as in the case of a LCO [63]:

$$\mathbf{S}(t) = -\frac{t}{T}\dot{\mathbf{y}}(t)\frac{\partial T}{\partial \mathbf{p}} + \mathbf{Z}(t).$$

2.3.2 The Boundary Value Problem

Since for NLCOs the initial conditions determine the periodic behavior together with the parameters, and there is no asymptotic behavior, the BVP solution is reduced to a single unknown. The period $T(\mathbf{p}, \mathbf{y}_0)$ of the system is not known *a priori*, but is easily determined, for example by the solution of a BVP for $T(\mathbf{p}, \mathbf{y}_0)$ subject to

$$\mathbf{y}(T(\mathbf{p}, \mathbf{y}_0), \mathbf{p}, \mathbf{y}_0) - \mathbf{y}_0 = \mathbf{0}. \tag{2.39}$$

When the BVP is differentiated with respect to the parameters, a matrix equation similar to Eq. (2.18) is obtained, where the matrix

$$\left[\begin{array}{cc} (\mathbf{M} - \mathbf{I}) & \dot{\mathbf{y}}(T, \mathbf{p}, \mathbf{y}_0) \end{array} \right] \tag{2.40}$$

has rank one, due to two possible scenarios. The rank of $(\mathbf{M}-\mathbf{I})$ can either be zero or one, depending on the nature of the dynamic system. In either case, (2.40) has rank one and n_y PLCs are needed to pose a BVP of full rank. A natural choice is to set all n_y initial conditions.

Period and Amplitude Sensitivities

The derivatives of the boundary condition in Eq. (2.39) with respect to parameters $\mathbf{p}$ and initial conditions $\mathbf{y}_0$ yield:

$$\dot{\mathbf{y}}(0,\mathbf{p},\mathbf{y}_0)\left.\frac{\partial T}{\partial \mathbf{p}}\right|_{\mathbf{p},\mathbf{y}_0} = -\mathbf{S}(T,\mathbf{p};\mathbf{0}) \tag{2.41}$$

and

$$\dot{\mathbf{y}}(0,\mathbf{p},\mathbf{y}_0)\left.\frac{\partial T}{\partial \mathbf{y}_0}\right|_{\mathbf{p},\mathbf{y}_0} = (\mathbf{I}-\mathbf{M}). \tag{2.42}$$

Eq. (2.41) can be solved for $\left.\frac{\partial T}{\partial \mathbf{p}}\right|_{\mathbf{p},\mathbf{y}_0}$. The rank of $(\mathbf{M}-\mathbf{I})$ determines the solution of Eq. (2.42). It is clear that in the case of $(\mathbf{I}-\mathbf{M})$ having rank zero, the initial conditions have no influence on the period of the oscillation. This is the case, for example, in the linear harmonic oscillator. The example presented in Section 2.6.3 is nonlinear and has a non-diagonalizable matrix $(\mathbf{I}-\mathbf{M})$ of rank one, still with all zero eigenvalues. In this case, because Eq. (2.40) has rank one, $(\mathbf{M}-\mathbf{I}) = \dot{\mathbf{y}}(T)\boldsymbol{\psi}$, where $\boldsymbol{\psi}$ is a row vector of length n_y. It follows that period sensitivities with respect to the initial conditions can be calculated and $\left.\frac{\partial T}{\partial \mathbf{y}_0}\right|_{\mathbf{p},\mathbf{y}_0} \equiv -\boldsymbol{\psi}$.

The amplitude sensitivities can be calculated in the same manner as described for LCOs.

Relative Phase Sensitivities

It is known that

$$\mathbf{S}(0,\mathbf{p},\mathbf{y}_0) = \mathbf{Z}(0,\mathbf{p},\mathbf{y}_0) = \mathbf{W}(0,\mathbf{p},\mathbf{y}_0) + \dot{\mathbf{y}}(0,\mathbf{p})\boldsymbol{\delta}(0,\mathbf{p},\mathbf{y}_0) = \mathbf{0}$$

and because, by construction the columns of $\mathbf{W}(0,\mathbf{p},\mathbf{y}_0)$ are orthogonal to $\dot{\mathbf{y}}(0,\mathbf{p})$,

$$\mathbf{W}(0,\mathbf{p},\mathbf{y}_0) = \mathbf{0}$$

and

$$\boldsymbol{\delta}(0, \mathbf{p}, \mathbf{y}_0) = \mathbf{0}.$$

However, neither $\mathbf{W}(t)$ nor $\boldsymbol{\delta}(t)$ are identically zero, as the example in Figure 2-4 shows. It follows that for any given point on the periodic orbit, the matrix $\mathbf{W}$ is not uniquely defined by the state variables, because the choice of PLC in the form of all initial conditions is arbitrary and any point on the cycle could have been chosen.

A relative phase sensitivity analysis can still be performed, and two examples will be shown here. To avoid repetition, the general case is discussed later in Section 2.4.3. Let the "relative phase" be defined here as a time difference β between the time zero, as defined by the set of initial conditions $\mathbf{y}_0$, and one differentiable PLC that locks one degree of freedom, e.g.,

$$y_i(t = \beta, \mathbf{p}, \mathbf{y}_0) = \psi. \tag{2.43}$$

This PLC can be differentiated with respect to the parameters, resulting, for this example, in

$$-\frac{\beta}{T}\dot{y}_i(\beta)\frac{\partial T}{\partial \mathbf{p}} + \mathbf{w}_i(\beta) + \dot{y}_i(\beta)\boldsymbol{\delta}(\beta) + \dot{y}_i(\beta)\frac{\partial \beta}{\partial \mathbf{p}} = \mathbf{0},$$

where $\mathbf{w}_i(\beta)$ is the i-th row of the matrix $\mathbf{W}(t)$. If $\dot{y}_i(\beta) \neq 0$, this equation can be solved to yield

$$\frac{\partial \beta}{\partial \mathbf{p}} = \frac{\beta}{T}\frac{\partial T}{\partial \mathbf{p}} - \frac{\mathbf{w}_i(\beta)}{\dot{y}_i(\beta)} - \boldsymbol{\delta}(\beta).$$

Again, it is important to notice that Eq. (2.43) is not a valid PLC at a point where $\dot{y}_i(\beta) = 0$, as discussed for the case of LCOs in Section 2.2.7.

Similarly, the method for peak-to-peak sensitivity calculation in Section 2.2.7 only needs to be modified slightly to be applicable to NLCOs. Instead of a first PLC, the time reference is defined by the inital condition, but the relative phase β is still defined by a PLC that locks the phase at a stationary point of a state variable y_j (and as discussed in Section 2.2.7, a point where $\ddot{y}_j(\beta(\mathbf{p}), \mathbf{p}, \mathbf{y}_0) = 0$ cannot be analyzed in this manner),

$$\dot{y}_j(\beta(\mathbf{p}), \mathbf{p}, \mathbf{y}_0) = 0. \tag{2.44}$$

Again, this PLC is differentiated with respect to $\mathbf{p}$ to yield

$$\left.\frac{\partial f_j}{\partial \mathbf{y}}\right|_{\mathbf{y}(\beta(\mathbf{p}),\mathbf{p};\mathbf{y}_0),\mathbf{p}} \left(\dot{\mathbf{y}}(\beta(\mathbf{p}),\mathbf{p};\mathbf{y}_0) \left.\frac{\partial \beta}{\partial \mathbf{p}}\right|_{\mathbf{p}} + \mathbf{S}\left(\beta(\mathbf{p}),\mathbf{p};\mathbf{0}\right) \right) + \left.\frac{\partial f_j}{\partial \mathbf{p}}\right|_{\mathbf{y}(\beta(\mathbf{p}),\mathbf{p};\mathbf{y}_0),\mathbf{p}} = \mathbf{0}. \quad (2.45)$$

which can be solved directly for $\left.\frac{\partial \beta}{\partial \mathbf{p}}\right|_{\mathbf{p}}$. Relative phases between two events defining a time β and a time α, respectively, on the periodic orbit can now be calculated simply by performing separate analyses with reference to the common time zero defined by the initial conditions, and then taking the difference, i.e., $\frac{\partial(\beta-\alpha)}{\partial \mathbf{p}} = \frac{\partial \beta}{\partial \mathbf{p}} - \frac{\partial \alpha}{\partial \mathbf{p}}$.

2.4 General Formulation for the Sensitivity Analysis of All Types of Oscillators

2.4.1 Intermediate-Type Oscillators

An intermediate-type oscillator in the context of this manuscript is a dynamic system with periodic orbits that is not described by the definitions for either the LCO or the NLCO. The monodromy matrix $\mathbf{M}$ can have k eigenvalues equal to one where $1 < k \leq n_y$. Then, the matrix (2.40) has rank m, where $1 < m \leq n_y$, and $(n_y + 1 - m)$ PLCs are needed.

Theorem 3. *Let n_u equal the number of linearly independent eigenvectors of $\mathbf{M}$ corresponding to eigenvalues equal to unity and let d be the degeneracy of the Jordan block corresponding to the eigenvector $\dot{\mathbf{y}}(T)$. Then the rank m of the matrix*

$$\begin{bmatrix} (\mathbf{M} - \mathbf{I}) & \dot{\mathbf{y}}(T) \end{bmatrix}$$

is given by

$$m = \begin{cases} 1 + n_y - n_u & \text{if } d = 0 \\ n_y - n_u & \text{otherwise.} \end{cases}$$

Proof. Let $\mathbf{T}$ be a matrix with $\dot{\mathbf{y}}(T)$ as its first column that takes $\mathbf{M}$ to its Jordan form. Applying the row and column operations

$$\mathbf{T}^{-1} \begin{bmatrix} (\mathbf{M} - \mathbf{I}) & \dot{\mathbf{y}}(T) \end{bmatrix} \begin{bmatrix} \mathbf{T} \\ 1 \end{bmatrix}$$

yields

$$\begin{bmatrix} \mathbf{N}_1 & & & & & \mathbf{e}_1 \\ & \mathbf{N}_2 & & & & \mathbf{0} \\ & & \ddots & & & \vdots \\ & & & \mathbf{N}_{n_u} & & \mathbf{0} \\ & & & & \mathbf{J} & \mathbf{0} \end{bmatrix}$$

where $\mathbf{N}_1, \ldots, \mathbf{N}_{n_u}$ are nilpotent Jordan blocks, $\mathbf{J}$ is a Jordan matrix corresponding to all the eigenvalues not equal to unity and $\mathbf{e}_1$ is the first unit vector of appropriate dimension. If $d = 0$ this matrix becomes

$$\begin{bmatrix} 0 & & & & & 1 \\ & \mathbf{N}_2 & & & & \mathbf{0} \\ & & \ddots & & & \vdots \\ & & & \mathbf{N}_{n_u} & & \mathbf{0} \\ & & & & \mathbf{J} & \mathbf{0} \end{bmatrix}$$

and it is clear that each nilpotent Jordan block reduces the rank by one, but the final column also contributes one pivot. If $d > 0$ then each nilpotent Jordan block reduces the rank by one and the final column does not contribute a pivot. □

Corollary 2. *For an oscillator $m = n_y$ iff $n_u = 1$ and $d = 0$ (LCO).*

Proof. If $n_u = 1$ and $d = 0$ (LCO) then $m = n_y$. If $m = n_y$ then

1. if $d = 0$ then $n_u = 1$,
2. if $d > 0$ then $n_u = 0$, contradicting $d > 0$.

□

Corollary 3. *If $m = 1$ then $\mathbf{M}$ has n_y eigenvalues equal to unity (NLCO).*

Proof. If $m = 1$ then $d \leq 1$ because otherwise the first nilpotent block contributes a second pivot. If $d = 0$ then $n_u = n_y$. If $d = 1$ then $n_u = n_y - 1$ and the additional eigenvalue equals unity. □

2.4.2 General Formulation of the BVP

The general BVP formulation is to solve the following equations for $T(\mathbf{p},\mathbf{q})$ and $\mathbf{y}_0(\mathbf{p},\mathbf{q})$

$$\mathbf{y}(T(\mathbf{p},\mathbf{q}),\mathbf{p};\mathbf{y}_0(\mathbf{p},\mathbf{q})) = \mathbf{y}_0(\mathbf{p},\mathbf{q}) \tag{2.46}$$

$$\mathbf{g}(\mathbf{y}_0(\mathbf{p},\mathbf{q}),\mathbf{p},\mathbf{q}) = \mathbf{0} \tag{2.47}$$

where $\mathbf{y}(T(\mathbf{p},\mathbf{q}),\mathbf{p};\mathbf{y}_0(\mathbf{p},\mathbf{q}))$ is given by the solution of Eq. (2.3) from the initial condition

$$\mathbf{y}(0,\mathbf{p};\mathbf{y}_0(\mathbf{p},\mathbf{q})) = \mathbf{y}_0(\mathbf{p},\mathbf{q}).$$

A distinction is made between the parameters $\mathbf{p}$ that appear in the right hand sides of the ODEs and the additional parameters $\mathbf{q}$ introduced by the PLC equations (2.47). In general the choice of the number and interpretation of the parameters $\mathbf{q}$ is arbitrary when formulating the PLC equations.

The number of PLC equations (2.47) introduced is dictated by the rank defficiency of the condition for a closed orbit (2.46). In addition, the Jacobian of the full system of Eqs. (2.46–2.47) must be full rank.

Period Sensitivities

Eqs. (2.46–2.47) can be formally differentiated with respect to $\mathbf{p}$ and $\mathbf{q}$, yielding period and initial condition sensitivities with respect to both.

$$\begin{gathered}
\dot{\mathbf{y}}(T,\mathbf{p};\mathbf{y}_0(\mathbf{p},\mathbf{q}))\left.\frac{\partial T}{\partial \mathbf{p}}\right|_{\mathbf{p},\mathbf{q}} + \left.\frac{\partial \mathbf{y}}{\partial \mathbf{y}_0}\right|_{T,\mathbf{y}_0,\mathbf{p},\mathbf{q}}\left.\frac{\partial \mathbf{y}_0}{\partial \mathbf{p}}\right|_{\mathbf{p},\mathbf{q}} \\
+\left(\left.\frac{\partial \mathbf{y}}{\partial \mathbf{p}}\right|_{T,\mathbf{y}_0,\mathbf{p},\mathbf{q}}\right)_{\mathbf{y}(0)=const.} = \left.\frac{\partial \mathbf{y}_0}{\partial \mathbf{p}}\right|_{\mathbf{p},\mathbf{q}} \\
\left.\frac{\partial \mathbf{g}}{\partial \mathbf{y}_0}\right|_{\mathbf{y}_0,\mathbf{p},\mathbf{q}}\left.\frac{\partial \mathbf{y}_0}{\partial \mathbf{p}}\right|_{\mathbf{p},\mathbf{q}} + \left.\frac{\partial \mathbf{g}}{\partial \mathbf{p}}\right|_{\mathbf{y}_0,\mathbf{p},\mathbf{q}} = \mathbf{0}
\end{gathered}$$

$$\dot{\mathbf{y}}(T,\mathbf{p};\mathbf{y}_0(\mathbf{p},\mathbf{q}))\left.\frac{\partial T}{\partial \mathbf{q}}\right|_{\mathbf{p},\mathbf{q}}+\left.\frac{\partial \mathbf{y}}{\partial \mathbf{y}_0}\right|_{T,\mathbf{y}_0,\mathbf{p},\mathbf{q}}\left.\frac{\partial \mathbf{y}_0}{\partial \mathbf{q}}\right|_{\mathbf{p},\mathbf{q}}=\left.\frac{\partial \mathbf{y}_0}{\partial \mathbf{q}}\right|_{\mathbf{p},\mathbf{q}}$$
$$\left.\frac{\partial \mathbf{g}}{\partial \mathbf{y}_0}\right|_{\mathbf{y}_0,\mathbf{p},\mathbf{q}}\left.\frac{\partial \mathbf{y}_0}{\partial \mathbf{q}}\right|_{\mathbf{p},\mathbf{q}}+\left.\frac{\partial \mathbf{g}}{\partial \mathbf{q}}\right|_{\mathbf{y}_0,\mathbf{p},\mathbf{q}}=\mathbf{0}$$

Both systems can then be solved for the unknowns $(\left.\frac{\partial \mathbf{y}_0}{\partial \mathbf{p}}\right|_{\mathbf{p},\mathbf{q}}, \left.\frac{\partial T}{\partial \mathbf{p}}\right|_{\mathbf{p},\mathbf{q}})$ and $(\left.\frac{\partial \mathbf{y}_0}{\partial \mathbf{q}}\right|_{\mathbf{p},\mathbf{q}}, \left.\frac{\partial T}{\partial \mathbf{q}}\right|_{\mathbf{p},\mathbf{q}})$, respectively.

Amplitude Sensitivities

When the sensitivity equations are integrated from the initial conditions $\left.\frac{\partial \mathbf{y}_0}{\partial \mathbf{p}}\right|_{\mathbf{p},\mathbf{q}}$ and $\left.\frac{\partial \mathbf{y}_0}{\partial \mathbf{q}}\right|_{\mathbf{p},\mathbf{q}}$, amplitude sensitivities with respect to both $\mathbf{p}$ and $\mathbf{q}$ can be computed as described in Section 2.2.6.

2.4.3 Relative Phase Sensitivities

Any type of phase β in reference to the time zero, which is implicitly defined by Eq. (2.47), can be analyzed if a valid, differentiable PLC is formulated. In general, a valid PLC is one that defines an isolated point which is guaranteed to exist for any parameter value in a neighborhood of the current value $\mathbf{p}$. Let this PLC be

$$h(\mathbf{y}(\beta(\mathbf{p},\mathbf{q}),\mathbf{p};\mathbf{y}_0(\mathbf{p},\mathbf{q})),\mathbf{p},\mathbf{y}_0(\mathbf{p},\mathbf{q}))=0 \tag{2.48}$$

which can be differentiated with respect to the parameters to yield

$$\left.\frac{\partial h}{\partial \mathbf{y}}\right|_{\mathbf{y}(\beta(\mathbf{p},\mathbf{q}),\mathbf{p};\mathbf{y}_0(\mathbf{p},\mathbf{q})),\mathbf{p},\mathbf{y}_0(\mathbf{p},\mathbf{q})}\left(\dot{\mathbf{y}}(\beta,\mathbf{p};\mathbf{y}_0(\mathbf{p},\mathbf{q}))\left.\frac{\partial \beta}{\partial \mathbf{p}}\right|_{\mathbf{p},\mathbf{q}}+\left.\frac{\partial \mathbf{y}}{\partial \mathbf{y}_0}\right|_{\beta,\mathbf{p},\mathbf{q},\mathbf{y}_0}\left.\frac{\partial \mathbf{y}_0}{\partial \mathbf{p}}\right|_{\mathbf{p},\mathbf{q}}\right.$$
$$\left.+\left(\left.\frac{\partial \mathbf{y}}{\partial \mathbf{p}}\right|_{\beta,\mathbf{p},\mathbf{q},\mathbf{y}_0}\right)_{\mathbf{y}_0=const.}\right)+\left.\frac{\partial h}{\partial \mathbf{p}}\right|_{\mathbf{y}(\beta(\mathbf{p},\mathbf{q}),\mathbf{p};\mathbf{y}_0(\mathbf{p},\mathbf{q})),\mathbf{p},\mathbf{y}_0(\mathbf{p},\mathbf{q})}$$
$$+\left.\frac{\partial h}{\partial \mathbf{y}_0}\right|_{\mathbf{y}(\beta(\mathbf{p},\mathbf{q}),\mathbf{p};\mathbf{y}_0(\mathbf{p},\mathbf{q})),\mathbf{p},\mathbf{y}_0(\mathbf{p},\mathbf{q})}\left.\frac{\partial \mathbf{y}_0}{\partial \mathbf{p}}\right|_{\mathbf{p},\mathbf{q}}=\mathbf{0}.$$

All parts of this equation are known except the relative phase sensitivities, $\left.\frac{\partial \beta}{\partial \mathbf{p}}\right|_{\mathbf{p},\mathbf{q}}$, which can now be computed easily and exactly. Similarly, the differentation of Eq. (2.48) can be

performed with respect to the PLC parameters $\mathbf{q}$ to yield

$$\left.\frac{\partial h}{\partial \mathbf{y}}\right|_{\mathbf{y}(\beta(\mathbf{p},\mathbf{q}),\mathbf{p};\mathbf{y}_0(\mathbf{p},\mathbf{q})),\mathbf{p},\mathbf{y}_0(\mathbf{p},\mathbf{q})} \left(\dot{\mathbf{y}}(\beta,\mathbf{p};\mathbf{y}_0(\mathbf{p},\mathbf{q})) \left.\frac{\partial \beta}{\partial \mathbf{q}}\right|_{\mathbf{p},\mathbf{q}} + \left.\frac{\partial \mathbf{y}}{\partial \mathbf{y}_0}\right|_{\beta,\mathbf{p},\mathbf{q},\mathbf{y}_0} \left.\frac{\partial \mathbf{y}_0}{\partial \mathbf{q}}\right|_{\mathbf{p},\mathbf{q}} \right)$$
$$+ \left.\frac{\partial h}{\partial \mathbf{q}}\right|_{\mathbf{y}(\beta(\mathbf{p},\mathbf{q}),\mathbf{p};\mathbf{y}_0(\mathbf{p},\mathbf{q})),\mathbf{p},\mathbf{y}_0(\mathbf{p},\mathbf{q})} + \left.\frac{\partial h}{\partial \mathbf{y}_0}\right|_{\mathbf{y}(\beta(\mathbf{p},\mathbf{q}),\mathbf{p};\mathbf{y}_0(\mathbf{p},\mathbf{q})),\mathbf{p},\mathbf{y}_0(\mathbf{p},\mathbf{q})} \left.\frac{\partial \mathbf{y}_0}{\partial \mathbf{q}}\right|_{\mathbf{p},\mathbf{q}} = \mathbf{0}.$$

2.5 Numerical Methods

The computationally most demanding part of performing the sensitivity analysis as described in this article is the solution of the BVP. Therefore, an efficient technique was developed to reduce the computational effort involved in this step.

2.5.1 Transformation of the BVP

In order to simplify the BVP shown in Eqs. (2.1) and (2.2), the problem was transformed to yield:

$$\hat{\mathbf{y}}(1,\mathbf{p};\hat{\mathbf{y}}_0) - \hat{\mathbf{y}}_0 = \mathbf{0} \tag{2.49}$$

$$f_i(\hat{\mathbf{y}}(0,\mathbf{p};\hat{\mathbf{y}}_0),\mathbf{p}) = 0 \tag{2.50}$$

where

$$\frac{d}{d\hat{t}}\hat{\mathbf{y}}(\hat{t},\mathbf{p};\hat{\mathbf{y}}_0) = T \cdot \mathbf{f}(\hat{\mathbf{y}}(\hat{t},\mathbf{p};\hat{\mathbf{y}}_0),\mathbf{p}),$$

thus allowing for integration to time 1 for all iterations of the BVP solution. For simplicity, the transformed state variables $\hat{\mathbf{y}}$ are taken to be $\mathbf{y}$, and the transformed time $\hat{t}$ will be called t for the remainder of this discussion.

2.5.2 Solution of the BVP

For the efficient solution of large-scale BVPs, an inexact Newton solver [81] was coupled with the stiff ODE solver CVODES [43]. In order to provide derivative information to the inexact Newton solver, directional sensitivities with respect to the variables of the BVP, $\mathbf{x} \equiv (\mathbf{y}_0, T)$, were integrated along with the original ODE system using the staggered-corrector method [28]. This technique avoids the calculation of the full matrix of sensitivities, thus reducing the total number of differential equations during integration by $n_y \times (n_y - 1)$ [78]. The

directional sensitivities $\mathbf{r} \equiv \mathbf{P}\mathbf{d}$ were integrated from time zero to time one, according to

$$\dot{\mathbf{y}} = T\mathbf{f}(\mathbf{y}, \mathbf{p})$$

$$\dot{\mathbf{r}} = T\frac{\partial \mathbf{f}}{\partial \mathbf{y}}\mathbf{r} + \mathbf{f}d_{n_y+1}$$

where $\mathbf{P}$ are the sensitivities of the state variables $\mathbf{y}$ with respect to the variables of the BVP, $\mathbf{x}$, and d_{1+n_y} is the T-coordinate of the current step of the Newton iterative solver. The initial conditions for this system are $\mathbf{r}_0 = \mathbf{P}_0\mathbf{d}$ with

$$\mathbf{P}_0 = \left[\begin{array}{cc} \mathbf{I}_{n_y} & \mathbf{0}_{1,n_y} \end{array} \right].$$

The Jacobian matrix of the BVP is the matrix obtained by partial differentiation of Eqns. (2.49-2.50) with respect to $\mathbf{x}$. However, it is not necessary to compute the entire matrix, because only the Jacobian-vector product of the BVP is required by the inexact Newton solver, which can be calculated directly from the chain rule and the directional sensitivities obtained after integration. The Jacobian-vector product is then

$$\mathbf{J}\mathbf{d} = \left[\begin{array}{c} \mathbf{r} - \mathbf{d}_{(1-n_y)} \\ \frac{\partial f_i}{\partial \mathbf{y}}\mathbf{d}_{(1-n_y)} \end{array} \right],$$

where $\mathbf{d}_{(1-n_y)}$ is the column vector containing the current step in the $\mathbf{y}_0$-coordinates.

Integration was performed in CVODES [43] with absolute and relative tolerances of 10^{-10} and 10^{-8}, respectively. The BVP was solved to a relative tolerance of 10^{-6} and absolute tolerance of 10^{-8}. No preconditioning was used.

Table 2.6 shows the effective system size for integration in comparison to the full sensitivity system. The method affords especially large savings of CPU time when the system has a large number of state variables.

It should be mentioned that for small systems, or for such LCOs that have a known short transient time (i.e., that approach the periodic orbit rapidly from any initial condition), it can be effective to solve the BVP simply by integrating over a sufficiently large time span, and using an event detection algorithm to assert sufficient convergence and to detect the period of oscillation. For the case of the NLCO, the solution of the BVP has only one independent variable, T, making this method preferable. It was used for the very small

example systems discussed in Sections 2.6.1 and 2.6.3. However, it is usually not known if a limit-cycle system has short transient times, and as system size increases, this method becomes inefficient.

2.5.3 Solution of the Sensitivity Equations

Once the BVP was solved, $\mathbf{M}$ and $\mathbf{S}(T, \mathbf{p}; \mathbf{0})$ were calculated from a sensitivity analysis over one period using the staggered-corrector sensitivity analysis functionality of CVODES [43] with full error control. The absolute and relative tolerances were set to 10^{-10} and 10^{-8}, respectively. The matrix operations to solve Eq. (2.17) were performed in MATLAB.

2.6 Applications and Comparison to Existing Methods

2.6.1 The Goodwin Oscillator - a LCO

The Goodwin oscillator is a small system comprising 3 states and 6 parameters. It has been used in the biological literature to model a very basic circadian clock [90]. It is governed by the set of nonlinear ODEs in Eq. (2.51), which can be interpreted as a mRNA concentration X, a Clock protein concentration Y and a transcription inhibition factor Z. Since the processes of transcription and translation are not chemical reactions, the system does not obey mass conservation, a fact that is closely related to the limit-cycle properties of the oscillator.

$$\begin{aligned} \frac{dX}{dt} &= p_1 \frac{1}{1+Z^9} - p_4 X \\ \frac{dY}{dt} &= p_2 X - p_5 Y \\ \frac{dZ}{dt} &= p_3 Y - p_6 Z \end{aligned} \tag{2.51}$$

The parameters used throughout this example are $\mathbf{p} = (2.6574, 1.5749, 1.2985, 0.1357,$ 0.1362, 0.1360). The BVP formulation described in Section 2.2.1 using the PLC $\dot{Z}(t=0) = 0$ was solved yielding the results given in Table 2.1.

Sensitivity Trajectories The trajectories for some of the state sensitivities as well as for $\mathbf{Z}(t)$, $\mathbf{W}(t)$ and $\boldsymbol{\delta}(t)$ are shown in Figure 2-2. As discussed earlier in this manuscript,

Table 2.1: Results of the sensitivity analysis for the Goodwin Oscillator. The resulting initial conditions were $X(0) = 0.0315$, $Y(0) = 0.1946$ and $Z(0) = 1.8582$, with a period of T=27.9613.

parameter	p_1	p_2	p_3	p_4	p_5	p_6
$\frac{\partial T}{\partial \mathbf{p}}$	0.0063	0.0106	0.0129	-68.6251	-68.7215	-68.6746
$\frac{\partial X_0}{\partial \mathbf{p}}$	0.0012	-0.0179	-0.0218	0.0489	0.1708	0.1718
$\frac{\partial Y_0}{\partial \mathbf{p}}$	0.0073	0.0123	-0.1349	-0.1438	-0.1412	1.2885
$\frac{\partial Z_0}{\partial \mathbf{p}}$	0.0696	0.1175	0.1425	-1.3735	-1.3488	-1.3608

it is difficult to compare sensitivity trajectories obtained by different methods. First, if the initial conditions $\mathbf{S}_0$ in Eq. (2.12) are set to zero, a non-decaying error is introduced. Second, since the computation of exact sensitivity trajectories relies on the use of a PLC, and since multiple PLCs are possible for any given point on the cycle, one cannot compare a solution obtained using a given PLC to any other solution using zero initial conditions due to the lack of a common reference point. If one attemped to calculate the bounded (purely periodic) part of the solution only, as has been done previously [56, 64], both of these sources of discrepancy remain. While one reference [99] mentions the need to define a time reference in order to obtain a unique sensitivity function, the influence of the initial condition – in particular as a function of the PLC – was neglected, and the influence of the PLC was assumed to be time invariant.

The results presented here emphasize the importance of a time reference for the calculation of sensitivity information, and introduce the notion of a PLC used for that purpose, thus allowing to isolate the shape and location sensitivities contained in $\mathbf{W}$, that are independent of the PLC.

Amplitude Sensitivities Previous sensitivity methods often relied on extracting partial sensitivity information for oscillating systems. What facilitated the computation of sensitivities at the extrema of a state variable y_i (as needed for the computation of the amplitude sensitivities) is the fact that at those times, all contributions but those of $\mathbf{w}_i(t_{extremum})$ drop because $\dot{y}_i(t_{extremum})$ is zero. Therefore these quantities could previously be estimated by waiting for the transient of the first term of Eq. (2.12) to decay, even in the absence of correct initial conditions for the sensitivities $\mathbf{S}$ [89, 56]. A graphical comparison to the method

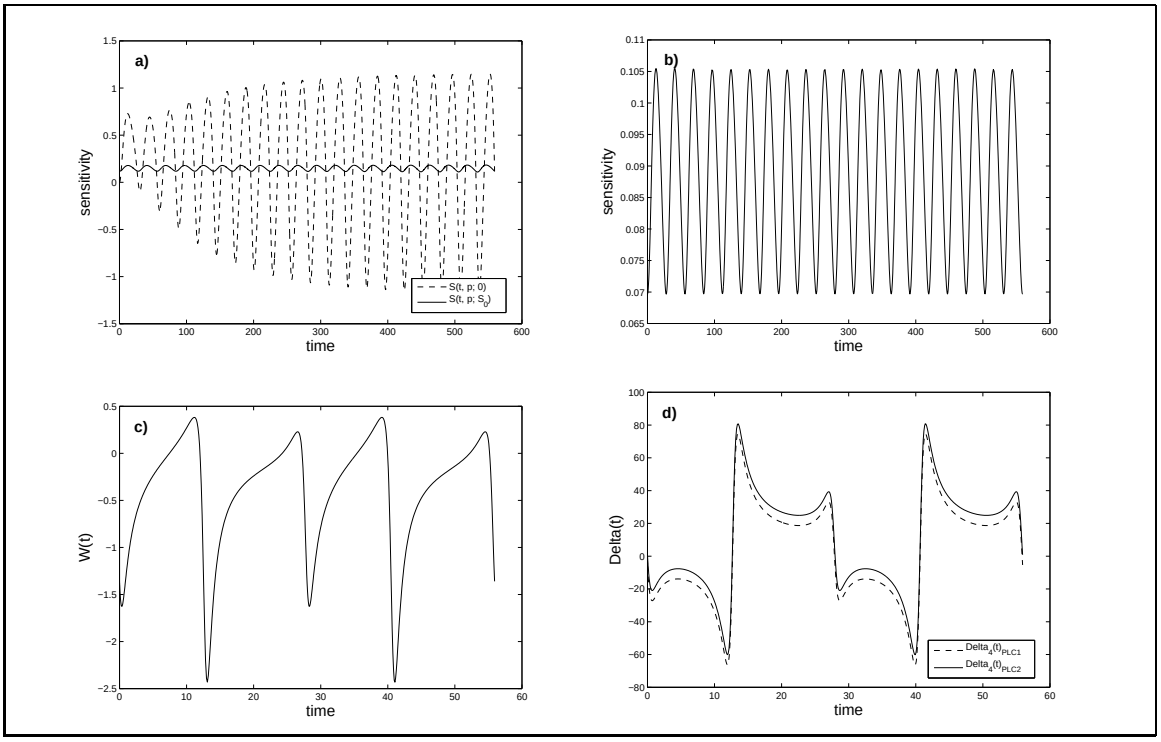

Figure 2-2: Sensitivity trajectories for the Goodwin Oscillator, all with respect to parameter p_4: a) full sensitivity of Z, as a function of initialization; $\mathbf{S}(t, \mathbf{p}; \mathbf{S}_0)$ (solid) vs. $\mathbf{S}(t, \mathbf{p}; \mathbf{0})$ (dashed) (both are unbounded, as verified over a longer integration period), b) period independent, periodic part $\mathbf{Z}(t, \mathbf{p}; \mathbf{S}_0)$, c) period and phase independent part $\mathbf{W}(t, \mathbf{p})$, d) relative phase sensitivity with respect to p_4, $\delta_{k4}(t, \mathbf{p})$, for two different PLCs (PLC$_1$: $\dot{Z}(0) = 0$, PLC$_2$: $Y(0) = 0.19457$).

proposed in this work is shown in Figure 2-3. The iterative method can take many periods of oscillation to converge to a close approximation of the exact value, which is obtained immediately using the boundary value method.

2.6.2 Relative Phase Sensitivities in the *Drosophila* Circadian Clock

A method for the calculation of peak-to-peak sensitivities was suggested by Gunawan et al. [37] based largely on previous work by Kramer *et al.* [56]. A very simple model of the *Drosophila* circadian clock [100] was analyzed. The method described in Section 2.2.7 of this work was applied to the same model using the same parameter values to allow for direct comparison. Numerical results are presented in Table 2.2. The peak-to-peak sensitivities as computed in this work agree very well with the finite difference approximation, with the maximum deviation being 0.06%. In comparison, previous results appear to compute the "period stretch" sensitivity of the peak-to-peak distance as result of the period sensitivity,

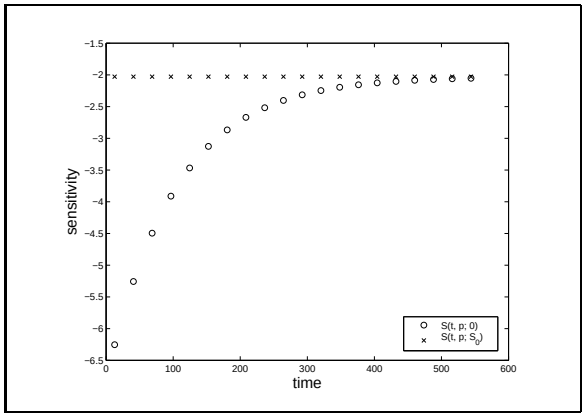

Figure 2-3: Results for the sensitivity of the extrema of Z with respect to parameter p_4 computed as described here (x) and as described in Reference [56] (o).

$\frac{\beta}{T}\frac{\partial T}{\partial \mathbf{p}}$, judged by the close match of the respective numerical results (maximum deviation 1.7%).

2.6.3 Application to the Lotka-Volterra Model - a Small NLCO

An example of a non-limit-cycle oscillator is the Lotka-Volterra Oscillator [63], which can be associated with a chemical reaction scheme such as

$$A + X \xrightarrow{p_1'} 2X$$
$$X + Y \xrightarrow{p_2} 2Y$$
$$B + Y \xrightarrow{p_3'} E,$$

where the concentrations A and B are constant and can be lumped with the rate parameters so that $p_1 = Ap_1'$ and $p_3 = Bp_3'$. Then the system can be written as:

$$\begin{aligned} \frac{dX}{dt} &= p_1 X - p_2 XY \\ \frac{dY}{dt} &= p_2 XY - p_3 Y. \end{aligned} \tag{2.52}$$

As the oscillator is based on a set of chemical reactions, it obeys mass conservation and it is clear that the initial conditions of X and Y will have an influence on the amplitude of the

Table 2.2: Results of the peak-to-peak sensitivity analysis for the *Drosophila* circadian oscillator [100]. The initial conditions of the state variables M and P at the maximum of M were $M(0) = 2.6444$ and $P(0) = 0.36244$, with a period of T=24.204. $\frac{\partial \beta}{\partial \mathbf{p}}$ = peak-to-peak sensitivities, FD = finite difference approximation of $\frac{\partial \beta}{\partial \mathbf{p}}$ (with a finite difference of $\epsilon = 0.01$), $\frac{\beta}{T}\frac{\partial T}{\partial \mathbf{p}}$ = overall phase shift induced by period sensitivity, $\frac{\partial \hat{\Phi}}{\partial \mathbf{p}}$ = peak-to-peak phase sensitivities from [37], FD = finite difference approximation of $\frac{\partial \hat{\Phi}}{\partial \mathbf{p}}$ from [37]

parameter	$\frac{\partial \beta}{\partial \mathbf{p}}$	FD	$\frac{\beta}{T}\frac{\partial T}{\partial \mathbf{p}}$	$\frac{\partial \hat{\Phi}}{\partial \mathbf{p}}$ [37]	FD [37]
ν_m	0.4938	0.4938	0.8653	0.8543	0.4923
k_m	-56.525	-56.490	-64.308	-63.457	-56.512
ν_p	0.9876	0.9876	1.7306	1.7014	0.9846
k_{p1}	0.0221	0.0221	-0.0138	-0.0135	0.0223
k_{p2}	-7.591	-7.5908	-10.878	-10.724	-7.6604
k_{p3}	-36.011	-35.991	-31.080	-30.635	-35.982
K_{eq}	-0.0001	-0.0001	0.0010	0.0010	-0.0001
P_{crit}	3.6138	3.6119	16.455	16.241	3.6333
J_p	-17.481	-17.473	-37.042	-36.517	-17.517

Table 2.3: Results of the period sensitivity analysis with respect to the parameters of the Lotka Volterra Oscillator described in Section 2.6.3. The parameterization of the system was $p_1 = p_2 = p_3 = 1.0$ with initial conditions $Y_0 = X_0 = 0.5$, resulting in a period of $T = 6.6939$. FD stands for finite difference approximation using $\epsilon = 0.001$.

parameter	p_1	p_2	p_3	X_0	Y_0
$\frac{\partial T}{\partial \mathbf{p}}$	-2.8077	-1.0786	-2.8077	-1.0786	-1.0786
$\frac{\partial T}{\partial \mathbf{p}}$[63]	-2.793	-1.120	-2.780	-1.1	-1.1
FD	-2.8092	-1.0804	-2.8092	-1.0766	-1.0766

oscillation. Sensitivity analysis with respect to initial values and parameters was performed for the parameterization given in reference [63]. Table 2.3 summarizes the results of the sensitivity analysis and compares them to a finite difference approximation. The methods presented in this work result in better agreement.

Some of the sensitivity trajectories for the Lotka-Volterra oscillators are shown in Fig. 2-4.

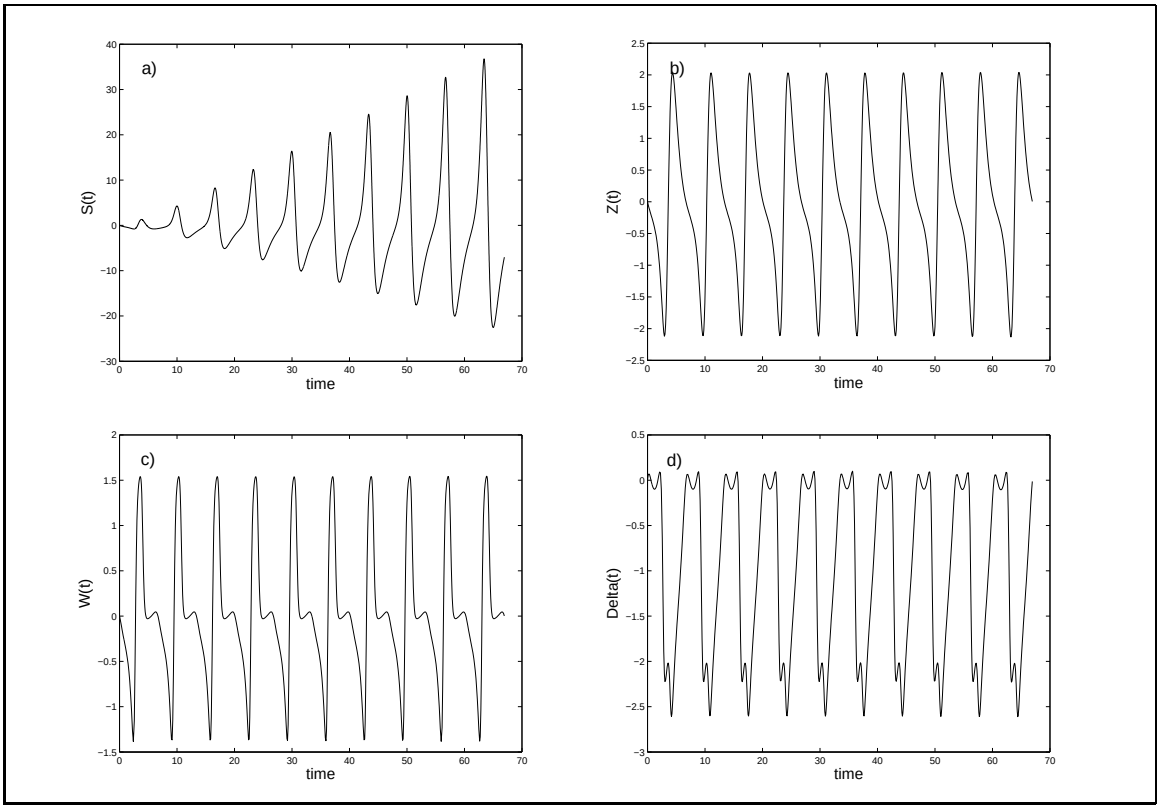

Figure 2-4: Sensitivity trajectories for the Lotka Volterra Oscillator, of state variable Y with respect to parameter p_3 over 10 periods of integration: a) unbounded, full sensitivity, $\mathbf{S}(t, \mathbf{p}; \mathbf{0})$, b) period independent, periodic part $\mathbf{Z}(t, \mathbf{p}; \mathbf{0})$, c) period and phase independent part $\mathbf{W}(t, \mathbf{p})$, d) relative phase sensitivity $\boldsymbol{\delta}(t, \mathbf{p})$ where the initial conditions chosen provide the PLC.

Relative Phase and Peak-to-Peak Sensitivities

Two different kinds of relative phase sensitivities were computed and both results compared favorably to a finite difference approximation, as shown in Table 2.4.

2.6.4 Application to a Small Intermediate-Type Oscillator

An example on an intermediate-type oscillator is the following linear system

$$\dot{\mathbf{y}} = \begin{bmatrix} 0 & p_1 & 0 \\ p_2 & 0 & 0 \\ p_2 & 0 & p_3 \end{bmatrix} \mathbf{y},$$

where $\mathbf{p} = (1, -1, -3)$. This system is a harmonic, 2-D oscillator coupled with a third variable which exponentially decays onto the the periodic orbit. Consequently, the mon-

Table 2.4: Results of the relative phase sensitivity analysis with respect to the parameters of the Lotka Volterra Oscillator described in Section 2.3.2. β_1 describes the peak-to-peak time distance between the time zero and the maximum of X, β_2 is the time to $X(\beta_2) = 0.7$. FD indicates the result of a finite difference approximation using $\epsilon = 0.001$.

parameter	p_1	p_2	p_3
$\frac{\partial \beta_1}{\partial \mathbf{p}}$	-3.9746	-0.4547	-1.0997
$\frac{\partial \beta_2}{\partial \mathbf{p}}$	-0.9711	0.4948	-0.1234
FD ($\beta 1$)	-3.9706	-0.4540	-1.0993
FD ($\beta 2$)	-0.9696	0.4951	-0.1234

odromy matrix $\mathbf{M}$ has two eigenvalues equal to one, and (2.40) has rank one, indicating the need for two phase locking conditions. A natural choice is to select $y_{1,0}(\mathbf{p}, \mathbf{q}) = q_1$ and $y_{2,0}(\mathbf{p}, \mathbf{q}) = q_2$, where $\mathbf{q} = (2, 0)$. Differentiation with respect to $\mathbf{p}$ and $\mathbf{q}$, respectively, then yields

$$\begin{bmatrix} (\mathbf{M} & - & \mathbf{I}) & \dot{\mathbf{y}}(T) \\ 1 & 0 & 0 & 0 \\ 0 & 1 & 0 & 0 \end{bmatrix} \begin{bmatrix} \frac{\partial \mathbf{y}_0}{\partial \mathbf{p}} \\ \frac{\partial T}{\partial \mathbf{p}} \end{bmatrix} = \begin{bmatrix} -\mathbf{S}(T, \mathbf{p}; \mathbf{0}) \\ 0 \quad 0 \quad 0 \\ 0 \quad 0 \quad 0 \end{bmatrix}$$

and

$$\begin{bmatrix} (\mathbf{M} & - & \mathbf{I}) & \dot{\mathbf{y}}(T) \\ 1 & 0 & 0 & 0 \\ 0 & 1 & 0 & 0 \end{bmatrix} \begin{bmatrix} \frac{\partial \mathbf{y}_0}{\partial \mathbf{q}} \\ \frac{\partial T}{\partial \mathbf{q}} \end{bmatrix} = \begin{bmatrix} 0 & 0 \\ 0 & 0 \\ 0 & 0 \\ 1 & 0 \\ 0 & 1 \end{bmatrix}.$$

The resulting sensitivities are $\frac{\partial T}{\partial \mathbf{p}} = \begin{bmatrix} -3.1416 & 3.1416 & 0 \end{bmatrix}, \frac{\partial T}{\partial \mathbf{q}} = \begin{bmatrix} 0 & 0 \end{bmatrix}$,

$$\frac{\partial \mathbf{y}_0}{\partial \mathbf{p}} = \begin{bmatrix} 0 & 0 & 0 \\ 0 & 0 & 0 \\ 0.06 & 0.54 & -0.16 \end{bmatrix}$$

and

$$\frac{\partial \mathbf{y}_0}{\partial \mathbf{q}} = \begin{bmatrix} 1 & 0 \\ 0 & 1 \\ -0.3 & 0.1 \end{bmatrix}.$$

Table 2.5: Results of the relative phase sensitivity analysis with respect to the parameters **p** and **q** of the Intermediate-Type Oscillator as described in Section 2.4.3. FD indicates the result of a finite difference approximation using $\epsilon = 0.001$.The relative phase was $\beta = 0.5247$.

parameter	p_1	p_2	p_3	q_1	q_2
$\frac{\partial\beta}{\partial\phi_i}$	0.0271	0.5525	0	-0.2898	0.5
FD	0.0274	0.5527	0.0005	-0.2885	0.4996

All results are in excellent agreement with the respective finite difference approximations (not shown), and are intuitive if one considers that the first two state variables form in fact a harmonic oscillator that behaves in pure NLCO fashion.

Relative Phase Sensitivities

The relative phase sensitivity of the phase β defined by the PLC $y_2(\beta) = -1$ was computed with respect to both the parameters **p** and **q**. The results are shown in Table 2.5 in comparison to a finite difference approximation. Good agreement is found between both numerical results.

2.6.5 Application to a Large LCO

The currently most detailed model of the mammalian circadian clock mechanism was published recently [29] and consists of 73 state variables and 231 parameters (after separating some of the repeatedly used 38 original model parameters). It describes five feedback loops, four of which are negative, and the remaining one is a positive feedback loop. Using mass action kinetics, the interactions between protein, mRNA and DNA species is modeled. In addition, transport processes are also included to distinguishs species with different intracellular localization. A detailed discussion of the results of the period sensitivity analysis of this model is given in a forthcoming publication [106]. In short, the period sensitivity analysis revealed that most high sensitivity parameters are located in the Per2 loop, and conversely, that most parameters in the Per2 loop have high period sensitivity. Therefore, the Per2 loop can be identified as the negative feedback loop which sets the period of oscillation. Sensitivity analysis allowed the discovery of a link between network structure and functionality encoded within it.

The computationally most expensive part of the method was the solution of the BVP,

Table 2.6: CPU times for the integration of the 73 state mammalian circadian clock oscillator, with or without different sensitivity systems, on a Pentium IV processor (2.2GHz, 1.0 GB of RAM). Full sensitivity system refers to the computation of the full sensitivity matrix with full error control for the entire integration. Direction sensitivity system refers to the computation of only a sensitivity matrix-vector product. 'Analytical Jacobian' indicates that an analytical expression for the Jacobian matrix was provided, 'Jacobian-vector-product by automatic differentiation' indicates that a subroutine was created using DAEPACK [98] which allows the efficient evaluation of the Jacobian-vector product directly. The integration of the system without sensitivity evaluation was included as a control for the comparison.

Sensitivity method	Sensitivities evaluated?	CPU time [sec]	Factor rel. to ODE system	Number of ODEs
Full sensitivity system,	No	0.201	1	73
analytical Jacobian	Yes	6.820	34	73+(74*73)
Directional sensitivities, analytical Jacobian	Yes	0.589	2.9	2*73
Directional sensitivities,	No	0.194	0.97	73
Jacobian-vector-product,	Yes	0.439	2.2	2*73
automatic differentiation				

whose CPU time depended mainly on the quality of the initial guess, i.e., on the number of iterations needed in NITSOL. A reasonable initial guess was generated by integrating the state variables only for a short period of time (1-2 estimated periods) to the point specified in the PLC. A typical run resulted then in approximately 10 iterations. Consequently, the use of directional sensitivities in the iterative Newton algorithm became a significant time saver. The CPU time necessary for integration of one period for the system is shown in Table 2.6. It should be mentioned that for the previous sensitivity analysis methods, the full sensitivity system must be integrated over at least tens of periods in order to obtain appropriate estimates for period and amplitude sensitivities, thereby making the solution of the BVP more than worthwhile in comparison.

The computation of the monodromy matrix and $\mathbf{S}(T, \mathbf{p}; \mathbf{0})$ required 5.71 and 19.7 seconds, respectively, and the matrix manipulations took approximately 0.15 seconds.

2.7 Conclusion

This work provides a unified treatment of the sensitivity analysis of oscillating systems, and their implicit derived properties such as period, phase and amplitude. A BVP is solved once, yielding the period sensitivities and the initial conditions for the sensitivity trajectories. The full sensitivity trajectories can then be computed, and decomposed into three parts, containing the influence of the period sensitiviy, phase sensitivity and amplitude sensitivity. All parts can be computed without approximations beyond the numerical error implicit in solving the BVP, and in numerically efficient ways. The focus of this work is to provide a well defined time reference by introducing the concept of PLCs, to identify the influence of the PLC on the sensitivity solution and also to isolate the shape and location sensitivities that are independent of the PLC. This provides a useful and intuitive framework for the computation of relevant quantities such as peak-to-peak sensitivities.

The methods are computationally competitive, because the computational cost of solving the BVP is outweighed by the advantages of a comprehensive method for sensitivity analysis of oscillators. Each of the quantities previously computed using iterative methods required an *a priori* unknown amount of integration time to achieve close approximation of the exact solution. Conversely, once the BVP is solved, any subsequent calculation only requires a minimum of computational effort, usually associated with integration times of under one period, which is a large improvement over previously suggested methods for those cases where appropriate methods existed.

Chapter 3

Sensitivity Analysis of a Small Mammalian Circadian Clock Model

Abstract

The mammalian circadian clock maintains gene expression and protein activation in a periodic manner that can entrain to daylight and influences a wide variety of biological processes. Here, two small models of the mammalian circadian clock, variants of each other representing different levels of molecular knowledge and abstraction, is analyzed comprehensively. The influence of individual reactions in the models on the characteristics of the circadian oscillation – namely, period, phase and amplitude – is studied using an exact and efficient sensitivity analysis method. The anlyses revealed a similar distribution of functional responsibilities between the two models. The period control is found to follow a different mechanism than the control of phase and amplitude. The control of phase and amplitude appears to be accomplished by a very similar set of reactions, involving all feedback loops in a model. The period is set by one negative feedback loop. The amplitudes for all molecular concentrations are controlled by a highly conserved set of reactions, and a consensus ranking for those is computed. Sensitivity similarities are used to analyze the degrees of freedom in the phase direction for each model. Most calculations are repeated for 10 alternative parameter sets for each model, in order to understand how much influence the exact parameterization has compared to the network architecture. The ability of the models to modify the length of the perceived day ("dawn-to-dusk") independently of the period was studied. Both models show a degree of flexibility with respect to this variation, although interestingly the simpler model with fewer feedback loops can more easily execute this task.

3.1 Introduction

The mammalian circadian clock is the molecular mechanism that drives the daily rhythms of many biological functions. For example, the secretion of hormones and the level of metabolic activity is partially under circadian control. Circadian rhythms are known to exist in several organs (including kidney, liver and thymus), in addition to the master clock, which resides in the suprachiasmatic nuclei (SCN) of the brain [26]. Circadian biology is becoming increasingly important in the context of chronopharmacology, where recent studies show that the timing of drug administration might have a strong influence on therapeutic success and on side effects [110, 79]. Circadian rhythms also play a role in shift work, jet-lag and military applications, where the ability of a human to perform and make decisions can be severely compromised by a lack of sleep, sunlight, and by being "misaligned" with the entraining signal (i.e., sunrise) for extended periods of time [74].

To take advantage of recent discoveries in circadian molecular biology and to devise treatment or management for the above mentioned situations, it is important to gain a full understanding of the functionality of the molecular pacemaker that causes these important effects. Moreover, to understand how biochemical networks carry out decision and control functions in biological systems, the development and application of modeling approaches is essential. The basic molecular biology of the circadian clock is well understood. Interlocked negative and positive feedback loops generate oscillations in the main clock gene products. At the center of the clock is a complex of two proteins, BMAL1 and CLOCK. This complex is the transcriptional activator of many other clock genes, including the three period genes *per1, per2* and *per3*, the cryptochrome genes *cry1* and *cry2* and nuclear orphan receptor gene family *rev-erb*. The protein products of the latter then regulate *bmal1* transcription together with PER2, thus closing several interlocked feedback loops. A number of post-translational steps, e.g., the phosphorylation of the period proteins PER1 and PER2, play a role in the regulation of the clock dynamics [106]. Furthermore, recent discoveries have added more detail to this mechanism such as the addition of the *dec* genes [45] and another nuclear orphan receptor ROR which acts on *bmal1* transcription [36, 91], both of which participate in feedback loops that are interlocked with the remaining clock mechanism.

As additional feedback loops are discovered, and the network as we know it becomes more intricate, several questions emerge. What is the advantage of such a complicated "wiring

scheme" in terms of oscillator performance? Do the extra feedback loops add flexibility to the network, or rather robustness? It was suggested in reference [85] that a larger number of feedback loops might increase the ability of a molecular network to track different phases. In fact, the notion has been advanced that the clock should be able to track both sunset and sunrise, given that the length of perceived day varies across the seasons in most locales [85, 26]. It is well known that the clock can entrain to different signals, most notably light input, which can be limited to short pulses during a window of sensitivity, but other signals, such as temperature and food supply have also been shown to impact entrainment [26]. The network must process this array of inputs yet maintain stable, robust 24-hour oscillations [26].

The present work extends previous research studying the distribution of responsibility for network functional characteristics across biochemical reactions forming network architecture. In previous work the reactions with the greatest effect on the period were identified using a well studied and detailed model of the mammalian circadian clock due to Forger & Peskin [29]. The result of that study highlights the importance of a contiguous portion of a negative feedback loop involving gene expression and phosphorylation of the gene product for Per2 in setting the period (Chapter 5). The results provide an intermediate view between properties set by a single reaction and emergent properties distributed throughout a network; A single process, involving multiple chemical reactions, was found to be dominant in setting the period. Here the theory for sensitivity analysis for oscillators presented in Chapter 2 is applied to more abstract models of the mammalian circadian clock, in which multiple sequential biochemical reactions are represented as a single reactions, and the determinants of not only the period but also the amplitude for individual species and different types of relative phases are analyzed.

3.1.1 The Becker-Weimann Model of the Mammalian Circadian Clock

There are several published mathematical models for the mammalian circadian clock. Some are detailed and large [29], others are of medium scale [68] and some are very small [12, 13]. All models have some omissions of known biology and vary in the level of inclusion of recently discovered interactions. Most are in the form of ordinary differential equations (ODEs) and are limit-cycle oscillators. The existence of different models of very different size suggests that studying the largest, most detailed model may lead to the most mechanistic, molecular

understanding, but the smaller, more abstracted models may produce a more conceptual understanding. It is especially interesting to study the degree to which results from smaller, more abstracted models map to results from larger, more detailed models, and vice versa.

In this work, a number of novel, sensitivity analysis-based methods were applied to a small mammalian circadian clock model [12] and its slightly larger variation [13]. The models are different in the level of molecular detail that is encapsulated and also in their network structures. The smaller model (7 concentrations, 24 rate constants and parameters) consists of one positive and one negative feedback loop. Protein and mRNA concentrations of Bmal1 and a lumped species termed the "Per2/Cry complex" are represented. Phosphorylation is not included in the model, nor is the differential action of Per1, Per2, Per3, Cry1 and Cry2. The only form of posttranslational regulation present is an activation step for BMAL1 that could represent the binding of CLOCK to BMAL1. PER2/CRY inhibits its own BMAL1-mediated expression, and BMAL1 increases its own expression; thus, two interlocking feedback loops are formed. The larger model (8 concentrations, 32 rate constants and parameters) has one additional negative feedback loop that is interlocked with the two other loops. The molecular species that performs the negative feedback is the REV-ERBα protein which downregulates the transcription of *bmal1*, while its own expression is promoted by BMAL1 and inhibited by PER2/CRY. All kinetics in the models are of mass-action type, except the terms for transcriptional control, which are modeled using Hill-type kinetic equations. The mutant behaviors of the two models are discussed with much attention to detail in the original publications.

Molecular data from circadian clock elements is usually presented on a time scale called "Circadian Time (CT)". CT =0 is defined as the onset of the subjective day, or dawn [26], and subjective dusk is CT=12. "Zeitgeber Time (ZT)" is the time schedule dictated by an external stimulus, called 'zeitgeber' (German: 'giver of time'). The molecular event that coincides with CT=0 is the beginning of the rise in *mCRY, mPer* and *mRev-Erb*α in the SCN clock [26, 91, 8, 77, 65, 87], although the timing can be shifted in the organ clocks according to data from liver, thymus, kidney and skeletal muscle [91, 36]. For all time references in this work, the minimum of nuclear Per2/Cry mRNA was chosen as the time reference CT=0 to be consistent with current literature.

3.2 Theory and Methods

Sensitivity Analysis of Oscillations

Sensitivity coefficients describe the effects of an infinitesimal perturbation of an input u on an output o,

$$s \equiv \frac{\partial o}{\partial u}.$$

In the context of deterministic dynamic models of biochemical networks, the sensitivities of molecular concentrations $\mathbf{y}$ with respect to the rate parameters $\mathbf{p}$ are often calculated, then $s_{ij} = \frac{\partial y_i}{\partial p_j}$ is the sensitivity of the ith concentration with respect to the jth parameter. In Chapter 2, it was shown that the parameter sensitivities in a limit-cycle oscillator have special properties and can be decomposed into three parts, according to

$$\mathbf{S}(t) = -\frac{t}{T}\dot{\mathbf{y}}(t)\frac{\partial T}{\partial \mathbf{p}} + \mathbf{W}(t) + \dot{\mathbf{y}}(t)\boldsymbol{\delta}(t). \tag{3.1}$$

Here, $\mathbf{S} \equiv \frac{\partial \mathbf{y}}{\partial \mathbf{p}}$ are the overall sensitivities of the states $\mathbf{y}$ with respect to the parameters $\mathbf{p}$, and $\frac{\partial T}{\partial \mathbf{p}}$ are the sensitivies of the period T of the oscillation with respect to the parameters. $\mathbf{W} \equiv \left(\frac{\partial \mathbf{y}}{\partial \mathbf{p}}\right)_{T(\mathbf{p})=const.,\phi(\mathbf{p})=const.}$ are the sensitivities of the states with respect to the parameters with period and phase kept constant, and it was shown in Chapter 2 that this quantity contains all amplitude information. In the final term, $\boldsymbol{\delta} \equiv \frac{\partial \phi}{\partial \mathbf{p}}$ is a phase sensitivity and contains information about the local acceleration or deceleration of the oscillation independently of the period and tangentially to the limit cycle, i.e., in the $\dot{\mathbf{y}}$-direction. It was shown in Chapter 2 that this information is needed and can be used to compute relative phase sensitivities, as mentioned briefly in Section 3.2. Both $\mathbf{W}(t)$ and $\boldsymbol{\delta}(t)$ are T-periodic, and in a limit-cycle oscillator (i.e., the type of oscillator used to model the circadian clock), $\mathbf{W}(t)$ is uniquely determined by the states (concentrations) at any given point on the cycle. On the other hand, $\boldsymbol{\delta}(t)$ is a function of the way the time $t = 0$ was defined for the system. A phase locking condition (PLC) is used to define mathematically a point on the limit-cycle trajectory that provides a reference point for the time $t = 0$, and the sensitivities $\boldsymbol{\delta}(t)$ depend on the choice of PLC. An important difference between limit-cycle oscillators and most other dynamical systems is the fact that the initial conditions of the parameter sensitivities are not zero. The parameters limit the choice of initial conditions to points on the limit cycle, and the PLC then defines one of those points. This leads to the fact

that $\mathbf{S}(0) \neq \mathbf{0}$, $\mathbf{W}(0) \neq \mathbf{0}$ and $\boldsymbol{\delta}(0) \neq \mathbf{0}$. A number of experimental [91, 36, 77, 8, 83, 65] and review publications [26, 87] were surveyed to identify the appropriate phase locking condition that could be used to represent CT=0 in the model. For the current work, the PLC was used that defined the time at which the Per2/Cry mRNA concentration attained a local minimum as time zero, implemented through setting its time derivative to zero.

Absolute and Relative Amplitude Sensitivities

In the context of this work, the absolute amplitude of a concentration is simply its level. This quantity is periodic in time, as are the associated absolute amplitude sensitivities $\mathbf{w}_i(t) = \left(\frac{\partial y_i(t)}{\partial \mathbf{p}}\right)_{T,\phi}$. The relative amplitude of a concentration is the difference between its maximum and minimum concentration. In Figure 3-1, the relative and mean absolute amplitudes for all species in both models are shown.

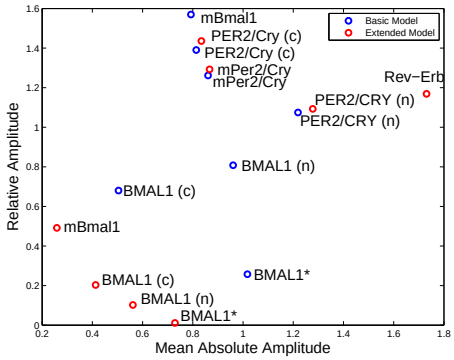

Figure 3-1: Relative and mean absolute amplitudes of all concentrations in both models

The relative amplitude of a species $y_i(t)$ is defined here as $A_i = \max_t y_i(t) - \min_t y_i(t)$. Its sensitivity with respect to the parameter p_j can be computed as

$$\frac{\partial A_i}{\partial p_j} = w_{i,j}(t_{y_i,max}) - w_{i,j}(t_{y_i,min}). \tag{3.2}$$

The times $t_{y_i,max}$ and $t_{y_i,min}$ are times at which the supremum and infimum of y_i are attained, respectively.

Relative Phase Sensitivities and Angular Relative Phase Sensitivities

The computation of relative phase sensitivities is somewhat more involved, and for a detailed treatment, the reader is referred to Chapter 2. In short, a relative phase is the time difference between two events on the limit cycle. Both events are defined with PLCs, and for the sake of simplicity, we will assume that one PLC defines the time reference $t = 0$. Then the relative phase β can be defined by the second PLC,

$$g(\mathbf{y}(\beta(\mathbf{p}), \mathbf{p}; \mathbf{y}_0(\mathbf{p})), \mathbf{p}, \mathbf{y}_0) = 0.$$

Differentiation with respect to the parameters yields

$$\begin{aligned}\frac{\partial g}{\partial \mathbf{y}}\Big|_{\mathbf{y}(\beta(\mathbf{p}),\mathbf{p};\mathbf{y}_0(\mathbf{p})),\mathbf{p},\mathbf{y}_0(\mathbf{p})} \Bigg(\dot{\mathbf{y}}(\beta, \mathbf{p}; \mathbf{y}_0(\mathbf{p}))\, \frac{\partial \beta}{\partial \mathbf{p}}\Big|_{\mathbf{p}} + \frac{\partial \mathbf{y}}{\partial \mathbf{y}_0}\Big|_{\beta,\mathbf{p},\mathbf{y}_0} \frac{\partial \mathbf{y}_0}{\partial \mathbf{p}}\Big|_{\mathbf{p}} \\ + \left(\frac{\partial \mathbf{y}}{\partial \mathbf{p}}\Big|_{\beta,\mathbf{p},\mathbf{y}_0}\right)_{\mathbf{y}_0 = const.}\Bigg) + \frac{\partial g}{\partial \mathbf{p}}\Big|_{\mathbf{y}(\beta(\mathbf{p}),\mathbf{p};\mathbf{y}_0(\mathbf{p})),\mathbf{p},\mathbf{y}_0(\mathbf{p})} \\ + \frac{\partial g}{\partial \mathbf{y}_0}\Big|_{\mathbf{y}(\beta(\mathbf{p}),\mathbf{p};\mathbf{y}_0(\mathbf{p})),\mathbf{p},\mathbf{y}_0(\mathbf{p})} \frac{\partial \mathbf{y}_0}{\partial \mathbf{p}}\Big|_{\mathbf{p}} = \mathbf{0}.\end{aligned}$$

This equation can be rewritten as

$$\begin{aligned}\frac{\partial g}{\partial \mathbf{y}}\Big|_{\mathbf{y}(\beta(\mathbf{p}),\mathbf{p};\mathbf{y}_0(\mathbf{p})),\mathbf{p},\mathbf{y}_0(\mathbf{p})} \left(\dot{\mathbf{y}}(\beta, \mathbf{p}; \mathbf{y}_0(\mathbf{p}))\, \frac{\partial \beta}{\partial \mathbf{p}}\Big|_{\mathbf{p}} + \mathbf{S}(\beta(\mathbf{p}))\right) + \frac{\partial g}{\partial \mathbf{p}}\Big|_{\mathbf{y}(\beta(\mathbf{p}),\mathbf{p};\mathbf{y}_0(\mathbf{p})),\mathbf{p},\mathbf{y}_0(\mathbf{p})} \\ + \frac{\partial g}{\partial \mathbf{y}_0}\Big|_{\mathbf{y}(\beta(\mathbf{p}),\mathbf{p};\mathbf{y}_0(\mathbf{p})),\mathbf{p},\mathbf{y}_0(\mathbf{p})} \mathbf{S}(0) = \mathbf{0}.\end{aligned}$$

which can be solved for the phase sensitivity $\frac{\partial \beta}{\partial \mathbf{p}}$. As shown in Chapter 2, another way to represent this sensitivity is

$$\frac{\partial \beta}{\partial \mathbf{p}} = \frac{\beta}{T}\frac{\partial T}{\partial \mathbf{p}} + \boldsymbol{\delta}^*(0) - \boldsymbol{\delta}(\beta), \tag{3.3}$$

where $\boldsymbol{\delta}(\beta)$ is the value of $\boldsymbol{\delta}$ at the time $t = \beta$ as shown in Eq. (3.1). $\boldsymbol{\delta}^*(0)$ is the value of $\boldsymbol{\delta}$ that would result at time zero, if instead of the original PLC that was used to define $t = 0$, the PLC that defines the event time $t = \beta$ was used.

Eq. (3.3) will be used to derive a relative phase sensitivity of particular interest: the angular relative phase sensitivity $\frac{\partial \gamma}{\partial \mathbf{p}}$. Eq. (3.3) shows the relative timing of two events is determined by two contributions. One is the overall period. Naturally, if the same exact limit cycle would oscillate faster, the relative timing between two events would shrink. The

other contribution is more interesting. The two events that define the beginning and end of the relative phase can move in time, as a function of the parameterization, in addition to the change imposed by the alteration of the period. This effect is represented by the pair of $\boldsymbol{\delta}$ sensitivities in the equation. In order to express the period-independent nature of this phase change, the phase angle γ of the phase β is computed as

$$\gamma = 360^\circ \frac{\beta}{T}, \tag{3.4}$$

or as the fraction of time (expressed in degrees) per period spend in the phase β. The angular relative phase sensitivity is then obtained by applying the chain rule,

$$\frac{\partial \left(360^\circ \frac{\beta}{T}\right)}{\partial \mathbf{p}} = \frac{360^\circ}{T}\frac{\partial \beta}{\partial \mathbf{p}} - \frac{360^\circ \beta}{T^2}\frac{\partial T}{\partial \mathbf{p}}. \tag{3.5}$$

By comparison with Eq. (3.3), it is clear that

$$\frac{\partial \gamma}{\partial \mathbf{p}} = \frac{360^\circ}{T}\left(\boldsymbol{\delta}^*(0) - \boldsymbol{\delta}(\beta)\right), \tag{3.6}$$

or, in other words, the second contribution to the overall (time) relative phase sensitivity can be interpreted as an angular relative phase sensitivity.

Period-Neutral Relative Phase Sensitivity Directions

In order to understand if a relative phase is hard or easy to change independently of the period, an orthogonal projection of the unscaled relative phase sensitivities to the unscaled period sensitivities was performed, where

$$\left(\frac{\partial \beta}{\partial \mathbf{p}}\right)_{T=const.} = \frac{\partial \beta}{\partial \mathbf{p}}\left(\mathbf{I} - \frac{\frac{\partial T}{\partial \mathbf{p}}^{\mathrm{T}}\frac{\partial T}{\partial \mathbf{p}}}{\|\frac{\partial T}{\partial \mathbf{p}}\|^2}\right). \tag{3.7}$$

The notation $\left(\frac{\partial \beta}{\partial \mathbf{p}}\right)_T$ for $\left(\frac{\partial \beta}{\partial \mathbf{p}}\right)_{T=const.}$ is going to be used for the remainer of this work. If instead of the relative phase sensitivity the angular relative phase sensitivity is used, the result is scaled by the factor $\frac{360^\circ}{T}$, i.e. $\left(\frac{\partial \beta}{\partial \mathbf{p}}\right)_T = \frac{T}{360^\circ}\left(\frac{\partial \gamma}{\partial \mathbf{p}}\right)_T$ The length of the resulting vector $\left(\frac{\partial \beta}{\partial \mathbf{p}}\right)_T$ relative to the period sensitivity vector $\frac{\partial T}{\partial \mathbf{p}}$ was computed as $L = \left\|\left(\frac{\partial \beta}{\partial \mathbf{p}}\right)_T\right\| / \left\|\frac{\partial T}{\partial \mathbf{p}}\right\|$. The angle between both vectors α was computed to provide complementary information,

where $\sin\alpha = \left\| \left(\frac{\partial \beta}{\partial \mathbf{p}} \right)_T \right\| / \left\| \frac{\partial \beta}{\partial \mathbf{p}} \right\|$. Figure 3-2 shows the relationships between the different vectors in 2D-view. Because β_{ij} is the (forward-counting) time difference between two events i and j, the relationship $T = \beta_{ij} + \beta_{ji}$ holds. The reason for the normalization of the length with respect to the period vector was to create a common basis for comparison for all phases in a model, and to make the measurements of two phases β_{ij} and β_{ji} symmetrical. Both should have the same absolute amount of period-invariant relative phase flexibility, but in the opposite direction. The angle between $\frac{\partial \beta_{ij}}{\partial \mathbf{p}}$ and $\frac{\partial T}{\partial \mathbf{p}}$ is equally telling to evaluate the possibility of a local, period-neutral phase variation. It is possible that in a given system, the phase sensitivity vector might be very orthogonal to the period sensitivity vector, but of small magnitude, thus making a phase modification difficult. Conversely, it is possible that a vector of large magnitude is almost parallel to the period sensitivity vector, and thus also hindering a period-neutral phase variation.

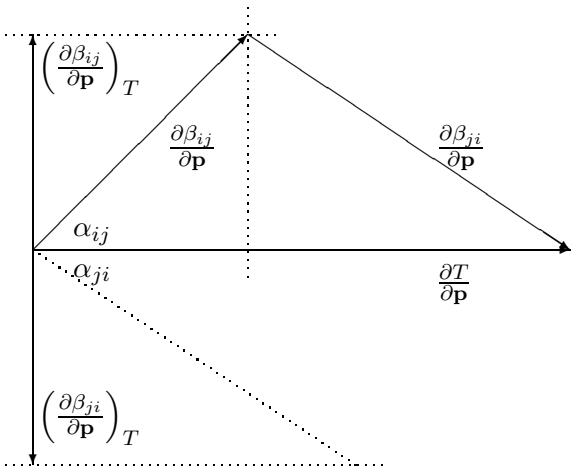

Figure 3-2: Illustration of the two metrics to measure the orthogonality and relative length of the vector $\left\| \left(\frac{\partial \beta_{ij}}{\partial \mathbf{p}} \right)_T \right\|$. The measure of orthogonality is $\sin\alpha_{ij} = \frac{\left\| \left(\frac{\partial \beta_{ij}}{\partial \mathbf{p}} \right)_T \right\|}{\left\| \frac{\partial \beta_{ij}}{\partial \mathbf{p}} \right\|}$. The measure of relative length is $L_{ij} = \frac{\left\| \left(\frac{\partial \beta_{ij}}{\partial \mathbf{p}} \right)_T \right\|}{\left\| \frac{\partial T}{\partial \mathbf{p}} \right\|}$. It should be noted that $\alpha_{ij} \neq \alpha_{ji}$ whereas $L_{ij} = L_{ji}$.

Phase Sensitivity Similarities

The concept of sensitivity similarities was recently extended and their meaning for the performance of chemical kinetic networks was discussed in [114]. In the present work, only

the following definition is used:

Global similarity: If for some $k, m \in \{1, 2, ..., n_p\}$ and $i \in \{1, 2, ..., n_y\}$ there exists a real number $\mu_{ikm} \in \mathbb{R}$ such that for all $\mathbf{y}_0 \in \mathbb{R}^{n_y}$

$$s_{ik}(t, \mathbf{p}) = \mu_{ikm} s_{im}(t, \mathbf{p}) \quad (0 \leq t \leq T_{end}), \tag{3.8}$$

then the parameters p_k and p_m are **globally similar** with respect to the state variable y_i with the similarity number μ_{ikm} on the time horizon of interest. (Because no other kind of similarity will be discussed, "similar" in the context of this work should be taken to mean "globally similar" as defined here.)

In other words, if the sensitivity of one variable with respect to one parameter at any time t is a constant multiple of the sensitivity of the same variable with respect to another parameter, the two parameters are termed globally similar. In reference [114] it is shown that the presence of different types of sensitivity similarities can be used to analyze functional properties of a network. In particular, a single parameter can reverse any perturbation over the entire range of t that is caused by modifications to any group of parameters that is similar to it. Conversely, a change in a parameter that has no similar counterpart is difficult to compensate for over the entire range of t under consideration. This idea is intriguing and inspired a similar type of analysis for oscillatory models in the present work.

Approximate Similarity Using Principal Component Analysis

In order to establish which groups of parameters are globally approximately similar in the sense of Eq. (3.8), all normalized δ_i are computed for the parameters $p_i, i \in \{1, 2, ..., n_p\}$ at time points $t_j, j \in \{0, 1, 2, ...100\}$ which are equally spaced over one period T. The result is a matrix $\mathbf{\Delta_N} \in \mathbb{R}^{n_p \times 101}$. If two parameters were exactly globally similar with respect to their phase sensitivity, then their normalized trajectories $\delta_{k,norm}(t) = \delta_{m,norm}(t),\ 0 \leq t \leq T$. In order to study and understand which groups of parameters are the most similar, the δ-trajectories had to be clustered according to a similarity measure and in as many clusters as there are similar modes (or manifolds) present in $\mathbf{\Delta}$. To determine the dimensionality of $\mathbf{\Delta}$ and the most populated modes, principal component analysis (PCA) was employed. PCA is a technique that allows one to represent a data set with multiple variables (here: n_p, the number of parameters and therefore δ-trajectories) in a lower-dimensional represen-

tation (here: number of modes). The eigenvalues associated with the principal components (or PCA axes) are called latent roots. It is typical to express the importance of a principal component as a percentage of the magnitude of that eigenvalue over the sum of all eigenvalues. That number is important to explain what percentage of data is explained by which principal component, and which principal components contribute so little that the system can be largely understood without them. Any mode contributing less than 1.0% was ignored here. The normalized principal components for each significant mode were used directly as mode centroids for the clustering of the δ-trajectories. For each mode, the negative of the component was termed "anti-mode". It was observed in the phase sensitivity data that the normalized trajectories often had symmetrical shapes, one being the negative (i.e. mirror image) of the other. The δ-trajectories were grouped by finding the closest principal component ("mode" or "anti-mode") for each one through using a least-squares measure of distance, and attributing the trajectory to that mode.

Alternative Parameter Sets

In order to understand the impact of a specific parameterization on the network performance, and to distinguish it from the effect of network architecture, alternative parameter sets were generated. The only criteria used here were to generate parameter sets that result in an oscillation of 23–25-hour period. The parameter values were randomly varied between –50% and +100% of their nominal values and the resulting dynamic behavior of the model was tested for oscillation in the desired period range. After 10 successful alternate parameter sets for each model were generated, the algorithm terminated. These parameter sets were then used without further curation to compute subsets of the data that was originally computed for the nominal parameter sets, to test for robustness. The alternative parameter sets are shown in Appendix A, Tables A.4 and A.5.

3.3 Results and Discussion

3.3.1 Period Sensitivities

Period sensitivities for both models in their nominal parameterization as well as for all alternative parameter sets were computed as described in Chapters 2 and 5. The sensitivities were scaled according to $\frac{\partial \ln T}{\partial \ln p_i} = \frac{p_i}{T}\frac{\partial T}{\partial p_i}$ so that the relative importance of each parameter p_i

in setting the period could be evaluated independently of the magnitude of the parameter. Figure 3-3 shows the rank-ordered, scaled period sensitivities $\frac{\partial \ln T}{\partial \ln \mathbf{p}}$ for both models under

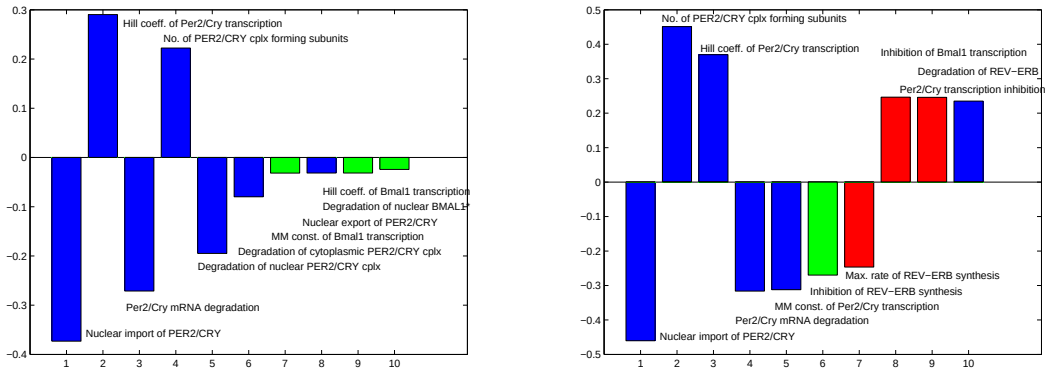

Figure 3-3: Scaled period sensitivities $\frac{\partial \ln T}{\partial \ln p_i}$, rank-ordered by absolute magnitude. Left: Top ten parameters and sensitivities in the basic model; Right: Model with REV-ERBα loop. Blue: Negative feedback loop - BMAL1* controls Per2/Cry expression. Green: Positive feedback loop of Bmal1 on itself (through Per2/Cry and Rev-Erbα if applicable). Red: Negative feedback loop where BMAL1 controls REV-ERBα expression

study. In each model, the period is strongly influenced by the primary negative feedback loop in which BMAL1* controls Per2/Cry expression (blue bars). Interestingly this pair of results agrees with a similar analysis carried out for a much more detailed, mechanistic model (Chapter 5). There, the period was strongly influenced by a small number of parameters all located within the Per2 negative feedback loop. The most noticable distinction between the two models, however, is that the sensitivities drop sharply for the basic model, that is, the influential parameters are highly localized within the network. The positive feedback loop does not participate significantly in setting the period (green bars). On the other hand, the extended model shows less localization of the high period sensitivities, and a marked participation of all 3 feedback loops in setting the period. It has been reported that Rev-Erbα deletions have an effect on the period through the "positive limb of the mammalian circadian oscillator [83]" — the period is shortened in Rev-Erb$\alpha^{-/-}$ mice. This experimental result might correspond to the influence of the positive feedback loop seen here in that the inhibition of Rev-Erbα synthesis has a large and negative period sensitivity. It is harder to analyze the rates of other Rev-Erbα-related reactions because those participate both in negative and positive feedback, leading to more complex effects.

3.3.2 Period Sensitivities for Alternative Parameter Sets

The same calculations were repeated for all alternative parameter sets. All ranked period sensitivites are shown in Figure 3-4. It is apparent that in the majority of cases, the negative feedback loop between Per2/Cry and BMAL1* dominates the period setting. The positive feedback loop has little influence on the period in the basic model. The distinction is less clear for the extended model, given that in this scenario both negative feedback loops participate in the positive feedback. However, the only parameter unique to the positive feedback does not appear at all in the ten parameters with the greatest period sensitivity.

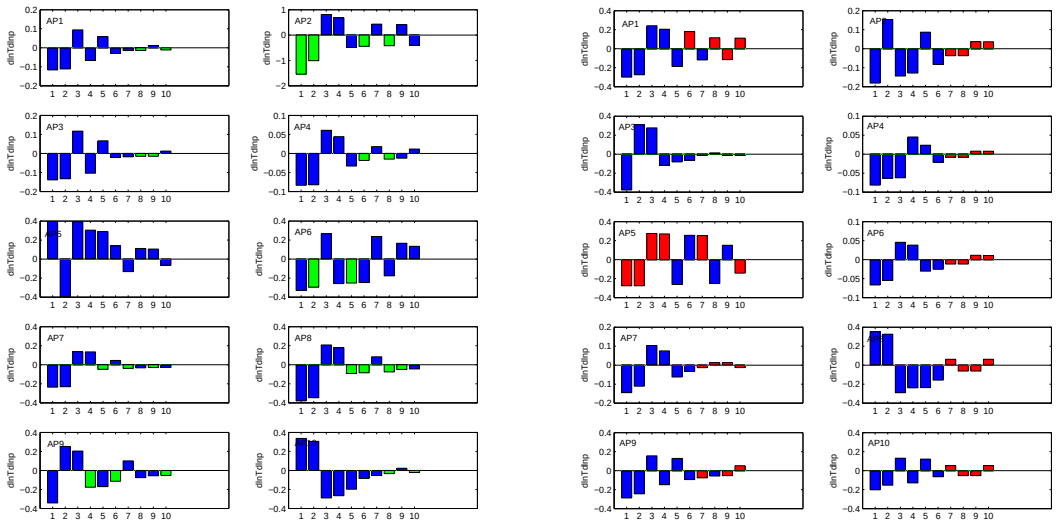

Figure 3-4: Scaled period sensitivities $\frac{\partial \ln T}{\partial \ln \mathbf{p}}$, rank-ordered by absolute magnitude, for the basic model (left) and the model with Rev-Erbα (right). The top ten sensitivities are shown. Blue: Negative feedback loop — BMAL1* controls Per2/Cry expression. Green: Positive feedback loop of Bmal1 on itself (through Per2/Cry and Rev-Erbα if applicable). Red: Negative feedback loop where BMAL1 controls REV-ERBα expression

In the basic model, a common set of parameters dominate the list of the ten with the greatest period sensitivity, and these correspond to indices 10, 5, 6, 8, 12, 9, as defined in Table A.1. Parameters 6 (Per2/Cry mRNA degradation), 10 and 12 (nuclear import and degradation rates of PER2/CRY) are closely related to parameters found to be prominent in the period setting in the mammalian clock in Chapter 5 using the large, detailed model by Forger and Peskin [29]. In that case they correspond to Per2 mRNA degradation and PER2 phosphorylation rates, which control nuclear trafficking and degradation of PER2/CRY.

In the extended model, the top parameters are similar to the ones in the basic model and different from the nominal parameterization of the extended model. Fewer parameters outside the Per2/Cry - BMAL1* feedback loop appear in the top ten of the alternative parameter rankings. It might suggest that Rev-Erbα is not necessary to generate an 24-h oscillation, which is experimentally known [83].

There is one especially intriguing parameter set (# 5) in which the two negative feedback loops have switched roles — the negative feedback of BMAL1 through Rev-Erbα now sets the period. The fact that this model parameterization behaves differently propagates through many of the other analyses in this work. To the extent that parameterizations leading to both behviors are consistent with available data, the different in behaviors and analyses are indicative of uncertainty.

3.3.3 Amplitude Sensitivities

The scaled amplitude sensitivities $\frac{p_j}{y_i} w_{ij}(t) = \frac{\partial \ln y_i(t)}{\partial \ln p_j}\Big|_{T,\phi}$ were computed for each species y_i with respect to all parameters over one period of time. Then the parameter sensitivities for each species were rank ordered according to the absolute area under the curve AUC, where

$$AUC(p_j, y_i) = \int_0^T \left\| \frac{p_j}{y_i} w_{ij}(t) \right\| dt.$$

In a second approach, the scaled amplitude sensitivities were ranked by their maximum magnitude. Both rankings were very similar in both models, so only the data based on the AUC-rankings is presented here. Tables 3.1 and 3.2 show the top ten parameter indices for the ranked amplitudes of each species.

First, it appears that a small group of reactions dominates the amplitude manipulation of all species in the basic model. (This set strongly overlaps that manipulating the phase, as shown later in this chapter in Figure 3-7.) This is a surprising result, because one might expect that the amplitude of each species might be strongly influenced by its own synthesis and degradation rates (transcription, translation, mRNA or protein degradation). Upon further inspection, it appears that only the degradation of Bmal1 mRNA (16) and of PER2/CRY in the nucleus (12) are involved in amplitude manipulation.

The manipulation of the amplitudes appears to be shared between reactions in the two feedback loops. The top 3 parameters are the same for the amplitudes of all species, and the

Table 3.1: Rankings of parameters by magnitude of AUC of scaled amplitude sensitivities for the basic model. The parameter indices of the top ten sensitivities are shown. A consensus sequence for the amplitude sensitivities was computed and is shown.

species	1	2	3	4	5	6	7	8	9	10
Per2/Cry mRNA	3	14	8	16	13	5	12	15	6	17
PER2/CRY cytosol	8	3	14	10	12	16	5	13	15	17
PER2/CRY nucleus	3	8	14	5	16	12	13	15	10	17
Bmal1 mRNA	14	3	8	15	16	13	5	10	12	17
BMAL1 cytosol	14	3	8	17	16	13	15	19	12	10
BMAL1 nucleus	14	3	8	16	17	13	15	12	21	10
BMAL1* nucleus	14	3	8	16	13	24	17	15	21	12
consensus	14	3	8	16	13	5	15	10	12	17
ranking for $\frac{\partial \phi}{\partial \ln \mathbf{p}}$	3	14	8	16	13	15	12	17	10	5
ranking for $\frac{\partial \ln T}{\partial \ln \mathbf{p}}$	10	5	6	8	12	9	14	11	24	15

Table 3.2: Rankings of parameters by magnitude of AUC of scaled amplitude sensitivities in the model including the Rev-Erbα loop. The parameter indices of the top ten sensitivities are shown. A consensus sequence for the amplitude sensitivities was computed and is shown.

species	1	2	3	4	5	6	7	8	9	10
Per2/Cry mRNA	3	8	2	25	29	27	26	5	31	10
PER2/CRY cytosol	8	3	2	27	25	29	31	26	10	5
PER2/CRY nucleus	3	2	8	31	27	29	25	26	17	16
Bmal1 mRNA	8	3	2	27	31	29	25	26	5	28
BMAL1 cytosol	27	31	29	25	3	8	2	26	17	16
BMAL1 nucleus	27	29	25	3	31	8	2	26	16	13
BMAL1* nucleus	27	29	25	31	3	8	2	26	16	13
REV-ERBα nucleus	8	3	2	27	31	29	25	26	28	5
consensus	8	3	2	27	31	29	25	26	16	5
ranking for $\frac{\partial \phi}{\partial \ln \mathbf{p}}$	3	2	27	8	25	29	26	31	10	12
ranking for $\frac{\partial \ln T}{\partial \ln \mathbf{p}}$	10	8	5	6	2	27	25	31	29	3

parameters in ranks 4 through 10 are very similar. This observation was used to compute a "consensus ranking" which forms a representative ranking of what might be considered "global" amplitude sensitivities. Each position in the ranking was given to the parameter that occupies this rank in the most individual amplitude rankings, unless it had already been used for a higher rank. In this case, the parameter index that appeared second most often in this position was chosen. The consensus ranking is shown in Table 3.1.

In the model with Rev-Erbα the amplitudes in the Bmal1 part of the system are manipulated by two sets of reactions. The first set involves transcriptional and translational control of Per2/Cry (2, 3, 5, 8); the second set includes Rev-Erbα synthesis and degradation (25, 26, 27, 29). The latter is found to determine the amplitude in the Bmal1 oscillations strongly, even more so than in the Per2/Cry oscillations, but surprisingly, not its own amplitude. The Bmal1-transcription parameters (14, 31, 17–24) do not play a significant role in the amplitude control, even in the Bmal1 species, except the mRNA degradation rate (16), which is the only degradation rate to play a role in amplitude control at all. Note that parameter number 27 (the inhibition constant of REV-ERBα synthesis) is the only parameter that is unique to the positive feedback loop in the larger model. This parameter has a large influence on amplitudes and phase, in particular on the amplitudes in the Bmal1 part of the network.

3.3.4 Amplitude Sensitivities for Alternative Parameter Sets

It remains true across the alternative parameter sets that for each parameterization, the rankings of amplitude sensitivities across the different molecular species is conserved and a consensus ranking can be computed. The consensus rankings for all alternative parameter sets are shown in Tables A.2 and A.3. In the basic model, parameters involved in Bmal1 transcription and translation (14, 15, 16) appear to play a relatively dominant role across the different parameterizations, and again, parameter 3 (inhibition constant of Per2/Cry transcription) is always in the top 4. This consensus is again correlated with the high ranked parameters in the phase sensitivity rankings (3, 14, 15, 16).

In the extended model, the dominant parameters are similar to those in the phase sensitivities. It is harder to see an overall consensus between the different parameter sets, and the phase and amplitude sensitivities are much less correlated in the ensemble of alternatively parameterized extended models. It could be hypothesized that the model with more

feedback loops has more ability to control amplitudes and phases separately.

3.3.5 Relative Amplitude Sensitivities

Shown in Figure 3-5 are the scaled relative amplitude sensitivities, ranked by magnitude. The relative amplitude is defined in Eq. (3.2) as the difference between the highest and lowest concentration for the molecule under study. The results found are similar to those in Section 3.3.3, but it is found that the amplitudes in the two different feedback loops have a slightly different set of reactions with high influence. We find that in the basic model, the relative amplitudes of the first 3 species (all Per2/Cry species) are controlled by parameters exclusively from the negative feedback loop, or in other words, parameters local to the loop. The top five parameters for these three cases also contain four of the top five parameters from the period sensitivity ranking, as shown in Table 3.3. Parameter #5 (Hill coeff. of Per2/Cry transcriptional inhibition) plays a larger role in the control of Per2/Cry relative amplitudes than for absolute ones, whereas the influence of parameter 14 is diminished. This parameter, the Michaelis constant of Bmal1 transcription, plays a role in regulating all Bmal1-related amplitudes, as one might expect. Overall, the relative amplitudes of the Bmal1 species, which participate in both feedback loops, are regulated by a combination of parameters from both feedback loops that is consistent throughout the four species.

It appears that the absolute amplitudes in the basic model are set by a consistent group of parameters for the entire network, and the relative amplitudes are determined by a similar set of parameters overall. However, the relative amplitudes have slightly more distinct mechanisms for local control.

For the extended model, the ranking of the scaled relative amplitudes shown in Figure 3-5 (right) and Table 3.4 is very consistent with the rankings of the absolute amplitudes shown in Table 3.2. The relative amplitudes of the first three species have slightly more influence from the parameters in the first negative feedback loop, but the effect is not as marked as in the basic model. Like the period sensitivity ranking, the relative amplitude sensitivity ranking drops off less steeply in the extended model if compared to the basic model.

One parameter that is highly influential in the amplitude sense in both models, but notably absent in the rankings for high period sensitivity, is parameter #3 (inhibition of Per2/Cry transcription), which regulates the feedback strength of the negative loop.

Table 3.3: Rankings of parameters by magnitude of scaled relative amplitude sensitivities $\frac{\partial \ln A_j}{\partial \ln \mathbf{p}} = \frac{\partial \ln y_{j,max}}{\partial \ln \mathbf{p}} - \frac{\partial \ln y_{j,min}}{\partial \ln \mathbf{p}}$ in the basic model. The parameter indices of the top ten sensitivities are shown.

species	1	2	3	4	5	6	7	8	9	10
Per2/Cry mRNA	8	5	12	3	10	6	7	14	24	16
PER2/CRY cytosol	8	10	3	12	5	14	6	24	16	1
PER2/CRY nucleus	8	3	5	12	10	14	24	16	1	15
Bmal1 mRNA	8	14	3	13	16	5	12	10	24	1
BMAL1 cytosol	8	14	3	17	13	16	5	10	12	19
BMAL1 nucleus	8	14	3	17	13	5	16	10	12	21
BMAL1* nucleus	8	14	3	10	5	13	17	16	22	12
ranking for $\frac{\partial \ln T}{\partial \ln \mathbf{p}}$	10	5	6	8	12	9	14	11	24	15

Table 3.4: Rankings of parameters by magnitude of scaled relative amplitude sensitivities $\frac{\partial \ln A_j}{\partial \ln \mathbf{p}} = \frac{\partial \ln y_{j,max}}{\partial \ln \mathbf{p}} - \frac{\partial \ln y_{j,min}}{\partial \ln \mathbf{p}}$ in the extended model. The parameter indices of the top ten sensitivities are shown.

species	1	2	3	4	5	6	7	8	9	10
Per2/Cry mRNA	8	2	3	5	27	29	31	25	12	26
PER2/CRY cytosol	8	3	2	27	29	31	25	5	26	10
PER2/CRY nucleus	8	3	2	27	29	31	25	26	5	12
Bmal1 mRNA	8	27	3	2	29	31	25	26	28	5
BMAL1 cytosol	8	27	3	2	29	31	25	26	5	28
BMAL1 nucleus	8	27	3	2	29	31	25	26	5	28
BMAL1* nucleus	8	27	2	3	29	25	31	26	5	10
REV-ERBα	8	27	2	3	31	5	28	29	25	26
ranking for $\frac{\partial \ln T}{\partial \ln \mathbf{p}}$	10	8	5	6	2	27	25	31	29	3

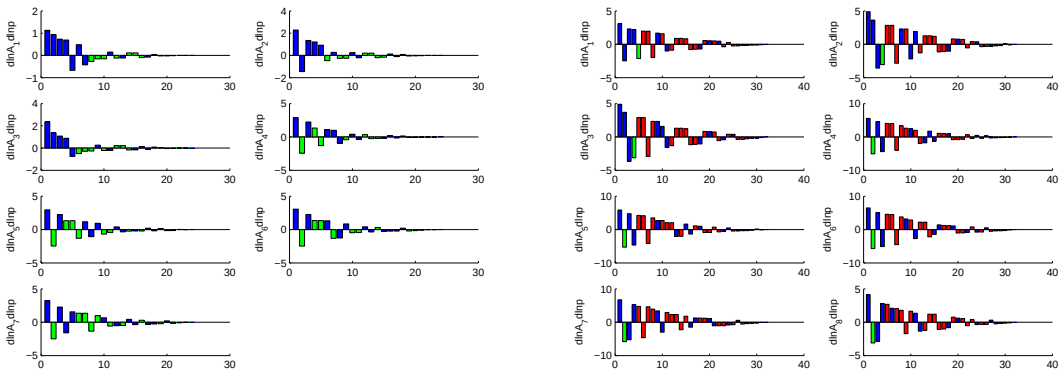

Figure 3-5: Left: Scaled relative amplitude sensitivities ($A_j = \frac{\partial \ln A_j}{\partial \ln \mathbf{p}}$) for all species in both nominal models, rank-ordered by absolute magnitude. All sensitivities are shown. Left: Basic model; Right: Model with REV-ERBα loop;

3.3.6 Phase Sensitivities

It is difficult to attribute an intuitive meaning to the vector $\boldsymbol{\delta}(t)$. It represents the local acceleration or deceleration at any point on the limit cycle, with reference to the time defined as $t = 0$. Or in other words, if one parameter p_i was changed by an infinitesimal amount ∂p_i, the point $\mathbf{y}(t^*)$ would be reached a tiny amount sooner (or later), so that the resulting $\partial t^* \approx \delta_i(t^*)\partial p_i$. In principle, a tiny change in p_i may cause the point $\mathbf{y}(t^*)$ to not exist anymore, but this information is separated out according to Eq. (3.1) and is represented in $\mathbf{w}_i(t^*)$, the ith column of $\mathbf{W}(t^*)$.

The phase sensitivities $\boldsymbol{\delta}(t)$ were computed for all parameters for one period of time. The resulting time trajectories are shown in Figure 3-6 both in scaled form ($p_j\delta_j(t) = \frac{\partial \phi}{\partial \ln p_j}\Big|_t$) and in normalized form ($\delta_{j,norm}(t) = \frac{\delta_j(t)}{\max_t(\delta_j(t))}$). The fact that the normalized δ-trajectories appear to occur in groups of similar shape will be investigated in detail in Section 3.3.8.

The phase sensitivites $\boldsymbol{\delta}$ were rank ordered. In order to capture their importance over the entire range $0 \leq t \leq T$, their AUC was computed and used for the ranking. Plotted in Figure 3-7 is however the maximum magnitude of any given δ-trajectory in order to allow for more meaningful comparison. (This sometimes leads to the rankings not being monotonically decreasing as one would usually expect.) It is interesting to see that in the basic model, the positive feedback loop participates significantly in the phase setting, but not in the period setting. It is more difficult to assess this for the extended model, due to the sharing of reactions in the positive and negative feedback loops in series, with only

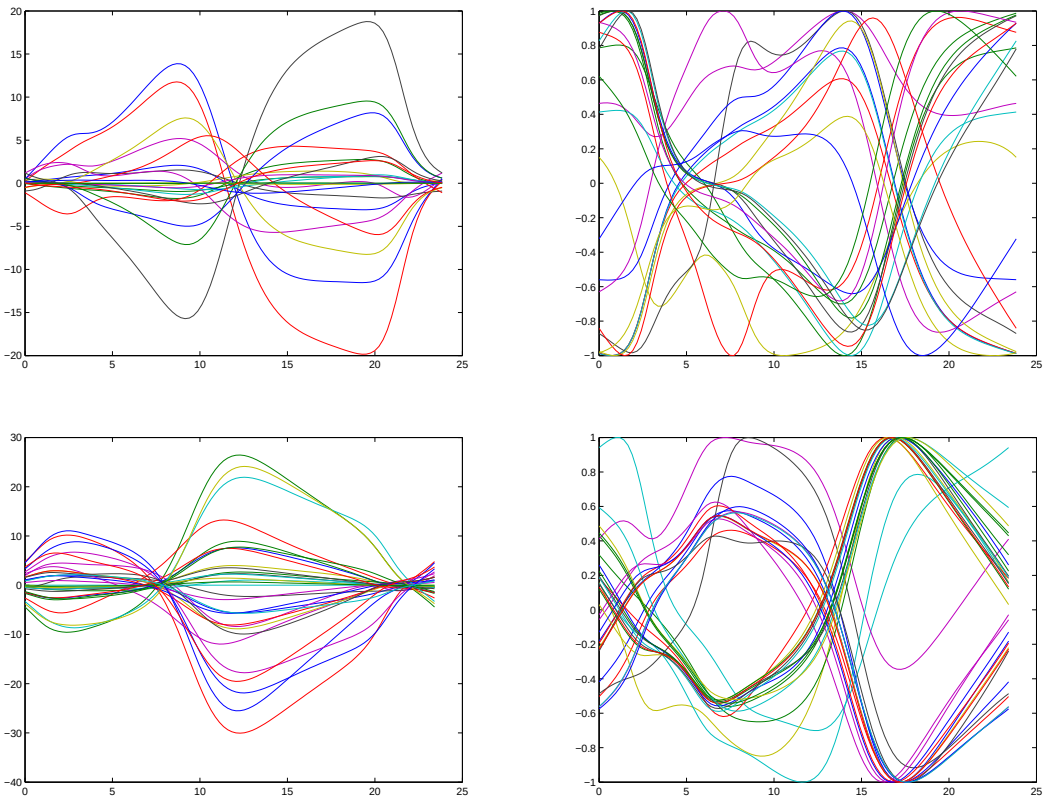

Figure 3-6: Left: Scaled phase sensitivities ($p_j\delta_j(t) = \frac{\partial\phi}{\partial lnp_j}\Big|_t$) over one period of time; Right: Normalized phase sensitivities ($\delta_{j,norm}(t) = \frac{\delta_j(t)}{\max_t(\delta_j(t))}$) over one period of time; Top: Basic model; Bottom: Model with REV-ERBα loop.

one parameter being unique to the positive feedback loop. That said, this single parameter plays a more prominent role in phase setting than in period setting. While the secondary negative feedback loop participates in the period setting as well, its influence is markedly larger in the phase sensitivites also.

3.3.7 Phase Sensitivities for Alternative Parameter Sets

In comparison to the period sensitivity rankings shown in Figure 3-8, the phase rankings show a stronger influence of positive feedback overall. This is easy to distinguish in the basic model. In the extended model, influences outside the first negative feedback loop are also much more prominent in the phase sensitivity rankings than in the period sensitivity rankings. The role of the positive feedback loop, however, cannot be distinguished as easily.

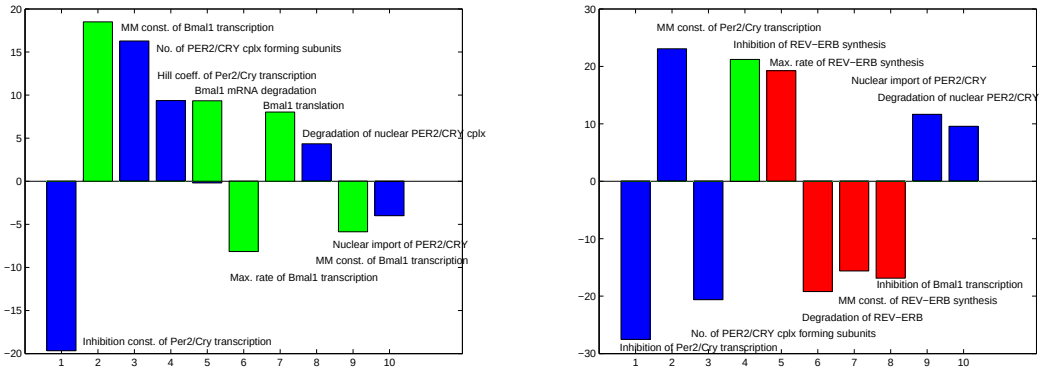

Figure 3-7: Top 10 peak, scaled phase sensitivities $\max\|\frac{\partial\phi}{\partial \ln p_i}\|$, ranked by absolute area under the curve. Left: Basic model; Right: Model with REV-ERBα loop. Blue: Negative feedback loop - BMAL1* controls Per2/Cry expression. Green: Positive feedback loop of Bmal1 on itself (through Per2/Cry and Rev-Erbα if applicable). Red: Negative feedback loop where BMAL1 controls REV-ERBα expression

The parameter indices for the top ten ranked parameters for all alternative parameter sets are included in Tables A.2 and A.3. In the basic model, the phase sensitivity rankings are most often dominated by parameters 3 (inhibition constant of Per2/Cry transcription) and 14 (MM constant of Bmal1 transcription), followed by 12 (degradation of nuclear PER2/CRY) and 15 (Hill coefficient of Bmal1 transcription).

In the extended model, the dominant parameters are 12 (degradation of PER2/CRY in the nucleus), 8 (number of PER2/CRY complex forming subunits), 25 (maximal rate of REV-ERBα synthesis), 29 (degradation of REV-ERBα), but the trend is modest and, again, the rankings are not in particularly close agreement with the nominal parameterization.

3.3.8 Phase Sensitivity Clusters

Here we apply the idea of sensitivity similarities described in Section 3.2 to the phase sensitivities $\boldsymbol{\delta}$. Upon inspection of the normalized phase sensitivities $\delta_{i,norm}(t) = \frac{\delta_i(t)}{\max_t \delta_i}$, where $\delta_i = \frac{\partial\phi}{\partial p_i}$, the sensitivities appear in groups of approximately similar trajectories over $0 \leq t \leq T$ (see Figure 3-6). The δ-trajectories were formally clustered into these groups as described in Section 3.2, with the aim of understanding which parameters have similar function in the network with respect to local acceleration and deceleration, and how many different groups exist (Figure 3-9). A first observation is the fact that most trajectories fall into the first mode. This is a general property of PCA-based clustering of data. PCA

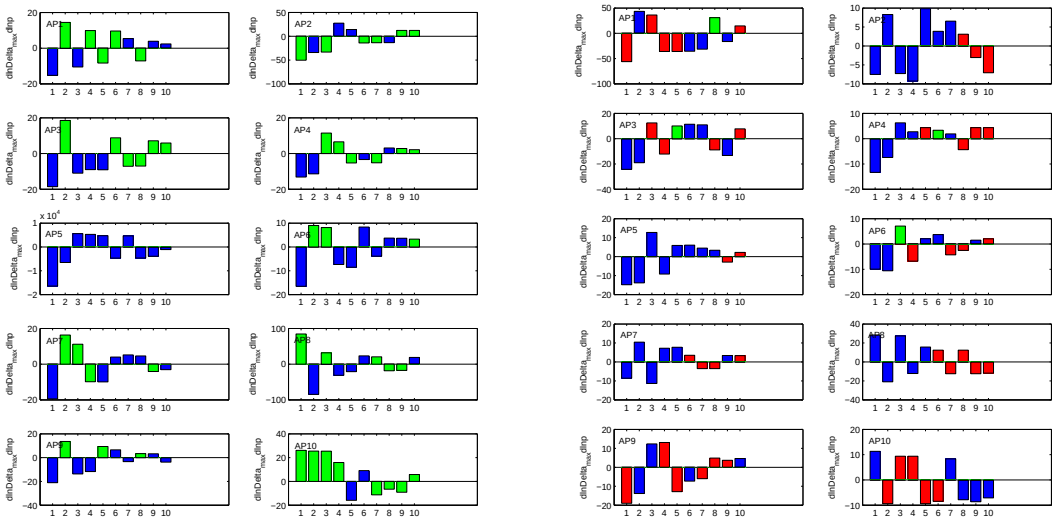

Figure 3-8: Top 10 peak, scaled phase sensitivities $\max\|\frac{\partial\phi}{\partial \ln p_i}\|$, rank ordered by absolute AUC for all alternative parameter sets in the basic model (left) and the model with Rev-Erbα (right). Blue: Negative feedback loop — BMAL1* controls Per2/Cry expression. Green: Positive feedback loop of Bmal1 on itself (through Per2/Cry and Rev-Erbα if applicable). Red: Negative feedback loop where BMAL1 controls REV-ERBα expression.

aims to explain as much as possible of the data using the first component. Nonetheless, the significance of the populations in the less populated modes, called "rare" modes, is discussed throughout the remainder of the chapter. The choice of PLC used to define the time $t = 0$ and to compute the δ-trajectories has an impact on the trajectories themselves, as shown in Theorem 2 (Chapter 2). Therefore, all phase-based clustering was repeated for a second PLC, using the nominal parameterizations for both models. The number of modes in a given parameterization, parameters in "rare" modes or large magnitude parameters appeared invariant to the choice of PLC (data not shown). It appears that even though the exact shape of the δ-trajectories depends on the PLC, their similarity properties do not depend on the PLC and are a function of the network model and parameterization only.

The basic model appears to have more modes than the extended model (Figure 3-9). Its latent roots (eigenvalues associated with the principal components) are also less strongly localized (i.e., the first component is less dominant) on the first mode than as in the extended model. The fact that the first mode dominates the phase sensitivities in the extended model also makes for lower intra-cluster variation. The question comes to mind if this property is specific to the given parameterization or inherent in the network structure.

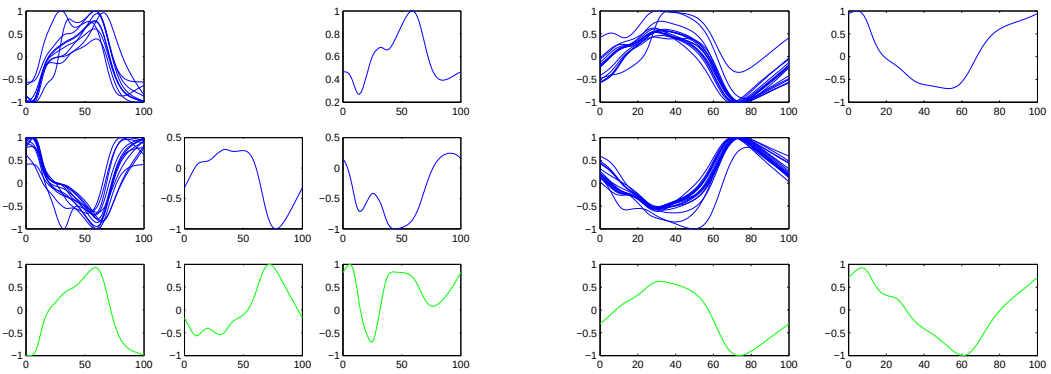

Figure 3-9: PCA based clustering of the normalized δ-trajectories over one period T. The time scale is normalized to $0 \leq \hat{t} \leq 100$. Each column represents once principal component. Top row: trajectories within the mode. Second row: trajectories within the "anti-mode". Bottom row (green): Principal component or cluster centroid. The latent roots in percent for each cluster are: Basic model (left): (87.5%, 10.3%, 1.0%); Extended model (right): (92.5%, 6.5%).

This is addressed in Section 3.3.9.

3.3.9 Phase Sensitivity Clusters for Alternative Parameter Sets

The same clustering based on sensitivity similarities was performed on all models with alternative parameter sets. It was found that in both network architectures, some parameterizations were found that led to several modes, versus in others few modes were populated. In general, it appears as though the number of significant modes is a function of network parameterization, and not of network architecture. This is especially surprising given that the current literature suggests a link between the number of feedback loops and phase flexibility [85].

In the basic model, one trend observed is that strong participation of the positive feedback loop in the period setting correlates with few modes in the phase sensitivities and the absence of a steep decline in the period sensitivites. I.e., a model parameterizer in this way can only do one thing. The situation in the extended model is harder to analyze. There appears significant freedom to establish quasi-24-hr oscillations using different types of strategies, as judged by the period sensitivities and the differing numbers of modes for the alternative parameter sets.

It appears that in many cases, there is a pair of one dominant mode and its anti-

mode, and then a few parameters that populate other, "rare" modes. It was observed that certain parameters appeared in those "rare" modes more often than others. For the basic model, those parameters included, in order of frequency, the transcription of Per2/Cry, the degradation of nuclear PER2/CRY as well as BMAL1 activation. The "rare" modes in the extended model are most often populated by the Per2/Cry transcription rate and the nuclear export rate of PER2/CRY. Of interest in this context is the fact that light input is thought to act through the regulation of Per trancription [26, 77]. As discussed previously, an alteration in a rate that belongs to a "rare" mode cannot be compensated by the network, and hence this choice of intervention point might be excellent if the network must undergo a phase shift, such as during jet lag.

Another interesting correlation was that one of the "rare" modes in the nominal parameteriztions for the basic model was populated by the activation rate of nuclear BMAL1. The (de)activation rates of Bmal1 was found in Section 3.3.11 to be crucial in the ability of the model to modify several of its relative phases without changing the period. The "rare" mode in the extended model was populated by the concentration of constitutively active BMAL1. This parameter was also found to play a significant role in the ability to modify a phase without altering the period, as discussed in Section 3.3.11. This could indicate that the existence of rare modes might be relevant in the context of phase modification.

In the extended model, a group of parameters often formed a secondary more populated mode and antimode pair involving a group of parameters that regulates the amount of REV-ERBα produced. This second, more populated mode often (but not always) included the reaction that is unique to the positive feedback loop (the inhibition constant of REV-ERBα synthesis). In the basic model, a second, higher populated mode is rarely found. It could be hypothesized that depending on the parameterization, an extra feedback loop could add the possibility of a second, robust (i.e., populated more than once) mode.

3.3.10 Angular Relative Phase Sensitivities

Circadian biology often discusses the following question: Given that the length of subjective day is not constant throughout the year (unless one lives on the equator), can the biological clock track dawn and dusk separately, and can it adjust its molecular events accordingly? In the models under study here, the impact of light is not represented. Thus, a more indirect method of analysis is needed that allows study of the model's ability to track different

phases. In this work, we cast this biological question in such a way that it is amenable to mathematical analysis. A relative phase in the mathematical context of this work is the angular phase γ (Eq. (3.4)) between two events relative to the period. The two events are defined by equations that describe the molecular events occurring at dawn and dusk. The dependency of this angular phase with respect to the model parameters is then calculated and compared to the dependency of the period on the same parameters. This analysis reveals the existence of mechanisms for changing the relative phase relationship of dawn and dusk wiht constant length of day. We term this relative phase flexibility.

Because it is not known how the circadian clock is read, or where its outputs are, the molecular events defining "dawn" and "dusk" are somewhat difficult to chose. As discussed in the Introduction, the minimum of Per2/Cry mRNA was chosen as the dawn time reference CT=0. From a survey of the experimental and review literature, the following molecular events happen at or near CT=12, or dusk. Bmal1 mRNA has risen half-way to its maximum concentration [83, 8, 87], Cry1 mRNA is near its highest concentration [8, 87], and Per1 and Per2 mRNA have declined to roughly half their peak concentrations [8, 87]. In order to evaluate the relative phase flexibility of the mammalian circadian models under study, each of these three molecular events were chosen as the second the PLC, and the results were compared. Note that this selection of PLCs contain some that relate to times at which concentrations cross an absolute threshold, rather a relative definition with respect to its peak level. This difference could result in a different phase sensitivity result, even if the same exact phase was detected. The results are shown in Figure 3-10, where the scaled angular relative phase sensitivities are shown in comparison to the period sensitivities and the amplitude sensitivities of the BMAL1* protein concentration in both models. In order to compare the network performance in the different scenarios, the angular phase sensitivities were scaled and ranked by absolute magnitude.

Tables 3.5 and 3.6 show that the high angular relative phase sensitivities are associated with overlapping but somewhat different sets of reactions for each choice of "dusk" PLC. Thus, it will be important to experimentally determine how the "dusk" and "dawn" signals are processed on the molecular level. Several of the reactions found to be important are involved in Per2/Cry transcriptional regulation (parameters # 2, 3, 5). The current partial understanding of light processing in the circadian clock has light input eventually resulting in increases transcription of Per1 and Per2 [26]. In the basic model, the high sensitiviy

Table 3.5: Rankings of parameters by magnitude of scaled angular relative phase sensitivities $\frac{\partial \ln \gamma}{\partial \ln \mathbf{p}}$ in the basic model. The parameter indices of the top ten sensitivities are shown.

PLC ("Dusk")	1	2	3	4	5	6	7	8	9	10
max of Per2/Cry mRNA	5	8	12	10	6	14	11	24	1	16
Bmal1 mRNA at 50%	8	14	3	5	13	15	12	16	10	24
Per2/Cry mRNA at 50%	5	3	7	12	6	14	9	8	2	17
ranking for $\frac{\partial \phi}{\partial \ln \mathbf{p}}$	3	14	8	5	16	13	15	12	17	10
ranking for $\frac{\partial \ln T}{\partial \ln \mathbf{p}}$	10	5	6	8	12	9	14	11	24	15

Table 3.6: Rankings of parameters by magnitude of scaled angular relative phase sensitivities $\frac{\partial \ln \gamma}{\partial \ln \mathbf{p}}$ in the extended model. The parameter indices of the top ten sensitivities are shown.

PLC ('Dusk')	1	2	3	4	5	6	7	8	9	10
max of Per2/Cry mRNA	8	5	2	27	29	31	25	3	26	12
Bmal1 mRNA at 50%	8	27	29	2	31	25	3	26	5	10
Per2/Cry mRNA at 50%	3	2	12	27	29	25	31	5	7	26
ranking for $\frac{\partial \phi}{\partial \ln \mathbf{p}}$	3	2	27	8	25	29	26	31	10	12
ranking for $\frac{\partial \ln T}{\partial \ln \mathbf{p}}$	10	8	5	6	2	27	25	31	29	3

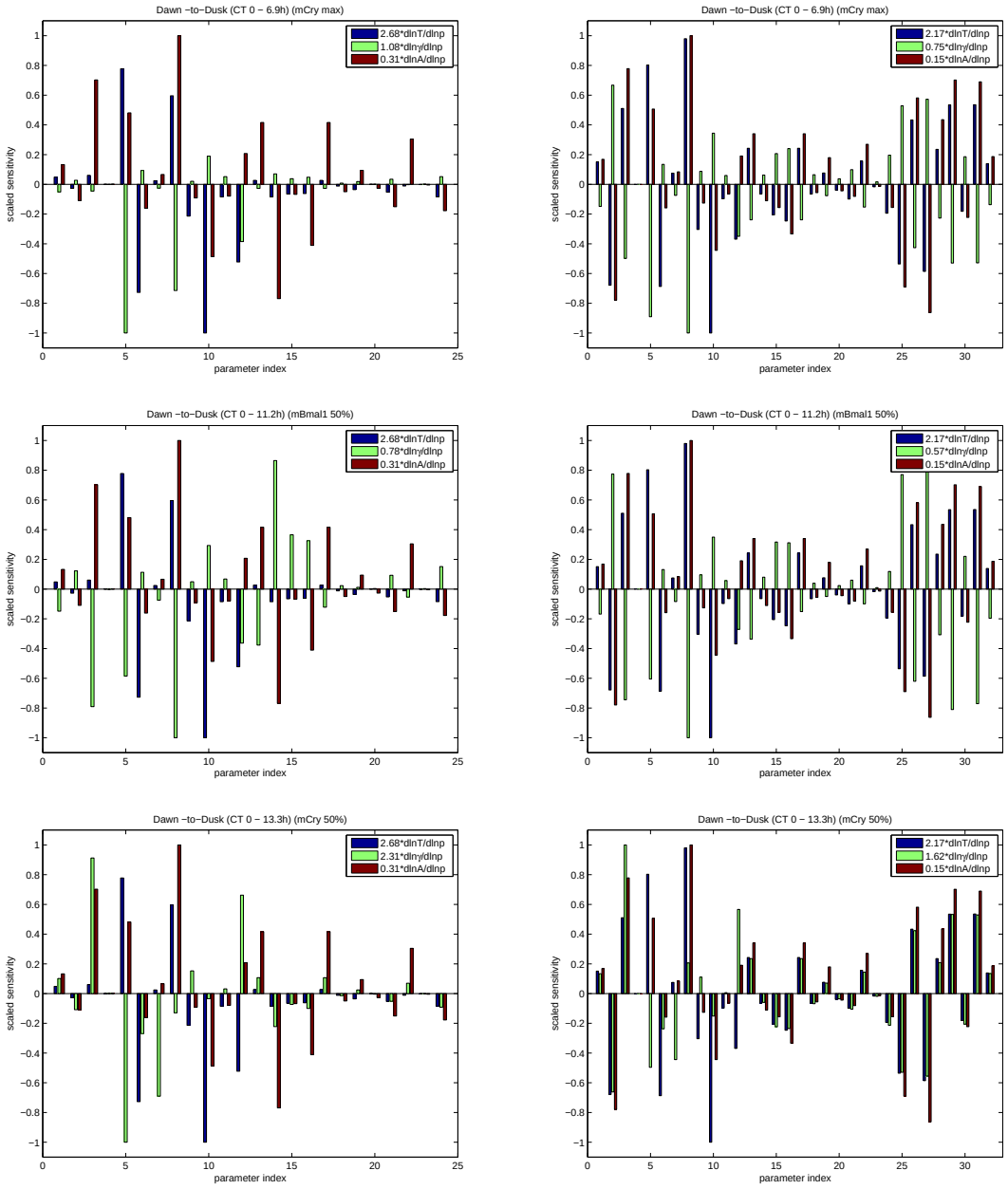

Figure 3-10: Relative, scaled angular phase sensitivities, amplitude sensitivities and period sensitivities in comparison. The period sensitivities for each parameter are plotted in blue, the angular relative phase sensitivites alone in green, the amplitude sensitivities for the amplitude of Bmal1* in red. Left: Basic model; Right: Extended model. Top: Definition of "dusk" is the maximum concentration of Per2/Cry mRNA; Middle: Definition of "dusk" is the point where Bmal1 mRNA exceeds 50% of its maximum concentration; Bottom: Definition of "dusk" is the point where Per2/Cry mRNA is less than 50% of its maximum concentration.

Table 3.7: Relationships between the vector $\left(\frac{\partial \beta}{\partial \mathbf{p}}\right)_T$ and the vector $\frac{\partial T}{\partial \mathbf{p}}$ for both the extended and the basic model.

PLC ('Dusk')	β (Basic)	L	α	β (Extended)	L	α
mCry1 max	6.91	0.296	51.5	6.85	0.380	50.2
50% of mBmal1	10.65	0.783	77.1	11.23	0.520	52.3
50% of mPer2	13.08	0.430	48.0	13.32	0.500	25.2

parameters are located primarily in the negative feedback loop (parameters # 1–12) with some participation of the positive feedback loop. In the extended model, the parameter unique to the positive feedback loop, # 27, is prominent, as are other parameters that belong to the positve and secondary negative feedback loop.

In principle, an important functional constraint of circadian rhythm networks is the ability to adjust phase and amplitude relationships without changing the period. Constant-period phase perturbations were explored by computing the angle and relative length of a period-neutral sensitivity vector as described in Section 3.2. The results of this calculation are shown in Table 3.7. Both models show period-neutral phase sensitivities of considerable magnitude and orthogonality. The most freedom appears to be in the timing between the "dawn" defined in terms of mCry1, and "dusk" defined in terms of mBmal1. The increased flexibility found in the Bmal1 part of the network is also found in the following section.

Model-wide Relative Phase Sensitivity Analysis

Having found in Section 3.3.10 that several relative phases appear to have significant sensitivity in the period neutral direction, one wonders if relative phase flexibility is a network wide property or if some relative phases are more flexible than others. In order to obtain a more exhaustive picture of the constant-period phase flexibilities, the sensitivities for the relative phase of the concentration peak for each species with that for each other species was computed. Each sensitivity vector was evaluated for its orthogonality to the period sensitivity vector. The relative length L of the projected vector is given in Tables 3.8 and 3.10 for each of the models. The angle α between the relative phase sensitivity vector and the period sensitivity vector for each phase is reported in Tables 3.9 and 3.11 for both models.

Table 3.8: Relative length of period-neutral peak-to-peak sensitivity to the period sensitivity vector $L = \left\| \left(\frac{\partial \beta}{\partial \mathbf{p}} \right)_T \right\| / \left\| \frac{\partial T}{\partial \mathbf{p}} \right\|$ from the peak of each species to the peak of each other species in the basic model. (n) indicates nuclear location, (c) indicates cytosolic location.

Species	P/C(c)	P/C(n)	mB(n)	B(c)	B(n)	B*(n)
Per2/Cry mRNA(n)	0.096	0.024	0.025	0.107	0.150	0.2451
PER2/CRY(c)		0.096	0.098	0.145	0.181	0.271
PER2/CRY(n)			0.026	0.115	0.160	0.264
Bmal1 mRNA(n)				0.107	0.155	0.256
BMAL1 (c)					0.150	0.241
BMAL1 (n)						0.211

Table 3.9: Angle $\alpha_{i,j}$ between peak-to-peak sensitivity vector and the period sensitivity vector, where $\sin(\alpha_{i,j}) = \left\| \left(\frac{\partial \beta_{i,j}}{\partial \mathbf{p}} \right)_T \right\| / \left\| \frac{\partial \beta}{\partial \mathbf{p}} \right\|$, from the peak of each species i to the peak of each other species j in the basic model. (n) indicates nuclear location, (c) indicates cytosolic location.

Species	P/C(c)	P/C(n)	mB(n)	B(c)	B(n)	B*(n)
Per2/Cry mRNA(n)	45.9	4.2	4.3	15.5	18.8	21.4
PER2/CRY(c)		22.8	22.7	26.3	27.5	27.0
PER2/CRY(n)			78.4	60.5	52.9	41.0
Bmal1 mRNA(n)				60.9	53.1	40.6
BMAL1 (c)					69.4	45.3
BMAL1 (n)						49.0

It is notable that in both models, there is a wide spread of values for both orthogonality metrics. The angle between relative phase direction and period direction ranges from 4.2° to 78.4° in the basic model, and from 3.4° to 64.8° in the extended model. The relative length of the period-neutral phase vector in comparison to the period vector ranges from 2.6% to 27.1% in the basic model and from 1.4% to 27.1% in the extended model. In both models, the phase with the largest angle has a very short length. However, this is not a general trend. Some phases have small angles and small lengths. A notable example of this in both models is the time difference between the peaks in Per2/Cry and Bmal1 mRNA. It appears that the relative phase between both mRNAs is fixed once the period is fixed. This insight is particularly interesting in light of experimental observations indicating that much

Table 3.10: Relative length of period-neutral peak-to-peak sensitivity to the period sensitivity vector $L = \left\| \left(\frac{\partial \beta}{\partial \mathbf{p}} \right) T \right\| / \left\| \frac{\partial T}{\partial \mathbf{p}} \right\|$ from the peak of each species to the peak of each other species in the extended model. (n) indicates nuclear location, (c) indicates cytosolic location.

Species	P/C(c)	P/C(n)	mB(n)	B(c)	B(n)	B*(n)	RE(n)
Per2/Cry mRNA(n)	0.047	0.017	0.021	0.086	0.140	0.150	0.154
PER2/CRY(c)		0.050	0.052	0.100	0.149	0.156	0.160
PER2/CRY(n)			0.014	0.081	0.135	0.155	0.170
Bmal1 mRNA(n)				0.080	0.140	0.165	0.172
BMAL1 (c)					0.127	0.175	0.207
BMAL1 (n)						0.129	0.238
BMAL1*(n)							0.164

of the phase control in the mammalian clock happens on the posttranslational level [33]. One hypothesis is that the mRNA level provides the underlying rhythm, while the details are regulated on the posttranscriptional level, which might be easier to adjust "on the fly".

When the largest angles in both models are analyzed, it appears that they are between the peaks of consecutive species in the molecular wiring of the positive feedback loop, from PER2/CRY in the nucleus to the Bmal1 mRNA in the cytosol, and the BMAL1 in cytosol and nucleus. Interestingly, the large angles "skip" the step through REV-ERBα in the extended model (which participates in a second, negative feedback loop). This observation might suggest that a positive feedback loop adds relative phase flexibility to a relatively static negative feedback loop. It is shown in the experiments of Section 3.3.11 that the angle is indeed the more significant indicator of flexibility, and that the length plays a less important role.

3.3.11 Can the Network Modify a Phase Over a Wide Range, Without Altering the Period?

Sensitivity information is local information; it is only valid for an infinitesimal perturbation from the point at which it was calculated. Thus, it is important to also examine whether local sensitivity information extends for larger parameter variations, such as those potentially undertaken by an organism either undergoing evolution or temporarily altering network performance to adapt to a change in environment. On a methodological level,

Table 3.11: Angle $\alpha_{i,j}$ between peak-to-peak sensitivity and the period sensitivity vector, where $\sin(\alpha_{i,j}) = \left\| \left(\frac{\partial \beta_{i,j}}{\partial \mathbf{p}} \right)_T \right\| / \left\| \frac{\partial \beta}{\partial \mathbf{p}} \right\|$, from the peak of each species i to the peak of each other species j in the extended model. (n) indicates nuclear location, (c) indicates cytosolic location.

Species	P/C(c)	P/C(n)	mB(n)	B(c)	B(n)	B*(n)	RE(n)
Per2/Cry mRNA(n)	27.7	3.4	4.2	12.7	15.6	9.3	7.5
PER2/CRY(c)		14.4	14.7	18.7	19.8	10.7	8.4
PER2/CRY(n)			64.8	38.8	31.5	13.8	10.9
Bmal1 mRNA(n)				37.7	32.2	14.6	11.0
BMAL1 (c)					46.9	18.2	14.8
BMAL1 (n)						17.5	19.6
BMAL1*(n)							7.5

it is also of interest to evaluate which of the two measures, α or L, computed in Section 3.3.10 corresponds better the ability of the network to modify the phase without altering the period.

Three relative phases in the basic model were selected for comparison. The relative phase β_1 with the largest angle $\alpha = 78.4°$ (but one of the shortest relative lengths $L = 0.026$) found in the basic model was the timing between the peak in nuclear PER2/CRY and Bmal1 mRNA. The relative phase β_2 with the longest relative length ($L = 0.271$) and a smaller angle ($\alpha = 27°$) was the time between the peaks of PER2/CRY complex in the cytosol and of BMAL1* activated transcriptional activator in the nucleus. Third, the relative phase β_3 with the smallest angle ($\alpha = 4.2°$) and the shortest relative length ($L = 0.024$) was between the peaks of Per2/Cry mRNA and nuclear PER2/CRY.

The question was, how far can the network take the process of adapting a phase without altering the period? To this end, a very rudimentary optimization procedure was implemented in which a small, constant size step in the direction of the period-neutral relative phase sensitivity was taken in parameter space. The step size was kept constant at $\Delta\mathbf{p} = \mu \left(\frac{\partial \beta}{\partial \mathbf{p}} \right)_T$. The step length μ was selected based on L, if L was larger, the step size μ was chosen smaller, and vice versa, to avoid going too far from the nominal point in one step. At the new parameterization, the new period and phase were determined and recorded. Then all sensitivities were recomputed and a new, period-neutral direction was found. This procedure was repeated until the period changed over 1% away from the

original value or no oscillation was detected at the new parameterization. At this point, the algorithm terminated. The resulting trajectories are represented in Figure 3-11, left column. The parameters at the end points were compared to the original parameters in Figure 3-11, right column.

The network has no trouble adapting the relative phase β_1 by as much as 93% (corresponding to a change by 1.3 hours) without disturbing the period by more than 1%. The relative phase β_2 could be modified by 13.3%, which corresponds to an absolute change of 2.2 hours. Interestingly, the same two parameters were largely responsible for this change as the change in β_1, even though the relative phase under study is in a different part of the network.

The relative phase β_3 could be modified by only 3.5% or 0.3 hours, neither a significant relative nor absolute amount. Parameter #23 was the main effector of this small change. If the first and third relative phases are compared, it appears that the angle α is important in measuring the ability of the network to adapt the phase without changing the period. Both relative phase sensitivities have almost the same length, yet one is signigficantly more flexible than the other.

All numerical experiments were repeated with half the stepsize ($\mu = 0.005$ or $\mu = 0.0005$, respectively. The results were only slightly different in that the first relative phase β_1 (large α, small L) was modified from 1.43 h to 2.66 h instead of 2.75 h, β_2 (large L, medium α) was modified from 17.02 h to 19.40 h instead of 19.28 h, β_3 (small α, small L) was modified by the exact same amount. This leads to the conclusion that the step sizes that were chosen originally lead to a reasonable representation of what the network can do.

The relative phase with the wider angle and shorter length could be modified by a larger relative amount (92% vs. 13%) but a smaller absolute time (1.3 h vs. 2.3 h) than the second phase with a medium angle and a longer length. Both phases can be changed to a significant degree. Interestingly, only two parameters are used to regulate all relative phases, as is seen in Figure 3-11, right hand sides, respectively. These two parameters, #11 and #23, are the rates of nuclear export of PER2/CRY and deactivation of BMAL1*. The eleventh parameter ranks eighths in scaled period sensitivities, but neither parameter's period sensitivity is very large in comparison to the top ranked. Both parameters represent processes in the network where posttranslational modification has been shown to play a role. PER2 phosphorylation by casein kinase I is shown to control nuclear trafficking and

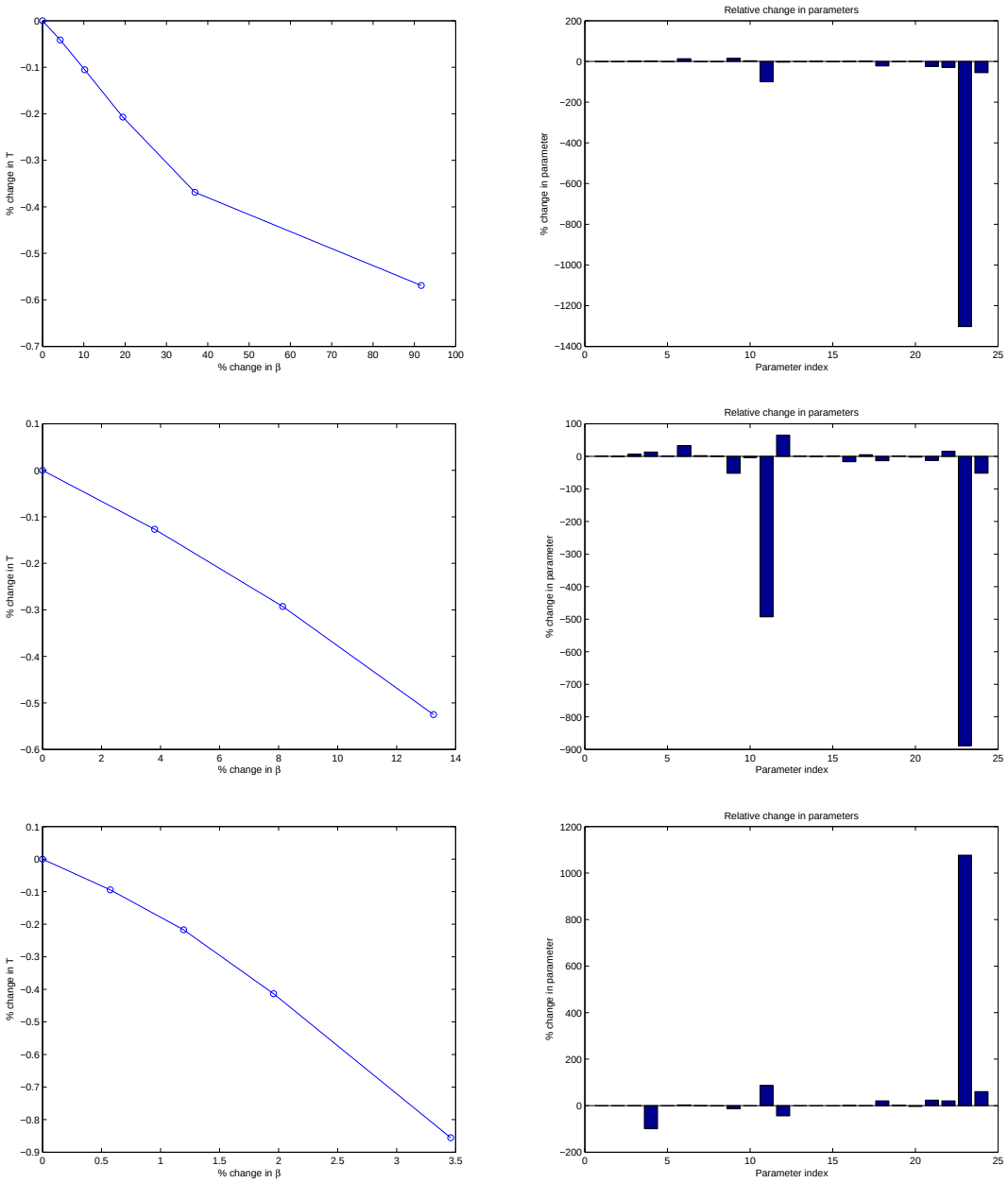

Figure 3-11: Trajectory of change of period and phase (left) and parameter changes (right) from a simple optimization aimed to increase three different phases β as much as possible without disturbing T more than 1%. Top: The phase $\beta_1 = 1.43h$, with the largest angle $\alpha = 78.4°$ and short length $L = 0.026$. The step size chosen was constant at $\mu = 0.01$. Middle: The relative phase $\beta_2 = 17.02h$, with the largest length $L = 0.271$ and intermediate size angle $\alpha = 27.0°$. The step size chosen was constant at $\mu = 0.001$. Bottom: The relative phase $\beta_3 = 7.46h$, with the smallest angle $\alpha = 4.2°$ and shortest length $L = 0.024$. The step size chosen was constant at $\mu = 0.01$

degradation [103]. The (de)activation step of BMAL1 is the binding of CLOCK, which is phosphorylated rhythmically as well [88]. The role of these two parameters is discussed further in Section 3.3.12.

3.3.12 The Length of Subjective Day in the Face of a Constant 24-hour Period

The significance of the length of subjective day and the calculation of its sensitivity was discussed in Section 3.3.10. To understand to what extent this sensitivity information is relevant in a biological context, it was studied how wide the quasi-linear region around the nominal point is for each model, in other words, how far can one walk into the period-neutral phase direction without losing its property of period-neutrality. This numerical experiment is different from the previous one in that the period neutral direction is not recalculated at each step, but rather steps are only taken in one direction. The phase tracked in this experiment was the first definition for the "dawn-to-dusk" time span, i.e., the time β between the minimum and the maxium of Per2/Cry mRNA. Both the basic and the extended models have significant angles α and lengths L of their period neutral phase sensitivity vector corresponding to this phase. The parameters with high relative phase sensitivity in the basic model typically also have significant period sensitivities, whereas in the extended model, parameters can be found that have limited period sensitivity but significant relative phase sensitivity (Figure 3-10). Can this correlation be used to evaluate whether the model can, through finite modification to rate constants, modify the relative phase without changing the period?

From the nominal parameterization of each model, steps in the period-neutral direction were taken, and the resulting period and phase change were recorded. The step size (always referring to distance from the nominal point, not from the previous point) was varied in the following increments: 0.00001, 0.00005, 0.0001, 0.0002, 0.0005, 0.001, 0.002, 0.005.

Results are shown in Figure 3-12 for both models. It is clear that the same relative step length μ results in much larger changes in the extended model, even thought the relative lengths L of both period-neutral relative phase sensitivities is only a factor 3 apart. In fact, for the extended model, no step size can be identified that would modify the phase β by a significant amount without also disturbing the period by a significant amount. It appears that the extended model is more non-linear in the sense that a slightly too large step in

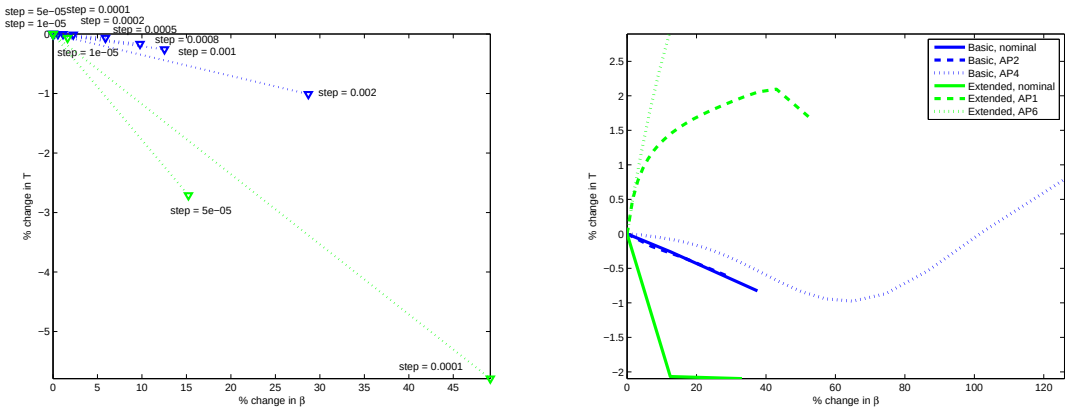

Figure 3-12: Period and "dawn-to-dusk" phase change after a finite parameter disturbance. Left: Steps of different size μ in the period-neutral phase direction for the nominal parameterization. Blue: Basic model; Green: Extended model. Right: Step-wise optimization of phase length while period is kept constant, for both nominal models and 2 alternative parameterizations each. Step size was constant at $\mu = 0.0001$ for all models, and at each point, the period-neutral search direction was recalculated.

what is the locally period-neutral direction results in significant period change, whereas in the basic model, a step with similarly sized change in phase is still causing a period change below 1%. It is intuitive that an additional feedback loop, in particular one with highly nonlinear terms, would add nonlinearity to the model.

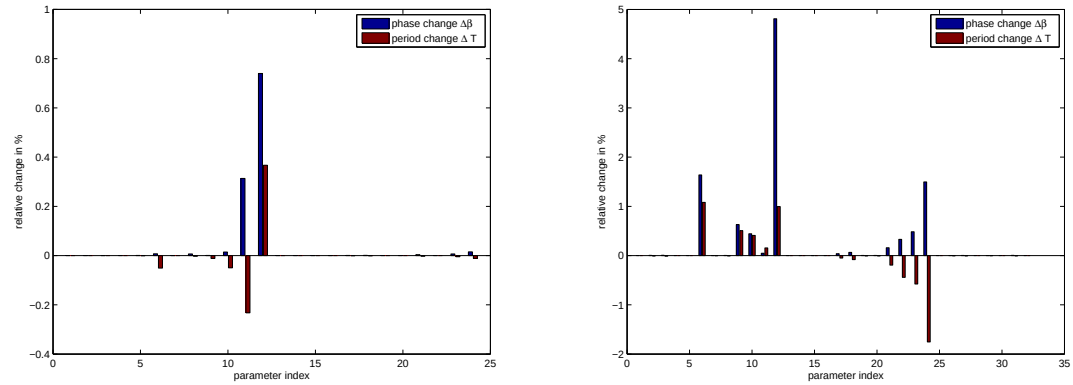

Figure 3-13: Mechanism of a period-neutral step in the phase direction. Shown is the relative change in % for each parameter. Left: Basic model; Right: Extended model

The mechanism behind a single step in the phase-neutral relative phase direction is visualized in Figure 3-13. In both cases, a small number of parameters are modified sig-

nificantly and produce both a change in relative phase and period. The relative change in phase is always positive, whereas the changes in period add up to a very small total change. It is interesting to see that in the extended model the number of changed parameters is larger by more than a proportional amount (given that the extended model has 33% more parameters in total). The mechanism for the maximum period-neutral phase change is more involved and requires a larger number of network-wide changes than in the basic model. In the basic model, a pair of reactions — the nuclear export rate and the degradation rate of the PER2/CRY complex — can accomplish the phase-neutral step almost completely. In the extended model, it appears as though two groups of parameters in two different parts of the network are necessary to make the period-neutral shift.

As a second experiment, the optimization procedure presented in Section 3.3.11 was repeated for this "dawn-to-dusk" relative phase definition. The step size was kept constant at $\Delta\mathbf{p} = \mu \left(\frac{\partial\beta}{\partial\mathbf{p}}\right)_T$. For the basic model experiments, the magnitude of the step change was $\mu = 0.001$, which always sufficed to produce at least one "feasible step" in parameter space, resulting in a period changed less than 1%. The numerical simulation shown in Figure 3-12 (right, solid blue line) indicates that the basic model is able to increase this relative phase by up to 35% without disturbing the period by more than 1%, corresponding to a change in phase of almost 3 hours. At the next step, the model left the oscillatory region and the algorithm terminated. It is astonishing to see the ability of a very small model to perform this task, even more so when one looks at the resulting parameterization in Figure 3-14.

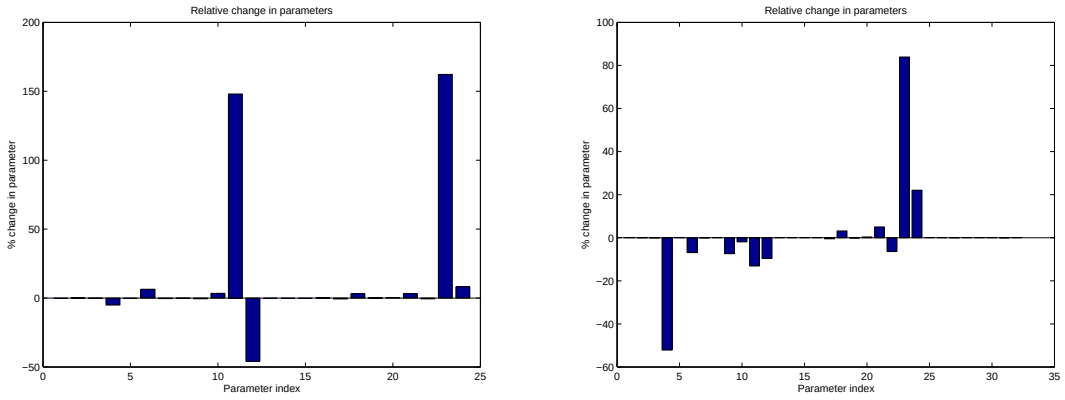

Figure 3-14: Relative parameter changes in % between beginning and end of the period-neutral phase change shown in Figure 3-12, right, for both nominal models. Left: Basic model; Right: Extended model

Only 3 parameters are changed significantly to effect this balanced change. These parameters are #23, #11 and #12, the rates of BMAL1* deactivation, and PER2/CRY nuclear export and degradation, as ordered by magnitude. The latter two parameters are ranked eighth and fifth for their period sensitivities, and similarly for their phase sensitivities; however, as seen in Figure 3-10 (top left), the period or relative phase sensitivities of the two most significant paramters (11 and 23) are not large. This suggests that a period-neutral phase modification might be a process that is somewhat uncoupled from the setting of the period (which is intuitive) *and* the setting of the phase (which is counter-intuitive). It is also interesting to note that the four different phases in the basic model that were considered in this study (Section 3.3.11 and here) are regulated in very similar ways. It could be hypothesized that the timing of most relative phases in the face of constant period of oscillation might be centrally controlled and uncoupled from the period control.

It is especially intriguing to see that the parameters with the largest impact are ones that are accessible to outside modification. The stability and nuclear localization of Per2 was shown previously to be of crucial importance and is regulated by a complicated phosphorylation pattern, which was shown to have an influence on both period and phase [103]. This phosphorylation pattern is caused by the casein kinase I family, which is the target of several signaling pathways [84]. The status of activation or inactivation of BMAL1* (which represents the BMAL1-CLOCK-complex (BCC)) depends on the availability of CLOCK. CLOCK is an essential component of the mammalian circadian clock, though its concentration does not exhibit a circadian rhythm [65]. It appears instead that CLOCK is rhythmically phosphorylated in at least 4 different forms [65, 105], which might affect its stability and nuclear trafficking [88]. In *Drosophila* it was shown that several input pathways, including the Ras and MAPK pathways, can regulate the activity of CLOCK [105].

The experiment was repeated for the extended model. The step size had to be reduced from $\mu = 0.001$ (at which level, no step could be taken without leaving the oscillatory regime, indicating a greater nonlinearity in the model behavior. Even with a new step size of only $\mu = 0.0001$, the phase could not be modified on the first step until the period was altered over 1%. Consequently, the threshold was raised to 3% permissible period alteration, and the results are shown in Figure 3-12 (right, green solid line). The phase was changed from CT=6.85 hours to CT=9.12 hours while the period changed from T=23.41 hours to T=22.92 hours. The next step resulted in a period of T=27.58 hours at which point the

algorithm terminated. Again, the right half of Figure 3-14 shows that only a fraction of the parameters are modified significantly. The most significant parameter changes were again #23, the deactivation rate of BMAL1* followed by parameter #4, the concentration of constitutive BMAL1*. Less significantly but not negligibly, the parameters 24 (BMAL1 activation), 11 and 12 (nuclear export and degradation of PER2/CRY) were modified as well. From the central role of the activity status of BMAL1, it could be hypothesized that the phosphorylation of CLOCK [65, 105] represents an opportunity for the network to modulate relative phase without greatly affecting the period, possibly together with the phosphorylation of PER2 which regulates its nuclear trafficking and degradation.

It is interesting that the extended model has less capability to modify this phase without the period, when one notices also that in this network the period sensitivities are less localized in the Per-related negative feedback loop and some contribution from other feedback loops is found in the high ranking period sensitivity parameters.

From the experiments presented here, it becomes clear that sensitivity information alone is not enough to judge and understand whether or not, and how, a model can achieve period-neutral phase shifting. One should note that parameters with very small relative phase sensitivities (#11, #23 in the basic model, #4, #23 in the extended model) are used chiefly to modify the phase in a period-neutral way, rather than balancing the effects of parameters with large phase sensitivities but also significant period sensitivites. A period-neutral relative phase sensitivity direction of significant length exists even in cases where such modification is difficult for the network to perform.

It is interesting to correlate this greater difficulty in modulating a phase without the period being altered with the number of modes found in the δ-trajectories, as described in Section 3.3.8. In order to study this effect, a total of four models with alternative parameters were picked. Alternative parameter sets 2 and 4 from the basic model were picked as having the fewest and most modes, respectively. For the extended model, alternative parameter sets 1 and 6 were picked according to the same standard. Table 3.12 shows the results for the period-neutral phase-change experiments.

3.3.13 How Functionality is Distributed Within the Two Networks

Several properties of the oscillation were investigated separately in this work. It is now discussed which trends and correlations were found in both models and across the alternative

Table 3.12: Period-neutral phase optimization for different parameterizations of both models. All step sizes were kept at 0.0001 for easy comparison of network performance.

Model	Modes	T	β	α	L	max % $\Delta\beta$	max % ΔT
Basic, nominal	3	23.84	6.92	51.5	0.296	37.5	-0.82
Basic AP Set 2	2	24.16	5.56	39.5	0.264	29.7	0.63
Basic AP Set 4	4	23.16	3.67	68.2	0.282	125	0.8
Extended, nominal	2	23.41	6.85	50.2	0.38	33.1	-2.10
Extended AP Set 1	2	24.27	6.57	84.7	0.36	52.3	1.7
Extended AP Set 6	4	23.10	4.16	74.0	0.279	12.0	2.9

parameter sets, and which relationships exist between the setting of different functions, the network parameterization and its architecture. Interestingly, some properties were relatively conserved across different network parameterizations. The period was always controlled by the negative feedback loop involving Per2/Cry. The amplitudes for all species in a model were always controled by a small number of parameters. The amplitude controls was performed by this group, in a centralized fashion for the entire model, for both model types and all alternative parameterizations. In the basic model, the high amplitude sensitivities almost always correlated strongly with the high phase sensitivities. This effect is observed to a lesser degree in the extended model, where it appears that phase and amplitudes might be controlled more independently. It was found overall that all parts of the networks contributed in the setting of amplitudes and phases. In both models, period control appears distinct in mechanism from phase and amplitude control, when the most influential parameters for each are compared. The positive feedback loop appears to play a stronger role in phase and amplitude sensitivities than in period sensitivities. Some of the parameters play a very prominent role in the amplitude and phase sensitivities, but a very insignificant one in the period setting. These parameters are #3, that indicates the strength of the negative feedback that PER2/CRY exerts on its own expression, as well as #14–17, that regulate the amount of Bmal1 produced.

The parameters that are very often found to be influential on period, phase, relative phase and amplitudes are #5 and even more so, #8 (the Hill coefficient of Per2/Cry transcription inhibition, and the number of Per2/Cry complex forming subunits, respectively). The latter is in its nature not related to a reaction rate, but rather a stoichiometric factor

which describes network architecture.

The control of relative amplitude, angular phase and period is compared network-wide in Figure 3-10. While there are parameters that have only one significant sensitivity (e.g., only a significant period sensitivity but negligible amplitude or angular phase sensitivity), overall the impression is that the control of these network functionalities is handled in a network-wide, concerted way. In other words, even though the most influential period parameters are not the same as the most influential parameters in an angular phase sense, it is nonetheless difficult to modify one without the other. Overall it can be said that the parameters #18–22 (the BMAL1 trafficking and degradation kinetics) have very little influence. In fact it is known that the clock can function without oscillations in Bmal1 (as is the case in Rev-Erb$\alpha^{-/-}$ mutants [26]) without much obvious detriment.

The ability to modify a particular relative phase indepedently of the period appeared also not to depend too strongly on the network parameterization. The small set of alternative parameterizations that were analyzed produced similar results in both models. It also did not seem to matter whether or not the period sensitivities strictly resided in the Per-related negative feedback loop, as seen in the basic, nominal model and its alternative parameter set #4, and in the alternative parameter set #6 in the extended model. In those parameterizations where other feedback loops participated in the period setting (Basic Model, alternative parameter set #2, and extended model in the nominal parameterization), a similar amount (compared to other parameterizations of the same model) of period-neutral phase shift was possible. This ability however, did depend on the number of feedback loops. The two models behaved significantly differently when finite steps in parameter directions were taken. It appears that the model with the additional negative feedback functions more nonlinearly, and is "stiffer" in this sense.

However, some of the more detailed network properties, such as the number of phase sensitivity modes depends strongly on the parameterization. The maximum number of significant modes that are computed using PCA across all alternative parameterization is higher for the extended model. This might correspond to the possibility to have more separate "rare" modes, i.e., more possibilities to process separate inputs, in a model with more feedback loops. However, the parameterization with fewer modes shows that this flexibility isn't automatically present just because there is another feedback loop.

When all phases between peaks of the species in a model were analyzed, it was found

that the phase sensitivities that were the most orthogonal to the period sensitivities were found within the positive feedback loops. The relative phases between the peaks in mRNA concentration of Per2/Cry and Bmal1 were very tightly constrained once the period is fixed. This might indicate that relative phase flexibility exists on a post-translational level, independently from a rather fixed schedule of transcriptional events.

3.4 Conclusions

It was shown that by calculating sensitivities of period, phases and amplitudes, a system-wide understanding of network performance can be gained. Because sensitivity information is, however, only valid at the nominal point, and is local, linearized information, it was of importance to explore the validity of the claims by expanding the range of parameter changes. It was shown that the sensitivity information of derived properties of the oscillation can be used to meaningfully manipulate the network in a non-local way, which aids in the understanding of network performance. It was shown that the networks possess the property that phase relationships can be varied without altering the period, a question that was often debated in circadian systems biology.

We find that one cannot make a general statement about the influence of the number of feedback loops on the flexibility of a network from sensitivity analysis alone. The basic and extended models in their nominal parameterizations have similarly orthogonal and long period-neutral phase sensitivity vectors. However, beyond the local information, the flexibility of the basic model at nominal parameterization is much larger when finite size steps are taken in parameter space to realize this design goal.

Overall we find the nominal extended model to be much less flexible. The amplitudes and relative amplitudes are all controlled by the same parameters. There are fewer modes in the phase sensitivities. There appears more stiffness in the network when phases are attempted to be changed without modifying the period.

There was some evidence found that relative phase flexibility might reside in the positive feedback loop, which is present in both models. It might be a preliminary working hypothesis emanating from this work to suggest that positive feedback adds flexibility, while negative feedback increases stiffness.

We find that many of the parameters that stood out, be that in the "rare" modes of the

δ-trajectories, or in the few parameters that act in a concerted fashion to modulate phase but not period, can be interpreted as potential points of permanent or transient input. Often times, signaling cascades are known to connect to the corresponding reactions. It is gratifying to see that even in a model at this level of abstraction and simplification, biological insight can be gained, and new hypotheses can be formed that can be the basis for future experimentation or intervention.

Chapter 4

An Extended Model of the Mammalian Circadian Clock

Abstract

The current most detailed model of the mammalian circaidan clock was extended to incorporate recent advances in experimental circadian biology. Several feedback loops and species have been added. The resulting model is about 50% larger in the number of variables and parameters than the original model. It accurately represents several known mutant phenotypes, entrains stably to light input, and has a free running period of 24.15 hours, close to that of humans. These realistic properties make the model a suitable candidate for furthering the current understanding of network behavior and function through the analysis of dynamical network models.

4.1 Introduction

4.1.1 The molecular biology of the mammalian circadian clock

The mammalian circadian clock is a biochemical network of molecular interactions, organized into a structure that includes a number feedback loops, that oscillates with a period of approximately 24 hours. Genes are expressed and proteins are modified rhythmically with all concentrations following cyclic trajectories. The circadian expression of clock-related genes is controlled by clock-related transcription factors.

The clock machinery has been modeled mathematically on different levels of detail [90, 68, 69, 29], and the models are often used to further the understanding of systematic network properties [59, 44, 94, 47, 10]. In this chapter, the most detailed current model of

the mammalian circadian clock [29] was extended in order to incorporate recent advances and findings in experimental circadian molecular biology. The aim was to create an up-to-date model, using mass-action kinetics exclusively, that reflects as much as possible the current knowledge and represents correct mutant and wild-type behavior. This model was created for further analysis using the phase sensitivity methods from Chapter 2, which is presented in Chapter 6. A summary of current knowledge in circadian molecular biology is presented next, followed by a review of the model by Forger & Peskin [29]. The extended model and its behaviors is described in Sections 4.2 through 4.2.1.

A transcriptional activator at the heart of the mammalian clock is a heterodimeric complex formed by the Clock protein CLK and the BMAL1 protein, called the Bmal1-Clock-Complex (BCC). Both BMAL1 and CLK are helix-loop-helix, PAS domain-containing transcription factors [93]. BMAL1 acts as a shuttle to facilitate the nuclear accumulation of CLK [60], and heterodimerization increases their degradation.

Although *clk* was the first mammalian clock gene to be identified [26], it is not as well studied as some of the others. $Clk^{+/-}$ mutant mice have a prolonged period, and homozygote mutants display an initially prolonged period that then decays into arrhythmicity in constant darkness [26]. It is expressed rhythmically in the mouse liver [65, 83] but not in the suprachiasmatic nucleus (SCN) [93], and it does not appear to control its own expression level through feedback, as shown through mutant studies. Preitner *et al.* [83] report that Rev-Erbα participates in regulating the Clk mRNA levels in the liver. Additionally, it appears that CLK is rhythmically phosphorylated in at least 4 different forms [65, 105], which might affect its stability and nuclear trafficking [88].

The BCC is a transcriptional activator of many other clock-related genes. It binds to CACGTG E-box sequences within the promotor regions of the three *per* (period) homologues [58], two *cry* (cryptochrome) homologues, the *ror* gene and the *rev-erb* genes. Bmal1 is expressed under the control of two upstream promotor regions called ROREs (retinoic acid receptor-related orphan receptor response elements). Both REV-ERBα and ROR have been shown to bind to both ROREs. While REV-ERBα represses *bmal1* expression [83], ROR increases it [36]. Beyond its role in its own feedback regulation through Bmal1, REV-ERBα regulates *clock* and *cry1* expression [83]. Because *cry1* expression is lowered by REV-ERBα, and CRY1 is an inhibitor of the BCC, which activates *rev-erb*α expression, a positive feedback loop is formed. In Figure 4-1, square arrowheads represent the negative

feedback interactions, while large, regular arrowheads indicate positive transcriptional control. A deletion of Rev-Erbα causes a shortened period, but more importantly, it causes the rhythmicity to cease in the Bmal1 concentrations. The rhythmicity in the other clock genes persists [83].

The BCC is inactivated by the binding of both CRY and all three PER proteins, probably through different mechanisms [2]. The CRY proteins have stronger inhibitory action than the PER proteins [58, 45]. This action closes five negative feedback loops affecting the expression of the *cry* and *per* genes. PER1 and PER2 in their different states of phosphorylation can enter and leave the nucleus at different rates and can form stable complexes with the kinases and either CRY protein [26, 2]. The PER proteins are rate limiting for this step and necessary for the nuclear import of the complex, making them the shuttle for nuclear CRY proteins [65]. PER2 plays a second, positive role in the regulation of *bmal1* expression [87, 83], thereby closing a positive feedback loop interlocked with the negative feedback through the BCC.

The BCC is also inactivated by another circadian protein family, that of DEC1 and DEC2 [45]. Both are basic helix-loop-helix transcription factors shown either to bind to BMAL1 or to compete for DNA binding, thereby influencing the transcription of *per1*. The DEC proteins are similarly strong transcriptional inhibitors than the CRY proteins, and are also rhythmically expressed in the SCN, and Dec1 expression was shown to respond to light pulses. The *dec* genes were shown to be expressed under positive control of the BCC. Much like the *per* and *cry* genes, they posess CACGTG E-boxes where the BCC binds [40, 54]. The negative autofeedback loops around the *dec* genes might interact with the other negative feedback loops, though details are not known.

The roles of the two *cry* homologues appear similar and perhaps redundant, in that neither of them is indispensable for rhythmicity. This is not so for the *per* homologs [112]; the deletion of *per3* unlike *per1* and *per2* hardly affects rhythmicity, and *per3* is hypothesized to play a role only as a potential output [8]. In humans, a single mutation in *per2* causes FASPS [97], and its loss causes arrhythmicity in mice [113, 8]. The phenotype of *per1* null mutant mice shows continued oscillations with unchanged period for 10–14 days but then loses rhythmicity in one study [8]. In another study, it was found that the absence of *per1* caused short periods but otherwise undisturbed rhythmicity [113]. On the molecular level, it was found that the loss of *per1* lowers the peak levels of certain clock proteins, but does

not affect mRNA levels in both studies. Disruption of *per2* expression results in reduced transcription levels of other clock genes and their protein levels. It was concluded that PER1 appears to participate predominantly in regulation at the posttranscriptional level [8, 113].

The PER proteins are phosphorylated by several isoforms of casein kinase 1 (CK1ϵ, CK1δ, and possibly others) in a complex manner that regulates their degradation and nuclear trafficking [103]. In particular, the phosphorylation pattern of PER2 was studied in detail, showing that its phosphorylation sites can be classified in 2 groups that yield opposite period phenotypes. One class of phosphorylation sites leads to an increase in degradation and a slight increase of nuclear import. A distinct phosphorylation site at Ser659 in mice (Ser662 in humans) significantly increases both the rate of nuclear import of phosphorylated PER2 as well as its stability [103]. This phosphorylation site is that of a known mutation in humans that leads to familial advanced sleep phase syndrome (FASPS) [97]. An alternate view of the importance of PER phosphorylation is given by Forger and coworkers [31], who showed that the *tau* mutation in CK1ϵ is not as previously thought a loss-of-function mutation, but instead a gain-of-function mutation specifically for the substrates PER1 and PER2 *in vivo*. Hyperphosphorylation is shown to lead to increased degradation rates; however different phosphorylation sites are not tracked individually, and the effects of their phosphorylation cannot distinguished in this study. On the other hand, Vanselow *et al.* [103] have identified 21 phosphorylation sites, only one of which — the FASPS site — was shown to increase stability; all others were shown to increase PER2 degradation. An increase in PER degradation might account for the shortened period phenotype found in hamsters with the *tau* mutation as well as humans with the FASPS mutation.

With the recent discovery of clock mechanisms based solely on posttranslational chains of events [75], namely, based on phosphorylation–dephorphorylation reactions, the question has been posed if there could possibly exist such a 'phoscillator' in mammals as well [73]. It is known that phosphorylation plays an integral role in the mammalian circadian clock, as discussed above. Furthermore, it was recently shown that the dephosphorylation of casein kinase 1 ϵ by protein phosphatase 5 (PP5) regulates its activity, and that the CRY proteins in turn regulate the activity of PP5 [80]. Furthermore, it was shown that protein phosphatase 1 (PP1) regulates the stability of PER2 by removing the phosphate groups that tag PER2 for ubiquitin-mediated degradation [32]. This new evidence might support

the existence of additional, non-transcriptional feedback loops in the mammalian circadian clock.

One of the most important features of the mammalian circadian clock is its ability to process input signals in the form of light, temperature, food or other stimuli, and entrain to a stable 24-hour oscillation that is in the correct phase with the entraining stimulus. In other words, the molecular network, even though it has a free running period (FRP) of slightly longer than 24 hours [20, 52], can be forced to oscillate at exactly 24 hours. Moreover, molecular events adapt in phase to match the entraining signal, so that, e.g., the molecular events signaling 'morning' will adjust to occur with the onset of light. It is not well understood how entraining signals are transmitted into the molecular clock, though it is known that the clock's ability to process input signals depends on the time of subjective day, due to a phenomenon called 'gating' [26]. It is known that Per1 mRNA increases very quickly after a light stimulus is applied during both early night (i.e., shortly after sunset) and late night [88]. On the other hand, Per2 mRNA levels rise slower [26], and only following signals introduced during early night [88]. The mRNA levels of Per3 and either Cry are not affected by light [26].

4.1.2 A critique of the current most detailed model of the circadian clock

Several mathematical models of circadian clock systems in different organisms have been formulated in recent years ([12, 68, 29, 101, 90, 68], among others), providing different levels of detail. The most detailed model of the mammalian circadian clock to date was published by Forger and Peskin in 2003 [29]. It describes the mechanistic action of 73 species (proteins and mRNA, both in the cytosol and the nucleus) and uses 38 parameters to model their interactions. The mathematical form of the model is a system of ordinary differential equations (ODEs), and all reactions are modeled using mass-action kinetics.

As shown in Figure 5-1, the model includes separate feedback loops for 2 homologs each of Cry and Per. The third Per homolog, Per3, is not included, as its role is not well understood and it is thought to participate mainly in the clock output [8]. Both CRY proteins inhibit the transcription of both *cry* and *per* genes by binding to the BCC. A fifth feedback loop models the positive feedback mediated by the REV-ERBα protein, which modulates *cry1* transcription. This feedback loop is parameterized in such a way that the resulting fluxes and concentrations are negligible, and the deletion of Rev-Erbα does not

cause any noticeable effects on the model's behavior. The influence of REV-ERBα on Clk or Bmal1 expression is omitted in the model. Bmal1 expression is not modeled at all, and the BCC concentration is modeled as having a constant value. This is a significant simplification, in particular because Bmal1 forms the 'anti-phase' to the oscillations of Per, Cry and Rev-Erbα, that are in phase with each other [26]. In some ways, this model could be compared to a Rev-Erb$\alpha^{-/-}$ mutant, because in those mutants, the Bmal1 levels are found to be constant.

The complex pattern of phosphorylation of PER species by the CK1 family is simplified so as to occur in 2 stages, performed by one kinase C at constant concentration, which plays the role of active kinase. Primary phosphorylation allows for binding to CRY and nuclear transport; a secondary phosphorylation event, which only occurs for PER1, prohibits nuclear entry. Dephosphorylation is not represented.

Light input is modeled as an increase in transcription of both *per1* and *per2*. While it is known that the two Per species respond differently to light input, details for the Per2 response are not fully elucidated, making this simplification a reasonable representation of current knowledge. The model entrains to dark–light cycles with an appropriate phase.

The model's authors set values for the 38 parameters through a combination of experimental data available from mouse SCN and liver cells and fitting to overall system behavior [29]. The same parameters are used multiple times in the network to represent different but similar reactions. For example, all mRNA export is governed by the same parameter, regardless of the mRNA species. The model has a total of 231 reactions. Under constant darkness conditions, the model is an autonomous oscillator of the limit-cycle type with a FRP of 24.3 hours. The model agrees reasonably well with wild-type and mutant behavior, but leaves out a certain number of findings that have recently been investigated in more detail. Several of those have been incorporated in an extended version of the model.

4.2 An extended model of the mammalian circadian clock

Based on thorough review of the circadian molecular biology experimental literature that has emerged since the model by Forger and Peskin was published in 2003, the model was extended. The extended model remains governed entirely by mass-action kinetics. Transcriptional activation and inhibition processes are modeled by representing the probability

of an inhibitor or activator being bound to the DNA, similar to the original model. The most signifiant alterations are the inclusion of Bmal1 and ROR expression. Additional work was done on representing the details of PER phosphorylation in accordance with the recent literature reports [31, 103].

Bmal1 is explicitly modeled, including its transcription, translation, nuclear trafficking and activation (i.e., the formation of the BCC, by binding to CLK, which is assumed to be present at sufficient concentration at all times, in agreement with data by Lee *et al.* [65]). In agreement with the data by Kwon *et al.* [60], the degradation rate for the BCC is much larger than that for BMAL1 alone. Bmal1 transcription is controlled by two RORE sites. While both REV-ERBα and ROR have been shown to bind to both sites [36], the effects are such that it is reasonable to simplify by including ROR binding to RORE1 only, and REV-ERBα binding to RORE2 only. This strategy avoids the need for an excessive number of transcription rate constants for each possible combination of bound and unbound states. The positive effect of PER2 on *bmal1* transcription is modeled to occur using a separate binding site and was assumed to be additive to the competitive regulation by ROR and REV-ERBα. This leads to a total of five transcription rate constants (neither ROR nor REV-ERBα bound, both bound or both combinations of one bound and one unbound, and the rate based on the bound PER2 site). The parameters were selected based on the observations reported in reference [36] regarding the relative importance of each effector, and so that the mutant behavior of a Rev-Erb$\alpha^{-/-}$ mutant would be correctly reproduced. The ability of the BCC to promote the transcription of Per, Cry, ROR and Rev-Erbα is assumed to be completely inhibited by the binding of either CRY alone or in any complex with either PER and/or the kinase CK1. CRY complexes can bind to the BCC while it is free, or while it is already bound to the DNA; however it is assumed that this binding only occurs in the nucleus.

In the original model a probability G was calculated to describe the likelihood of a Cry complex to be bound to the BCC at the E-box sites. This probability was the same for all E-box sites in the model (i.e., for Per, Cry and Rev-Erbα transcriptional control). In the extended model the DNA binding sites are modeled separately for both Pers and Crys and for Rev-Erbα and ROR. Their probabilities of having BCC bound are labeled G1BCC through G6BCC; likewise their probabilities of having BCC and a Cry complex bound are G1BCCRn through G6BCCRn. This detailed representation does not add dynamical detail

to the model, because all parameters for all DNA binding and unbinding are the same for the six sites. However, it does allow for a more detailed, unlumped sensitivity analysis. In other words, it can be observed which of the DNA binding sites might be the most important for the implementation of a particular network behavior.

The species ROR is also modeled in detail, with transcription, translation, nuclear trafficking and DNA binding to the RORE site of Bmal1 represented. ROR is assumed to be under the same transcriptional control by the BCC as the PER proteins, at its G6BCC binding site.

The phosphorylation pattern of PER2 was updated in light of findings by Vanselow *et al.* [103], allowing for a two-level pattern of PER2 phosphorylation to regulate nuclear transport. The basic mechanism of phosphorylation is taken from the model suggested in reference [103], with the parameterization adapted so that the absolute parameter values agree approximately with [31] and the original model [29]. The relative values were inspired by [103] and fine-tuned to match the model behavior to data [31].

The light input remained unchanged from the original model, with the same positive influence on light on the transcription of Per1 and Per2.

Omissions in the extended model include the lack of an explicit representation of *clock*, *per3*, and the *dec* genes, mainly because too little information on their quantitative behavior was found in the literature. Likewise, dephosphorylation is not represented in the model.

The extended model consists of 115 concentrations and 64 parameters, many of which are reused for multiple reactions. The mathematical form of the model is a system of ordinary differential equations, whose dynamical behavior in constant conditions is that of an autonomous limit-cycle oscillator. The total number of reactions in the model is 447. A simplified scheme of all reactions and species and their interactions is shown in Figure 4-1.

The values for the 64 model parameters were chosen based on the parameters published by Forger and Peskin [29], with some alterations to fit as much mutant data and wild-type behavior as possible. The relative timing of a number of molecular events was used to refine model parameters. Experimental data are available for the timing of the peaks of mRNA levels for the different clock genes. These data are always represented in a relative fashion, so that the peak concentration equals 100%. The timing of the peaks for different molecular species was collected from experimental literature and compiled in Table 4.1. Molecular data from circadian clock experiments are usually presented on a time scale

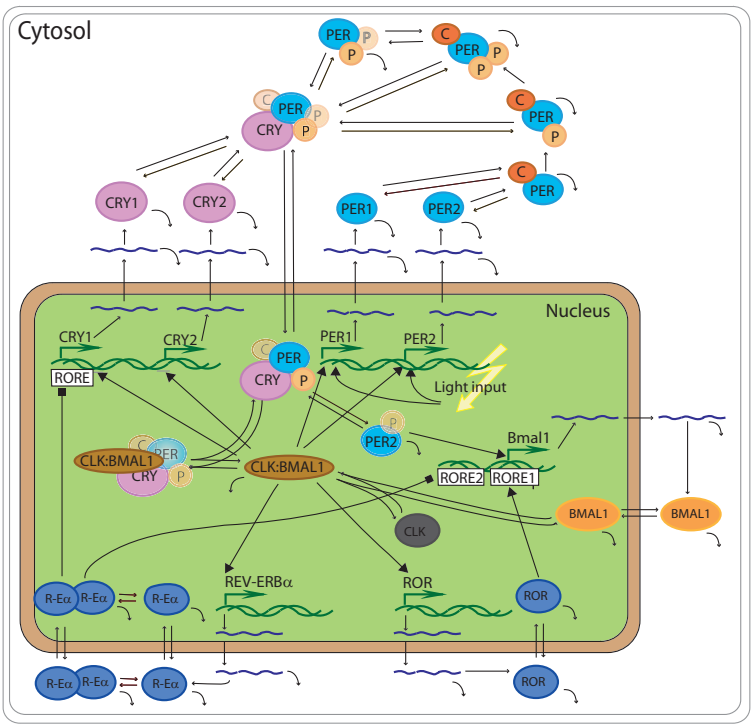

Figure 4-1: Overview of all species and reactions in the extended model. Small arrowheads - reactions; Large arrowheads - transcriptional activation; Square arrowheads - transcriptional inhibition; curved arrows -degradation; In several cases, the multiplicity of a large number of different complexes has been represented by making parts of the complex transparent, to show its optional nature.

called 'Circadian Time (CT)', where CT=0 corresponds with the onset of dawn, or the onset of the subjective day [26]. Subjective dusk is CT=12. 'Zeitgeber Time (ZT)' is the time schedule dictated by an external stimulus, called 'zeitgeber' (German: 'giver of time'), and is sometimes used interchangeably with CT.

It is noticeable that there is wide variability in the experimental data; nevertheless, some general trends are recognizable. The first mRNA concentrations to peak are those of ROR and Rev-Erbα, followed by peaks in Per1, then Per2 mRNA. The peak in Cry1 mRNA follows late in the day, then Bmal1 mRNA peaks either late at night or very early in the morning. It is also observed in the experimental literature that the relative amplitudes of the different mRNA species are different. Both Per mRNAs have minimum concentrations as low as 10%, whereas Cry1 mRNA is rarely seen to drop below 40% of its maximum value. Bmal1 mRNA shows a wide variation of relative mRNA levels, sometimes the oscillation is barely detectable [91, 8]; other times it is strong with the minimum level close to zero [91],

Table 4.1: Peak times in CT (h) in mRNA level for different mammalian clock genes

Publication	Cry1	Per1	Per2	Bmal1	ROR	Rev-Erbα
Preitner *et al.* (liver) [83]	22		16	22		7
Reppert & Weaver (SCN) [87]	10	6	8	18		
Bae *et al.* (SCN) [8]	8-12	4-8	8	20		
Sato *et al.* (SCN) [91]	9-15	9	9	18	6-10	6
Sato *et al.* (liver)	22	12	15	21-2	18	6
Shearman *et al.* (SCN) [93]	10			18-23		
Lee *et al.* (liver) [65]	15	9	9	21-3		
Guillaumond *et al.* (thymus, muscle) [36]				22-2		6-10
Okamura *et al.* (SCN) [77]	12	4	8			
Extended Model	7.9	7.1	7.7	22.7	7.6	7.1

even for data within the same tissue. Bmal1 expression, together with ROR and Rev-Erbα expression is also the most tissue specific [36, 91], with significant differences between liver, SCN or other tissue data.

4.2.1 Model Equations and Parameters

The model equations given here use the following abbreviations: M - mRNA concentration; Po - Per1; Pt - Per2; Ro - Cry1; Rt - Cry2; Rv - Rev-Erbα; n - nuclear localization; c - cytosolic localization; G - likelihood of BCC to be bound to DNA; p - phosphorylated; pp - doubly phosphorylated; C - free kinase CK1;

1. dG1BCC/dt = binGBCC*BCCn*(1-G1BCC-G1BCCRn) - unbinGBCC*G1BCC - bin2GBCC*G1BCC*Rn + unbin2GBCC*G1BCCR
2. dGRv/dt = binRv*RvnRvn *(1 - GRv) - unbinRv*GRv
3. dMnRo/dt = trRo*G1BCC*$(1 - GRv)^3$ - tmc*MnRo
4. dMcRo/dt = tmc*MnRo - umR*McRo
5. dMnRt/dt = trRt*G2BCC- tmc*MnRt
6. dMcRt/dt = tmc*MnRt - umR*McRt
7. dMnPo/dt = trPo*$G3BCC^5$ + L - tmc*MnPo
8. dMcPo/dt = tmc*MnPo - umPo*McPo
9. dMnPt/dt = trPt*$G4BCC^5$ + L - tmc*MnPt

10. dMcPt/dt = tmc*MnPt - umPt*McPt

11. dMnRv/dt = trRv*G5BCC^3 - tmc*MnRv

12. dMcRv/dt = tmc*MnRv - umRv*McRv

13. dRv/dt = tlrv*McRv - 2*arv*Rv*Rv + 2*drv*RvRv - nl*Rv + ne*Rvn - uRv*Rv

14. dRvn/dt = - 2*Nf*arv*Rvn*Rvn + 2*drv*RvnRvn + nl*Rv - ne*Rvn - uRv*Rvn

15. dRvRv/dt = arv*Rv*Rv - drv*RvRv - nl*RvRv + ne*RvnRvn - 2*uRv*RvRv

16. dRvnRvn/dt = Nf*arv*Rvn*Rvn - drv*RvnRvn + nl*RvRv - ne*RvnRvn
- 2*uRv*RvnRvn

17. dPo/dt = tlp*McPo - ac*Po*C + dc*PoC - upu*Po

18. dPt/dt = tlp*McPt - ac*Pt*C + dc*PtC - upu*Pt

19. dPoC/dt = ac*Po*C - dc*PoC - hoo*PoC - upu*PoC

20. dPtC/dt = ac*Pt*C - dc*PtC - hot*PtC - upu*PtC

21. dPopC/dt = hoo*PoC + ac*Pop*C - dc*PopC - up*PopC - hto*PopC - nl*PopC + ne*PonpCn - ar*PopC*Ro + dr*PopCRo - ar*PopC*Rt + dr*PopCRt

22. dPtpC/dt = hot*PtC + ac*Ptp*C - dc*PtpC - up*PtpC - ht*PtpC - nl*PtpC + ne*PtnpCn - ar*PtpC*Ro + dr*PtpCRo - ar*PtpC*Rt + dr*PtpCRt

23. dPop/dt = - ac*Pop*C+ dc*PopC - up*Pop - ar*Pop*Ro + dr*PopRo - ar*Pop*Rt + dr*PopRt - nl*Pop + ne*Ponp

24. dPtp/dt = - ac*Ptp*C + dc*PtpC - up*Ptp - ar*Ptp*Ro + dr*PtpRo - ar*Ptp*Rt + dr*PtpRt - nl*Ptp + ne*Ptnp

25. dPoppC/dt = hto*PopC - up*PoppC + ac*Popp*C- dc*PoppC + ne*PonppCn - ar*PoppC*Ro + dr*PoppCRo - ar*PoppC*Rt + dr*PoppCRt

26. dPtppC/dt = ht*PtpC - upp*PtppC + ac*Ptpp*C - dc*PtppC + ne*PtnppCn - ar*PtppC*Ro + dr*PtppCRo - ar*PtppC*Rt + dr*PtppCRt - nlpp*PtppC

27. dPopRo/dt = ar*Pop*Ro - dr*PopRo - ac*PopRo*C + dc*PopCRo - nl*PopRo + ne*PonpRon

28. dPtpRo/dt = ar*Ptp*Ro - dr*PtpRo - ac*PtpRo*C + dc*PtpCRo - nl*PtpRo + ne*PtnpRon

29. dPopRt/dt = ar*Pop*Rt - dr*PopRt - ac*PopRt*C + dc*PopCRt - nl*PopRt + ne*PonpRtn

30. dPtpRt/dt = ar*Ptp*Rt - dr*PtpRt - ac*PtpRt*C + dc*PtpCRt - nl*PtpRt
+ ne*PtnpRtn

31. dPoppRo/dt = ar*Popp*Ro - dr*PoppRo - ac*PoppRo*C + dc*PoppCRo
+ ne*PonppRon

32. dPoppRt/dt = ar*Popp*Rt - dr*PoppRt - ac*PoppRt*C + dc*PoppCRt
+ ne*PonppRtn

33. dPtppRo/dt = ar*Ptpp*Ro - dr*PtppRo - ac*PtppRo*C + dc*PtppCRo
+ ne*PtnppRon - nlpp*PtppRo

34. dPtppRt/dt = ar*Ptpp*Rt - dr*PtppRt - ac*PtppRt*C + dc*PtppCRt + ne*PtnppRtn
- nlpp*PtppRt

35. dPopp/dt = - ac*Popp*C + dc*PoppC + ne*Ponpp - ar*Popp*Ro + dr*PoppRo -
ar*Popp*Rt + dr*PoppRt - up*Popp

36. dPtpp/dt = - ac*Ptpp*C+ dc*PtppC + ne*Ptnpp - ar*Ptpp*Ro + dr*PtppRo -
ar*Ptpp*Rt + dr*PtppRt - upp*Ptpp - nlpp*Ptpp

37. dPopCRo/dt = ar*PopC*Ro - dr*PopCRo + ac*PopRo*C- dc*PopCRo - nl*PopCRo
+ ne*PonpCnRon - hto*PopCRo

38. dPtpCRo/dt = ar*PtpC*Ro - dr*PtpCRo + ac*PtpRo*C - dc*PtpCRo - nl*PtpCRo
+ ne*PtnpCnRon - ht*PtpCRo

39. dPopCRt/dt = ar*PopC*Rt - dr*PopCRt + ac*PopRt*C- dc*PopCRt - nl*PopCRt
+ ne*PonpCnRtn - hto*PopCRt

40. dPtpCRt/dt = ar*PtpC*Rt - dr*PtpCRt + ac*PtpRt*C - dc*PtpCRt - nl*PtpCRt
+ ne*PtnpCnRtn - ht*PtpCRt

41. dPoppCRo/dt = ar*PoppC*Ro - dr*PoppCRo + ac*PoppRo*C - dc*PoppCRo
+ ne*PonppCnRon + hto*PopCRo

42. dPtppCRo/dt = ar*PtppC*Ro - dr*PtppCRo + ac*PtppRo*C - dc*PtppCRo
+ ne*PtnppCnRon + ht*PtpCRo - nlpp*PtppCRo

43. dPoppCRt/dt = ar*PoppC*Rt - dr*PoppCRt + ac*PoppRt*C - dc*PoppCRt
+ ne*PonppCnRtn + hto*PopCRt

44. dPtppCRt/dt = ar*PtppC*Rt - dr*PtppCRt + ac*PtppRt*C - dc*PtppCRt
+ ne*PtnppCnRtn + ht*PtpCRt - nlpp*PtppCRt

45. dRo/dt = - ar*Ro*Pop - ar*Ro*Popp - ar*Ro*PopC - ar*Ro*PoppC + dr*PopRo
+ dr*PoppRo + dr*PopCRo + dr*PoppCRo - ar*Ro*Ptp - ar*Ro*Ptpp - ar*Ro*PtpC -
ar*Ro*PtppC
+ dr*PtpRo + dr*PtppRo + dr*PtpCRo + dr*PtppCRo + tlr*McRo - uro*Ro

46. dRt/dt = - ar*Rt*Pop - ar*Rt*Popp - ar*Rt*PopC - ar*Rt*PoppC + dr*PopRt
+ dr*PoppRt + dr*PopCRt + dr*PoppCRt - ar*Rt*Ptp - ar*Rt*Ptpp - ar*Rt*PtpC -
ar*Rt*PtppC + dr*PtpRt + dr*PtppRt + dr*PtpCRt + dr*PtppCRt + tlr*McRt - urt*Rt
47. dPonpCn/dt = ac*Nf*Ponp*Cn - dc*PonpCn - hto*PonpCn + nl*PopC - ne*PonpCn
- ar*Nf*PonpCn*Ron + dr*PonpCnRon - ar*Nf*PonpCn*Rtn + dr*PonpCnRtn
- up*PonpCn
48. dPtnpCn/dt = ac*Nf*Ptnp*Cn - dc*PtnpCn - ht*PtnpCn + nl*PtpC - ne*PtnpCn
- ar*Nf*PtnpCn*Ron + dr*PtnpCnRon - ar*Nf*PtnpCn*Rtn + dr*PtnpCnRtn
- up*PtnpCn
49. dPonp/dt = - ac*Nf*Ponp*Cn + dc*PonpCn - ar*Nf*Ponp*Ron + dr*PonpRon
- ar*Nf*Ponp*Rtn + dr*PonpRtn + nl*Pop - ne*Ponp - up*Ponp
50. dPtnp/dt = - ac*Nf*Ptnp*Cn + dc*PtnpCn - ar*Nf*Ptnp*Ron + dr*PtnpRon
- ar*Nf*Ptnp*Rtn + dr*PtnpRtn + nl*Ptp - ne*Ptnp - up*Ptnp
51. dPonppCn/dt = hto*PonpCn + ac*Nf*Ponpp*Cn - dc*PonppCn
- ar*Nf*PonppCn*Ron - ne*PonppCn + dr*PonppCnRon - ar*Nf*PonppCn*Rtn
+ dr*PonppCnRtn - up*PonppCn
52. dPtnppCn/dt = ht*PtnpCn + ac*Nf*Ptnpp*Cn - dc*PtnppCn - ne*PtnppCn +
nlpp*PtppC - ar*Nf*PtnppCn*Ron + dr*PtnppCnRon - ar*Nf*PtnppCn*Rtn
+ dr*PtnppCnRtn - uppn*PtnppCn
53. dPonpRon/dt = ar*Nf*Ponp*Ron - dr*PonpRon - ac*Nf*PonpRon*Cn
+ dc*PonpCnRon + nl*PopRo - ne*PonpRon - binBCCRn*PonpRon*BCCn
+ unbinBCCRn*BCCPonpRon
54. dPtnpRon/dt = ar*Nf*Ptnp*Ron - dr*PtnpRon - ac*Nf*PtnpRon*Cn
+ dc*PtnpCnRon + nl*PtpRo - ne*PtnpRon - binBCCRn*PtnpRon*BCCn
+ unbinBCCRn*BCCPtnpRon
55. dPonpRtn/dt = ar*Nf*Ponp*Rtn - dr*PonpRtn - ac*Nf*PonpRtn*Cn
+ dc*PonpCnRtn + nl*PopRt - ne*PonpRtn- binBCCRn*PonpRtn*BCCn
+ unbinBCCRn*BCCPonpRtn
56. dPtnpRtn/dt = ar*Nf*Ptnp*Rtn - dr*PtnpRtn - ac*Nf*PtnpRtn*Cn + dc*PtnpCnRtn
+ nl*PtpRt - ne*PtnpRtn- binBCCRn*PtnpRtn*BCCn + unbinBCCRn*BCCPtnpRtn
57. dPonppRon/dt = ar*Nf*Ponpp*Ron - dr*PonppRon - ac*Nf*PonppRon*Cn
- ne*PonppRon + dc*PonppCnRon - binBCCRn*PonppRon*BCCn

+ unbinBCCRn*BCCPonppRon

58. dPtnppRon/dt = ar*Nf*Ptnpp*Ron - dr*PtnppRon - ac*Nf*PtnppRon*Cn
+ dc*PtnppCnRon - ne*PtnppRon + nlpp*PtppRo- binBCCRn*PtnppRon*BCCn + unbinBCCRn*BCCPtnppRon

59. dPonppRtn/dt = ar*Nf*Ponpp*Rtn - dr*PonppRtn - ac*Nf*PonppRtn*Cn
+ dc*PonppCnRtn - ne*PonppRtn- binBCCRn*PonppRtn*BCCn
+ unbinBCCRn*BCCPonppRtn

60. dPtnppRtn/dt = ar*Nf*Ptnpp*Rtn - dr*PtnppRtn
- ac*Nf*PtnppRtn*Cn + dc*PtnppCnRtn - ne*PtnppRtn + nlpp*PtppRt
- binBCCRn*PtnppRtn*BCCn + unbinBCCRn*BCCPtnppRtn

61. dPonpp/dt = - ac*Nf*Ponpp*Cn + dc*PonppCn - ne*Ponpp
- ar*Nf*Ponpp*Ron + dr*PonppRon - ar*Nf*Ponpp*Rtn + dr*PonppRtn - up*Ponpp

62. dPtnpp/dt = - ac*Nf*Ptnpp*Cn + dc*PtnppCn - ne*Ptnpp
- ar*Nf*Ptnpp*Ron + dr*PtnppRon - ar*Nf*Ptnpp*Rtn + dr*PtnppRtn - uppn*Ptnpp
+ nlpp*Ptpp

63. dPonpCnRon/dt = ar*Nf*PonpCn*Ron - dr*PonpCnRon + ac*Nf*PonpRon*Cn
- dc*PonpCnRon + nl*PopCRo - ne*PonpCnRon - hto*PonpCnRon
- binBCCRn*PonpCnRon*BCCn + unbinBCCRn*BCCPonpCnRon

64. dPtnpCnRon/dt = ar*Nf*PtnpCn*Ron - dr*PtnpCnRon + ac*Nf*PtnpRon*Cn
- dc*PtnpCnRon + nl*PtpCRo - ne*PtnpCnRon - ht*PtnpCnRon
- binBCCRn*PtnpCnRon*BCCn + unbinBCCRn*BCCPtnpCnRon

65. dPonpCnRtn/dt = ar*Nf*PonpCn*Rtn - dr*PonpCnRtn + ac*Nf*PonpRtn*Cn
- dc*PonpCnRtn + nl*PopCRt - ne*PonpCnRtn - hto*PonpCnRtn
- binBCCRn*PonpCnRtn*BCCn + unbinBCCRn*BCCPonpCnRtn

66. dPtnpCnRtn/dt = ar*Nf*PtnpCn*Rtn - dr*PtnpCnRtn + ac*Nf*PtnpRtn*Cn
- dc*PtnpCnRtn + nl*PtpCRt - ne*PtnpCnRtn - ht*PtnpCnRtn
- binBCCRn*PtnpCnRtn*BCCn + unbinBCCRn*BCCPtnpCnRtn

67. dPonppCnRon/dt = ar*Nf*PonppCn*Ron - dr*PonppCnRon + ac*Nf*PonppRon*Cn
- dc*PonppCnRon - ne*PonppCnRon + hto*PonpCnRon- binBCCRn*PonppCnRon*BCCn
+ unbinBCCRn*BCCPonppCnRon

68. dPtnppCnRon/dt = ar*Nf*PtnppCn*Ron - dr*PtnppCnRon + ac*Nf*PtnppRon*Cn
- dc*PtnppCnRon - ne*PtnppCnRon+ nlpp*PtppCRo + ht*PtnpCnRon

- binBCCRn*PtnppCnRon*BCCn + unbinBCCRn*BCCPtnppCnRon

69. dPonppCnRtn/dt = ar*Nf*PonppCn*Rtn - dr*PonppCnRtn + ac*Nf*PonppRtn*Cn
- dc*PonppCnRtn - ne*PonppCnRtn + hto*PonpCnRtn - binBCCRn*PonppCnRtn*BCCn
+ unbinBCCRn*BCCPonppCnRtn

70. dPtnppCnRtn/dt = ar*Nf*PtnppCn*Rtn - dr*PtnppCnRtn + ac*Nf*PtnppRtn*Cn
- dc*PtnppCnRtn - ne*PtnppCnRtn + nlpp*PoppCRt + ht*PtnpCnRtn
- binBCCRn*PtnppCnRtn*BCCn + unbinBCCRn*BCCPtnppCnRtn

71. dRon/dt = - ar*Nf*Ron*Ponp - ar*Nf*Ron*Ponpp - ar*Nf*Ron*PonpCn
- ar*Nf*Ron*PonppCn + dr*PonpRon + dr*PonppRon + dr*PonpCnRon
+ dr*PonppCnRon - ar*Nf*Ron*Ptnp - ar*Nf*Ron*Ptnpp - ar*Nf*Ron*PtnpCn
-ar*Nf*Ron*PtnppCn + dr*PtnpRon + dr*PtnppRon + dr*PtnpCnRon
+ dr*PtnppCnRon - uro*Ron - bin*Ron*BCCn + unbin*BCCRon

72. dRtn/dt = - ar*Nf*Rtn*Ponp - ar*Nf*Rtn*Ponpp - ar*Nf*Rtn*PonpCn
- ar*Nf*Rtn*PonppCn + dr*PonpRtn + dr*PonppRtn + dr*PonpCnRtn
+ dr*PonppCnRtn - ar*Nf*Rtn*Ptnp - ar*Nf*Rtn*Ptnpp - ar*Nf*Rtn*PtnpCn
- ar*Nf*Rtn*PtnppCn + dr*PtnpRtn + dr*PtnppRtn + dr*PtnpCnRtn
+ dr*PtnppCnRtn - urt*Rtn - bin*Rtn*BCCn + unbin*BCCRtn

73. dCn/dt = - ac*Nf*Cn*Ponp - ac*Nf*Cn*Ponpp - ac*Nf*Cn*PonpRon
- ac*Nf*Cn*PonppRon + dc*PonpCn + dc*PonppCn + dc*PonpCnRon
+ dc*PonppCnRon - ac*Nf*Cn*Ptnp - ac*Nf*Cn*Ptnpp - ac*Nf*Cn*PtnpRon
- ac*Nf*Cn*PtnppRon + dc*PtnpCn + dc*PtnppCn + dc*PtnpCnRon
+ dc*PtnppCnRon - ac*Nf*Cn*PonpRtn - ac*Nf*Cn*PonppRtn + dc*PonpCnRtn
+ dc*PonppCnRtn - ac*Nf*Cn*PtnpRtn - ac*Nf*Cn*PtnppRtn + dc*PtnpCnRtn
+ dc*PtnppCnRtn + up*PonpCn + up*PonppCn + up*PtnpCn + uppn*PtnppCn

74. dGRORE1/dt = binROR*RORn*(1-GRORE1) - unbinROR*GRORE1

75. dGRORE2/dt = binRE*RvnRvn*(1-GRORE2) - unbinRE*GRORE2

76. dGPER2/dt = binPer2*(Ptn_T)*(1-GPER2) - unbinPER2*GPER2

77. dMnBmal1/dt = trB1*(1-GRORE1)*(1-GRORE2) + trB2*(1-GRORE1)*GRORE2
+ trB3*GRORE1*(1-GRORE2) + trB4*GRORE1*GRORE2 + trB5*GPER2
- tmc*MnBmal1

78. dMcBmal1/dt = tmc*MnBmal1 - umB*McBmal1

79. dBmal1n/dt = tlB*McBmal1 - uB*Bmal1n + neB* Bmal1n

- nlB*Bmal1c- actB*Bmal1n + deactB*BCCn

80. dBmal1c/dt = - neB* Bmal1n + nlB*Bmal1 - actB*Bmal1c

+ deactB*BCC - uBc*Bmal1c

81. dBCCc/dt = actB*Bmal1c - deactB*BCCc - uBCC*BCCc

- nlBCC*BCCc - neBCC*BCCn

82. dBCCn/dt = nlBCC*BCCc - neBCC*BCCn - uBCCn*BCCn + actB*Bmal1n - de-

actB*BCCn - bin*Rn*BCCn - unbin*BCCRn$_T$

83. dBCCPonpRon/dt = bin*PonpRon*BCCn - unbin*BCCPonpRon

84. dBCCPtnpRon/dt = bin*PtnpRon*BCCn - unbin*BCCPtnpRon

85. dG1BCCRn/dt = binGBCCR*BCCRn$_T$*(1-G1BCC-G1BCCRn)

- unbinGBBCR*G1BCCRn + bin*G1BCC*Rn - unbin*G1BCCRn

86. dMnROR/dt = trROR*G6BCC^5 -tmc*MnROR

87. dMcROR/dt = tmc*MnROR - umROR*McROR

88. dROR/dt = tlROR*McROR - nl*ROR + ne*RORn - uROR*ROR

89. dRORn/dt = nl*ROR - ne*RORn - uRORn*RORn

90. dBCCPonpRtn/dt = bin*PonpRtn*BCCn - unbin*BCCPonpRtn

91. dBCCPtnpRtn/dt = bin*PtnpRtn*BCCn - unbin*BCCPtnpRtn

92. dBCCPonppRon/dt = bin*PonppRon*BCCn - unbin*BCCPonppRon

93. dBCCPtnppRon/dt = bin*PtnppRon*BCCn - unbin*BCCPtnppRon

94. dBCCPonppRtn/dt = bin*PonppRtn*BCCn - unbin*BCCPonppRtn

95. dBCCPtnppRtn/dt = bin*PtnppRtn*BCCn - unbin*BCCPtnppRtn

96. dBCCPonpCnRon/dt = bin*PonpCnRon*BCCn - unbin*BCCPonpCnRon

97. dBCCPtnpCnRon/dt = bin*PtnpCnRon*BCCn - unbin*BCCPtnpCnRon

98. dBCCPonpCnRtn/dt = bin*PonpCnRtn*BCCn - unbin*BCCPonpCnRtn

99. dBCCPtnpCnRtn/dt = bin*PtnpCnRtn*BCCn - unbin*BCCPtnpCnRtn

100. dBCCPonppCnRon/dt = bin*PonppCnRon*BCCn - unbin*BCCPonppCnRon

101. dBCCPtnppCnRon/dt = bin*PtnppCnRon*BCCn - unbin*BCCPtnppCnRon

102. dBCCPonppCnRtn/dt = bin*PonppCnRtn*BCCn - unbin*BCCPonppCnRtn

103. dBCCPtnppCnRtn/dt = bin*PtnppCnRtn*BCCn - unbin*BCCPtnppCnRtn

104. dBCCRon/dt = bin*Ron*BCCn - unbin*BCCRon

105. dBCCRtn/dt = bin*Rtn*BCCn - unbin*BCCRtn

106. dG2BCC/dt = binGBCC*BCCn*(1-G2BCC-G2BCCRn) - unbinGBCC*G2BCC

- bin2GBCC*G2BCC*Rn + unbin2GBCC*G2BCCR

107. dG3BCC/dt = binGBCC*BCCn*(1-G3BCC-G3BCCRn) - unbinGBCC*G3BCC

- bin2GBCC*G3BCC*Rn + unbin2GBCC*G3BCCR

108. dG4BCC/dt = binGBCC*BCCn*(1-G4BCC-G4BCCRn) - unbinGBCC*G4BCC

- bin2GBCC*G4BCC*Rn + unbin2GBCC*G4BCCR

109. dG5BCC/dt = binGBCC*BCCn*(1-G5BCC-G5BCCRn) - unbinGBCC*G5BCC

- bin2GBCC*G5BCC*Rn + unbin2GBCC*G5BCCR

110. dG6BCC/dt = binGBCC*BCCn*(1-G6BCC-G6BCCRn) - unbinGBCC*G6BCC

- bin2GBCC*G6BCC*Rn + unbin2GBCC*G6BCCR

111. dG2BCCRn/dt = binGBCCR*BCCRn$_T$*(1-G2BCC-G2BCCRn)

- unbinGBBCR*G2BCCRn + bin*G2BCC*Rn - unbin*G2BCCRn

112. dG3BCCRn/dt = binGBCCR*BCCRn$_T$*(1-G3BCC-G3BCCRn)

- unbinGBBCR*G3BCCRn + bin*G3BCC*Rn - unbin*G3BCCRn

113. dG4BCCRn/dt = binGBCCR*BCCRn$_T$*(1-G4BCC-G4BCCRn)

- unbinGBBCR*G4BCCRn + bin*G4BCC*Rn - unbin*G4BCCRn

114. dG5BCCRn/dt = binGBCCR*BCCRn$_T$*(1-G5BCC-G5BCCRn)

- unbinGBBCR*G5BCCRn + bin*G5BCC*Rn - unbin*G5BCCRn

115. dG6BCCRn/dt = binGBCCR*BCCRn$_T$*(1-G6BCC-G6BCCRn)

- unbinGBBCR*G6BCCRn + bin*G6BCC*Rn - unbin*G6BCCRn

Algebraic relations:

C = Ct - (PoC + PtC + PopC + PtpC + PoppC + PtppC + PopCRo + PopCRt + PtpCRo + PtpCRt + PoppCRo + PoppCRt + PtppCRo + PtppCRt + PonpCn + PtnpCn + PonppCn + PtnppCn + PonpCnRon + PonpCnRtn + PtnpCnRon + PtnpCnRtn + PonppCnRon + PonppCnRtn + PtnppCnRon + PtnppCnRtn + Cn)

Rn = (Ron + PonpRon + PonppRon + PonpCnRon + PonppCnRon + PtnpRon + PtnppRon + PtnpCnRon + PtnppCnRon + Rtn + PonpRtn + PonppRtn + PonpCnRtn + PonppCnRtn + PtnpRtn + PtnppRtn + PtnpCnRtn + PtnppCnRtn BCCRn = BCCRon + BCCPonpRon + BCCPonppRon + BCCPonpCnRon + BCCPonppCnRon + BCCPtnpRon + PtnppRon + BCCPtnpCnRon + BCCPtnppCnRon + BCCRtn + BCCPonpRtn + BCCPonppRtn + BCCPonpCnRtn + BCCPonppCnRtn + BCCPtnpRtn + BCCPtnppRtn + BCCPtnpCnRtn + BCCPtnppCnRtn

$\mathbf{Ptn}_T$ = PtnpCn + Ptnp + PtnppCn + PtnpRon + PtnpRtn + PtnppRon + PtnppRtn + Ptnpp + PtnpCnRon + PtnpCnRtn + PtnppCnRon + PtnppCnRtn

$\mathbf{BCCRn}_T$ = BCCPonpRon + BCCPtnpRon + BCCPonpRtn + BCCPtnpRtn + BCCPonppRon + BCCPtnppRon + BCCPonppRtn + BCCPtnppRtn + BCCPonpCnRon + BCCPtnpCnRon + BCCPonpCnRtn + BCCPtnpCnRtn + BCCPonppCnRon + BCCPtnppCnRon + BCCPonppCnRtn + BCCPtnppCnRtn +BCCRon + BCCRtn

4.2.2 Wild-type and mutant dynamic behavior of the extended model

With the model equations and parameterization as shown in Section 4.2.1 and Table 4.2, the model oscillates at constant darkness with a period of 24.15 h, which is close to the period length of 24.19 h found in humans [20, 52]. The model entrains to an outside light stimulus. This stimulus can be applied phase-shifted with respect to a wide range of phases of the constant-darkness oscillation, and stably leads to entrainment. Low levels of Cry1 total mRNA are found at the beginning of the subjective day, in agreement with experimental data summarized in Table 4.1.

In Figure 4-2, left, the time data for all nuclear mRNA concentration is shown, where ZT=0 corresponds to the onset of the subjective day (dawn), the time at which the light stimulus was switched on. For comparison, the same data is plotted for the original model on the right.

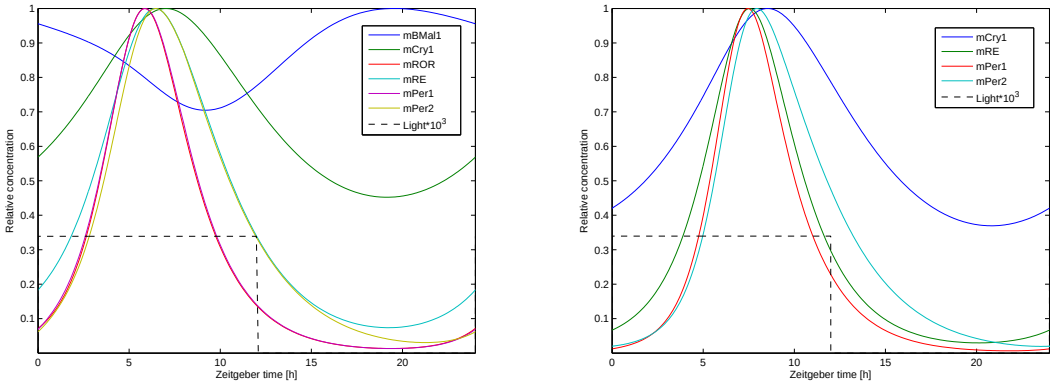

Figure 4-2: Left: Relative mRNA levels in the extended model. Right: Relative mRNA levels in the original model. The combined concentrations of nuclear and cytosolic mRNA are normalized to their maximum level and plotted. The light stimulus was applied to entrain the model for several periods, and is shown (black, dashed). ZT=0 corresponds to the onset of light (dawn). ZT=12 corresponds to dusk.

Table 4.2: Parameterization for the extended model of the mammalian circadian clock

Index	Abbreviation	Meaning	Value
1	tlp	Per translation	10.75
2	tlr	Cry translation	1.108
3	tlrv	Rev-Erbα translation	2.720
4	up	degradation of free PERp	3.646
5	upu	degradation of free PER	0.0882
6	hto	second phosphorylation of PER1	0.194
7	uro	degradation of free CRY1	0.4686
8	urt	degradation of free CRY2	0.6384
9	ac	binding of PER to CK1	0.4999
10	dc	unbinding of PER to CK1	5.468
11	ar	binding of PER to CRY	0.2860
12	dr	unbinding of PER from Cry	0.3784
13	nl	nuclear import (proteins)	2.48
14	ne	nuclear export (proteins)	0.7665
15	nlpp	nuclear import of PER2pp	7.525
16	hoo	first phosphorylation of PER1	0.3075
17	hot	first phosphorylation of PER2	0.4838
18	ht	second phosphorylation of PER2	0.4838
19	Ct	casein kinase 1 concentration	8.290
20	bin	binding of CRY to BCC	1587.2
21	unbin	unbinding of CRY from BCC	5.117
22	trPo	Per 1 transcription	322.5
23	trPt	Per 2 transcription	322.5
24	trRo	Cry 1 transcription	7.525
25	trRt	Cry2 transcription	7.525
26	trRv	Rev-Erbα transcription	53.75
27	tmc	mRNA export	0.4515
28	arv	dimerization of REV-ERBα	0.2258
29	drv	undimerization of REV-ERBα	3.889
30	binRv	binding of REV-ERBα dimers to *cry1*	0.1430
31	unbinRv	unbinding of REV-ERBα dimers to *cry1*	23.44
32	uRv	degradation of REV-ERBα	1.742
33	umPo	degradation of Per1 mRNA	6.676
34	umPt	degradation of Per2 mRNA	0.4053
35	umR	degradation of Cry mRNA	0.4838
36	umRv	degradation of Rev-Erbα mRNA	0.5483
37	Lon	strength of Light Stimulus	3.644×10^{-4}
38	Nf	nuclear/Cytosol volume	124.5
39	upp	degradation of PER2pp	0.086
40	uppn	degradation of PER2npp	0.86

41	binGBCCR	binding of BCC to DNA	10750
42	unbinGBCCR	unbinding of BCC from DNA	0.1075
43	binROR	binding of ROR to RORE	1290
44	unbinROR	unbinding of ROR from RORE	0.215
45	binRE	binding of RE to RORE	107.5
46	unbinRE	unbinding of RE from RORE	2.15
47	binPer2	binding of PER2 to *bmal1*	10.75
48	unbinPer2	unbinding of PER2 from *bmal1*	10.75
49	trB1	Bmal1 basal transcripton	1.075
50	trB2	Bmal1 transcripton, RE bound, ROR unbound	0.01075
51	trB3	Bmal1 transcripton, RE unbound, ROR bound	5.375
52	trB4	Bmal1 transcripton, RE bound, ROR bound	1.075
53	trB5	Bmal1 transcripton, PER2 bound	1.613
54	umB	Bmal1 mRNA degradation	75.25
55	tlB	Bmal1 translation	0.43
56	uB	BMAL1 degradation	5.375
57	actB	BMAL1 activation (CLK binding)	21.5
58	deactB	BCC unbinding	2.15
59	uBCC	BCC degradation	537.5
60	trROR	ROR transcription	1075.0
61	umROR	ROR mRNA degradation	1720.0
62	tlROR	ROR translation	2.15
63	uROR	ROR degradation	5.375

It is found that Bmal1 mRNA oscillates in anti-phase with all other mRNAs, as known from the literature, with its peak being at ZT=22.7 h. The timing of Cry, Per, ROR and Rev-Erbα mRNA is closely related (similar to the original model), with Rev-Erbα and Per1 showing peaks at ZT=7.1 h, ROR and Per2 at ZT=7.6 h and 7.7 h, respectively, and Cry1 peaking last at ZT=7.9 h. While the peak in Cry1 happens sooner than reported in the literature, the overall order of events reproduces well the literature described in Section 4.2.

The relative amounts of Per, ROR, and Rev-Erbα message have larger relative amplitude; their levels drop below 10 % in the very early morning. The relative level of Cry1 mRNA does not decrease as much, creating a smaller relative amplitude, as observed in experimental data [91, 8, 65, 77]. The relative amplitude of Bmal1 message is the smallest. Bmal1 related experimental data shows a large variation, both in relative amplitudes as well as in peak times. In some cases [8], data from SCN shows a relative amplitude in a range similar to the model. A larger relative amplitude in mBmal1 can be produced by changing several parameters, however this generally caused later peak times for mBmal1, which is more similar to data from liver tissue [91, 65].

The mutant behavior of the extended model is in good agreement with experimental data and is shown in Figure 4.2.2. The Per1$^{-/-}$ phenotype (parameter p(22) set to zero) is rhythmic, its period however is slightly prolonged. Experimentally it was found that Per1$^{-/-}$ phenotypes do have a working clock, albeit with a shortened period [112].

The Per2$^{-/-}$ mutant (p(23)=0) does not have a working clock; none of the concentrations oscillate, and if Per2 transcription is stopped suddenly, the system undergoes damped oscillation with a significantly shortened period. The same behavior was found in the original model as well as in experimental studies [113, 8]. The Cry1$^{-/-}$ mutant (p(24)=0) shows rhythmic behavior with slightly shortened period, in agreement with the experimental literature [102]. Cry2$^{-/-}$ (p(25)=0) is still rhythmic, although with slightly lengthened period, again, in agreement with known data [102]. Rev-Eb$\alpha^{-/-}$ (p(26)=0) shows a reduced amplitude of the mBmal1 oscillation, while the other clock species continute to oscillate at a slightly prolonged period. This is seen experimentally, although the period is shortened in experimental findings [83]. The ROR mutant (p(60)=0) shows little effect on the model behavior and period, and no experimental data was found for comparison. Not shown are the Bmal1$^{-/-}$ mutant data, Per1/Per2 double mutant and Cry1/Cry2 double mutant data. All of those mutants were found to be arrhythmic, in agreement with the literature [8, 87].

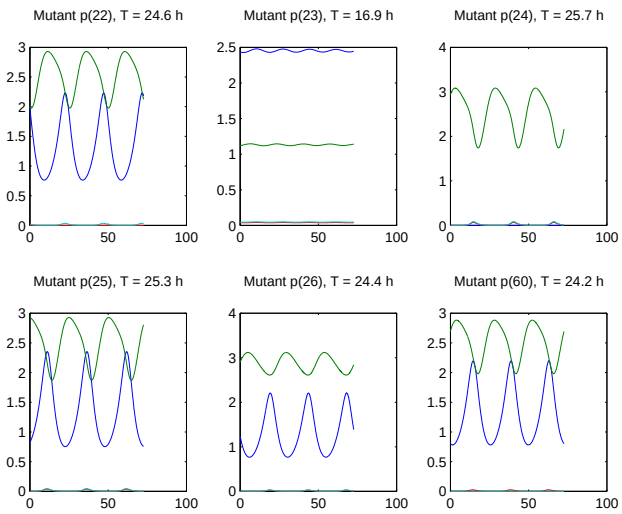

Figure 4-3: Mutant behavior of six mutants of the extended model. Blue - mCry1 total mRNA; Green - Bmal1 total mRNA. The parameter that is indicated by p(i) was set to zero, the parameter indices can be found in Table 4.2.

4.2.3 Circadian Time and the Phase Locking Condition

For further analysis, in particular phase sensitivitiy analysis of the clock, a phase locking condition (PLC) is needed to mark a molecular event that represents 'dawn' in the model. A number of experimental [91, 36, 77, 8, 83, 65] and review publications [26, 87] were surveyed to identify the appropriate PLC that would be used to represent CT=0. The molecular event that coincides with CT=0 most consistently is the beginning of the rise in *mCRY, mPer* and *mRev-Erbα* in the SCN clock [26, 91, 8, 77, 65, 87], although the timing can be shifted in the organ clocks according to data from liver, thymus, kidney, and skeletal muscle in [91, 36]. For implementation in the model, the minimum of total Cry1 mRNA (i.e., the sum of nuclear and cytosolic Cry1 mRNA concentrations) was chosen as the time reference CT=0 as a result of the literature survey. This definition shifts all molecular events by 4.7 hours in comparison to the entrained time, or ZT. Thus the peak times of Cry1, Per1, Per2, ROR, Rev-Erbα and Bmal1 mRNA happen at CT=12.7, 11.7, 12.4, 12.4, 11.8 and 3.2 h, respectively. This definition matches the peak of Cry1 mRNA closer to the time at which it is usually observed, around noon. The timing of the peak in Bmal1 mRNA is now more in agreement with data from the liver, than from the SCN.

4.2.4 Numerical Methods

The model was developed in MATLAB and integrated using ode15s (MATLAB Version 7.4.0.287 2007a, The Mathworks, Natick, MA). The times of peaks and troughs of the model species were determined using the 'Events' function in MATLAB. The model was also written in C for integration and sensitivity analysis using CVODES, a stiff nonlinear solver with sensitivity analysis capabilities [43]. The periodicity of the solution was confirmed by solving the BVP as described in Chapter 2.

4.3 Conclusions

The model that was developed as part of this thesis work represents many details of current mammalian circadian biology. It represents correctly the behavior of wild-type SCN cells and several of their mutants. It improves upon the existing, most detailed models through the addition of several feedback looks, among them positive feedback loops that were shown to be important experimentally. It is now possible to evaluate how the addition of several feedback loops has changed model behavior and performance. Because the anti-phase of oscillation in the Bmal1 species is represented, it is possible to compare the behavior of this very detailed model with simpler and more abstracted models of the mammalian circadian clock that represent this feedback loop, such as the models by Becker-Weimann *et al.* [12]. It can be very useful to study small, abstracted models to gain understanding of general design strategies, and to learn about the benefits of structural features such as additional feedback loops. However, it is very important to be able to match the insights gained in those small models to the molecular processes that implement the dynamical behavior physically. With the creation of this very detailed model that represents all physical processes with mass action kinetics, it is expected that not only the molecular mechanisms of certain clock functionalities or dysfunctions could be understood, but also points of interest for intervention and clock input or output could be identified. The hope is that beyond simulation and analysis, the model will provide inspiration for further experimental inquiry and elucidation of ever more detail of the workings of the mammalian circadian clock.

Chapter 5

Period Sensitivity Analysis of the Mammalian Circadian Clock[1]

Abstract

Processes that repeat in time, such as the cell cycle, the circadian rhythm and seasonal variations, are prevalent in biology. Mathematical models can represent our knowledge of the underlying mechanisms, and numerical methods can then facilitate analysis which forms the foundation for a more integrated understanding as well as for design and intervention. Here, the intracellular molecular network responsible for the mammalian circadian clock system was studied. A new formulation of detailed sensitivity analysis is introduced and applied to elucidate the influence of individual rate processes, represented through their parameters, on network functional characteristics. One of 4 negative feedback loops in the model, the Per2 loop, was uniquely identified as most responsible for setting the period of oscillation; none of the other feedback loops were found to play as substantial a role. The analysis further suggested that the activity of the kinases CK1δ and CK1ϵ were well placed within the network such that they could be instrumental in implementing short-term adjustments to the period in the circadian clock system. The numerical results reported here are supported by previously published experimental data.

5.1 Introduction

The circadian clock is a well studied oscillatory biological system. It is nearly ubiquitous in eukaryotes and is found in similar versions in very different organisms, from unicellular cyanobacteria through filamentous fungi and plants to mammals [25]. It provides a mechanism for adaptation to the changing environment following a 24-hour cycle, by, for

[1]The work presented in this chapter was published with P. I. Barton and B. Tidor in PLoS Computational Biology in 2007 [106].

example, readying the organism in advance for the next event of the day. In addition to establishing periods of wakefulness and rest, the mammalian circadian clock regulates many bodily functions, such as renal and liver activity and the release of appropriate hormones at different times [26]. The circadian clock is the pacemaker that in its normal function is responsible for the impact of shift work and jet-lag on alertness, behavior, and health, and whose misregulation plays a role in such disorders as familial advanced sleep phase syndrome (FASPS). In patients afflicted with FASPS, a shortened intrinsic period makes it difficult for affected individuals to have a normal work and social life. In addition to these more well known effects, circadian rhythms also play a role in pathogenesis and can guide optimal treatment for diseases including arthritis, asthma, cancer, cardiovascular disease, diabetes, duodenal ulcers, hypercholesterolemia, and seasonal affective disorder [70, 110]. In many instances, circadian rhythms can be exploited to minimize dosage and side effects by timing appropriate therapies to the peak times of disease activity or symptoms, including pain [110]. A better understanding of the circadian clock and its workings might contribute to improved treatment of these disorders.

Current models of circadian clocks show behaviors consistent with known biology and anticipated from engineering principles, such as a persistence of the free running period (FRP) in the absence of a daily stimulus and the ability to entrain to periodic external signals [26]. Additionally, the circadian clock, particularly that of organisms lacking temperature regulation, exhibits temperature compensation - the period of oscillation is insensitive to changes in the external temperature [26]. Despite detailed studies on the molecular as well as the systems level [2, 86, 90], open questions persist. Some can be addressed using mathematical analysis of the biological models, and examples from this class form the focus of the current work. Is there a difference in mechanism between phase advance and phase delay, as suggested by experimental observation that phase delay happens much more rapidly than phase advance [86]? Which input pathways could potentially play a role in managing such phase responses? Is the fact that the FRP of the human circadian clock is slightly larger than 24 hours related to the difference in phase advance and delay?

As a first step towards answering such questions, which typically involve the simultaneous analysis of several network characteristics, we focus on the period specific biochemical properties of the mammalian circadian network. We discuss which network structures are involved in setting the FRP, as revealed by detailed sensitivity analysis. The distribution of

this responsibility within the network gives important clues towards a further understanding of the principles and concepts underlying network design. Intimately related to studying where in the network the FRP is regulated is the study of possible mechanisms present to modify the FRP temporarily or persistently, in order to accommodate external fluctuations. How flexibly can the system adjust to changing external situations, for example by undergoing phase shifts? A potential point of intervention for the short-term management of the FRP is suggested here. The fundamental biochemical pathways involved in the clock systems of different eukaryotic species are well known and have the same essential components. Negative feedback regulation of transcription is always present and often interlocked with positive feedback, thus increasing the complexity. Nuclear transport of transcriptional regulators is a central process in forming the feedback loops [26]. At the heart of the mammalian clock is the Clock protein CLK, which acts together with BMAL1 in a heterodimeric complex (BCC). BCC is a transcriptional activator of the three *per* (period) homologues, two *cry* (cryptochrome) homologues, and the *rev-erbα* gene. REV-ERBα represses *bmal1* expression, and regulates *clock* and *cry1* expression [83]. Because *cry1* expression is lowered by REV-ERBα, and CRY1 is an inhibitor of the BCC, which activates rev-erbα expression, a positive feedback loop is formed. The PER proteins are phosphorylated by several isoforms of casein kinase 1 (CK1ϵ, CK1δ, and possibly others) in a complex manner that regulates their degradation and nuclear trafficking [103]. PER1 and PER2 can form stable complexes with the kinases and either CRY protein [26, 3]. The PER proteins are rate limiting for this step and necessary for the nuclear import of the complex, making them the shuttle for nuclear CRY proteins [65]. Nuclear CRY and PER proteins all have an inhibitory effect on the activity of the BCC, probably following different mechanisms [3], thereby closing four negative feedback loops affecting the expression of *cry* and *per* genes. PER2 plays a second role in the positive regulation of *bmal1* expression [87]. Of the *per* homologues, *per3* is the only one whose deletion hardly affects the rhythmicity of the system. While the roles of the two *cry* homologues appear similar and perhaps redundant, this is not so for the *per* homologues [112]. In humans, a single mutation in *per2* causes FASPS [97], and its loss causes arrhythmicity in mice [113, 8]. The behavioral phenotypes of *per1* null mutant mice were similar to those of *per2* mutants; however, comparison of the molecular consequences of the mutations revealed significant differences between the two. Disruption of *per2* expression was reported to result in reduced transcription levels of other

clock genes, whereas PER1 appears to act predominantly at the posttranscriptional level [8]. An overview of the molecular mechanism of the circadian clock is found in references [26] and [87].

Several mathematical models of circadian clock systems in different organisms have been formulated in recent years (references [90, 100, 29, 35, 68], among others), providing different levels of detail. The most detailed model of the mammalian circadian clock to date was published by Forger and Peskin in 2003 [29] and was used for the current study. It describes the mechanistic action of 73 species (proteins and mRNA, both in the cytosol and the nucleus) and uses 38 parameters to model their interactions. The mathematical form of the model is a system of ordinary differential equations (ODEs), and all reactions are modeled using mass action kinetics. As shown in Figure 5-1, the model includes separate feedback loops for 2 homologues each of Cry and Per. The third Per homologue, Per3, is not included, as its role is not well understood and it is thought to participate mainly in the clock output [26]. Both CRY proteins inhibit the transcription of both *cry*s and *per*s by binding to the BCC. A fifth feedback loop models the positive feedback mediated by the REV-ERBα protein, which modulates *cry1* transcription. The effect of REV-ERBα on *clk* expression is omitted in the model. The complex pattern of phosphorylation of PER species by the CK1 family is simplified so as to occur in 2 stages, performed by one kinase C at constant concentration, which plays the role of active kinase concentration. A primary phosphorylation allows for binding to CRY and nuclear transport. A secondary phosphorylation, which only occurs for Per1, prohibits nuclear entry. The BCC concentration is modeled as having a constant value, which is a simplification, as *bmal1* is rhythmically expressed, probably under positive feedback control of PER2 [87] and ROR [36] as well as negative feedback control of REV-ERBα [83]. The model's authors set values for the 38 parameters through a combination of experimental data available from mouse SCN and liver cells, and fitting to overall system behavior [29]. Under constant darkness conditions, the model is an autonomous oscillator of the limit cycle type and has a FRP of 24.3 hours. The model encapsulates mathematically much of what is known about the mammalian circadian biochemistry, with a few omissions and simplifications. New discoveries will undoubtedly lead to improved versions of the model. As is, it is an excellent basis for theoretical investigation of this interesting and important network control system. The model agrees well with wild-type and mutant behavior.

Circadian clock models are generally limit cycle oscillators, a characteristic of which is robustness of period and amplitude with respect to perturbations in their state variables (corresponding to concentrations or activities here). Mathematically, such systems will asymptotically approach the limit cycle trajectory from any initial condition in the region of attraction of the limit cycle. The shape and situation of the limit cycle depends only on the parameters of the system. This property, however, can make it more difficult to study these systems. Without knowing the exact limit cycle trajectory, iterations over several periods of oscillation are needed to approximate it. It is not clear a priori how many periods are needed to reach the limit cycle to a given tolerance. At the same time, the exact limit cycle properties (period, amplitudes, relative phases) are of direct biological interest. In this article, we present a new method for the exact computation of sensitivity trajectories of limit cycle oscillators and sensitivities of derived quantities with respect to model parameters. Sensitivity analysis probes how a small variation of a parameter or initial condition away from a reference solution influences the trajectories of the state variables, and of derived quantities. Applied to biological systems, sensitivity analysis can help to analyze how changes in rate parameters or temporary perturbations in protein or mRNA concentrations can influence the behavior of a system. It is becoming a standard tool for systems biologists. The use of various sensitivity metrics has been explored in a variety of network biology studies [49, 46] including a number of simpler models of circadian rhythms [69, 94, 48]. However, the exact sensitivity analysis of oscillating systems is more challenging than for other dynamic systems [48, 89]. It has been shown that the parametric sensitivities of periodic systems can be decomposed into a bounded and an unbounded part according to

$$\mathbf{S}(t) = -\frac{t}{T}\dot{\mathbf{y}}(t)\frac{\partial T}{\partial \mathbf{p}} + \mathbf{Z}(t)$$

where $\mathbf{Z}(t)$ is the periodic matrix containing the parametric sensitivities at constant period. This part is sometimes referred to as the 'cleaned out' sensitivities [99], as opposed to the 'raw' sensitivities , and is reported to contain information on shape and amplitude of the oscillation [63]. In order to achieve this decomposition, two conditions have to be met. First, the exact computation of the period sensitivities is required. Second, appropriate initial conditions for have to be found. Since one is interested in initial conditions of the state variables that lie on the periodic orbit, which in its shape and location depends on

the system parameters, those initial conditions are not independent of the parameters. Consequently, the sensitivities cannot be initialized with the zero matrix as usual in other dynamic systems. An incorrect initialization of the sensitivities leads to an unbounded error of unknown magnitude [89]. In the current work we have derived a rigorous procedure for computing the sensitivity of the period of a limit cycle oscillator with respect to model parameters and applied this to the most detailed model of circadian rhythms available [29]. This has provided a particularly high-resolution view of the role different model elements play in setting the period of oscillation and for the first time highlighted that reactions involving Per2 have an especially strong effect on the period. Interestingly, the results point to a series of steps forming a reaction cycle, rather than to any particular step in that cycle.

We describe and apply a strategy that identifies the exact limit cycle trajectory by solving a boundary value problem (BVP) and then using the solution of this BVP to calculate the exact sensitivities of state variables, amplitudes, and period of the oscillation without resorting to the iterative methods typically used for limit cycle systems. Here we applied our sensitivity analysis methodology to study the limit cycle circadian clock model of Forger & Peskin [29]. Because the same parameters are used in multiple places throughout the model, the individual sensitivities were computed on a per-reaction basis, rather than a per-parameter basis. Due to parameter sharing, the 38 model parameters describe 231 reactions in the model. Sensitivity analysis was performed using both the original 38 lumped parameters or with an unlumped parameter set in which the effect of each of the 231 reaction rate parameters was probed individually. The unlumping as described in Section 5.5 does not change the physical model but rather provides a more detailed analysis of the roles of individual physical and chemical reactions. Meaningful results were only obtained in the unlumped calculation, rather than the lumped sensitivities obtained when analyzing the original model parameters directly, which simultaneously affected multiple reactions. This analysis revealed that the period setting is strongly dominated by processes within the Per2 feedback loop, but not the subtly different Per1 loop. The mechanism of this responsibility distribution is elucidated in several numerical experiments and supported by published experimental results. Moreover, a potential mechanism for short-term period adjustment is identified and discussed, namely the activity of casein kinase 1 isoforms.

5.2 Results

5.2.1 Most high-impact parameters are located in the Per2 loop

The relative sensitivities of the FRP T with respect to each parameter pj on a per-reaction basis, , were calculated, and then rank-ordered by magnitude. Results for the top ten ranked sensitivities are graphically represented in Figures 5-1 and 5-2. Per2 related reactions dominate by far in their influence on the period in the system. Eight of the ten highest magnitude sensitivities are Per2 related (including expression, transport, reaction, and degradation of Per2), and only one is not directly related to the Per2 feedback loop (nuclear export rate of Cry1 mRNA). The overwhelming dominance of Per2 processes in influencing clock period in the model is particularly interesting given that *per2* mutations are linked to FASPS [97].

Figure 5-2 shows that the top ranked sensitivities are significantly larger than the remainder, indicating a strongly localized distribution of sensitivity of the period within the network. At the same time, there is no single parameter (and therefore process or reaction) found to be the only control for increasing or decreasing the period of oscillation; rather, the period setting responsibilities are shared among a number of processes within the Per2 negative feedback loop. Likewise, the localization of high sensitivity within the network cannot be attributed to a class of reaction or process (such as phosphorylation, translation, or transcription).

In order to test the influence of the exact network parameterization on the results shown here, additional parameter sets were created (see Section 5.5). The period sensitivity rankings of all modified parameter sets correlate highly with the nominal parameter set (Spearman rank correlation factors between 0.890 and 0.966), which is surprising given the large number of parameters with negligible period sensitivity. The majority of the top ten parameters shown in Figure 5-2 (6.3 of them on average) are found in the top ten of the modified sets, an average of 4.3 of the original top 5 parameters are found in the top 5 of the modified sets and the original top 6 parameters are represented in 9 of the modified top tens. The casein kinase concentration ranks sixth or higher in all but two of them, and tenth or higher in all but one. An average of 5.8 parameters in the top ten is Per2 related. Thus, the results presented here do not depend very strongly on the particular parameter values in the Forger and Peskin model, but instead appear to be a property of this class of

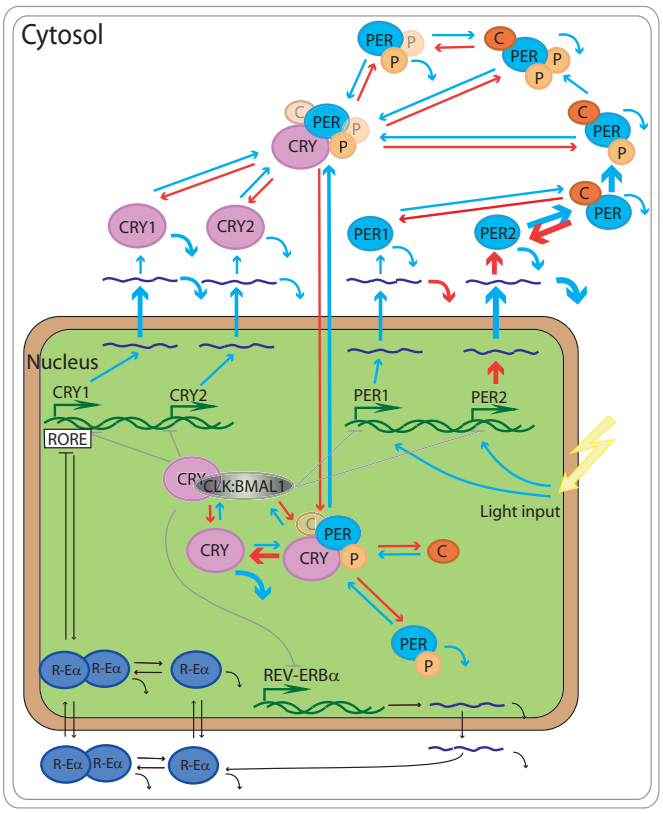

Figure 5-1: Graphical representation of results of detailed sensitivity analysis. Red, positive sensitivity; blue, negative sensitivity; black, zero sensitivity; gray, not modeled explicitly; thick arrow, large magnitude; thin arrow, small magnitude; curved arrow, degradation; R-Eα, REV-ERBα; RORE, target sequence for retinoic acid-related orphan receptor R-Eα on Cry1 promotor; P, phosphorylated; C, CK1; The CRY-CLK:BMAL1 complex does not inhibit transcription but rather diverts active CLK:BMAL1 from the transcription initiation site. The effect of light input is modeled as an increase in *per1* and *per2* transcription, identical in both. In the interest of visualization, only Per2 pertinent sensitivities are represented where one arrow represents multiple processes. In those cases, the Per2-related sensitivities were always significantly larger in magnitude than any other sensitivities.

models in the neighborhood of the parameterization developed by Forger and Peskin [29].

5.2.2 Differences between the Per1 and Per2 loops

Although Per1 and Per2 carry out similar reactions, only Per2 is singled out as highly significant in affecting the period of oscillation. Model dissection was used to analyze the source of this difference. There are four differences between Per1 and Per2 in the original model. One is a topological difference, in that PER1 can be phosphorylated a second time, which masks its nuclear localization sequence; doubly phosphorylated PER1 or any of its

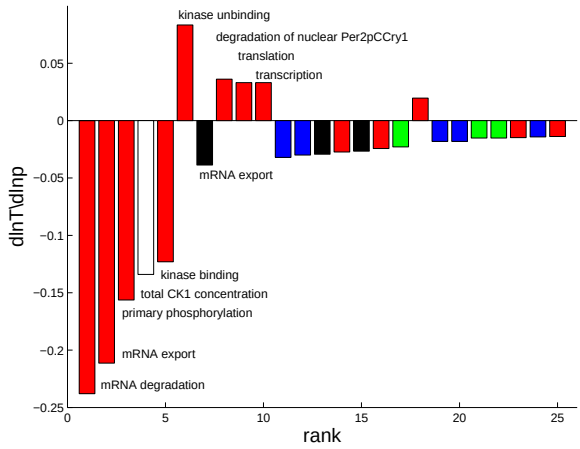

Figure 5-2: Top 25 ranked sensitivities ordered by relative period sensitivitiy. Black bars indicate Cry1-related parameters, blue bars indicated Cry2-related parameters, green bars indicate Per1-related parameters, and red bars indicate Per2-related parameters. The white bar represents a single, special parameter representing the total kinase concentration. Where Cry- and Per-related parameters overlap, the Per-species colors are shown. "Per2pCCry1" describes a complex of once-phosphorylated PER2 with the kinase C and CRY1.

complexes cannot enter the nucleus. The remaining 3 differences are purely parametrical and of different relative magnitude - differences in transcription rates (the *per1* rate being 2.6-fold higher), rates of first phosphorylation (the PER2 rate being 5-fold higher), and mRNA degradation rates (the Per1 rate being 16-fold higher). These differences cause the PER2 concentration to be roughly 2.5 times that of PER1, with minima and maxima occurring at almost the same times; the PER1 concentration is not negligible, however. The loss of Per1 alone does not abolish rhythmicity, but the loss of Per2 alone leads to a slowly decaying amplitude of the oscillation [29].

Each of the differences was studied in individual numerical experiments. In a first set of numerical "mutations", the rates that are different between Per1 and Per2 were made equal at either the value of the Per1 specific rate or the value of the Per2 specific rate . Then the sensitivity analysis was repeated and the ranking of the resulting sensitivities was compared to the ranking shown in Figure 5-2 (results not shown). In short, the findings pointed towards the mRNA degradation rate as well as the rate of primary phosphorylation being influential in making Per2 the period setting feedback loop. In order to observe this effect more clearly, the rates of the same reactions were reversed in the next set of

numerical experiments, before repeating the sensitivity analysis and ranking comparison as before. The results are shown in Figure 5-3. Neither the only topological difference, nor

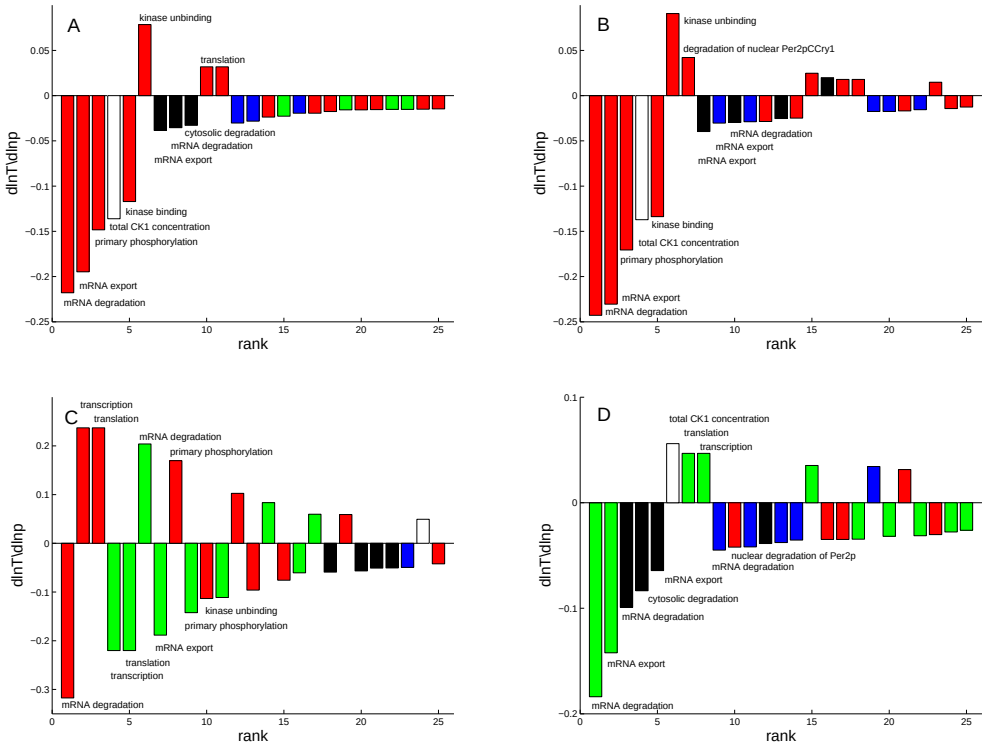

Figure 5-3: Top 25 ranked period sensitivities for different numerical experiments – Flipped rate parameters. Flipped rate parameters between Per1 and Per2 for (A) secondary phosphorylation rate, (B) transcription rate, (C) primary phosphorylation rate, and (D) mRNA degradation rate. Black – Cry1-related parameter; Blue – Cry2-related parameter; Green – Per1-related parameter; Red – Per2-related parameter; Where Cry- and Per-related parameters overlap, the Per-species colors are shown.

the different transcription rates for *per1* and *per2* are crucial for the differential behavior of the two homologues (Figures 5-3 A and B), as the sensitivity ranking remains largely unchanged.

When the rates of primary phosphorylation were reversed, the maximum sensitivity in the network increased. While the highest magnitude sensitivity remained the Per2 mRNA degradation rate, Per1 specific rates now appeared almost alternating with the Per2 specific rates, as if in this scenario the two share the period setting responsibility (Figure 5-3 C), yet the overall concentrations of Per1 and Per2 concentration remain largely unchanged. When the rates of mRNA degradation were reversed for both genes, a subset of Per1 specific rates

moved up in the ranking and at the same time, the maximum sensitivity found decreased in magnitude significantly (Figure 5-3 D). Per1 in this scenario dominated the period setting, and its concentration was now a factor of 20 larger than the Per2 concentration. When both of the rates for mRNA degradation and primary phosphorylation were reversed simultaneously, a clear role reversal between Per1 and Per2 occurred (Figure 5-4). We can thus say that the combined action of mRNA degradation and primary phosphorylation of Per2, in comparison to Per1, are what cause the Per2 loop to dominate in setting the period of the circadian clock.

It should be noted that the rates of mRNA degradation in the original model are more different in a relative sense than the rates of primary phosphorylation. The quantitative results obtained here may vary upon a more exact determination of the parameter values used in the model. However, the qualitative insights gained from the numerical experiments performed in this work appear to be robust to changes in parameter values.

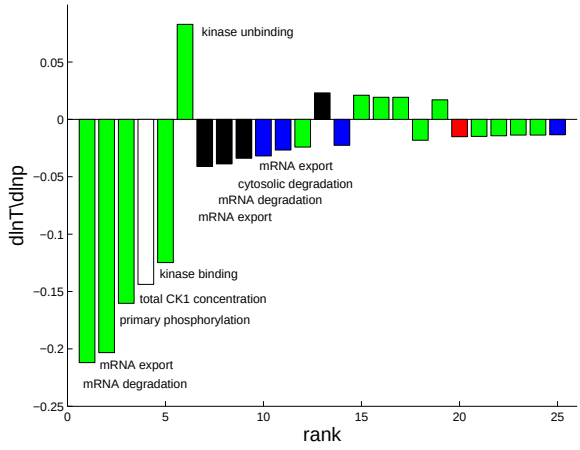

Figure 5-4: Top 25 ranked period sensitivities when mRNA degradation rate and primary phosphorylation rate for Per1 and Per2 were reversed. The color assignment is identical to Figure 5-2.

5.2.3 The CK1 kinase activity alone can alter the period over a wide range

The analysis of period sensitivities identified the total active concentration of casein kinase 1 isoforms (CK1) as well as the kinase binding kinetics as being among the main determinants

of the period. As the sensitivity analysis measures the effects of local (infinitesimal) parameter variations, a possible mechanism for modulating the period of the system through modulating the amount of active kinase in the system was verified by parametric studies. The results are shown in Figure 5-5.

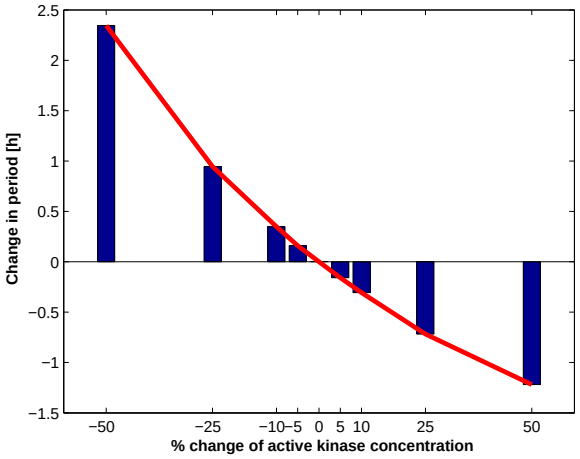

Figure 5-5: Changes in the period as a result of variation in kinase CK1 concentration. All other parameters remain constant.

The kinase concentration allows for modulation of the period over a wide range of parameter values. By varying the parameter 50% up or down, the period was changed by -5% or +9.7% (-1.25 to 2.4 hours), respectively. The sensitivity of the period with respect to kinase concentration remains negative, as the period becomes shorter with increasing kinase concentration and vice versa, over the entire range. It is assumed that a temporary change in the period will cause a permanent phase shift, a process called "parametric entrainment" in the circadian literature [26]. The results shown in Figure 5-5 suggest that by modulation of the kinase concentration, it is relatively easier to produce a phase delay (a temporary decrease of kinase concentration, leading to a temporarily longer period) than it is to produce a phase advance, as shown by the larger magnitude period variation achieved for a 50% decrease in kinase concentration compared to a 50% increase. A similar difference is noted in the maximum amplitude of the phase response curve (PRC) shown in Figure 5-6, where the phase shift as the result of a short-term step change in active kinase concentration is shown as a function of time. This figure shows, again, that the same absolute change in kinase concentration at the right time results in a longer delay but shorter advance. The

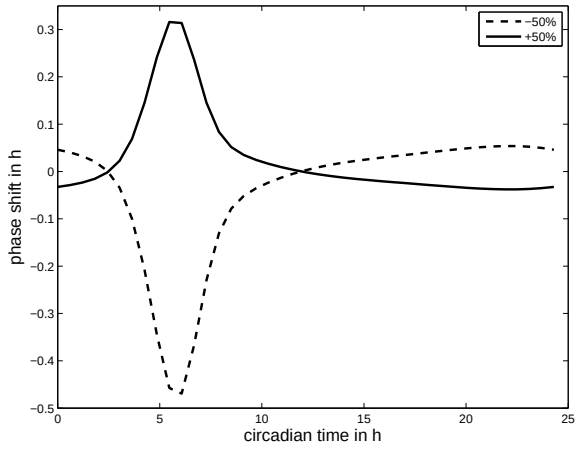

Figure 5-6: Phase Response Curve for CK1 concentration. The phase response indicated by the ordinate is the permanent effect that was caused by a 50% up or down shift in active kinase concentration of 30 min duration. A positive phase shift indicates a phase advance, a negative one phase delay. The starting time of the step change corresponds to the time indicated by the abscissa. Circadian time zero corresponds to dawn.

results also show that the magnitude of phase shift depends dramatically on when during the day the kinase modification is applied, both for delay and advance. It should be noticed that changes in period shown in Figure 5-5 correspond to a stationary property of the system. In contrast, the response measured in Figure 5-6 describes a transient effect of a short-term disturbance of the system - the short-term parameter change does not allow for the system to approach its perturbed stationary state.

5.3 Discussion

5.3.1 The Per2 loop sets the period

The results presented for the circadian clock system in mammals suggest a strongly localized distribution of functionality within the network. Through detailed analysis of the period sensitivities, it was shown that the period of oscillation is set by parameters distributed throughout the Per2 negative feedback loop. The ten parameters with the greatest period sensitivities are dominated by Per2-related species, likewise Per2-related reactions have high sensitivities.

Within the Per2 feedback loop there is a self-consistency as to the effects on the length of

the period; changes that accelerate (decelerate) progress through the loop lead to a shorter (longer) period. For example, multiple processes that reduce the half-life of Per2 mRNA all produce a shortened period. These processes include faster mRNA degradation, faster mRNA export, and interestingly, slower transcription. Likewise, faster kinase binding or phosphorylation lead to faster migration of CRY1 bound species into the nucleus, which closes the negative feedback loop faster and results in a shorter period. Interestingly, PER2 and CRY1 interoperate to control the rate of nuclear transport of the phosphorylated complex. Changes that prolong the half-life for CRY1 in the nucleus (faster dissociation of PER2 bound CRY1 species and slower CRY1 degradation) result in a longer period, a fact that was recently confirmed in experimental studies [19]. Changes can also be understood through their effects on altering concentrations. Increases to the cytosolic concentrations of CRY1 (faster nuclear export of CRY1 and bound species, faster transcription, or faster translation) lead to shorter periods. Because unbound CRY cannot migrate from nucleus to cytosol, a delay of CRY1 in the nucleus shows the feedback from the Per2 loop and lengthens the period. Processes that increase the amount of Per2 produced (faster Per2 transcription or translation, or slower mRNA degradation) ten to lead to a longer period. This self-consistency makes intuitive sense of the network structure-function relationship computed here and lends additional support to the notion that the results are not overly dependent on the details of the particular model implementation here.

Published experimental results indicate that the roles of Per1 and Per2 in the circadian clock mechanism are not redundant [112, 8]. Our findings confirm these results on a network analysis level: the Per2 feedback loop carries responsibility that Per1 does not share. Due to the detailed and comprehensive model, the mechanistic detail behind this organization could be analyzed to show that the values of two reaction rates, the rates of mRNA degradation and of primary phosphorylation of Per2, cause this feedback loop to dominate period setting. In another computational study [108], mRNA degradation rates were found to be highly influential on the period of oscillation throughout a set of four different circadian clock models, not including the model studied here. The present study provides further insight in that it is mainly only one mRNA degradation rate, that of Per2, that matters most. Even the second most sensitive mRNA degradation rate, that of Cry1, is only 20% as significant with respect to the period. It should be noted that the authors of the model also report a sensitivity called "sensitivity of the badness of the fit" [29]. This quantity is only indirectly

related to the period sensitivity, and is also only computed for the 38 "lumped" original parameters. Without dissecting the multiple roles of the original parameters, the Per2 loop cannot be identified as the period setting feedback loop, nor does it become obvious how the period setting responsibility is distributed throughout the loop.

5.3.2 The positive feedback loop may not participate in period setting

The sensitivities of the period with respect to all parameters associated with the Rev-Erbα loop were zero, suggesting that the Rev-Erbα loop may not participate in setting the period for this model. This hypothesis was confirmed by removal of the entire loop without consequence for the period (results not shown). Interestingly, this is an area where the model appears to disagree with experiment; experiments show that, while Rev-Erbα is not essential for rhythmicity, period length and phase shifting behavior are altered in null mutants [83], although less so than in Per2 null mutants [113, 8].

In this portion of the model, the action of REV-ERBα on Bmal1 expression is omitted, and the Rev-Erbα loop is parameterized in such a way that the resulting concentrations are essentially zero [47]. To test whether inaccuracies in the Rev-Erbα portion of the model could compromise conclusions regarding the role of the Per2 loop, simulations and sensitivities were computed for artificially manipulated versions of the model that substantially increased the activity of the Rev-Erbα loop. Even when the flux through the Rev-Erbα loop was increased by five orders of magnitude (by increasing the transcription and translation rates and decreasing the degradation rates), and the corresponding sensitivities became significant and moved up the ranks (ranging from 168th to 225th in the original parameterization versus 68th to 168th for the increased flux model), the top 50 ranking parameter sensitivities did not change significantly.

Furthermore, in accordance with recent findings in the experimental literature [36, 55], we have constructed an alternate version of the model (Supplementary Dataset S3, available online at http://www.ploscompbiol.org) with a sixth feedback loop involving ROR (retinoid acid-related orphan receptor). This receptor was found to have an opposing role to Rev-Erbα in the control of Bmal1 expression. While Bmal1 was still not explicitly represented, we included the indirect effect of ROR as well as that of Rev-Erbα on the transcriptional activity of all circadian genes in the model. This change resulted in the use of 4 new state variables and 10 new parameters. The preliminary parameterization of this sixth

feedback loop was done using qualitative insights from the experimental data, and chosen so that the peak in ROR would follow the peak of REV-ERBα in the nucleus and so that transcriptional control of ROR would be similar to that of Per2. The transcription rate of *rev-erb*α was increased one hundred fold to make the corresponding concentrations more significant. Those modifications to the original model did not alter mutant behavior, period or the results presented in this paper. The ranking of relative period sensitivities remains virtually unchanged. The ten new parameters ranked between 148 and 218 out of 241. This suggests that while there are still discrepancies between the known biology and the model that will undoubtedly be resolved through future work, the results shown here are not sensitive to changes in this part of the model.

5.3.3 A potential mechanism for accelerating or decelerating the oscillation

It is of interest for the understanding of network design, as well as potential therapeutic interventions, to identify possible points of intervention for period control. Furthermore, it is known that parametric entrainment (which relies on period modulation to control the phase of oscillation) plays a role in the mammalian circadian clock, although details are not understood [26]. The total casein kinase 1 concentration appeared fourth in the rank-ordered sensitivities and is a quantity that deserves special attention. While it is modeled here as a constant quantity, it realistically represents a concentration of active kinase, which may not be constant throughout the cycle. Some of the other top ten parameters can be modified by genetic mutation on a long time scale (such as the mRNA degradation rate), or a medium time scale (such as transcriptional regulation). However, the (active) kinase concentration could potentially be regulated both on a very short time scale by post-translational modification through an input signaling pathway or a medium time scale through transcriptional regulation. In fact, CK1ϵ is known to inactivate itself by autophosphorylation, a process that is counteracted by cellular phosphatases [55]. It has been suggested that such phosphatases can be activated by signaling pathways such as the Wnt pathway [84] so as to activate CK1ϵ as a result of a signaling cascade.

A comparison with experimental results for period-related abnormalities reveals that PER2 phosphorylation by casein kinase 1 has significant involvement in setting the period. It has been shown experimentally that in individuals with one type of FASPS, the human

per2 gene is mutated at the site of its phosphorylation by CK1ϵ. This mutation causes hypophosphorylation and ultimately a phase advance, which is typically associated with a shortened FRP [97]. In individuals with another type of FASPS, the *ck1δ* gene is altered [109].

In hamsters, a mutation called τ in *ck1ε* causes a short circadian period. For the Forger and Peskin model an increased rate of primary Per2 phosphorylation predicts a shortened period. This finding contradicted the prior observation that the *tau* mutation was a loss-of -function mutation of CK1ϵ in *in vitro* experiments [71], thus leading to the discovery of the differential action of CK1ϵ on clock-related versus generic substrates. Recent findings have confirmed that the τ mutation is in fact a gain-of-function mutation with respect to the phosphorylation of PER2 [31].

It should be noted that the exact pattern and functional consequences of Per2 phosphorylation are simplified in the model [29]. More recently, its details have been investigated [103], providing additional insight. In broad terms, there are two effects of mPER2 phosphorylation. The phosphorylation site involved in FASPS (Ser 659) was shown to increase nuclear retention and stabilization of mPer2. Phosphorylation at other sites of Per2 leads to increased degradation. Only the latter effect is represented in the model used for this. In order to substantiate the results in this study in the light of more recent experimental data, the phosphorylation pattern suggested in [103] was incorporated into the model. No new species were created, since the original model includes a doubly phosphorylated Per2 species already. Only three rate parameters were added to the model (nuclear import rate of Per2pp species, modified degradation rates for nuclear and cytosolic Per2pp species). The previously unused rate of secondary phosphorylation rate of Per2 was reassigned. Parameter values were chosen to closely reflect the relative rates as published in reference [103], based on the rate values in the original model. I.e., the rate of secondary phosphorylation was set equal to that of primary phosphorylation, as suggested in [103], at the value published in [29]. The modified model in MATLAB format can be found in the Supplemental Information (Dataset S2, available online at http://www.ploscompbiol.org). This very preliminary parameterization resulted in a period of 23.82 hours, the mutant behavior with respect to knockouts as described in [29] was unchanged. Again, the parameters were unlumped and the sensitivity analysis and ranking was repeated. The top 6 parameters are the same in sign and very similar in magnitude than those of the original model, confirming the dom-

inant role of Per2 again. The twice phosphorylated PER2 species appear twice in the top ten (rank 7 and 9, unbinding from CRY1 and degradation, respectively), and the unbinding and binding kinetics between CRY1 and CLK:BMAL1 take rank 8 and 10, respectively. The period sensitivity with respect to the secondary phosphorylation rate is smaller than that of the first, (rank 64 vs. rank 3) and positive, as expected.

The details might not be represented exactly in the original model, yet it correctly reflects the notion that the phosphorylation rate of PER2 is one of the main period setting parameters, consistent with the wealth of results presented here highlighting the pivotal role of the management of Per2 related nuclear trafficking in setting the period. It was previously shown in experiments that the circadian clock in humans, as well as in mice, takes longer to phase advance than phase delay, if exposed to jet-lag conditions in the form of a 6-hour time shift during daylight hours [86]. Jet lag is a transient phenomenon that in this case lasted several days, during which the organism is thrown off the steady-state periodic cycle and resets its new phase according to an entraining signal. While the PRC provides some insight in the phase shifting behavior of the clock in response to an outside stimulus, relating this steady-state response to a transient, jet-lag situation is generally difficult. During jet lag, the relative timing between 'clock time' and 'entrainment time' changes continuously, the system is not at its steady state, and the response to a stimulus in a (nonlinear) limit-cycle system depends on the state of the system at which the stimulus is received. In fact, a recent computational study shows that designing an optimal input stimulus for rapid phase resetting is nontrivial even if the PRC is well known [9].

In the following discussion, the focus is therefore not on the exact mechanism of overcoming jet lag in the mammalian circadian clock model, but rather the apparent similarities in the asymmetry between phase delay and phase advance between observations in jet-lagged mice and the numerical experiments performed in this work. It is sometimes argued that this difference is caused by the FRP being longer than 24 hours, however the results presented here are in reference to the innate FRP of 24.3 hours. New experimental results have furthermore identified the FRP in humans to be closer to 24 hours than previously reported [20, 52].

It is apparent that there could be a number of places in the network through which phase shifts can be introduced. For example, it has been suggested that Per1 is important during discrete entrainment, the phase response to transitions in the light stimuli, and is especially

receptive to such signals during the night [4]. During the 6-hour advance phase shift induced in the experiment by Reddy et al., the light onset occurred in the middle of the former night, temporarily inducing Per1 mRNA [86]; however, the phase shift achieved in this experiment was markedly slower than the phase delay response. To produce the phase delay, the new light onset corresponds to the former noontime, which coincides with the time at which the kinase concentration is most influential as seen in Figure 5-6. While the discussion here is solely circumstantial and we have no formal proof that the kinase concentration is involved in the asymmetric phase shifting reported in [86], our observations in Figures 5-5 and 5-6 show similarity in the sense that phase delay is accomplished relatively easier than phase advance. In addition, the particular shape of the PRC in Figure 5-6 shows a large bias towards phase advance (delay) for increased (decreased) kinase activity; in other words the PRC itself is asymmetric. If the kinase concentration is modulated throughout the cycle, the PRC suggests an effect only in the desired direction or else, if the modulation happens at a phase-shifted time, little effect at all. This could make the adaptation to a new phase during a transient situation such as jet lag easier to control. Thus we hypothesize that the kinase concentration (activity) could be a particularly convenient control point. It may be used by the natural system, for example as an additional way to process entrainment inputs during the day, especially those of long signal duration, thus acting as the control element for continuous entrainment discussed earlier. The kinase concentration may also be useful as a therapeutic point of intervention. Figure 5-5 shows that a 50% change in kinase concentration can lead to a 1 - 2 hour phase shift per day, and larger changes increase that shift further.

While the exact molecular biology of the phase advance versus delay response is beyond the scope of a purely computational study, it is discussed next that a molecular basis for differences between phase advance and phase delay can be identified for this model system. The mechanistic reason for the differences between phase advance and delay in this model is that once PER2 is phosphorylated, two processes compete for it. Phosphorylated PER2 can be either degraded or bound by the CRY proteins, which protects them from degradation. Increased kinase activity results in more phosphorylated PER2 being formed, but it is also degraded at a higher rate. Therefore, the feedback loop is accelerated. In comparison, if the kinase activity is decreased, the PER2 concentration in the cytosol increases until the rate of phosphorylation, which is proportional to the product of PER2 concentration and

kinase concentration, is equal to the maximum phosphorylation rate in the wild type. No process is competing with the slowed down phosphorylation rate and the phase delayed nuclear import of PER-CRY complex.

Taken together, these results suggest that control of the active kinase concentration is a possible way for the system to modify the period (therapeutically or naturally), especially on short time scales and following entrainment signals received during daytime.

5.4 Conclusions

This study illustrates computational approaches for probing structure-function relationships in network models - namely by showing how sensitivity analysis of a sufficiently detailed mechanistic model can relate theoretical results to experimental findings. The technique can be used both for refining the biological model and understanding the implications of network design for normal operation, disease, and therapeutic intervention.

5.5 Materials and Methods

5.5.1 The Boundary Value Problem

An ODE model for a biological system is analyzed, where $\mathbf{y}(t, \mathbf{p}) \in \Re^{n_y}$ are usually concentrations of protein, mRNA, or other species. The parameters $\mathbf{p} \in \Re^{n_p}$ are typically reaction rate constants in mechanistic models, or lumped rates of processes such as transport between compartments. Given a fixed value for $\mathbf{p}$, initial conditions on the limit cycle and the period of the oscillator are identified by solving a boundary value problem (BVP) for initial condition $\mathbf{y}_0(\mathbf{p})$ and period $T(\mathbf{p})$ subject to a periodicity condition

$$\mathbf{y}(T(\mathbf{p}), \mathbf{p}; \mathbf{y}_0(\mathbf{p})) - \mathbf{y}_0(\mathbf{p}) = \mathbf{0} \tag{5.1}$$

and a phase locking condition

$$\dot{y}_i(0, \mathbf{p}; \mathbf{y}_0(\mathbf{p})) = 0 \tag{5.2}$$

for some arbitrary $i \in \}1, ..., n_y\{$, with the limit cycle trajectory $\mathbf{y}(t, \mathbf{p}; \mathbf{y}_0(\mathbf{p}))$ given by the solution of

$$\frac{d}{dt}\mathbf{y}(t, \mathbf{p}; \mathbf{y}_0(\mathbf{p})) = \mathbf{f}(\mathbf{y}(t, \mathbf{p}; \mathbf{y}_0(\mathbf{p})), \mathbf{p}), \tag{5.3}$$

and $\mathbf{y}(0, \mathbf{p}; \mathbf{y}_0(\mathbf{p})) = \mathbf{y}_0(\mathbf{p})$. From this, we obtain initial conditions for the state variables that lie on the limit cycle. The $(n_y + 1)$st condition in Eq. (5.2) fixes the solution to a point on the limit cycle where the state variable y_i is stationary. Any arbitrary state variable can be chosen for this constraint. This BVP was solved using NITSOL, an inexact Newton solver [81], and CVODES, a stiff ODE solver with sensitivity analysis capabilities, for the integration of the dynamic system [43].

5.5.2 Sensitivity Analysis for Limit Cycle Oscillators

In most dynamic systems, the parametric sensitivities $s_{ij} \equiv \frac{\partial y_i}{\partial p_j}$ for a system such as Eq. (5.3) are integrated from zero initial conditions according to

$$\frac{d}{dt}\mathbf{S}\left(t, \mathbf{p}; \left.\frac{\partial \mathbf{y}_0}{\partial \mathbf{p}}\right|_{\mathbf{p}}\right) = \mathbf{A}(t, \mathbf{p})\mathbf{S}\left(t, \mathbf{p}; \left.\frac{\partial \mathbf{y}_0}{\partial \mathbf{p}}\right|_{\mathbf{p}}\right) + \mathbf{B}(t, \mathbf{p}) \tag{5.4}$$

where $\mathbf{A} = \frac{\partial \mathbf{f}}{\partial \mathbf{y}}$ and $\mathbf{B} = \frac{\partial \mathbf{f}}{\partial \mathbf{p}}$. In the case of the solution of a BVP in a limit cycle system, Eq. (5.4) still applies; however setting the initial conditions to zero would not be correct. The initial conditions $\mathbf{y}_0(\mathbf{p})$ are now dependent on the parameters. Because this dependency is implicit through the solution of Eqs. (5.1-5.2), it is not immediately clear how to set the initial conditions $\left.\frac{\partial \mathbf{y}_0}{\partial \mathbf{p}}\right|_{\mathbf{p}}$ for the system in Eq. (5.4) correctly. This problem is solved as follows. The set of Eqs. (5.1-5.2) can be differentiated with respect to the parameters $\mathbf{p}$, and written in matrix form yielding the following expression

$$\begin{bmatrix} (\mathbf{I} - \mathbf{M}(\mathbf{p})) & -\dot{\mathbf{y}}(T, \mathbf{p}; \mathbf{y}_0(\mathbf{p})) \\ \left.\frac{\partial f_i}{\partial \mathbf{y}}\right|_{\mathbf{y}_0(\mathbf{p}), \mathbf{p}} & 0 \end{bmatrix} \begin{bmatrix} \left.\frac{\partial \mathbf{y}_0}{\partial \mathbf{p}}\right|_{\mathbf{p}} \\ \left.\frac{\partial T}{\partial \mathbf{p}}\right|_{\mathbf{p}} \end{bmatrix} = \begin{bmatrix} \mathbf{S}(T(\mathbf{p}), \mathbf{p}; \mathbf{0}) \\ -\left.\frac{\partial f_i}{\partial \mathbf{p}}\right|_{\mathbf{y}_0(\mathbf{p}), \mathbf{p}} \end{bmatrix} \tag{5.5}$$

where $\mathbf{I}$ is the identity matrix, and $\mathbf{S}(T, \mathbf{p}; \mathbf{0})$ is the solution at time $T(\mathbf{p})$ of sensitivity Eq. (5.4)for zero as the initial condition. The matrix $\mathbf{M}$ is $\left.\frac{\partial \mathbf{y}}{\partial \mathbf{y}_0}\right|_{T(\mathbf{p}), \mathbf{p}, \mathbf{y}_0(\mathbf{p})}$, the matrix of sensitivities of the state variables with respect to their initial conditions at $T(\mathbf{p})$. This matrix is also termed the Monodromy matrix of the sensitivity system. For more detailed explanation, see reference [89]. The matrix Eq. (5.5) can be solved for the matrix of unknowns. The calculation of the sensitivity trajectories $\mathbf{S}(t, \mathbf{p}; \left.\frac{\partial \mathbf{y}_0}{\partial \mathbf{p}}\right|_{\mathbf{p}})$ can then easily and exactly be performed by integrating Eq. 95.4) starting from $\left.\frac{\partial \mathbf{y}_0}{\partial \mathbf{p}}\right|_{\mathbf{p}}$, allowing the decomposition into a periodic part and an unbounded part as described previously. This

method, in contrast to some previous publications [48, 111], enables the exact computation of the period sensitivities rather than approximating the result by truncation of a limit or by integration of the entire system for sufficiently long time, resulting in significantly less computational effort and, in principle, exact results. All matrix manipulations were performed in MATLAB 7.4.0 (R2007a). The circadian clock model was obtained as a MATHEMATICA file from http://www.pnas.org/cgi/content/full/2036281100/DC1/6 and was re-written as MATLAB code (available as Supplementary Material Dataset S1, online at http://www.ploscompbiol.org).

5.5.3 Unlumping of the parameters

The original model has 38 rate parameters, many of which are used in multiple roles within the reaction network. E.g., the mRNA export rate is the same for all mRNA species. In a "lumped" sensitivity analysis, a parameter may be shown to have great impact on the period of oscillation. However, on a network analysis level, one is interested to see which of its multiple roles is the most important in the setting of the period. Therefore, the parameter was "unlumped", meaning new parameters were assigned to each species that is affected by it so that each new parameter corresponds to a unique chemical reaction or physical process. The parameter values of all those were the same than the value of the original, single parameter. In other words, the model itself did not change during this process, but it is now possible to distinguish the different roles a parameter might play. Doing so does not necessarily imply that the organism has the capability to independently control the unlumped parameters.

5.5.4 Alternative Parameter Sets

The original set of 38 parameters was modified by first randomly choosing 10 parameters, then by randomly modifying their value either by a factor two up or down. The resulting model was simulated over 40 nominal periods in order to approach the limit cycle. If the apparent period (time difference between the last and second-to-last minimum in the CRY1 concentration) was between 23.5 and 25 hours, the model was subjected to the boundary value problem solver. This selection criterion was chosen because it is known that the mammalian clock oscillates roughly in this range of periods, and it is irrelevant to investigate parameterizations with known, unphysical periods. 15 such models were generated, 11 out of

those were converged easily; the others were discarded. Possible reasons for non-convergence include the presence of damped oscillations, which would not have been detected in the earlier test. By inspection, it was found that the modified parameters included both low and high sensitivity parameters in the nominal model. The parameter values of the 11 final models are found in Table B.2, along with the resulting period and ranking of the top 25 sensitivities.

Chapter 6

Structure–Function Relationships Between the Biochemical Architecture of the Mammalian Circadian Clock and the Functional Properties of Its Oscillation

Abstract

A pair of related, large, detailed models of the mammalian circadian clock are subjected to sensitivity analysis of the phases, amplitudes and period of their circadian oscillation. The mechanisms for manipulation of each of these features are compared and it is found that certain commonalities exist. Most features were found to be highly sensitive with respect to changes in a small group of parameters, indicating that a balanced control of several features at the same time requires concerted action throughout the network. Using the example of period-neutral phase changes, such mechanisms are discovered and discussed, both on the scale of infinitesimal as well as finite perturbations. Furthermore, it is demonstrated that relative phase sensitivity analysis is a suitable tool to study the ability of the circadian clock to track several phases simultaneously, while keeping a constant period. However, it is also shown that in order to make biologically significant discoveries, the mechanism of detection of relevant phases such as "dawn" and "dusk" must be known at a molecular level.

6.1 Introduction

The mammalian circadian clock is a molecular network that consists of several negative and positive feedback loops. Part of its functionality is to generate 24-hour oscillations which provide mammals with a time-keeping framework. Interactions of the clock with other biochemical signals provide a very precise schedule of events that include the production of different hormones at different times of day, digestive activity at times when the body anticipates food, and liver and kidney activity at times when the body anticipates a need to process waste. The particular network structure of genetic and biochemical signaling reactions organized into multiple, seemingly redundant feedback loops raises the possibility of discerning structure–function relationships at a variety of levels of abstraction. For example, in their 2004 review, Lakin-Thomas & Brody indicate that particular pieces of the clock might be responsible for particular functions [61]. In an experimental study of *per2* expression, separate mechanisms for rhythm generation and for phase control were found recently [2], further suggesting potentially separate control mechanisms for both. In this work, it was shown in Chapter 5 that a portion of one feedback loop carries dominant responsibility for setting the period in the mammalian circadian clock. This framing lays the groundwork for understanding detailed relationships between functionalities of the clock and their implementation at a molecular level and perhaps also for assigning functional roles to seemingly redundant feedback loops.

In this study several types of sensitivities are computed. In some other studies the local sensitivities of the fit between model trajectories and experimental data are computed with respect to the model parameters, with the goal of identifying the extent to which the parameters are locally determined by the data [17, 39]. Here our goal is quite different. We are interested in quantifying the extent to which functional properties of the system are determined or affected by each chemical reaction. The functional properties that we investigate for this limit-cycle oscillator include the period (which is the same for all species), the amplitude of each species, and relative phase relationships between pairs of species. Because each chemical reaction is controlled by a single rate parameter, it is useful to compute sensitivities with respect to parameters as a metric for the effect of individual reactions on network properties. Our goal is to elucidate network structure–function properties as well as to implement specific changes in network behavior through manipulation of individual

reactions. A second, related question that is treated in this study is related to the ability of the circadian clock mechanism to process more than one entraining signal at a time. It is known, for example, that the clock can entrain to signals other than light; for example, it can entrain to temperature cycles and cycles in nutritional availability. Related to this observation is the question of whether the clock can track separate signals simultaneously and continuously. This is often phrased as the "ability to track several phases". An intuitive example is the circannually varying length of the subjective day. Winter days are shorter than summer days, although the 24-h period of the clock is maintained. So how does the clock account for this varying length of day? Is there a signal for "dusk" that can be processed separately from a signal for "dawn"? How is the "signal capacity", expressed as the number of independent signals the network can track, related to network structure? In particular, it has been suggested that the number of feedback loops in a clock mechanism is related to the ability of the mechanism to track several phases [85]. This suggestion is examined in detail in the current work, in the context of the most detailed, published mechanistic model of the mammalian circadian clock. This model was extended in Chapter 4 using recent experimental findings to include several additional feedback loops.

Numerical experimentation demonstrated that while both the original and extended model entrain with a stable "morning" phase to the light input signal as shown in Figure 4-2, the time at which the light is switched off does not significantly affect the time courses of mRNA concentrations (data not shown). Therefore, it was concluded that any mechanism that would allow for "dusk tracking' is not explicitly included in the models studied here. It seems that there might be two possibilities for the tracking of a second phase for "dusk". One is that at or before dusk, an input signal is processed that would cause a phase adjustment. This mechanism would be similar to the discrete entrainment caused by a step change in an entrainment signal at dawn, which adjusts the phase once daily to match the period of the entraining signal [26]. However, a second possibility might be that an input related to seasonal change would cause a permanent parameter change in the mechanism, which could slowly vary the time at which dusk occurs throughout the year. This mechanism could be similar to the continuous entrainment mechanism, which is found in some species, e.g., birds, and might play a role in mammals [26]. Due to the lack of explicit abilities to model the relative length of the perceived day, computing the relative phase sensitivities of the model parameters in constant darkness appears to be an appropriate numerical experiment

to evaluate the models's performance. The results are expected to pertain to the second proposed mechanism, since they indicate how permanent parameter changes would affect clock performance.

The scaled, relative phase sensitivity of a given relative phase of interest with respect to each of the 324 or 447 unlumped parameters is calculated and the group of the most highly relative-phase-sensitive parameters is analyzed for the apparent mechanism of phase setting and its overlap with the group of highly period-sensitive parameters. By determining key reaction or transport rates for the setting of different phases that might be representative of the way the day length is represented molecularly, it may be possible to identify candidate mechanisms that would allow for the change of day length over the course of a season.

On a more general level, it is then interesting to study the general ability of the model to control different phases independently of each other. Ideally, one would like to analyze exhaustively the network's abilities to control phases independently. However, there is an infinite number of possible ways to define different phases and their parameter dependencies. Thus, this study is limited to investigating a small number of relative phases that are possibly relevant to the biology or the network structure. After analyzing how individual relative phases are controlled in either model, it is attempted to understand how the network could adapt to change a phase independently of the period. This task involves changing some of the reaction rate parameters in a finite manner, and thus goes beyond the local sensitivity information that describes the effects of infinitesimal perturbations. For the set of numerical experiments that is performed here, the models with lumped parameterization are used, considering the fact that the unlumped parameters might not be independently accessible to manipulation. The relative phase sensitivity information is used to select a period-neutral direction in parameter space in which maximum phase change is expected. It is studied how far the model can take the process of changing a phase independently of the period, by using a very basic gradient-based optimization technique.

6.1.1 Angular Relative Phase Sensitivity

A relative phase is defined in the context of this work as the difference in time between two events on the periodic orbit. In mathematical terms, both events can be described by phase locking conditions (PLCs), as discussed in Chapter 2. If the mathematical definitions for the beginning and end of the relative phase are differentiable, we can calculate how

the relative timing between the two events depends on the network parameterization. This was explained in detail in Section 2.2.7. It is important to remember that identical times on the periodic orbit can be defined using different PLCs, but this can lead to different relative phase sensitivities. This is shown graphically in Figure 2-1 and will be important in understanding the results presented in this chapter. In Chapter 3 it was explained that one of the more descriptive definitions of phase is the angular relative phase, or γ. If the relative phase β is a time difference between two events, then the relative phase angle γ of the phase β is defined as

$$\gamma = 360^\circ \frac{\beta}{T}. \tag{6.1}$$

Its sensitivity $\frac{\partial \gamma}{\partial \mathbf{p}}$ with respect to the parameters is

$$\frac{\partial \left(360^\circ \frac{\beta}{T}\right)}{\partial \mathbf{p}} = \frac{360^\circ}{T}\frac{\partial \beta}{\partial \mathbf{p}} - \frac{360^\circ \beta}{T^2}\frac{\partial T}{\partial \mathbf{p}}, \tag{6.2}$$

which follows directly from the chain rule. This sensitivity describes the change of the phase angle as a result of an infinitesimal parameter change, where the change of period is taken into account and normalized out. Thus the relative phase sensitivity $\frac{\partial \beta}{\partial \mathbf{p}}$ describes the change in time between a pair of events, whereas the relative angular phase sensitivity $\frac{\partial \gamma}{\partial \mathbf{p}}$ describes the change in phase angle. Two events that remain 180° apart in the circadian day after a finite perturbation of a parameter increases the period by 6 hours will have a $\Delta\beta$ of 6 hours but a $\Delta\gamma$ of 0°.

6.1.2 Definition of the Dawn-to-Dusk Time Distance

The time at which the concentration of *mCry1* reaches a minimum was used to represent subjective dawn, or CT=0, in the model (see Section 4.2.3; CT is circadian time). In order to study the flexibility of the model with respect to variations in the length of subjective day (dawn-to-dusk) while maintaining a 24-hour period, a second PLC needs to be identified for the definition of "dusk" (CT=12 in most laboratory experiments). From a survey of the experimental and review literature, the following molecular events happen at or near CT=12. *mBmal1* has risen half-way to its maximum concentration [83, 8, 87], *mCry1* is near its highest concentration [8, 87], and *mPer1* and *mPer2* have declined to roughly half their peak concentrations [8, 87]. Because Forger and Peskin [29] do not represent Bmal1

transcription explicitly, the corresponding PLC cannot be employed in this model. Thus, in order to evaluate the relative phase flexibility of the mammalian circadian models under study, the maximum of total Cry1 mRNA concentration was chosen as a first definition of dusk. This phase is called 'mCry1 dusk' for the remainder of this Chapter, and it occurs at CT = 11.88 or 12.002 h in the original and extended model, respectively. A second definition was the time at which *mPer2* crosses 50% of its peak concentration. This phase is called 'mPer2 dusk' for the remainder of this Chapter, and it occurs at CT = 15.38 or 15.04 h in the original and extended model, respectively. These choices allow for a direct comparison of phase flexibility in both models.

6.2 Results

Two models form the basis for the results presented here — the original model of Forger and Peskin and an extended version that augments the original with additional details and recent findings. Moreover, as sensitivities with respect to rate parameters were computed, the results depend on the degree to which the parameters have been lumped (see Chapter 5). The rate parameters are lumped if two seperate physical processes are represented with one parameter, which means that only one sensitivity can be calculated for this rate parameter. We unlump them by assigning individual parameters with the same value to each reaction, and calculating separate sensitivities for each. For example, it is common to use a common rate parameter for nuclear export for all mRNA species. When we are interested in understanding the individual contribution of each reaction to functional network properties, we unlump the parameters. However, when we consider re-engineering new properties into the network, we may choose to lump together parameters representing properties that we are unlikely to be able to manipulate independently.

For the study presented here, the models were unlumped even further than in our previous work in Chapter 5, in order to distinguish the DNA binding events separately for each of the BCC-controlled species. This leads to 4 additional differential equations in the original model, and to 10 additional equations in the extended model. These equations are redundant in that the state variables they govern (i.e., the likelihoods of BCC or BCC–Cry complexes to be bound to the different DNA sites) are exactly the same as in the original, lumped variables. However, this procedure allows one to probe individually the

reactions that determine the binding kinetics for each, and the results of the unlumping are worthwhile. Doing so increases the number of parameters to 324 in the original model, and 447 in the extended model. As before, the parameter values are unchanged from the lumped model, and there is no difference between a simulation of the lumped versus unlumped models.

6.2.1 Period Sensitivities

As a first basis for comparison, the period sensitivities for both models were calculated and rank-ordered (Figure 6-1). Here, the label "GBCCRn" indicates the probability of a BCC–Cry complex being bound to a DNA binding site, and "GBCC" indicates that the free BCC is bound to a DNA binding site. Both models show a very similar pattern of

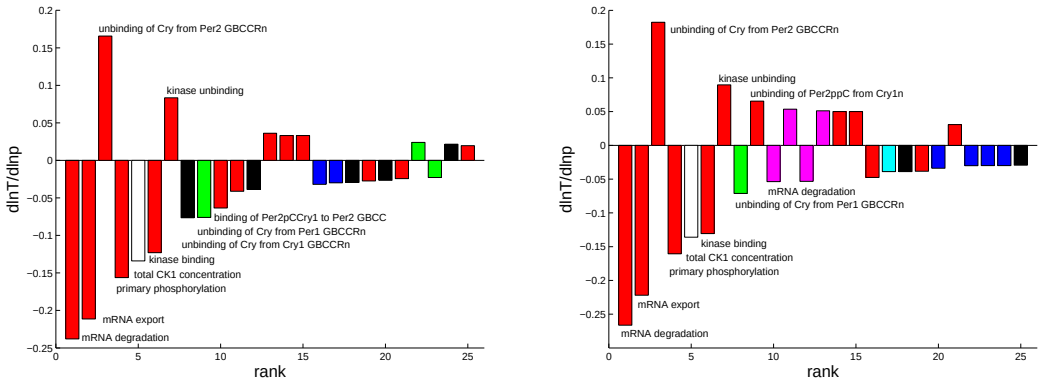

(a) (b)

Figure 6-1: The top 25 scaled period sensitivities ranked by absolute magnitude for unlumped models. (a) Original model; (b) Extended Model; Black, Cry1-related parameter; blue, Cry2-related parameter; green, Per1-related parameter; red, Per2-related parameter; magenta, Bmal1-related parameter; cyan, Rev-Erbα-related parameter; yellow, ROR-related parameter.

parameters with high, scaled period sensitivities, with the magnitudes of the sensitivities being comparable. As discussed in detail for the original model in Chapter 5, a set of largely contiguous reactions in the Per2 negative feedback loop dominate the period setting in both models, with mRNA export and degradation being the most significant. The unlumping of the DNA binding kinetics has further revealed that the unbinding of Cry complexes from the Per2 transcriptional control element is the third most important reaction in setting the

period. The fourth through seventh ranked parameters in both models are reactions related to Per2 phosphorylation, which was discussed in detail in Sections 5.2.1 and 5.3.3. Not shown on the graph is the fact that the secondary phosphorylation of Per2 has the opposite effect on the period as the primary phosphorylation, as suggested in reference [103]. In the extended model, parameters regulating the transcription and mRNA kinetics of Bmal1 are ranked tenth through thirteenth. This is consistent with the experimental observation that the Bmal1$^{-/-}$ phenotype is arrhythmic [8, 87].

6.2.2 Amplitude Sensitivities

The scaled relative amplitude sensitivities were computed for the seven mRNA species in the extended model. The relative amplitude of the total mRNA (nuclear plus cytosolic) for each species was calculated as the difference between maximum and minimum concentration. The sensitivity of this quantity was calculated as described in Chapter 2. Shown in Figures 6-2 and 6-3 are the top 25 reactions of the extended model, ranked by absolute magnitude of their scaled amplitude sensitivity. The results for the original model are very similar and are not shown.

Throughout the seven amplitudes it is consistently seen that the transcription reaction of the respective mRNA together with the unbinding reaction of Cry-complexes from the BCC on the respective DNA-binding site are the largest impact reactions. This makes intuitive sense, in that both reactions affect transcription. However, that they specifically affect amplitude and that they would be somewhat more important than the binding reactions for the Cry complexes is not immediately clear. Interestingly, there is a second set of parameters that appears common between all seven amplitudes studied. The rate of Cry unbinding from the BCC at the Per2 DNA binding site is ranked in the top three of all amplitudes. The nuclear export of Per2 mRNA is in the top eight in all but one of the amplitudes. Other parameters that repeatedly appear in the top 25 are the rate of unbinding of Per2ppC (the complex of twice-phosphorylated Per2 with CK1 kinase) from Cry1 as well as the degradation rates of nuclear Per2ppC and nuclear Cry1. This observation demonstrates a combination of local and central control over the amplitudes of the mRNA oscillations in both computational models.

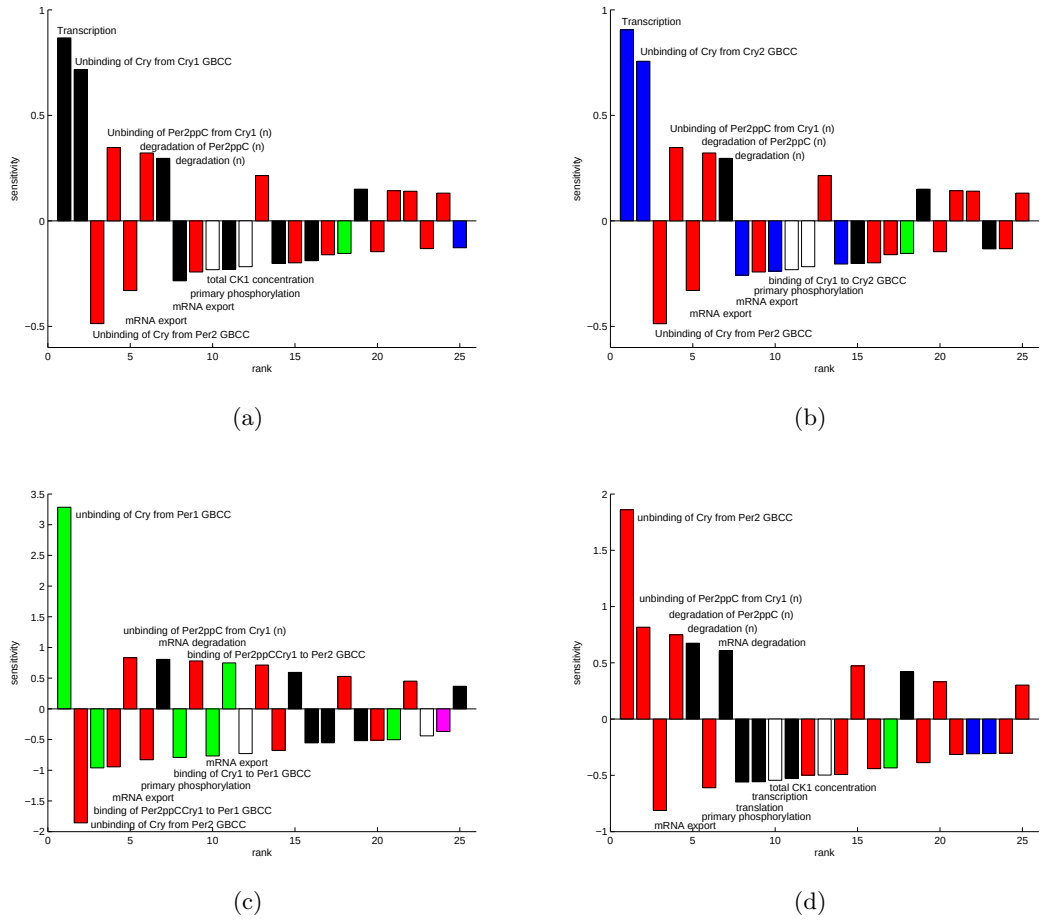

Figure 6-2: Scaled, rank-ordered relative amplitude sensitivities for the different mRNA concentrations, in the extended model; (a) *mCry1*; (b) *mCry2*; (c) *mPer1*; (d) *mPer2*; black, Cry1-related parameter; blue, Cry2-related parameter; green, Per1-related parameter; red, Per2-related parameter; magenta, Bmal1-related parameter; cyan, Rev-Erbα-related parameter; yellow, ROR-related parameter.

6.2.3 Relative Angular Phase Sensitivities

The scaled relative angular phase sensitivities $\frac{\partial \ln \gamma}{\partial \ln \mathbf{p}}$ for two differently defined dawn-to-dusk relative phases were computed for the original and extended models using unlumped parameters (Figure 6-4). Dawn was defined as the point at which *mCry1* reaches a minimum concentration and dusk was defined alternatively as "mCry1 dusk" or "mPer2 dusk" as described in Section 6.1.2. The results are similar between the two models; the results for the extended model will be discussed, as they provide more detail. When the peak of mCry1 is used as the marker for dusk, the two dominant sensitivities are degradation and export

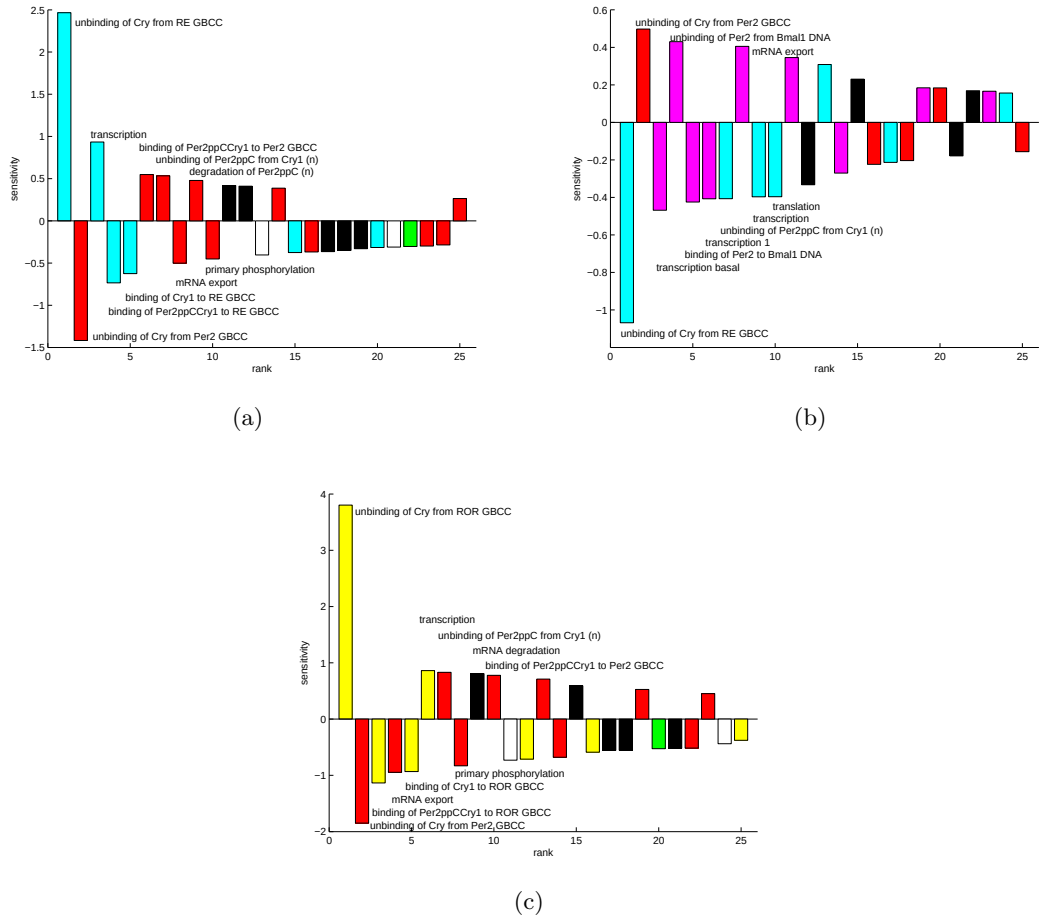

Figure 6-3: Scaled, rank-ordered relative amplitude sensitivities for the different mRNA concentrations, in the extended model; (a) *mRE*; (b) *mBmal1*; (c) *mROR*; black, Cry1-related parameter; blue, Cry2-related parameter; green, Per1-related parameter; red, Per2-related parameter; magenta, Bmal1-related parameter; cyan, Rev-Erbα-related parameter; yellow, ROR-related parameter.

of Cry1 mRNA. This is interesting, given that both PLCs that define the beginning and end of apparent daytime were formulated with reference to *mCry1*, but it is noteworthy that reactions involving *mCry1* synthesis do not dominate. The degradation and export reactions dominate the relative angular phase between trough and peak. The reactions that follow in the ranking are reminiscent of the high-period sensitivities shown in Figure 6-1, and mostly located in the Per2 negative feedback loop. That is, reactions that strongly affect the period do not do so exclusively. They also affect phase relationships. It is important to note that period-changing reactions are not unalterable in the context of a 24-hour day. Rather, compensating changes in such reactions can lead to unaltered period yet changed

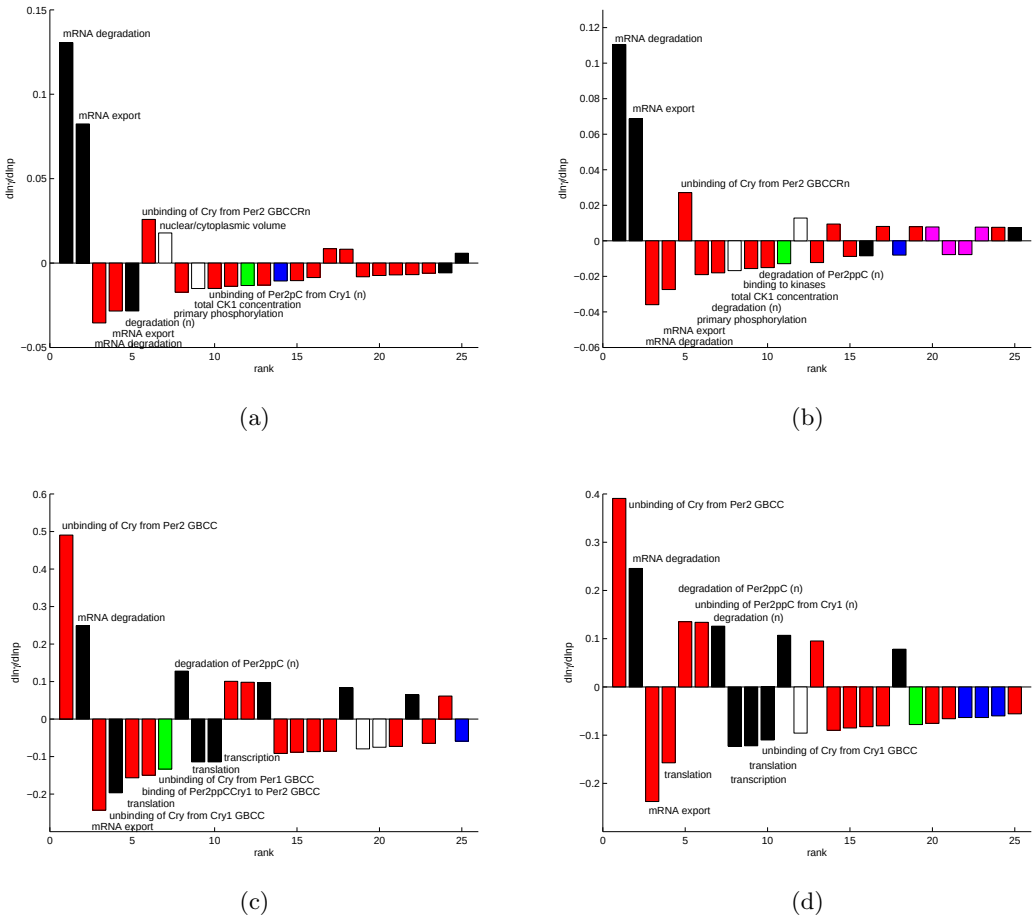

Figure 6-4: Scaled relative angular phase sensitivities $\frac{\partial \ln \gamma}{\partial \ln \mathbf{p}}$ for the dawn-to-dusk phase, ranked by absolute magnitude. (a) Original model, mCry1 dusk; (b) Extended Model, mCry1 dusk; (c) Original model, mPer2 dusk; (d) Extended model, mPer2 dusk; Black, Cry1-related parameter; blue, Cry2-related parameter; green, Per1-related parameter; red, Per2-related parameter; magenta, Bmal1-related parameter; cyan, Rev-Erbα-related parameter; yellow, ROR-related parameter.

phase relationships.

Conversely, when daytime was defined using a definition of dusk that involves the Per2 mRNA concentration (but the same, Cry1-based definition of dawn), the Per2 related reactions moved even farther to the top of the ranking and the Cry1 mRNA degradation remains the second most influential. A group of Cry1 related parameters populates ranks 7–11; these reactions are all important in determining the amount of Cry1 in circulation (transcription, translation, the binding of the inhibitory Cry-complexes from the BCC at the Cry1 binding site and degradation of nuclear and cytosolic CRY1). Interestingly, a number of reactions

were found to be of significant influence in the relative angular phase sensitivities that were already found previously to be important in setting the period and amplitudes of the mRNA oscillations. This finding will be discussed in more detail in Section 6.2.4.

The second definition of the relative phase not only leads to somewhat different sensitivity rankings, but also to higher magnitudes of scaled sensitivity than found in the previous definition. This observation leads to the conclusion that if one is to understand how the clock could regulate the dawn-to-dusk phase, it is important to understand how both dawn and dusk are "tracked" on a molecular basis. This knowledge could be important for understanding the molecular origin of seasonal affective disorder and possibly could point towards novel therapeutic intervention.

6.2.4 Network-wide Relative Angular Phase Sensitivities

To obtain a more general, network-wide picture of the phase sensitivities in the model, an additional six phases were defined. The phase angles between the peaks and troughs of the total mRNA concentrations of Cry2, Per1, Per2, Rev-Erbα, Bmal1, and ROR in the extended model were computed together with their sensitivities. The corresponding phase in Cry1 mRNA is same as the dawn-to-dusk phase with "mCry1 dusk". The resulting rankings based on absolute magnitude of scaled relative angular phase sensitivity are shown in Figure 6-5.

It is found that the export and degradation rates of the mRNA that defined the phase are in most cases the reactions with the largest influence on the peak-to-trough phase angle. As before, these parameters will be called "local" to the network function studied. These are followed by a surprisingly conserved set of parameters, some of which have been found to be important in period and amplitude setting as well, including the unbinding of Per2ppC from Cry1, the degradation of Per2ppC, and the export and degradation rates of Per2 mRNA. One other reaction that is consistenly present is the degradation of nuclear Cry1. It should be noted that the mBmal1 phase deviates somewhat from this pattern, as was the case in the amplitude study. This species' expression is regulated very differently than the rest, which are all controlled by the same mechanism through BCC and its inhibition by Cry and their complexes.

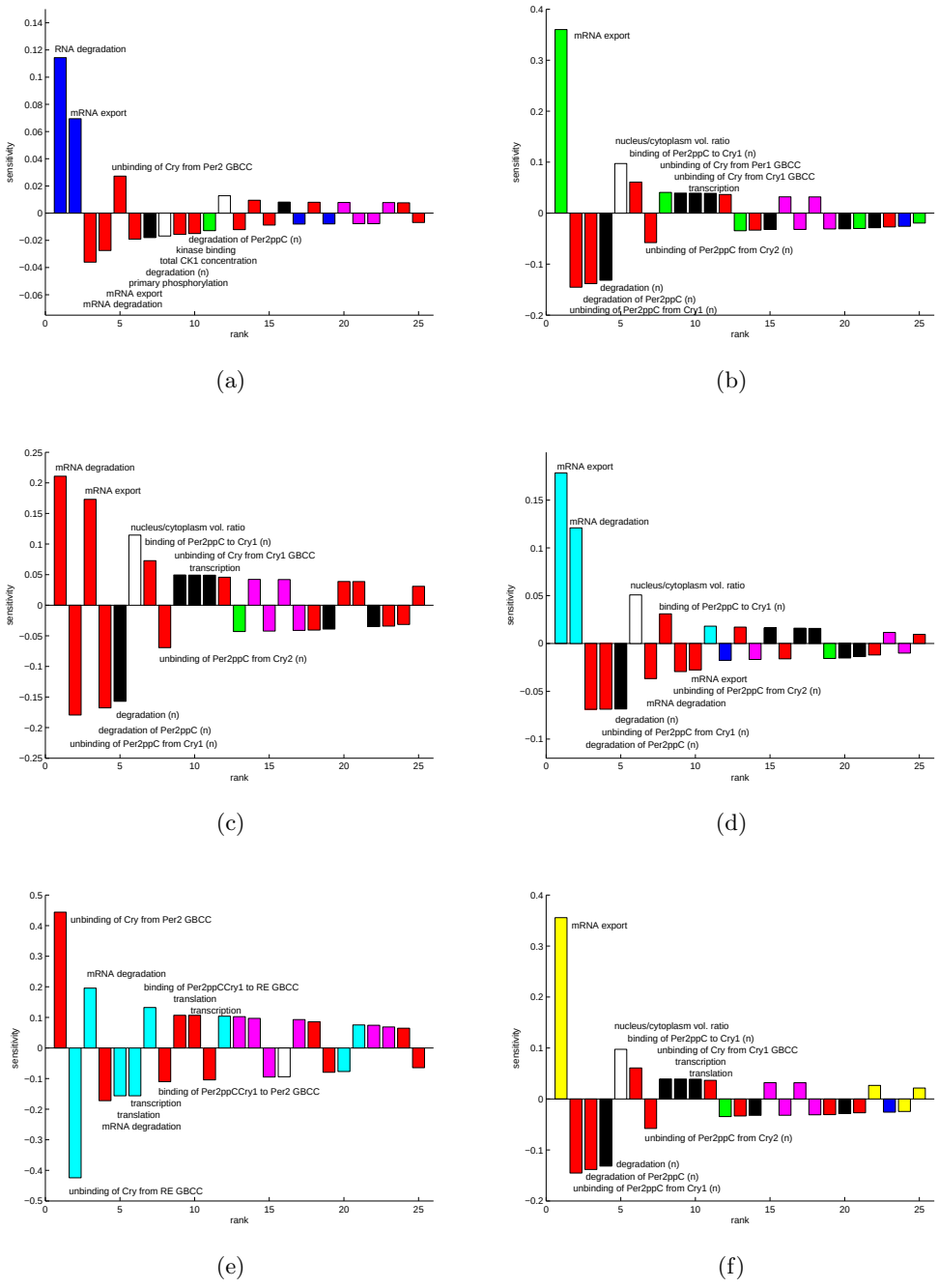

Figure 6-5: Scaled relative angular phase sensitivities $\frac{\partial \ln \gamma}{\partial \ln \mathbf{p}}$ for the peak-to-trough phase of different mRNA concentrations, ranked by absolute magnitude in the extended model; (a) *mCry2*; (b) *mPer1*; (c) *mPer2*; (d) *mRE*; (e) *mBmal1*; (f) *mROR*;Black, Cry1-related parameter; blue, Cry2-related parameter; green, Per1-related parameter; red, Per2-related parameter; magenta, Bmal1-related parameter; cyan, Rev-Erbα-related parameter; yellow, ROR-related parameter.

6.2.5 The Circadian Clock is Not Modular

In modular design such as found in man-made devices, one expects a one-to-one correspondence between structure and function. Our early results on the circadian clock supported a modular design strategy: all high period sensitivities were found in just one out of several feedback loops [106]. Throughout this loop, the period sensitivities were high, and in other feedback loops the period sensitivities were low. Thus, this feedback loop bears primary responsibility for setting the period. This finding is confirmed in the more detailed analysis in Section 6.2.1. It is however only part of a bigger picture, as the subsequent results show. It appears that a significant fraction of the parameters that are important in setting the period are also important in setting other properties of the oscillation, such as the setting of relative phase angles or relative amplitudes. Both phases and amplitudes can be located entirely in other feedback loops yet still be regulated indirectly and in part through the Per2 negative feedback loop.

This set of result leads to a new interpretation, namely that the clock design is not modular in the same sense as man-made, engineered systems. If one of the "key parameters" (i.e., parameters with high sensitivities in several functions) is changed, several clock functions might be altered simultaneously. Conversely, altering one clock property might necessarily entail changing another, and controlled, concerted changes of functions might require balanced modifications to several reactions throughout the network. This hypothesis is considered in the remainder of this section.

6.2.6 How Independent Are Period and Dawn-to-dusk Phases?

As it is recognized that some clock properties can only be tuned in concert with others, we return to the question of whether with this network one can independently vary the length of perceived day (or sunlit day), while maintaining a 24-hour period. The angle α between the period sensitivity vector and the relative phase sensitivity vector for both models was computed, as previously shown in Section 3.2. As demonstrated in Figure 3-2, this angle should give an indication to understand how orthogonal the relative-phase sensitivity vector is to the period sensitivity vector. The range of angles is by definition between zero and 90°, and a large angle should provide an indication that it is possible to modify the period and the relative phase fairly independently. The angles for both definitions of 'dusk' and

Table 6.1: Relative angles and lengths of the period-neutral phase sensitivity vectors in the original and extended models of the mammalian circadian clock.

Model	Original	Extended
CT (mCry1 dusk)	12.00	11.88
Rel. Length L (mCry1 dusk)	0.259	0.181
Angle α (mCry1 dusk)	26.6	18.3
CT (mPer2 dusk)	15.38	15.05
Rel. Length L (mPer2 dusk)	0.787	0.673
Angle α (mPer2 dusk)	41.6	33.2

both models are shown in Table 6.1. A period-neutral relative phase sensitivity vector was also calculated, and its length compared to the length of the period sensitivity vector. This relative length L is also reported in Table 6.1. The make-up of the period-neutral relative phase sensitivity vector is discussed in Section 6.2.8

It was previously shown in Section 3.3.10 that the angle might provide a better measure of the phase flexibility of the model than the relative length L. For both definitions of "dusk", it is found that the original model has a larger angle, and the angle is larger for the second, rather than for the first definition of "dusk". This observation is related to the finding in the sensitivity rankings, where it was shown that the corresponding sensitivities are larger, and more different from the period sensitivities in this case. Again the two different angles reflect the need to know mechanistically how dawn and dusk are tracked in the clock, if one wants to understand the underlying flexibility of the clock with respect to this phase.

6.2.7 Peak-to-Peak Relative Phase Sensitivities

In the absence of specific knowledge regarding how individual phases might be set and tracked, it was thought to be interesting to attempt to gain a more systematic impression of how different phases throughout the network are regulated and how flexible they are in the face of a constant period. Ideally, one would like to obtain a network-wide picture for which events and their timings are interrelated, and which ones can change without affecting others. However, as previously mentioned, this is not possible due to the infinite number of relative phases in the network. Thus, a smaller number of events was selected for a pairwise

study. The relative timing between peaks in total mRNA concentration was calculated and each phase's relative sensitivity was computed. The angle α between this vector and the period sensitivity vector was computed as in the previous section. In other words, it was studied how the timings between peaks of mRNA can be varied locally, depending on the parameters, and how independent this variation is from a variation of the period. The angles α are represented in Tables 6.2 for the original model and Table 6.3 for the extended model.

Table 6.2: Relative angles of peak-to-peak sensitivities in the original model of the mammalian circadian clock. Rows: Beginning of the phase is the peak in this mRNA concentration; Columns: End of the phase is the peak in this mRNA concentration.

mRNA	*mCry2*	*mPer1*	*mPer2*	*mRev-Erbα*
mCry1	87.7	84.9	76.1	83.6
mCry2		87.6	72.9	86.3
mPer1			57.9	87.7
mPer2				58.6

Table 6.3: Relative angles and lengths of the period-neutral phase sensitivity vectors in the extended model of the mammalian circadian clock. Rows: Beginning of the phase is the peak in this mRNA concentration; Columns: End of the phase is the peak in this mRNA concentration.

mRNA	*mCry2*	*mPer1*	*mPer2*	*mRev-Erbα*	*mBmal1*	*mROR*
mCry1	88.6	88.3	70.0	87.3	26.4	89.1
mCry2		86.6	68.1	88.9	26.7	87.4
mPer1			62.70	83.3	26.5	88.7
mPer2				55.41	25.04	61.33
mRev-Erbα					24.94	84.56
mBmal1						26.59

It is very noticeable that the angles throughout the original model are very large, with the lowest being 57.9° and the highest being 87.7°. In other words, several of the phases shown here appear almost completely locally independent of the period. In the extended model, a similar picture is found, with the exception of phases that involve Bmal1 mRNA, which appear with markedly smaller angles of 24.9° to 26.7°. In other words, the largest

angle found involving the peak time of Bmal1 mRNA is much smaller than the smallest angle found in any phase not involving the Bmal1 mRNA concentration.

It appears that the timing between peaks of mBmal1 and any other mRNA species is hard to vary independently of the period. All the other peak-to-peak timings can be varied practially independently of the period. All species except Bmal1 also oscillate "in phase" with each other, whereas the Bmal1 species oscillates "in anti-phase". It is this antiphasic oscillation which closes all the feedback loops of the other species, since the BCC is necessary for transcription of all species but Bmal1. The result found here might indicate that the anti-phasic nature coupled with the need for BCC to close the feedback loop means that the peak time of mBmal1 is coupled to the period of oscillation in such a way that any phase involving mBmal1 is less flexible (i.e., has a smaller angle α).

6.2.8 Period-neutral Relative Phase Sensitivities

For the relative phase sensitivities computed in Section 6.2.3, the period-neutral direction in parameter space was calculated using Equation 3.7. The result is a period-neutral relative phase sensitivity direction $\left(\frac{\partial\beta}{\partial\mathbf{p}}\right)_T$. An infinitesimally small step in parameter space in this direction results in maximum relative phase change with zero period change. It is very important to appreciate the fact that all the results presented here are only to be interpreted in the context of this entire vector. Any individual parameter change will not result in a period-neutral relative phase change.

The largest contributions of the period-neutral phase direction were sorted by absolute magnitude ($\|\left(\frac{\partial\beta}{\partial p_i}\right)_T\|$) or relative magnitude ($\|\frac{p_i}{\beta}\left(\frac{\partial\beta}{\partial p_i}\right)_T\| = \|\frac{\partial \ln\beta}{\partial \ln p_i}\|$) and are shown in Figure 6-6 for the original model and Figure 6-7 for the extended model, for both definitions of "dusk". It is found in both models that the period-neutral phase direction is made up of parameter changes that are only slightly different from the top-ranking relative angular phase sensitivity parameters in Figure 6-4.

The mechanism of a period-neutral relative phase change is examined more closely. A step of length one was taken into the period-neutral phase direction. The change in % of phase and period caused by each individual parameter change was calculated and is shown in Figure 6-8. It becomes clear that this change requires a concerted effort. For the mCry1 dusk definition (top row), most of the phase change (green) is accomplished by changing just two parameters, the Cry1 mRNA export and degradation rates, in both

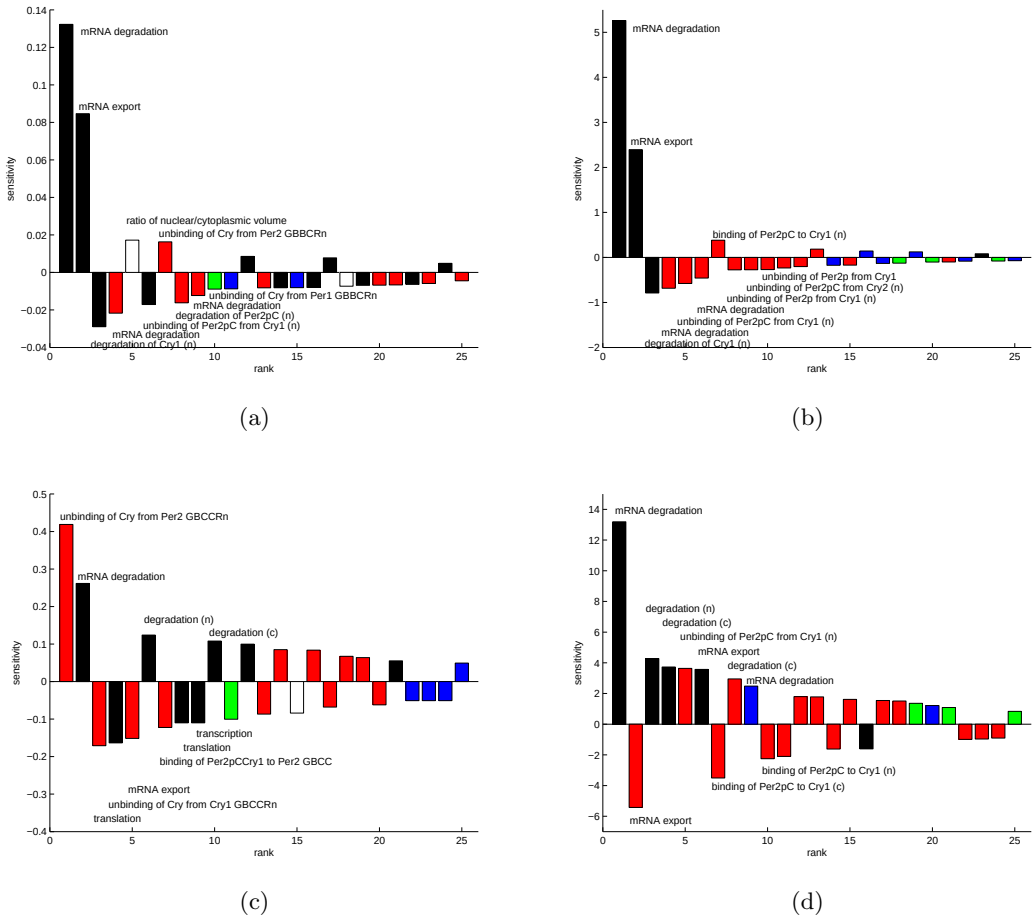

Figure 6-6: Period-neutral relative phase direction for the dusk-to-dawn phase in the original model, ranked by absolute magnitude of step size. (a) mCry1 dusk, ranked by relative stepsize; (b) mCry1 dusk, ranked by absolute stepsize; (c) mPer2 dusk, ranked by relative stepsize; (d) mPer2 dusk, ranked by absolute stepsize; Black, Cry1-related parameter; blue, Cry2-related parameter; green, Per1-related parameter; red, Per2-related parameter. The sensitivities represented here are part of a sensitivity direction, and can only be considered in the context of the entire vector.

models. However, to compensate for the period change (magenta) it takes a group of four (in the original model) or six (in the extended model) parameters that participate significantly. The mechanism is different for the second, mPer2-based, definition of dusk. The phase change is implemented by contributions of the first ten parameters, with the first parameter making the biggest contribution by far, but the others contributing significantly. Throughout the same parameters, the period changes occur such that they balance each other, with again 4 and 6 significant changes in both models, respectively. It should be

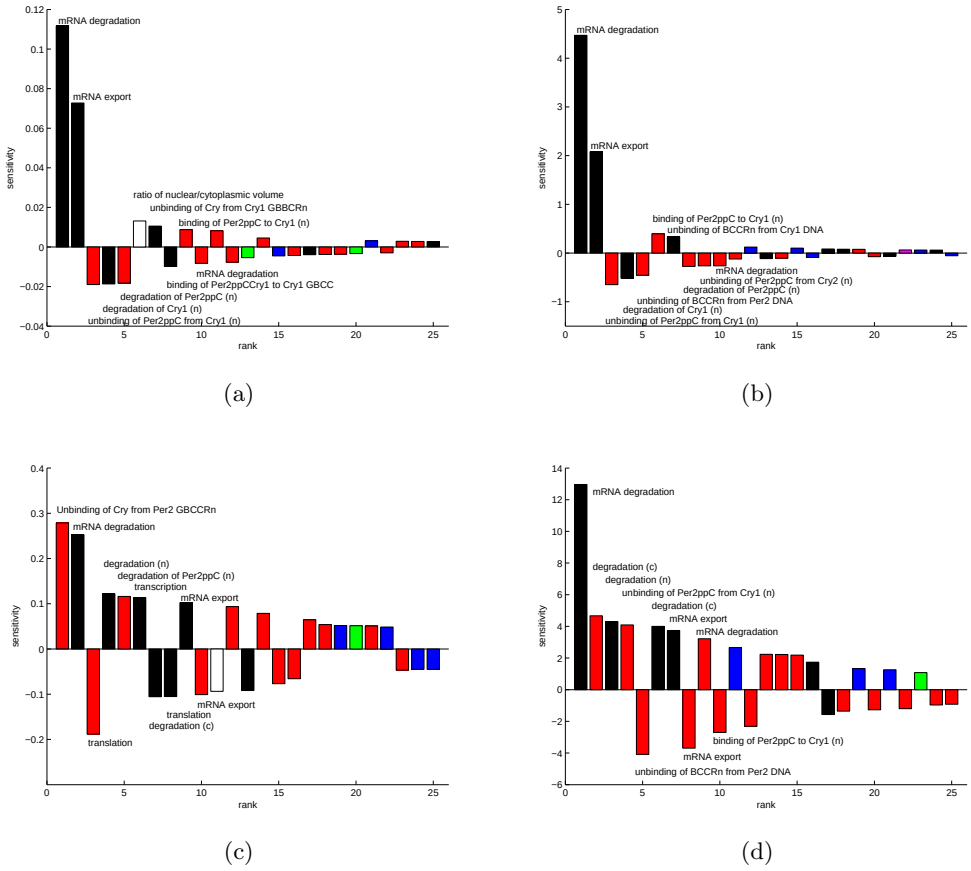

Figure 6-7: Period-neutral relative phase direction for the dusk-to-dawn phase in the extended model, ranked by absolute magnitude of step size.(a) mCry1 dusk, ranked by relative stepsize; (b) mCry1 dusk, ranked by absolute stepsize; (c) mPer2 dusk, ranked by relative stepsize; (d) mPer2 dusk, ranked by absolute stepsize; Black, Cry1-related parameter; blue, Cry2-related parameter; green, Per1-related parameter; red, Per2-related parameter; magenta, Bmal1-related parameter; cyan, Rev-Erbα-related parameter; yellow, ROR-related parameter. The sensitivities represented here are part of a sensitivity direction, and can only be considered in the context of the entire vector.

emphasized again that this balanced parameter modification is needed for the maximum phase change with zero period change. It might be possible to modify the phase in a period-neutral manner using a simpler mechanism, however the phase change achieved would be smaller.

This result is a graphical representation of what was found throughout this study. Modifying one property significantly (here, a relative phase) without another (here, the period) requires a concerted effort of several parameter changes. The parameters changed here,

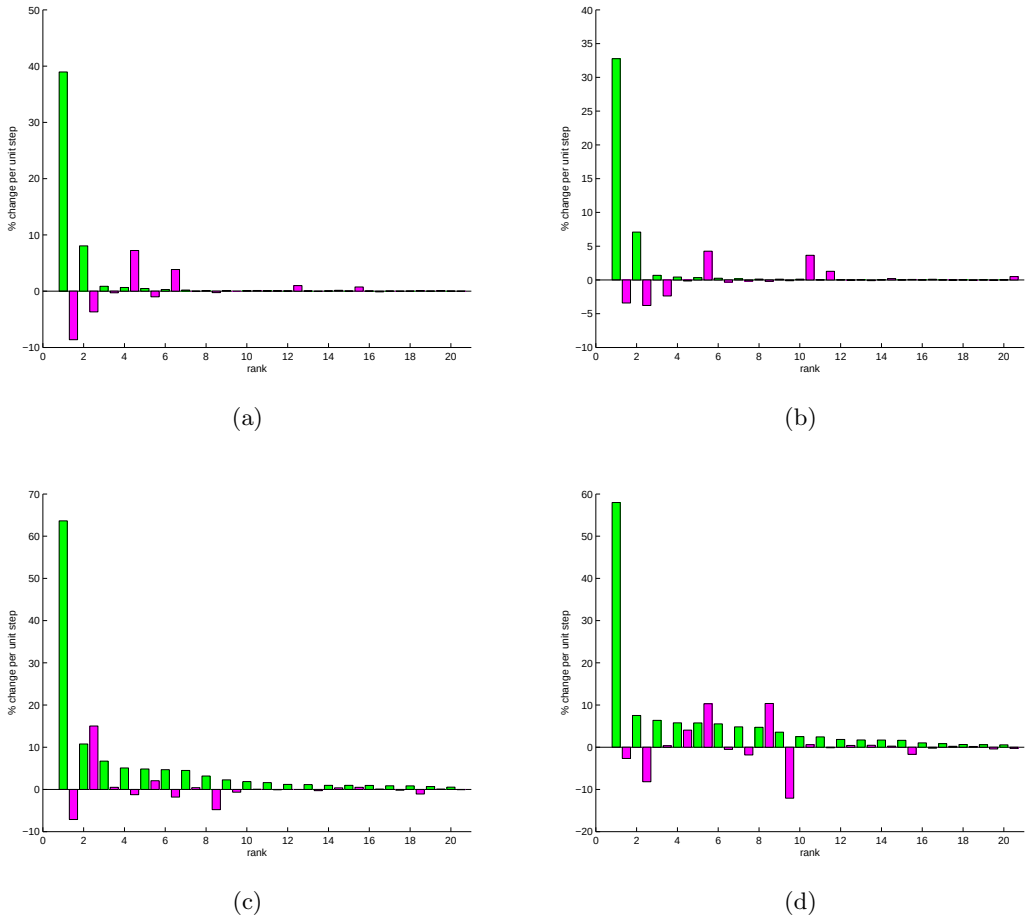

Figure 6-8: Changes in relative phase (green) and period (magenta) caused by a step in period-neutral phase direction. (a) Original model, mCry1 dusk; (b) Extended model, mCry1 dusk; (c) Original model, mPer2 dusk; (d) Extended model, mPer2 dusk; The order of parameters is taken from the ranking by absolute parameter change in Figure 6-6 and 6-7, right side, respectively.

again, include some of the parameters that were found to be "key players" in setting the period, mRNA amplitudes and relative phases in the extended model, such as the Per2 mRNA export rate, the degradation nuclear Cry1, the unbinding of Per2ppC from Cry1 and the degradation of Per2ppC.

6.2.9 Can the Lumped Models Finitely Adjust the Dawn-to-dusk Phase Without Changing the Period?

Both models' ability to change the dawn-to-dusk distance in a finite way is considered next. The dusk definition used here and in the remainder of the study is the maximum in Cry1 mRNA. In order to not overestimate the models' ability to change individual parameters, the numerical experiments shown here were all performed on the lumped ones. The sensitivity calculations that were presented before for the unlumped models are repeated here for the lumped models. Figure 6-9 shows the top ranked parameters based on the magnitude of their scaled relative angular phase sensitivity, $\|\frac{\partial \ln \gamma}{\partial \ln p_i}\|$, along with the rankings based on the magnitudes of relative (top right) and absolute (bottom left) parameter sensitivities in the period-neutral phase direction, $\|\frac{p_i}{\beta}\left(\frac{\partial \beta}{\partial p_i}\right)_T\|$ and $\|\left(\frac{\partial \beta}{\partial p_i}\right)_T\|$, respectively. The mechanism of period-neutral phase change is shown in the bottom, right graph. The same results are shown in Figure 6-10 for the extended model. The results shown here do not add any detail to the previous, detailed sensitivity analyses and are only shown for completeness. The mechanism for period-neutral phase setting is also similar to the detailed models and still involves a group of six to eight parameters in both models, respectively.

How Local is the Sensitivity Information?

The knowledge that sensitivity information is inherently local begs the question if the computation of a period-neutral phase direction is meaningful in a sense beyond infinitesimal variations. To understand how far the linear approximation made in sensitivity analysis is valid, steps of different, finite size in parameter space are taken into the period-neutral phase direction for each model. Results are shown in Figure 6-11, where the absolute step sizes σ are reported relative to the lengths of the two different vectors, so that $\Delta\mathbf{p} = \sigma\left(\frac{\partial \beta}{\partial \mathbf{p}}\right)_T$ for each model.

For both models, smaller steps result in significant phase change with negligible period change. Thus, sensitivity information is valuable to understand how small parameter variation can affect the phase behavior of the model. As the stepsize increases, the period is more and more affected, and an obvious non-linear relationship between phase and period is found as for both models eventually the phase decreases while the period increases further.

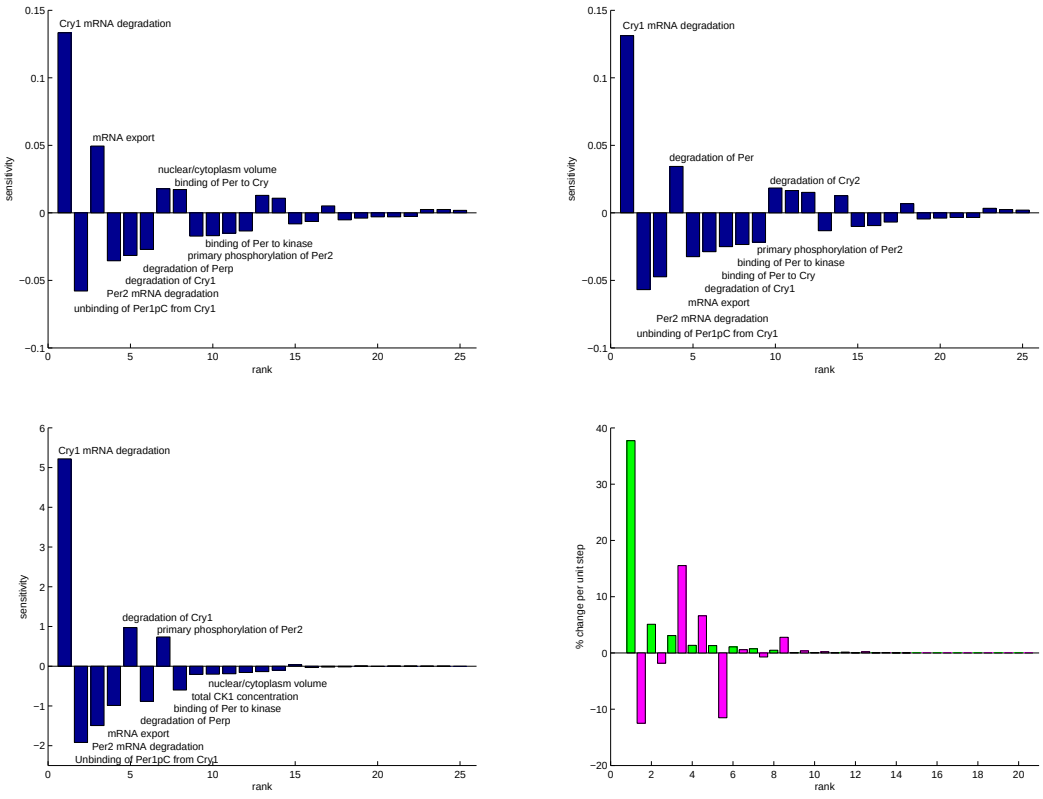

Figure 6-9: Dawn-to-dusk in the original model. The dusk definition was the mCry1 dusk. Top left: Scaled relative Dawn-to-Dusk angular phase sensitivities $\frac{\partial \ln \gamma}{\partial \ln \mathbf{p}}$ in the lumped, original model. Top right: Ranked absolute magnitudes of relative period-neutral lumped phase sensitivities $\frac{\mathbf{p}}{\beta}\left(\frac{\partial \beta}{\partial \mathbf{p}}\right)_T$. Bottom left: Ranked absolute magnitudes of absolute period-neutral lumped phase sensitivities $\left(\frac{\partial \beta}{\partial \mathbf{p}}\right)_T$. Bottom right: Changes in relative phase β (green) and period (magenta) caused by a step in period-neutral phase direction. The order of parameters is taken from the ranking by absolute parameter change in bottom, left.

Stepwise Change in Period-Neutral Phase

A very simple optimization procedure was used to study whether the mammalian circadian clock can vary the dawn-to-dusk distance over a wider range of values. Again, the period-neutral phase direction was computed. Then a step of normalized length $\gamma = 0.1$ was taken in parameter space, so that $\mathbf{\Delta p} = \frac{\gamma}{\|\left(\frac{\partial \beta}{\partial \mathbf{p}}\right)_T\|}\left(\frac{\partial \beta}{\partial \mathbf{p}}\right)_T$. The normalization allows for better comparison between the two models. At the new parameterization, a new period-neutral phase direction was computed, normalized, and another step of the same length was taken. The results of this procedure for both the original and the extended model are shown in

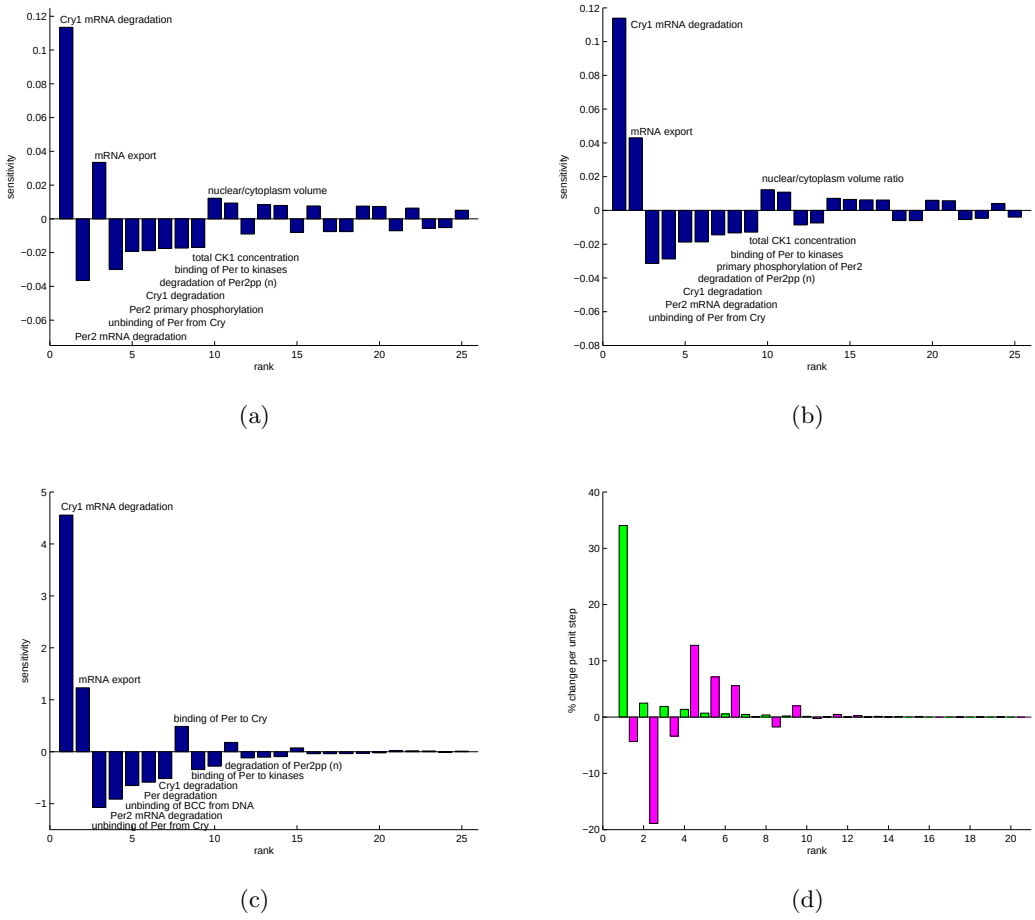

Figure 6-10: Dawn-to-dusk in the extended model. The dusk definition was the mCry1 dusk. (a) Scaled relative Dawn-to-Dusk angular phase sensitivities $\frac{\partial \ln \gamma}{\partial \ln \mathbf{p}}$ in the lumped, original model. (b) Ranked absolute magnitudes of relative period-neutral lumped phase sensitivities $\frac{\mathbf{p}}{\beta}\left(\frac{\partial \beta}{\partial \mathbf{p}}\right)_T$. (c) Ranked absolute magnitudes of absolute period-neutral lumped phase sensitivities $\left(\frac{\partial \beta}{\partial \mathbf{p}}\right)_T$. (d) Changes in relative phase β (green) and period (magenta) caused by a step in period-neutral phase direction. The order of parameters is taken from the ranking by absolute parameter change in bottom, left.

Figure 6-12.

Both models appear to have a very similar range of values in which the length of the subjective day can fall. Both models can increase the length of subjective day by approximately two hours, while not changing the period by more than 2% (or one half-hour). Interestingly, as the last value in either figure is approached, the models show different behavior. The original model continues to show oscillatory behavior, and in the next step the phase can be further lengthened, however, the period exceeds the 2% limit and thus the next step

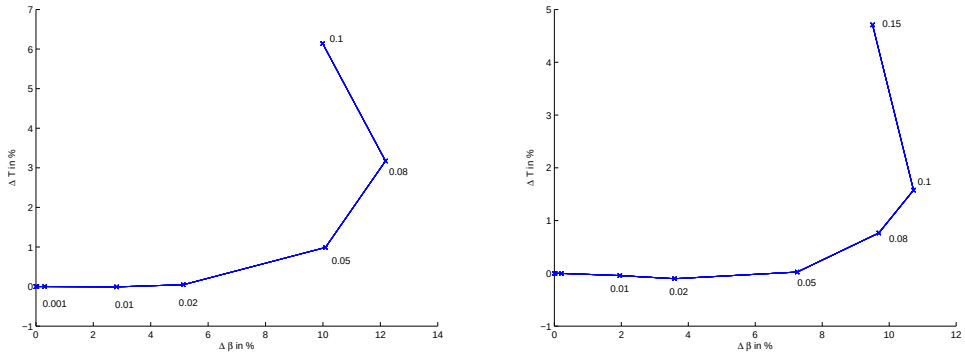

(a) (b)

Figure 6-11: Changes in relative phase and period caused by a steps of different sizes σ in the period-neutral phase direction for lumped parameterization of both models. The relative phase was defined by the time between the minimum and maximum total *mCry1* concentration. (a) Original model; (b) Extended model.

was rejected. In the extended model, the model enters a regime of damped oscillation, the period shortens dramatically, and eventually the oscillation is lost, as more steps are taken.

6.3 Discussion and Conclusions

There are two main conclusions that can be drawn from the work presented in this Chapter. First, it is observed that the mammalian circadian clock model is not modular in the way functionality is distributed within the network structures. While one feedback loop sets the period, a small number of "key parameters" were found to play an important role in the setting of the period, the amplitudes and phases under study. These "key parameters" were mainly located in the Per2 negative feedback loop as well, but they do not form a contiguous stretch of reactions. Rather, they appear to act at certain key points in the loop. This result is somewhat counterintuitive, given that the clock has so many feedback loops which could be hypothesized to be functional modules that add specific functionality and given that hints at a more modular mechanism were discovered experimentally [2]. To add more detail, it appears that the "centralized" part of the amplitude and phase control in the form of the "key parameters" is prominently present in all species whose expression is under similar control by the BCC. The expression of Bmal1 is regulated differently, which is reflected to a certain degree in different profiles of high-sensitivity parameters. Some

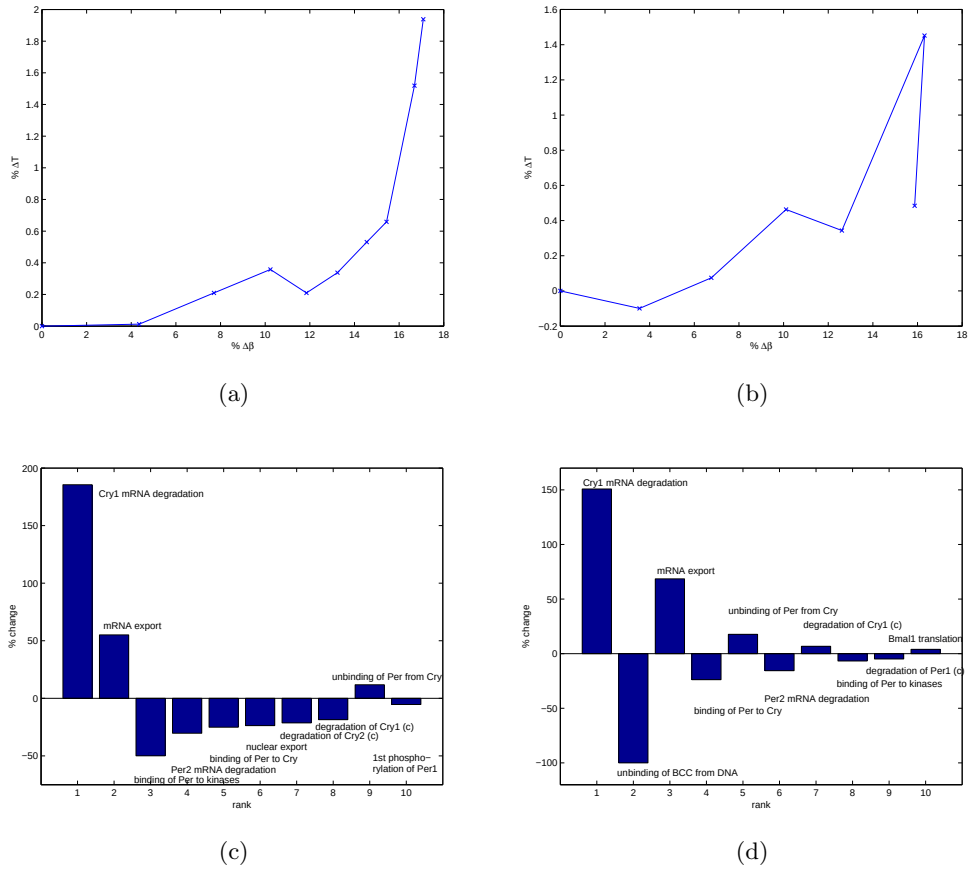

Figure 6-12: Changes in relative phase and period caused by a series of steps of constant size in the period-neutral phase direction for lumped parameterization of both models. At each step, the best period-neutral direction was recomputed and normalized to length one. The step size was $\gamma = 0.1$. The relative phase was defined by the time between the minimum and maximum total *mCry1* concentration. (a) Original model; (b) Extended model. (c) Changes in parameters at the end of optimization, ranked by relative magnitude for the original and (d) extended model

"key parameters" however still appear in the top of the rankings. All amplitudes and relative phases have a significant proportion of high-sensitivity, "local" parameters, i.e., parameters that are involved in the feedback loop in which the phase is measured. The control of these functions appears shared between central control mechanisms and local control mechanisms. Others have found similar overlap between the sensitivity profiles of different network functionalities, in different models of the ciracadian clock [10, 37], suggesting that this overlap might be a general property of circadian clock models.

In the second main result, it is found that there is very little difference between the

original and the extended model. In other words, the addition of several feedback loops appears to have neither constrained nor extended the network's abilities to perform the functions that were considered here. This insight adds further support to the notion that additional feedback loops do not appear to be additional functional modules.

It was shown here that sensitivity analysis, in particular different kinds of phase sensitivity analyses, are useful in understanding network dynamics and trade-offs in functionality. It was also observed that knowing the molecular background for what one studies with mathematical tools is crucial to obtain a meaningful result. In order to perform a detailed, mathematical analysis of the implementation of a variable-length perceived day in the mammalian clock, more detailed experimental knowledge is needed. One experiment that would shed light into the correct definition of "dawn" and "dusk" would be to expose laboratory animals to different L:D (light:dark) ratios while maintaining an overall 24-hour period. Then, by recording the resulting mRNA concentrations over time, one could determine what happens on a molecular level when the timing of dawn and dusk change, which would be useful in formulating the PLCs needed for the mathematical analysis that is performed here. Furthermore, if more detailed information is found eventually, it would be of interest to implement an even more detailed version of the extended model that could account for both dawn and dusk tracking. Then the sensitivity analysis method could be extended to forced oscillations and the relevant studies could be undertaken under entrained conditions.

Chapter 7

Feature-Based Parameter Fitting for Oscillatory Systems Biology Models

Abstract

The mathematical modeling of biological or physical systems under study is part of almost all research in systems biology. An important part of the modeling process is the choice of parameter values, which in the best case is derived directly from experimental knowledge. When such knowledge is not available, parameters are fitted, usually by matching numerical results from model simulations to experimental data points using techniques such as least squares. However, the availability and quality of different types of data vary widely, creating challenges that are discussed here. In addition, it is shown here that least squares fitting can be difficult for oscillatory models. In this work, we propose to use dynamical model features directly for parameter fitting. Data like the timing of particular events or the period of oscillation is often more readily available and more reliably obtained than concentration time-series data. We provide a mathematical formulation to perform parameter fitting so that model features match features known from experimental biology. Examples of such features include timing of events such as transitions between cell cycle phases, timing of peaks in concentrations of protein or mRNA, the existence of oscillations or damped oscillations, as well as their frequencies. An example of the application of this strategy is taken from circadian biology. While feature-based parameter fitting can be a stand-alone technique, it is fully compatible with simultaneous concentration-based parameter fitting, and may show its greatest promise in this context.

7.1 Introduction

The formulation of mathematical models that capture the current knowledge of a particular biological network is a promising avenue of research in systems biology. Through the application of mathematical models, general properties of the system can be understood and analyzed to a depth that goes beyond understanding individual reaction mechanisms and is more predictive than mere rationalization of observation affords. A necessary part of most modeling approaches is parameterization. Parameter values have to be identified in such a way that the model's behavior closely resembles what is known from experimental biology. In the best case, the model parameters represent individual chemical reactions with rates individually determined from experiments. However, this scenario is not always realistic, and it is often necessary to fit the model behavior to the available measured data. By varying the parameters in a systematic way, it can be possible to identify a parameterization that yields the best match between simulation and experiment. Two requirements for success in this process are that enough data is available and that the model is able to represent the data at the optimal parameterization. If the optimized parameters match experimental data sufficiently better than all others it may represent the most likely parameterization.

This work is concerned with parameter estimation for dynamical models of biological systems that are formulated as systems of nonlinear ordinary differential equations (ODEs). The dynamical system is written as

$$\dot{\mathbf{y}}(t, \mathbf{p}; \mathbf{y}_0) = \mathbf{f}(\mathbf{y}(t, \mathbf{p}; \mathbf{y}_0), \mathbf{p}), \tag{7.1}$$

where $\mathbf{y}$ are the states, or concentrations, in the model, and $\mathbf{p}$ are the model parameters, which can be chemical reaction rate constants or constants associated with transport or other physical processes.

7.1.1 Existing Methods for Parameter Estimation

A method commonly used for parameter estimation in biological models is least-squares (LS) fitting. It involves the minimization of the squared error between experimental data $\mathbf{x}_{data}$ and model, or model-derived, data $\mathbf{x}_{fit}$. The data are typically species concentrations over a time horizon that is determined by the experimental setup, in which case $\mathbf{x}(t, \mathbf{p}) = \mathbf{y}(t, \mathbf{p})$. Alternatively, a measurement function of the concentration data is, used in which case

$\mathbf{x}(t, \mathbf{p}) = \mathbf{g}(\mathbf{y}(t, \mathbf{p}))$ [11]. Regardless of which type of data is used, least-squares fitting involves minimizing an objective or cost function

$$\Omega(\mathbf{p}) = \sum_{i=1}^{n_{data}} \omega_i (\mathbf{x}_{fit}(t_i, \mathbf{p}) - \mathbf{x}_{data}(t_i))^2, \tag{7.2}$$

where ω_i are optional weighing or scaling factors that are assumed to be one for the remainder of this chapter. The goal of any parameter estimation procedure is to minimize Ω and moreover, to find a unique, isolated minimum. As is evident from the formulation, the quality of fit can depend strongly on the number of experimental measurements, n_{data}, and the dimensionality of the vector $\mathbf{x}(t_i)$, or in other words on the ability to measure many relevant concentrations in the system. It is essential to measure enough of the most informative, yet experimentally accessible, concentrations y_i at each time. This issue is addressed in the field of identifiability and experimental design, e.g. in references [51, 15, 57, 7]. Often, gradient-based local optimization techniques are used to minimize Ω, where the gradient information can easily be obtained by integrating the model sensitivities $s_{jk} = \frac{\partial y_j}{\partial p_k}$ along with the model states $\mathbf{y}$ over the time horizon, e.g., using software packages such as CVODES [43] or Jacobian [1]. The LS algorithm is widely available to systems biologists in software packages such as Jacobian and the MATLAB SimBio Toolbox (The Mathworks, Inc.; Natick, MA, USA). A second prevalent method for parameter fitting is called maximum likelihood estimation, which relates the likelihood of the experimental observation being produced by a parameterized model to the likelihood of the parameter set. If a normal distribution of experimental noise is assumed, the ML estimation is mathematically equivalent to LS estimation. A good overview of the current state of parameter fitting in systems biology is given in reference [51]. This chapter uses LS fitting for all comparisons mainly because the feature-based method is both competitive and fully compatible with it.

7.1.2 Feature-based Parameter Estimation

The main concept of feature-based parameter estimation is to specifically reward agreement between dynamical features in model and experiment rather than between concentration data. Features extracted from experiments and from models are compared, as is the concentration data in the conventional LS approach. The details of this formulation are discussed in Section 7.2.2. Examples of model features include the timing and height of a peak in

a measurable concentration, or the existence and period of an oscillation. This strategy has a conceptual advantage in that the model can be fit directly to what the biologist knows is important for system function. The strategy changes the scope of the optimization formulations; in particular, constraints are introduced which are not typically present in conventional LS algorithms. The ramifications of having constraints in the context of parameter identifiability are discussed in Section 7.2.3. The cost function surface depends on the structure of the cost function; different surfaces can have different properties (i.e., convexity, smoothness). One surface may be significantly more convex than another (i.e., fewer local minima), which can lead to substantial improvement in parameter identification, particularly if the initial guess for the parameterizations is poor.

7.1.3 Types of Available Data

Examples for concentration data that might be available for parameter fitting include data from mass spectrometry; fluorescence based measurements of protein concentrations *in vitro* or *in vivo* from single cells, cell extracts or cell culture; microarray data; data derived from optical processing of different types of blots; to name a few. This multitude of sources and different measuring techniques causes several challenges. Data is generally noisy, concentrations can often only be determined in a relative or indirect fashion, and it can be hard to combine concentration data obtained in different laboratories or experiments due to the lack of common controls. Often, concentration data is represented in normalized form, where the maximum observed concentration is 100%, to mitigate some of these effects. We have observed, however, that what is often more comparable between experiments from different sources is what will be called "feature data" for the remainder of this work. An example is the timing of events such as peaks in concentrations. This is particularly so if they repeat in periodic biological systems, as is the case for the circadian clock. Another example is the order of a sequence of events in the form of peaks of different cyclins in the cell cycle. In fact, it is sometimes possible to determine feature data without measuring any concentration data of the modeled species, e.g., the period of oscillation in the circadian clock can be determined using activity data from laboratory animals [26], and the time spent in different phases of the cell cycle can be determined by measuring DNA content.

7.2 Mathematical Methods

7.2.1 Example Features and Their Sensitivities

Period of Oscillation

The period of oscillation is a feature that is very important in the fitting of oscillatory systems. It can be determined by solving a boundary value problem to find the exact periodic orbit of the oscillation. Its sensitivity with respect to the system parameters can then be calculated as shown in Chapter 2.

Peak Time

If the timing of a peak in species y_i, or the relative timing between peaks, is of interest for parameter fitting, the following equation can be used to, not necessarily uniquely, define that time

$$f_i(\mathbf{y}(t_{peak}, \mathbf{p}; \mathbf{y}_0), \mathbf{p}) = 0. \tag{7.3}$$

Eq. (7.3) can be differentiated with respect to the parameters $\mathbf{p}$ to yield

$$\frac{\partial f_i}{\partial \mathbf{y}} \left(\left.\frac{d\mathbf{y}}{dt}\right|_{t=t_{peak}} \frac{\partial t_{peak}}{\partial \mathbf{p}} + \left.\frac{\partial \mathbf{y}}{\partial \mathbf{y}_0}\right|_{t=t_{peak}} \frac{\partial \mathbf{y}_0}{\partial \mathbf{p}} + \left.\frac{\partial \mathbf{y}}{\partial \mathbf{p}}\right|_{t=t_{peak}} \right) + \frac{\partial f_i}{\partial \mathbf{p}} = \mathbf{0}, \tag{7.4}$$

where $\frac{\partial t_{peak}}{\partial \mathbf{p}}$ is the desired sensitivity information (or peak time sensitivity). In limit-cycle oscillatory systems, special attention should be paid to the quantity $\frac{\partial \mathbf{y}_0}{\partial \mathbf{p}}$, the calculation of which is detailed in Chapter 2.

Peak Height (Amplitude)

Using a peak height as a feature for parameter fitting requires finding the peak time, and then using the concentration of the desired species $y_i(t_{peak}, \mathbf{p}; \mathbf{y}_0)$ at that time. Its sensitivity $\frac{dy_i}{d\mathbf{p}}$ is computed according to

$$\frac{dy_i}{d\mathbf{p}} = \left.\frac{\partial y_i}{\partial \mathbf{p}}\right|_{t=t_{peak}} + \left.\frac{\partial y_i}{\partial \mathbf{y}_0}\right|_{t=t_{peak}} \frac{\partial \mathbf{y}_0}{\partial \mathbf{p}}.$$

Threshold Crossing Time

The time at which a concentration y_i crosses a threshold α can be defined as

$$y_i(t_{cross}, \mathbf{p}; \mathbf{y}_0) = \alpha,$$

and differentiated to yield

$$\left.\frac{\partial y_i}{\partial \mathbf{p}}\right|_{t=t_{cross}} + \left.\frac{\partial y_i}{\partial \mathbf{y}_0}\right|_{t=t_{cross}} \frac{\partial \mathbf{y}_0}{\partial \mathbf{p}} + \left.\frac{dy_i}{dt}\right|_{t=t_{cross}} \frac{\partial t_{cross}}{\partial \mathbf{p}} = \mathbf{0}.$$

Here again, the quantity $\frac{\partial t_{cross}}{\partial \mathbf{p}}$ is the sensitivity information of interest.

It should be noted that the term $\frac{\partial \mathbf{y}_0}{\partial \mathbf{p}}$ appears in most of the sensitivity equations for the feature sensitivities. This quantity is sometimes overlooked, but needed in some situations. One example is a limit-cycle oscillator, where the starting point at time zero lies on the periodic orbit. Another example is a system that is at a steady state at time zero. In both of those cases, the starting point for the dynamic simulation, $\mathbf{y}_0(\mathbf{p})$, depends on the parameters of the system, because the parameters determine the steady state or periodic orbit. If it can be ascertained that the initial conditions of the dynamic simulation are independent of the parameters, as is the case in a non-limit-cycle oscillator, the term drops and the equations simplify accordingly.

7.2.2 Optimization Formulation for Parameter Estimation

Direct Method Using Feature Sensitivities

The optimization itself is then similar to a least-squares formulation, but instead of the concentrations, the feature data now appear in the cost function

$$\Omega(\mathbf{p}) = \sum_{i=1}^{n_f} \omega_i(\phi_i(\mathbf{p}) - \phi_{i,data})^2, \tag{7.5}$$

where Ω is the cost function, n_f is the total number of features fitted, ω_i are optional weighting coefficients, ϕ_{data} is the feature data from experimental or other knowledge, and ϕ_{fit} is the feature prediction from simulation. The problem statement is then simply

$$\min_{\mathbf{p}} \Omega(\mathbf{p}) \tag{7.6}$$

A gradient-based numerical optimization algorithm further requires the input of gradient information, or in other words the sensitivity of the cost function with respect to the parameters. The chain rule can be applied to the cost function, and then the sensitivities of the features can be substituted into the resulting equation,

$$\frac{\partial \Omega}{\partial \mathbf{p}}(\mathbf{p}) = \sum_{i=1}^{n_f} 2\omega_i(\phi_i(\mathbf{p}) - \phi_{i,data})\frac{\partial \phi_i}{\partial \mathbf{p}}(\mathbf{p}). \tag{7.7}$$

The only constraints are typically upper and lower bounds on parameter values known from experiments or derived from physical feasibility considerations, and the constraint derivatives are either zero (for constraints not related to the parameter) or one (for constraints relevant to the parameter). A severe limitation of this approach is the problem of leaving the implicit feasible region. In other words, if one of the features disappears (e.g., the optimization algorithm leaves the oscillatory region and there is no period to measure as a feature), the algorithm has difficulty recovering. This limitation applies in particular to the initial guess used for the parameter estimation. If no initial guess is known that yields features with reasonable values, the algorithm cannot even begin. This limitation is addressed in a second approach.

Independent Optimization Variables

An alternative to the above direct method is to treat the measured features as well as the parameters as independent variables, and then to use constraints to ensure that all of the independent variables are consistent (i.e., the current solution is feasible). The resulting problem statement is

$$\min_{\mathbf{p},\boldsymbol{\phi},\mathbf{y}_0} \Omega(\mathbf{p}, \boldsymbol{\phi}, \mathbf{y}_0) \tag{7.8}$$

$$\text{s.t.} \qquad \mathbf{g}(\boldsymbol{\phi}, \mathbf{p}, \mathbf{y}_0) = \mathbf{0} \tag{7.9}$$

where

$$\Omega(\mathbf{p}, \boldsymbol{\phi}, \mathbf{y}_0) = \sum_{i=1}^{n_f} \omega_i(\phi_i - \phi_{i,data})^2, \tag{7.10}$$

and $\mathbf{g}(\boldsymbol{\phi}, \mathbf{p}, \mathbf{y}_0) = \mathbf{0}$ is a system of equations defining all features $\boldsymbol{\phi}$ and any dependency of $\mathbf{y}_0$ on $\mathbf{p}$, as is the case in limit-cycle oscillators. An example using this approach is described in Section 7.3.2.

In this approach the cost function is the same as in the previous strategy. However, the dependency of the features and initial conditions on the parameters has been removed from the cost function and is transferred into the constraints of the optimization. This eliminates the need to compute feature sensitivities during the optimization, and all gradient information for cost function and gradients only contains the sensitivities $\frac{\partial \mathbf{y}}{\partial \mathbf{p}}$, which can be computed easily. This strategy has been found to be numerically more robust for the optimization of oscillatory systems. It possesses an implicit control against crossing bifurcations into a parameter region where the oscillatory behavior disappears. The same properties direct an initial guess that does not oscillate into the feaasible region. This event corresponds to a constraint violation, and gradients can be computed to direct the search back into the feasible region. The exact mechanism depends on the algorithm of the optimization software used to solve the problem.

7.2.3 Feature Fitting in the Context of Identifiability

The concept of structural identifiability was introduced by Bellman & Aström in 1970 [14]. The problem formulated there is to decide, given a model and set of measured outputs, whether it is possible to determine all parameters uniquely. The approach they used is a least-squares based cost function $\Omega(\mathbf{p})$ in an unconstrained optimization. The term "local identifiability" is defined as $\Omega(\mathbf{p})$ having a strict local minimum at $\Omega(\mathbf{p}_{nom})$ where $\mathbf{p}_{nom}$ is the nominal parameterization at which the measured output was generated (i.e., it is *a priori* unknown). Global identifiability requires a global minimum, and a sufficient condition is that the Hessian of the cost function $\Omega_{\mathbf{pp}}$ is positive definite (implying strict convexity of $\Omega(\mathbf{p})$) for all $\mathbf{p}$ in the range considered. Structural identifiability implies that the local or global identifiability properties of a given model hold for almost all nominal values of $\mathbf{p}$ (except on a set of measure zero) [50]. For nonlinear, dynamic problems it is challenging to assess the properties of the Hessian matrix of any cost function over the entire parameter range [57], and algorithms developed for the study of *a priori* global identifiability are scarce [6]. Both global and structural identifiability analyses are beyond the scope of the work presented here, and local identifiability is evaluated *a posteriori* at the nominal point in

parameter space.

Assuming the idealized case that the model is correct and no error is present in the experimental data, the value of the least-squares problem in Eq. (7.2) at the true solution is zero. At this point the second-order information in the Hessian matrix vanishes and the first-order sensitivity matrix determines the properties of the Hessian at that point:

$$\Omega_{\mathbf{pp}}(\mathbf{p}) = \sum_{i=1}^{n_{data}} \sum_{j=1}^{n_y} 2 \frac{\partial y_{i,j}}{\partial \mathbf{p}}(\mathbf{p}) \frac{\partial y_{i,j}}{\partial \mathbf{p}}(\mathbf{p})^{\mathrm{T}} - \sum_{i=1}^{n_{data}} \sum_{j=1}^{n_y} 2(y_{data,i,j} - y_{i,j}(\mathbf{p})) \frac{\partial^2 y_{i,j}}{\partial \mathbf{p}^2}(\mathbf{p}). \quad (7.11)$$

It is assumed that the concentrations $\mathbf{y}$ can be directly determined experimentally and n_y is the number of measured concentrations. The first term in Eq. (7.11) corresponds to the Fisher Information Matrix (FIM), when measurement errors are mutually independent and follow a standard normal distribution ($N(0,1)$)

$$\mathbf{F}(\mathbf{p}) = \sum_i \frac{\partial \mathbf{y}_i}{\partial \mathbf{p}}(\mathbf{p}) \frac{\partial \mathbf{y}_i}{\partial \mathbf{p}}(\mathbf{p})^{\mathrm{T}}.$$

This matrix has been used to evaluate local identifiability [57, 15, 39, 7, 50]. The eigenvalue spectrum of the FIM is informative, as it indicates the local shape of the minimum. One single, zero eigenvalue makes the system locally unidentifiable [15, 39] because it corresponds to a one-dimensional "valley" in the cost function surface. A parameter variation in the direction of the valley (i.e., direction of the associated eigenvector) results in no change of the cost function $\Omega(\mathbf{p})$.

The following general observation is made when one compares the literature on local identifiability with the approach presented in this work. In the LS fitting method (e.g., [14, 50, 39]), an unconstrained optimization problem is formulated, i.e., the analysis of the Hessian of the cost function at the solution point is sufficient to understand the quality of the solution found. However, in the case of feature fitting, the feasible region is further constrained by equality constraints. It is therefore true that the feasible region of the constrained optimization problem in feature fitting must be a subset of the feasible region without the equality constraints. In other words, if one analyzes only the Hessian of the cost function at the solution point, the local identifiability of the system can be underestimated.

To evaluate identifiability in a constrained parameter estimation problem, the nullspace of the Hessian $\mathcal{N}(\Omega_{\mathbf{pp}})$ was projected into the row space of a matrix describing the linearized

constraints,

$$\mathbf{A} = [\nabla \mathbf{g}].$$

$\mathbf{A}$ thus has as many rows as there are constraints. The dimension of the subspace

$$\mathcal{W} = \mathbf{A}^{\mathrm{T}}(\mathbf{A}\mathbf{A}^{\mathrm{T}})^{-1}\mathbf{A}\mathcal{N}(\Omega_{\mathbf{pp}}),$$

$dim(\mathcal{W})$ is a measure of how much the constraints have limited the possible solutions to the parameter estimation problem. An identifiability score can be computed as

$$\sigma = rank(\Omega_{\mathbf{pp}}) + dim(\mathcal{W}). \tag{7.12}$$

If s is equal to the number of variables in the parameter estimation problem, the system is uniquely locally identifiable. If σ is smaller, one or more parameters or directions in parameter space are unconstrained and the system is unidentifiable.

This realization indicates that the period is a particularly "potent" feature. Its definition requires n equality constraints that define the BVP, which results in a system of equations of rank n in the case of a limit-cycle oscillator, similar to Eq. (2.18). This potential to reduce the dimensionality of the feasible region by up to n dimensions, combined with the fact that the period is typically easy to determine experimentally, makes this feature extremely useful for parameter estimation.

7.3 Results and Discussion

7.3.1 Motivational Examples

The Fitting Strategy Changes the Cost Function Surface

In the following, an abstract, motivational example is given to show how the different fitting strategies result in different cost functions. The single feature in this model is assumed to be a peak time of a concentration c, and the time course of that same concentration is used for comparison. Presumably, different parameterizations $\mathbf{p}_i$ lead to different model behaviors, some of which might have peaks in concentration c (Figure 7-1, left). Depending on the cost function used to evaluate the quality of fit, very different results are obtained for the same parameterization. If least-squares fitting based on concentration data is performed,

the cost function value for peak times away from the true peak time will be virtually constant in this simple example. A steady-state solution for c with no peak, as found for parameterization $\mathbf{p}_3$, might be competitive with those solutions, having the same or even lower error compared to those parameterizations that show the desired peaking behavior. If the parameter search is begun in a region with this property, the cost function gradient is too close to zero to lead the search effectively to the true parameterization (Figure 7-1, right). On the other hand, the search based on the peak time has a two-fold advantage. First, only parameterizations that produce the desired behavior are allowed in the search. Second, the resulting cost function gradient points toward the true parameterization, no matter how far the peak time of the initial guess is away from the true peak time (Figure 7-1, right).

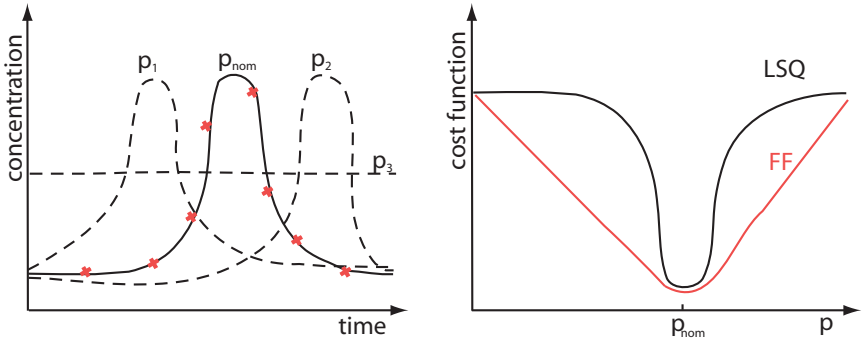

Figure 7-1: Left: Data (red) and model trajectories depending (solid and dashed lines) for 4 different parameterizations. Right: Cost functions for different fitting strategies. Red, cost function for peak-time based feature fit; black, cost function for concentration-based least-squares fit.

This effect is illustrated by a numerical example with only two parameters, which allows for plotting of the cost function directly. Two parameters in a harmonic oscillator were fit. The hypothetical concentration $c(t)$ over time was calculated as

$$c(t, \omega, \alpha) = \sin(\omega t + \alpha), \tag{7.13}$$

where the nominal parameterization was the frequency $\omega_{nom} = 1.0$ and the phase $\alpha_{nom} = 0.0$. The least-squares cost function was calculated as

$$\Omega_{LSQ}(\omega, \alpha) = \int_0^{3T} (c_{nom}(t) - c(t, \omega, \alpha))^2 dt, \tag{7.14}$$

where $T = 2\pi/\omega$ was period of the current parameterization. The features used for fitting in this example were the times at which $c(t)$ peaks, $t_{peak,i}$, resulting in a cost funtion

$$\Omega_{FF}(\omega, \alpha) = \sum_{i=1}^{3} (t_{peak,nom,i} - t_{peak,i}(\omega, \alpha))^2, \tag{7.15}$$

where the equality constraints of the corresponding "independent variables"-optimization formulation would correspond to $g_i = \frac{dc}{dt}(t_{peak,i}, \omega, \alpha)$ for each peak over the first three periods. The cost function surfaces for both examples were calculated over a range of -90% to $+100\%$ for the frequency ω and -100% to $+100\%$ for the phase α, and are shown in Figure 7-2. It is shown that the cost function surface, in particular in the frequency

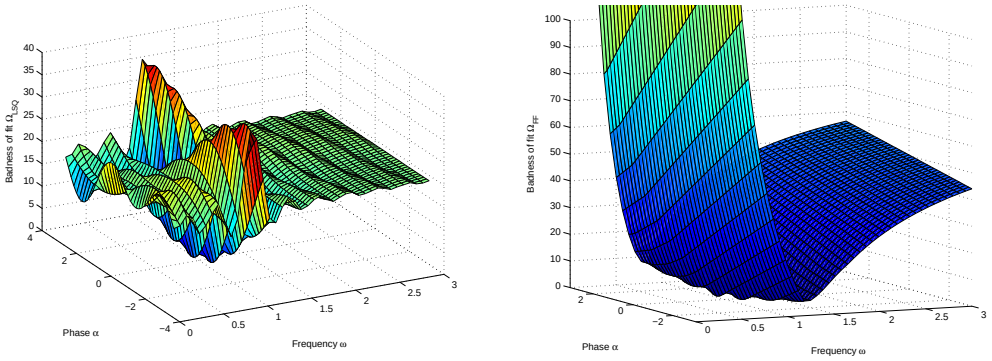

Figure 7-2: Cost function surface for least-square, concentration-based parameter estimation (left) compared to feature based (right) parameter estimation based on the period and phase of a sine-wave function. The nominal point is in both cases at phase $\alpha = 0$ and frequency $\omega = 1$.

direction, is more convex for the feature fit approach. In the LS approach, the cost function surface is shallow and rippled when far away from the minimum; a local optimizer might be unable to locate the true (global) minimum at the nominal point. Near the minimum Ω_{LSQ} is highly non-convex, making convergence difficult as well. In both approaches a similar amount of non-convexity in the phase direction persists. This example shows how the approach to fitting can change the shape of the resulting cost function significantly, and it is this observation that motivates the feature fitting approach.

Certain Features Can Dominate the Least-Squares Fitting Cost Function

Here, an example from the circadian literature is used to demonstrate how a feature (the period of oscillation) can dominate the error in a least-squares-fitting approach. In their 2003 publication, Forger and Peskin provide information on which of the 38 parameters contribute more or less to the "badness of fit" at the best fit parameter choice [29]. This "badness of fit" is an evaluation in the least-squares sense of the mRNA concentrations at several time points as well as scaled, relative peak- and trough-concentrations of proteins where data were available. A relative sensitivity is computed where the effect of a 10% parameter change on the "badness of fit" is evaluated. In Figure 7-3, this quantity is plotted together with the scaled sensitivity of the period with respect to the corresponding parameter.

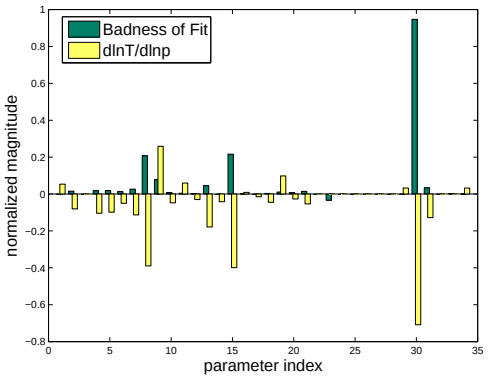

Figure 7-3: Comparison between the feature sensitivity $\frac{\partial \ln T}{\partial \ln \mathbf{p}}$ and the scaled sensitivity of the "Badness of the Fit" as reported by Forger & Peskin [29] for a concentration-based least-squares fit. Both data sets were normalized by the length of the respective sensitivity vector for all parameters, for direct, relative comparison.

It is noticeable that there are several parameters where the sensitivity of the "badness of the fit" is very large. Those same parameters have high magnitudes of scaled period sensitivities. In fact, the parameters with the top ten magnitudes in both measures are the same and their order is barely different. Also, both measures result in a small number of parameter sensitivities being significantly larger than most. It appears that the effect that worsens the quality of fit is not the change of the concentrations that are being measured in the cost function, but rather the change in overall period of oscillation. If the period in the model does not fit the period of the data, this effect dominates the error. In other words,

the optimization procedure might weigh the agreement in the period more than agreement in individual concentrations, which may not be the intended outcome.

7.3.2 Application to the Goodwin Circadian Oscillator

In a comparative study, one feature-based approach to parameter estimation was compared side-by-side to a conventional, least-squares-based approach using two different data sets. The methods were applied to the Goodwin oscillator, a small circadian clock model that was presented previously in Section 2.6.1. In all cases, a significant number of converged optimization runs was generated, and the results were compared in two different metrics. First, the resulting fit model was scored against perfect data (i.e., continuous data from the model in nominal parameterization in all concentrations, starting from the nominal initial conditions). Second, the estimated parameters were compared to the nominal parameters. The mean and standard deviations of both scoring metrics are shown.

Problem Formulation

The least-squares (LS) problem was formulated as follows:

$$\min_{\mathbf{y}_0,\mathbf{p}} \sum_{i=1}^{6} (\mathbf{y}_{data}(t_i) - \mathbf{y}(t_i, \mathbf{p}; \mathbf{y}_0))^2, \tag{7.16}$$

where $\mathbf{y}_{data}(t_i)$ as well as $\mathbf{y}(t_i, \mathbf{p}; \mathbf{y}_0)$ were either the complete 3-dimensional vector of concentrations (labeled LSQ - 3×6), or only the last concentration (labeled LSQ - 1×6). The two situations correspond to different amounts of experimental data available, because it is not always possible to measure concentrations for all species of a model. This approach was numerically implemented using the *fmincon* function in the MATLAB Optimization Toolbox version 3.1.1., which uses a a trust-region dogleg algorithm with BFGS Hessian update in its medium-scale setting. The only bounds that were used were upper and lower bounds on the parameters and initial conditions.

Alternatively, the feature fitting approach was formulated as

$$\begin{aligned} \min_{\mathbf{y}_0,\mathbf{p},\phi,T} \quad & (T_{data} - T)^2 + (\phi_{data} - \phi)^2 \\ \text{s.t.} \quad & f_3(\mathbf{y}(0,\mathbf{p};\mathbf{y}_0),\mathbf{p}) = 0 \\ & \mathbf{y}(T,\mathbf{p};\mathbf{y}_0) - \mathbf{y}_0 = \mathbf{0} \\ & f_2(\mathbf{y}(\phi,\mathbf{p};\mathbf{y}_0),\mathbf{p}) = 0 \\ & f_1(\mathbf{y}(0,\mathbf{p};\mathbf{y}_0),\mathbf{p}) \leq 1e^{-4}. \end{aligned} \tag{7.17}$$

The cost function contains the least-squares type error of two features, the period of oscillation, and the peak time of species 2. The first constraint, which is a phase locking condition to specify the time zero reference (as discussed in Chapter 2), is an implicit third feature. The fourth constraint is an inequality constraint that excludes stationary points from the feasible region. This approach is numerically more difficult due to the presence of multiple nonlinear constraints and was implemented in C, using the software packages SNOPT [34] for the constrained optimization and CVODES [43] for the integration of the differential equations. The nominal parameterization used to generate the data $\mathbf{y}_{data}(t_i)$, T_{data} and ϕ_{data} were $\mathbf{p}_{nom} = (6.0, 3.287, 2.250, 0.153, 0.153, 0.114)$, $\mathbf{y}_{0,nom} = (0.01, 0.117, 2.307)$. This parameterization yields a $T_{data} = 27.0$ and $\phi_{data} = 10.0$. In both methods, the upper and lower bounds on the parameters were the same at $\mathbf{p}_{LB} = (2.0, 2.0, 1.0, 0.1, 0.1, 0.1)$ and $\mathbf{p}_{UB} = (6.0, 6.0, 6.0, 2.0, 2.0, 2.0)$ and the initial conditions were the same, at $\mathbf{y}_{0,LB} = (0.005, 0.1, 2.0)$ and $\mathbf{y}_{0,UB} = (0.015, 0.15, 2.5)$.

Using the parameter bounds, 500 initial guesses were randomly generated for the parameters and initial conditions. All 500 were used to generate 65 converged feature fitting optimization runs. Only the first 100 were used to generate 80 (LSQ - 3×6) and 73 (LSQ - 1×6) converged runs for the two different LSQ optimization runs, respectively. A converged run was one in which the optimizer terminated with an optimal solution with the value of the cost function $\Omega_{fit} \leq 0.001$.

The results are shown in Figures 7-4 and 7-5. First, the fit models of all converged runs are scored against the perfect (nominal) trajectory in all concentrations. The error is calculated as

$$\epsilon(\mathbf{p}) = \int_0^{T_{data}} (\mathbf{y}_{data}(t) - \mathbf{y}(t,\mathbf{p};\mathbf{y}_0))^2 dt, \tag{7.18}$$

This error is plotted in Figure 7-4 (left), and its mean and standard deviation in Figure 7-4 (right). The resulting parameterizations are represented in Figure 7-5 where the

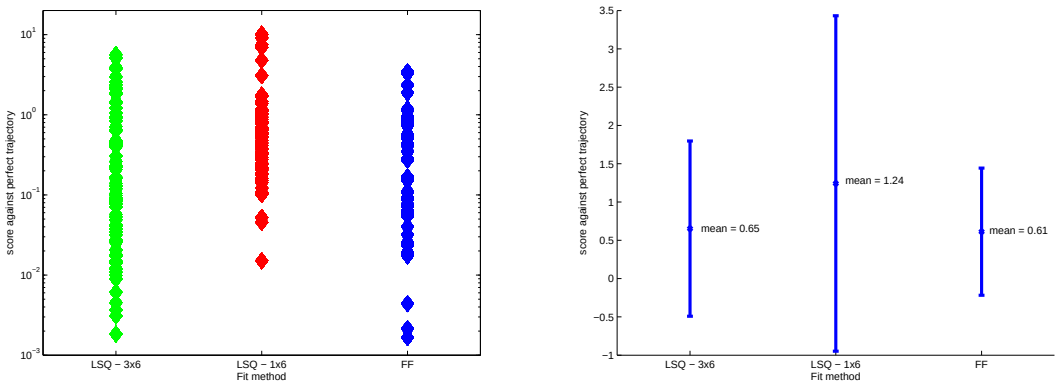

Figure 7-4: Error against the nominal trajectories for all converged runs for the three different fitting algorithms. Left: Error ϵ for all runs; Right: Mean and standard deviation for all runs; LSQ - 3×6: 6 data points in all three concentrations were available for least-squares fitting; LSQ - 1×6: 6 data points in one concentration (Z) were available for least-squares fitting; FF: Feature fitting based on period and peak time of concentration (Y);

mean and standard deviation for each parameter is shown as a function of the fitting method. It is found that only in the case of the feature fitting approach do the nominal parameter values fall within one standard deviation of the mean parameter value found by the fitting algorithm. The mean fit parameter values are always closer to the true value for the feature fit than for either of the other methods. In particular, for parameters k_4 through k_6, the parameters were identified uniquely with very small deviations. These parameters were found to have high period sensitivities in Section 2.6.1 (at a different parameterization). The scaled period sensitivity vector at the nominal point is $\frac{\partial \ln T}{\partial \ln \mathbf{p}} = (0.000125, 0.00071, -0.00035, -0.370, -0.370, -0.232)$ and the scaled phase sensitivity vector is $\frac{\partial \ln \phi}{\partial \ln \mathbf{p}} = (0.0001, 0.0013, 0.0006, 0.387, 0.386, 0.241)$. In both cases, parameters k_4 through k_6 had orders of magnitude larger sensitivities than the first three parameters.

Thus using data on three features resulted in a fit that is very competitive to the fit obtained using a relatively complete set of concentration data. It is superior to a fit where only one out of three concentrations was measured. If judged by parameter identification, the feature-based fit performs better than both concentration-based least-squares fits.

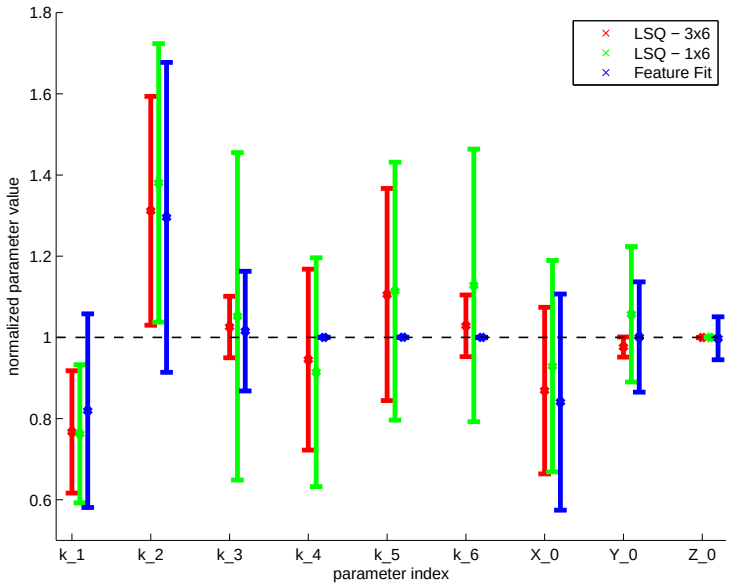

Figure 7-5: Mean and standard deviation of normalized parameterizations $\mathbf{p}/\mathbf{p}_{nom}$ after fitting, depending on the algorithm. LSQ - 3×6: 6 data points in all three concentrations were available for least-squares fitting; LSQ - 1×6: 6 data points in one concentration (Z) were available for least-squares fitting; FF: Feature fitting based on period and peak time of concentration (Y);

Local Identifiability Evaluation

The identifiability score σ is determined for the nominal solution of the Goodwin oscillator, $\mathbf{p}_{nom}$, given different combinations of concentration time-series and feature data. It is assumed that either only the concentration Z is experimentally measurable, or that both concentrations Y and Z are measurable. Time series with equally spaced data points are generated for different numbers of data points, ranging from 3 to 16. These sets of concentration time series data are evaluated for local identifiability, alone and in comparison with different combinations of feature data, using Eq. (7.12). For direct comparison, the identifiability score is adjusted for the number of features used in the cost function, which increases the number of variables but also the rank of the Hessian by the same value. The score reported here is $\sigma = rank(\Omega_{\mathbf{pp}}) + dim(\mathcal{W}) - n_{feature}$, and its maximum value is $\sigma = 9$ for all cases. The results are shown in Figure 7-6. In both cases, the identifiability score that can be reached by increasing the number of time points reaches a plateau at $\sigma = 6$ and $\sigma = 8$ respectively. Feature data can then increase the identifiability score, though

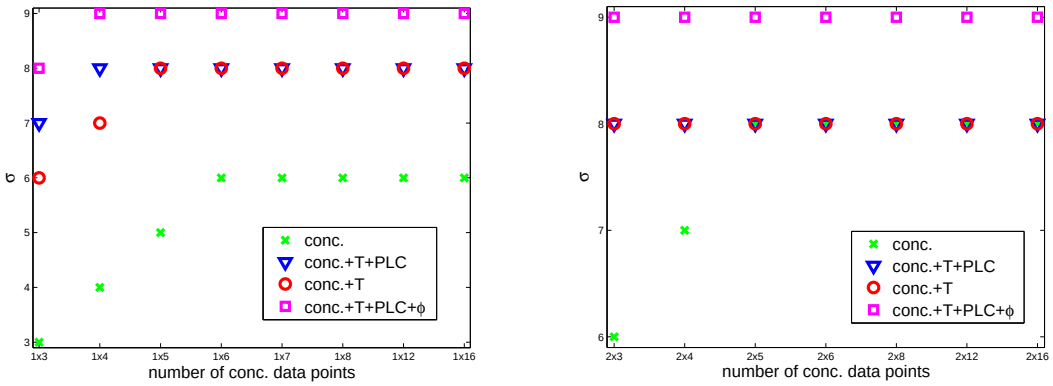

Figure 7-6: Identifiability score σ for the Goodwin oscillator and different amounts of concentration and feature information. The score σ is adjusted for the number of features used, so that full identifiability always corresponds to $\sigma = 9$. Left: One concentration is experimentally measurable. Right: Two concentrations are experimentally measurable. A cut-off of $1e^{-4}$ for an eigenvalue was used to determine that the associated eigendirection was essentially unconstrained. "PLC" indicates that the first constraint in Eq. (7.18) was used, "T" indicates that the second constraint was used and "ϕ" indicates that the third constraint was used.

more so if only one concentration is measurable. If two concentrations are measurable and five or more data points are available, the two features period and PLC do not increase the identifiability score. In both cases, full identifiability ($\sigma = 9$) is reached only by using the available features, period T and relative phase ϕ, even if relatively many time points are available in the concentration data. It is evident that feature data adds most information under data-poor circumstances, which is often the case in biological system of moderate to large scale.

7.3.3 An argument for mass-action kinetics

In many instances in the history of biological model formulations, certain known "formulae" were employed in cases where a particular feature or behavior was desired in the final model. Examples include the use of Hill equations, Michaelis-Menten terms and Goldbeter-Koshland switches [68, 100]. These formulations are very useful in cases where the corresponding assumptions are justified and where the model parameters can be mapped back to actual physical processes. However, in many biological situations, such assumptions are not easy to validate. The method presented here allows fitting of any model topology, in

particular pure mass-action models, directly to the desired feature behavior. This enables the modeler to stay closer to the biochemical reality while representing behavior typically associated with higher-order functional forms. The resulting parameter fit will be meaningful because the parameter set maps directly to physical processes such as binding events, chemical reactions or transport processes.

7.4 Conclusions

The cost function surface of a parameter estimation optimization depends on the formulation. It was shown here that the use of suitable feature-based cost functions can result in a more convex cost function surface in at least one dimension, with a steeper gradient towards the true minimum. Second, it was shown that feature fitting can provide a competitive parameter estimation using different types of data than concentration data. In particular, the period appears to be a feature that contains a large amount of information that is useful for parameter estimation, likely due to the implicit definition of a higher-dimensional boundary value problem in the constraints of the feature-based optimization algorithm. Furthermore, feature fitting can be an alternative or a complement to concentration-data based parameter fitting, given that the cost function itself can be added to any least-squares approach. One known problem with fitting parameters in biological models to data, even when large amounts of high quality data are available, is that some parameters will be poorly constrained [39]. Adding other dimensions to the cost function in the form of desired feature behavior of the fitted model can only help to constrain parameters further, and in a biologically meaningful way.

Chapter 8

Conclusions

Several contributions are made in this thesis. First, a rigorous mathematical treatment of sensitivity analysis for all types of autonomous oscillators is presented. The previously neglected influence of the phase locking condition (PLC) on the solution of the sensitivity equations is demonstrated to have important effects for understanding and computing relative phase sensitivities. Through a three-part decomposition of the sensitivities, the influence of a given parameter on the period, phases and amplitudes of the system is distinguished and made accessible for analysis. Moreover, the application of sensitivity analysis to models of the mammalian circadian clock can result in meaningful insights, under certain conditions. First, the sensitivity analysis has to be applied to a model with sufficient physical basis that the individual parameters have meaning on a molecular, mechanistic basis. Second, in particular for phase sensitivity analysis, it is very important to cast any biolgical observation into the correct mathematical formulation. If the choice of PLC does not represent the biology behind the tracking of the phase, the resulting phase sensitivities will not be biologically meaningful (although they might be interesting on a structural level for more abstract network analysis). When a detailed, mechanistic model is available, and the sensitivity analysis is well tailored to a biological question or observation, it was shown that one can obtain results that explain the mechanistic basis of a biological feature, can give an indication of the involvement of certain network structures (negative or positive feedback loops) in its control, and can link information gained from experiments back to structural insight at the network level.

It deserves mention that as biological knowledge expands, the models representing this

knowledge will grow in size and their mathematical analysis will depend on having tools available that scale well. Each of the methods developed and presented in this thesis work well for models of considerable size, such as those that were analyzed here and scale favorably as model size increases further.

Through system-wide analyses a general picture of the network design can be gained. While after performing period sensitivity analysis alone, it seemed as though there might be a one-to-one correspondence between network architecture and function, this first impression was modified after studying several relative angular phase sensitivities in the same network. When several performance metrics were compared (amplitudes, phases, period), the resulting picture was that there exist certain "key parameters" that are involved in controling almost all of them. This new insight moves the emphasis away from the hypothesis of a modular network design and towards a picture of an integrated network design in which all functions are carefully balanced against each other and are implemented in a concerted fashion.

The biggest limitation of sensitivity analysis is its local nature. Therefore, a clear future direction for this work would be to use dynamic optimization for the study of network behavior as a function of network parameterization. In Chapters 3 and 6 some work in this direction was presented, where the phase was modified over a wide range while a constant period was maintained. Of course, the algorithm used there was very simplistic and more definite answers could likely be obtained by using more sophisticated optimization software (e.g., SNOPT [34]) that determine the optimal step size at each step along with the optimal search direction. By observing how two or more network performance metrics can or cannot be modified independently, insights into network performance under multi-objective challenges from the outside might be gained. Multiple simultaneous demands are likely to be present in nature. For example, it is reasonable to think that a minimum amplitude must be maintained in order to be able to process clock output. At the same time, the period should be kept constant, while relative phases may be adapted to match different contingencies. Given the observation that multiple network functions might locally be regulated in a concerted way, it would be interesting to see how this compromise and concerted action translates beyond the local scope.

In order to gain the most biologically meaningful results, the model must be kept as close as possible to the most recent advances in molecular circadian biology. In Chapter 4 it was

demonstrated that the extended model developed here shows good agreement with mutant behaviors and other experimental data. The choice of parameterization for biological models is notoriously difficult for several reasons. One is that experimental data for individual reaction rate constants is scarce. Second, even with a significant amount of data, biological models often seem to exhibit a certain "sloppiness" in their parameter estimation [39]; in other words it is impossible to identify all parameters uniquely. However, the choice of parameterization has a significant impact on the results of sensitivity analysis. In this work, only one parameterization for the extended model was studied extensively, whereas several others could be identified that matched the data equally well. For comparison purposes, the parameterization closest to the original model by Forger and Peskin was used, but in general, no such restriction needs to be made. In order to obtain a more complete picture, it might be beneficial to establish a set of likely parameterizations, which might all match the known mutant behavior and trajectory data equally well, and perform sensitivity analysis on the resulting ensemble of models. In doing so, conclusions and predictions could be made from commonalities among models, whereas disagreement might indicate the need for further experimentation [16].

A complementary approach was suggested in Chapter 7, where it was shown that feature sensitivity analysis can be useful in parameter estimation, and a procedure was presented that helped to identify more parameters than through concentration-based least squares fitting alone. This approach could be used for larger models and is fully compatible with any other type of least-square based fitting algorithm. Such a combination, used with as much of the experimental data as available, might narrow the parameter choices that are available for the extended model considerably.

Appendix A

Data for Alternative Parameter Sets in Chapter 3

Table A.1: Parameter indices and descriptions. Parameters of index 25 and higher are unique to the extended model and represented in italics.

Index	Description
1	Max. rate of Per2/Cry transcription
2	MM const. of Per2.Cry transcription
3	Inhibition constant of Per2/Cry transcription
4	Concentration of constitutive activator
5	Hill coeff. of Per2/Cry transcription inhibition
6	Per2/Cry mRNA degradation
7	Per2/Cry complex formation
8	No. of Per2/Cry complex forming subunits
9	PER2/CRY (c) degradation
10	PER2/CRY nuclear import
11	PER2/CRY nuclear export
12	PER2/CRY (c) degradation
13	Max. rate of Bmal1 transcription
14	MM rate of Bmal1 transcription
15	Hill coeff. of Bmal1 transcription activation
16	Bmal1 mRNA degradation
17	BMAL1 translation
18	BMAL1(c) degradation
19	BMAL1 nuclear import
20	BMAL1 nuclear export
21	BMAL1(n) degradation
22	BMAL1(n) activation
23	BMAL1*(n) deactivation
24	BMAL1*(n) degradation
25	Max. rate of REV-ERBα synthesis
26	MM const. of REV-ERBα synthesis
27	Inhibition constant of REV-ERBα synthesis
28	Hill coeff. of inhibition of REV-ERBα synthesis
29	REV-ERBα degradation
30	Hill coeff. of activation of Per2/Cry transcription
31	Inhibition const. of Bmal1 transcription
32	Hill coeff. of activation of REV-ERBα synthesis

Table A.2: Consensus rankings of parameters by magnitude of AUC of scaled amplitude sensitivities in the basic model for alternative parameter sets (AP1-AP10).

Parameter set	1	2	3	4	5	6	7	8	9	10
AP1 (Amp)	14	3	8	12	16	6	13	5	17	10
AP1 (Phase)	3	14	16	8	13	12	15	5	17	6
AP1 (Per)	10	6	5	12	8	9	11	24	15	14
AP2 (Amp)	15	14	3	8	1	24	13	2	5	17
AP2 (Phase)	15	3	14	8	1	24	16	2	13	17
AP2 (Per)	15	14	3	8	12	24	1	5	16	2
AP3 (Amp)	14	3	8	16	17	13	15	5	10	12
AP3 (Phase)	14	3	8	16	5	13	15	17	10	6
AP3 (Per)	6	12	5	10	8	11	9	24	14	1
AP4 (Amp)	3	14	12	8	16	5	13	17	10	6
AP4 (Phase)	3	14	12	8	16	13	17	5	6	10
AP4 (Per)	6	10	5	8	12	14	24	3	9	1
AP5 (Amp)	15	14	3	1	6	2	4	16	13	5
AP5 (Phase)	3	12	7	10	8	1	6	2	4	9
AP5 (Per)	1	2	4	5	8	10	6	3	12	7
AP6 (Amp)	15	14	3	8	16	17	13	1	2	24
AP6 (Phase)	3	15	14	10	12	8	5	1	2	16
AP6 (Per)	6	15	5	10	12	14	8	9	3	1
AP7 (Amp)	3	14	16	13	5	12	6	8	5	10
AP7 (Phase)	3	14	5	16	13	12	8	6	17	10
AP7 (Per)	10	6	5	8	14	3	24	12	9	16
AP8 (Amp)	14	3	15	12	6	8	5	16	13	17
AP8 (Phase)	14	3	15	12	6	8	16	13	5	17
AP8 (Per)	6	10	5	8	24	14	15	3	21	9
AP9 (Amp)	15	14	3	8	12	10	16	6	5	1
AP9 (Phase)	3	15	8	14	12	10	5	1	16	2
AP9 (Per)	10	5	8	6	15	14	3	9	12	24
AP10 (Amp)	16	13	8	3	14	5	22	21	7	15
AP10 (Phase)	13	16	17	14	3	8	5	21	15	24
AP10 (Per)	5	8	10	12	6	9	11	14	3	24

Table A.3: Consensus rankings of parameters by magnitude of AUC of scaled amplitude sensitivities in the model including the Rev-Erbα loop for all alternative parameter sets (AP1-AP10).

Parameter set	1	2	3	4	5	6	7	8	9	10
AP1 (Amp)	26	2	31	29	25	27	8	3	16	13
AP1 (Phase)	26	2	25	29	31	3	8	27	5	16
AP1 (Per)	10	6	8	5	12	26	2	25	31	29
AP2 (Amp)	8	13	17	14	3	5	2	32	24	6
AP2 (Phase)	5	3	30	10	12	8	2	16	13	28
AP2 (Per)	12	5	10	6	9	8	13	17	16	24
AP3 (Amp)	25	29	10	27	17	3	13	17	8	26
AP3 (Phase)	3	8	5	25	29	27	10	2	31	16
AP3 (Per)	10	5	8	12	9	6	11	27	16	3
AP4 (Amp)	28	3	10	8	12	2	16	14	27	12
AP4 (Phase)	3	12	8	5	10	2	6	28	27	25
AP4 (Per)	12	6	10	5	9	8	13	17	16	14
AP5 (Amp)	3	13	5	14	16	12	17	24	8	27
AP5 (Phase)	5	3	30	2	12	16	13	14	10	17
AP5 (Per)	13	17	16	14	6	5	24	10	8	22
AP6 (Amp)	3	13	17	14	10	27	28	26	12	17
AP6 (Phase)	3	12	5	10	27	28	6	8	2	26
AP6 (Per)	6	10	5	12	8	9	13	17	16	14
AP7 (Amp)	8	6	17	10	3	12	5	19	13	27
AP7 (Phase)	3	8	10	5	12	16	13	6	17	14
AP7 (Per)	5	8	12	9	10	6	13	14	16	17
AP8 (Amp)	8	5	30	10	3	22	17	18	24	2
AP8 (Phase)	5	30	3	8	10	13	14	16	17	24
AP8 (Per)	5	8	12	9	10	6	13	14	16	17
AP9 (Amp)	26	25	2	10	8	15	24	16	13	17
AP9 (Phase)	26	3	2	25	29	5	12	24	6	22
AP9 (Per)	6	10	5	2	8	9	26	12	29	25
AP10 (Amp)	13	17	27	14	24	22	21	2	5	30
AP10 (Phase)	5	17	16	13	14	2	24	3	30	22
AP10 (Per)	6	12	5	10	8	9	13	16	17	14

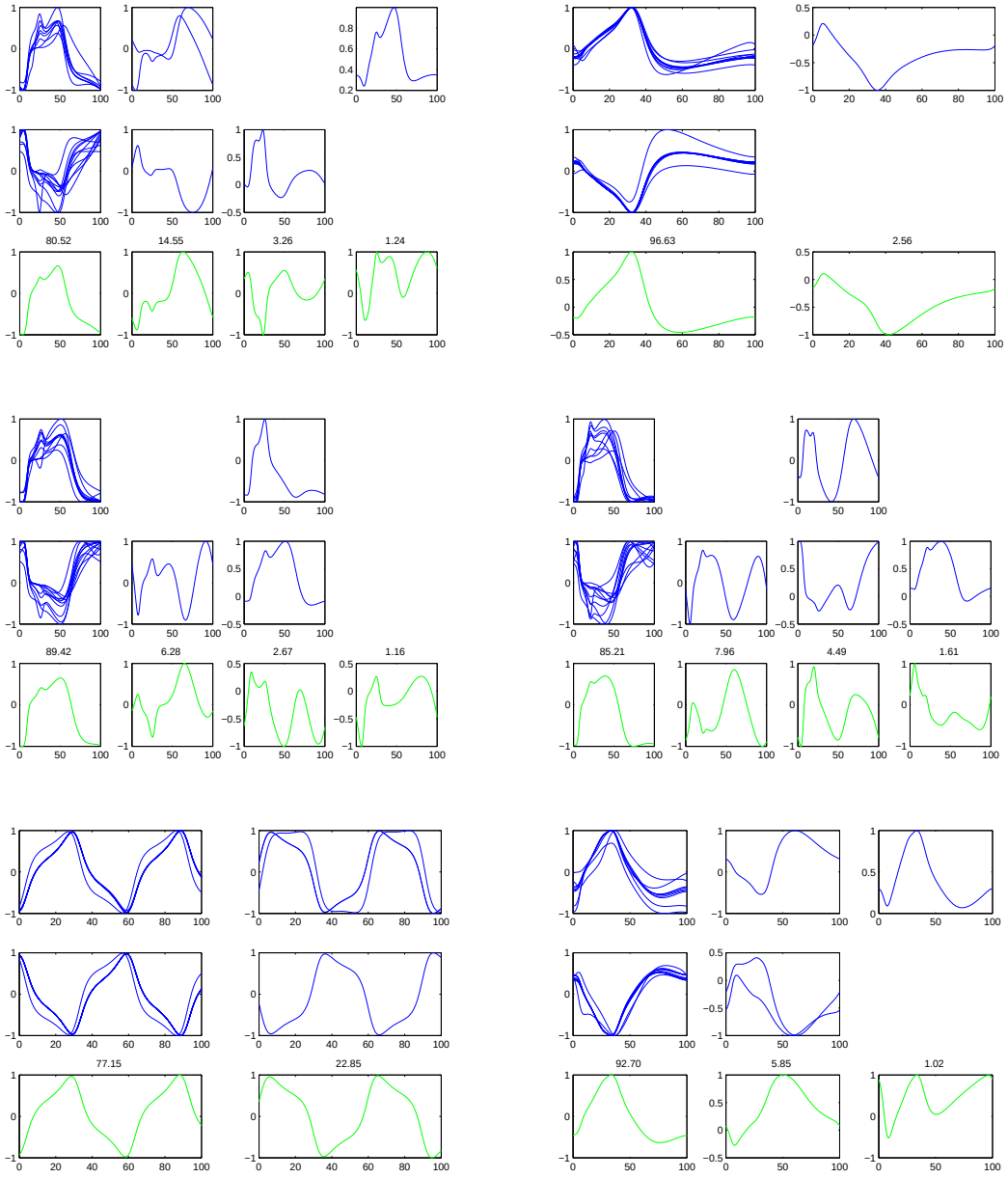

Figure A-1: PCA based clustering of the δ-trajectories for basic model alternative parameter sets 1-6. Each column represents once principal component. Top row: trajectories within the mode. Second row: trajectories within the "anti-mode". Bottom row (green): Principal component or cluster centroid.

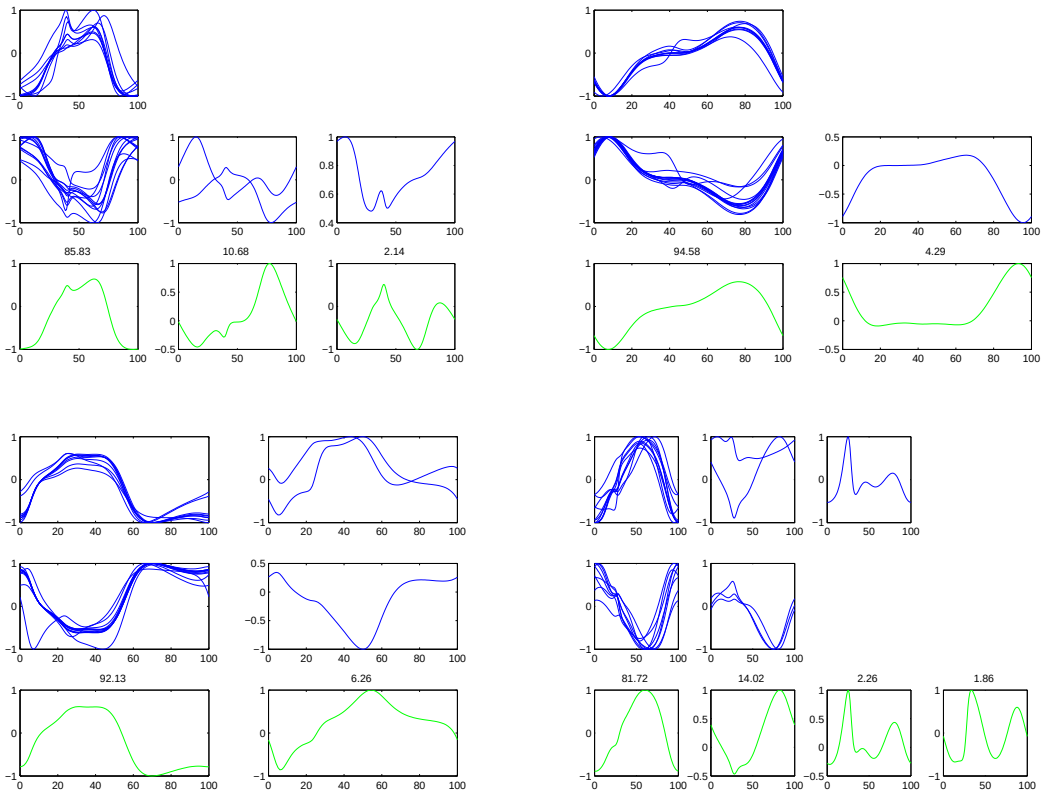

Figure A-2: PCA based clustering of the δ-trajectories for basic model alternative parameter sets 7-10. Each column represents once principal component. Top row: trajectories within the mode. Second row: trajectories within the "anti-mode". Bottom row (green): Principal component or cluster centroid.

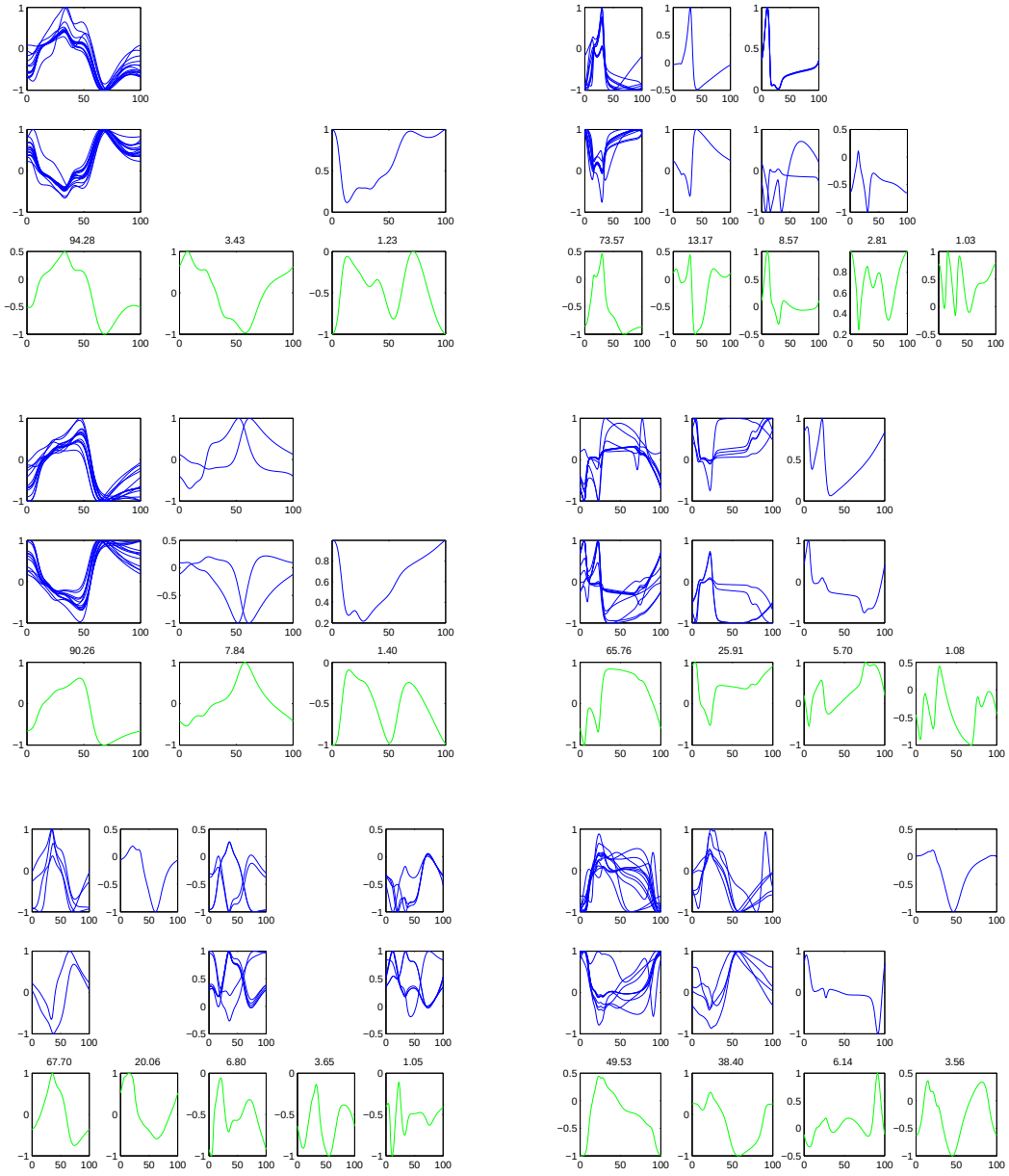

Figure A-3: PCA based clustering of the δ-trajectories for extended model alternative parameter sets 1-6. Each column represents once principal component. Top row: trajectories within the mode. Second row: trajectories within the "anti-mode". Bottom row (green): Principal component or cluster centroid.

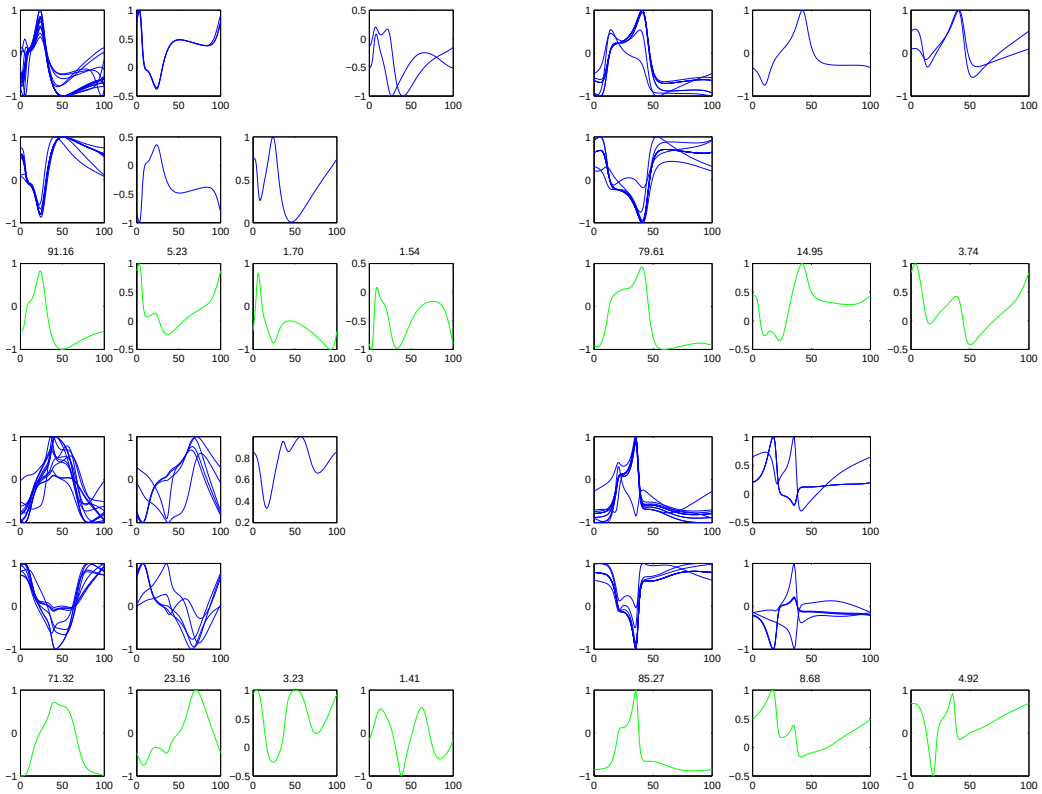

Figure A-4: PCA based clustering of the δ-trajectories for extended model alternative parameter sets 7-10. Each column represents once principal component. Top row: trajectories within the mode. Second row: trajectories within the "anti-mode". Bottom row (green): Principal component or cluster centroid.

Table A.4: Alternative parameter sets (APi), and the resulting period of oscillation for the basic model.

j	AP1	AP2	AP3	AP4	AP5	AP6	AP7	AP8	AP9	AP10
1	16.948	5.3762	11.538	15.541	16.423	9.4634	7.6179	15.849	12.147	12.963
2	1.9219	1.5185	0.72606	1.967	1.6232	0.75005	1.0672	0.52879	0.73794	0.58793
3	0.50307	0.43483	0.5211	0.96559	0.49207	0.77701	0.91474	0.36897	0.30359	0.72536
4	0.011866	0.0096603	0.0057659	0.018825	0.018053	0.013811	0.018744	0.017675	0.0074928	0.015844
5	10.128	13.103	11.765	15.647	8.2183	12.367	7.723	7.5819	9.6084	9.4873
6	0.13272	0.071764	0.14687	0.15305	0.12755	0.12127	0.19646	0.19733	0.084221	0.11395
7	0.41987	0.53558	0.57556	0.30906	0.23914	0.38889	0.27974	0.29022	0.5575	0.26265
8	3.1419	2.2377	2.267	3.0129	3.4407	1.5888	3.7329	2.857	3.1449	1.3716
9	0.066545	0.092017	0.028563	0.053147	0.099436	0.095459	0.031556	0.030147	0.086471	0.048232
10	0.26227	0.17646	0.17291	0.35706	0.45197	0.18727	0.25333	0.22123	0.40024	0.1689
11	0.035313	0.01749	0.037398	0.033827	0.023915	0.021095	0.012636	0.015619	0.013819	0.029749
12	0.13156	0.19194	0.21944	0.12807	0.20036	0.12403	0.078007	0.060601	0.085849	0.15256
13	5.7909	5.2434	5.6102	2.8112	2.4221	4.8888	2.0122	2.6068	3.0136	7.0463
14	3.5055	4.0476	3.2513	3.5194	4.2369	4.0131	2.3412	1.2423	3.055	1.1773
15	2.2511	2.7372	3.5502	4.6652	5.8604	2.7283	3.2224	5.3156	3.0142	3.2651
16	0.63441	0.7086	0.64566	0.7465	0.86234	1.4961	0.45843	1.1419	0.64032	0.79196
17	0.24444	0.32395	0.4772	0.448	0.1422	0.12801	0.17367	0.47953	0.15176	0.34017
18	0.10846	0.057606	0.058059	0.10853	0.041939	0.087784	0.05229	0.036854	0.10568	0.037084
19	0.40192	0.54758	0.51108	0.33498	0.27955	0.62827	0.70382	0.63693	0.76067	0.47272
20	0.041124	0.1128	0.044158	0.1033	0.031673	0.10153	0.044913	0.042738	0.038017	0.047785
21	0.078582	0.082612	0.20207	0.21218	0.14608	0.15541	0.14981	0.097508	0.12397	0.16849
22	0.14344	0.16784	0.092998	0.17135	0.069093	0.11584	0.15252	0.070324	0.13677	0.14812
23	0.0037021	0.003358	0.001595	0.0031332	0.0043118	0.0042981	0.0054928	0.0036765	0.0057972	0.0051884
24	0.14079	0.16728	0.10819	0.14993	0.13119	0.11233	0.13267	0.15033	0.048505	0.15665
T	24.238	24.117	24.216	23.122	23.174	23.326	23.701	23.378	24.503	24.532

Table A.5: Alternative parameter sets (APi), and the resulting period of oscillation for the extended model.

j	AP1	AP2	AP3	AP4	AP5	AP6	AP7	AP8	AP9	AP10
1	24.113	18.357	29.836	26.16	17.706	16.889	17.977	28.74	9.8219	20.569
2	0.78665	1.4326	0.51986	1.2076	1.9555	1.6336	0.71526	0.79336	1.4445	0.79131
3	0.33667	0.84649	0.61133	1.1918	1.2115	0.97433	1.0825	1.2063	0.64732	1.1945
4	0.0014254	0.0017861	0.00066616	0.0010587	0.0010782	0.0011091	0.0019001	0.0019251	0.00069789	0.0015786
5	7.2969	6.4912	10.873	11.524	10.12	15.51	9.8032	8.1469	9.8746	7.171
6	0.13078	0.10601	0.073071	0.14712	0.16104	0.18768	0.064134	0.094811	0.16529	0.21061
7	0.20296	0.37864	0.27547	0.53999	0.38963	0.29843	0.30302	0.25677	0.50019	0.24932
8	2.1539	3.4864	2.4171	3.2377	2.5518	3.3361	3.4798	1.6592	3.0736	3.3261
9	0.043366	0.0957	0.098295	0.056944	0.091382	0.13932	0.12788	0.12639	0.09613	0.06651
10	0.20499	0.17603	0.45644	0.16835	0.28335	0.30459	0.23766	0.13284	0.25391	0.13216
11	0.031313	0.036483	0.016474	0.016494	0.032606	0.032954	0.02323	0.028832	0.017935	0.026318
12	0.1411	0.19251	0.098654	0.23748	0.070647	0.097437	0.21139	0.14092	0.060379	0.15689
13	3.2078	5.795	4.9807	4.7145	5.3285	3.3246	2.4646	5.0086	5.9107	2.699
14	0.57898	0.79877	0.64719	1.4025	1.1718	1.8855	1.8834	1.2299	1.1169	1.5293
15	5.4331	3.8594	2.7728	4.3961	4.8853	5.2269	1.997	5.8492	2.5623	3.3535
16	2.4854	2.3754	3.5967	1.799	1.0282	0.90344	2.6073	0.97291	1.085	1.5386
17	0.079644	0.10462	0.12333	0.10408	0.11364	0.15253	0.20766	0.26548	0.18209	0.19336
18	0.026116	0.020629	0.04767	0.053097	0.015587	0.051238	0.039103	0.016537	0.017873	0.026655
19	0.19831	0.21543	0.24068	0.28046	0.2285	0.25147	0.23946	0.23252	0.11319	0.20568
20	0.03774	0.074566	0.1146	0.062649	0.065986	0.043952	0.094361	0.08607	0.1074	0.064746
21	0.03626	0.022435	0.054461	0.044406	0.040901	0.054349	0.034704	0.037035	0.056421	0.022393
22	0.043536	0.054614	0.048677	0.052601	0.049908	0.026935	0.055541	0.018544	0.035791	0.015405
23	0.0035366	0.0028077	0.0058623	0.0035036	0.0041181	0.003249	0.0041119	0.0022721	0.0027815	0.0043574
24	0.027673	0.024501	0.026507	0.019284	0.021261	0.029554	0.038916	0.033259	0.026623	0.025676
25	9.6404	13.95	10.633	17.274	8.8036	20.522	7.1693	7.694	17.661	16.925
26	1.6652	1.382	1.38	0.69298	1.3859	1.7573	1.7606	1.9977	1.411	1.4465
27	2.0752	0.68734	1.3677	2.1954	1.0028	0.71365	2.157	0.68326	1.3152	1.3226
28	3.0201	2.2012	1.6414	3.0285	3.4113	2.803	3.9414	3.6475	1.0509	3.0908
29	2.5649	1.6523	1.9026	1.6781	2.3725	1.0762	2.9953	1.7865	2.0334	2.5888
30	8.8397	3.3373	4.8962	4.0958	4.0227	2.7882	3.7609	6.3736	6.2542	7.626
31	0.75673	1.3578	1.5838	0.75482	1.7177	0.87667	0.64014	1.0488	0.90119	1.775
32	1.9053	1.1783	0.61243	1.5647	1.5974	1.5249	1.1574	1.9349	1.9451	1.1885
T	24.244	23.348	23.43	24.596	23.062	23.058	24.412	24.216	24.156	23.21

Appendix B

Alternative Parameter Sets for Chapter 5

*

Table B.1: Alternative lumped parameter sets (APi), and the resulting period of oscillation for the model by Forger % Peskin [29]. Rankings of the top 25, scaled period sensitivities $\frac{\partial \ln T}{\partial \ln \mathbf{p}}$ by absolute magnitude, for the alternative parameter sets presented in Table B.2. The parameter indices of the unlumped parameters are shown for each alternative parameter set and each of the top 25 ranks.

rank	AP1	AP2	AP3	AP4	AP5	AP6	AP7	AP8	AP9	AP10	AP11
1	10.0	20.0	10.0	10.0	10.0	10.0	10.0	10.0	10.0	10.0	20.0
2	1.031	1.031	1.031	1.031	1.031	1.031	1.031	1.031	1.031	1.031	1.031
3	2.533	2.533	2.533	2.533	2.533	2.533	2.533	2.533	5.067	2.533	1.267
4	6.784	3.392	1.696	6.784	3.392	1.696	1.696	1.696	3.392	3.392	1.696
5	0.165	0.082	0.165	0.082	0.082	0.165	0.165	0.082	0.165	0.082	0.082
6	0.090	0.090	0.045	0.090	0.090	0.045	0.090	0.180	0.090	0.180	0.180
7	0.436	0.872	0.436	0.872	0.436	0.436	0.436	0.436	0.436	0.872	0.436
8	0.594	0.594	0.594	0.297	0.594	0.594	1.188	0.297	0.297	0.594	0.594
9	0.465	0.465	0.465	0.465	0.465	0.465	0.465	0.465	0.465	0.465	0.465
10	5.087	10.17	5.087	5.087	10.17	5.087	5.087	5.087	10.17	5.087	5.087
11	0.266	0.266	0.133	0.266	0.266	0.133	0.266	0.533	0.133	0.266	0.266
12	0.352	0.352	0.352	0.352	0.176	0.352	0.352	0.352	0.352	0.352	0.352
13	2.307	1.153	1.153	2.307	2.307	1.153	1.153	1.153	2.307	2.307	2.307
14	0.713	0.713	0.713	0.713	0.713	0.713	0.713	0.713	0.713	0.357	0.713
15	0.836	0.418	0.836	0.836	0.836	0.836	0.836	0.418	0.836	1.673	0.836
16	0.143	0.143	0.143	0.286	0.286	0.143	0.286	0.286	0.572	0.286	0.572
17	1.453	1.453	1.453	0.727	1.453	1.453	1.453	1.453	0.727	1.453	1.453
18	0.000	0.000	0.000	0.000	0.000	0.000	0.000	0.000	0.000	0.000	0.000
19	15.42	7.712	7.712	7.712	7.712	7.712	7.712	7.712	7.712	15.42	7.712
20	738.3	1476.5	1476.5	1476.5	1476.5	1476.5	1476.5	1476.5	1476.5	2953.0	
21	23.78	23.78	23.78	47.56	11.89	23.78	11.89	23.78	23.78	23.78	23.78
22	807.4	807.4	1614.8	807.4	807.4	1614.8	807.4	807.4	1614.8	807.4	807.4
23	308.8	308.8	308.8	308.8	308.8	308.8	308.8	308.8	308.8	154.4	308.8
24	9.034	4.517	9.034	9.034	18.069	9.034	9.034	9.034	9.034	9.034	9.034
25	15.323	7.662	7.662	7.662	15.323	7.662	7.662	7.662	7.662	7.662	7.662

26	0.046	0.046	0.023	0.046	0.046	0.023	0.046	0.046	0.046	0.046	0.046
27	0.420	0.420	0.420	0.420	0.420	0.420	0.420	0.420	0.420	0.420	0.420
28	0.210	0.210	0.210	0.210	0.421	0.210	0.210	0.105	0.210	0.105	0.210
29	1.809	3.618	3.618	1.809	3.618	3.618	7.236	3.618	3.618	1.809	3.618
30	0.133	0.066	0.133	0.133	0.066	0.133	0.066	0.133	0.266	0.133	0.066
31	21.76	21.76	10.88	43.53	21.76	10.88	21.76	21.76	21.76	21.76	21.76
32	16.25	16.25	16.25	16.25	32.51	16.25	16.25	16.25	16.25	16.25	16.25
33	6.211	12.42	6.211	6.211	6.211	6.211	3.106	6.211	3.106	3.106	6.211
34	0.188	0.377	0.377	0.377	0.377	0.377	0.377	0.377	0.377	0.377	0.377
35	0.299	0.597	0.299	0.597	0.597	0.299	0.299	0.597	0.299	0.299	0.299
36	15.11	15.11	7.56	15.11	7.56	7.56	15.11	30.22	15.11	15.11	7.56
37	0.00017	0.00034	0.00034	0.00034	0.00034	0.00034	0.00017	0.00034	0.00034	0.00017	0.00034
38	115.8	115.8	115.8	57.9	57.9	115.8	231.5	115.8	115.8	115.8	231.5
T	23.96	23.99	24.75	24.85	24.25	24.65	23.96	23.67	24.06	24.41	24.32

Table B.2: Rankings of the top 25, scaled period sensitivities $\frac{\partial \ln T}{\partial \ln \mathbf{p}}$ by absolute magnitude, for the alternative parameter sets presented in Table B.2. The parameter indices of the unlumped parameters are shown for each alternative parameter set and each of the top 25 ranks.

j	AP1	AP2	AP3	AP4	AP5	AP6	AP7	AP8	AP9	AP10	AP11
1	224	34	34	34	34	34	34	34	34	34	34
2	17	224	224	224	224	224	224	224	223	224	224
3	34	222	17	8	17	17	17	17	16	180	19
4	66	17	19	17	19	19	19	19	39	211	17
5	19	19	66	231	66	66	66	66	23	17	66
6	65	231	91	19	91	91	91	91	9	66	91
7	222	66	27	222	64	27	27	21	224	209	223
8	91	8	35	66	27	35	223	20	22	24	16
9	35	149	56	211	7	56	35	27	1	2	23
10	231	91	7	91	35	7	209	38	19	25	39
11	7	211	209	65	56	222	7	222	10	40	171
12	209	201	222	39	23	40	199	223	56	99	21
13	211	27	65	23	39	22	56	201	64	173	1
14	27	43	23	56	222	23	171	56	33	93	22
15	38	38	39	149	184	39	23	211	27	39	20
16	49	56	171	24	163	147	39	165	43	23	27
17	39	65	199	2	65	65	16	2	5	190	9
18	23	147	223	223	223	231	163	24	41	91	163
19	134	23	43	157	38	149	40	16	231	179	33
20	180	39	147	40	209	155	25	39	222	97	64
21	8	64	231	25	43	58	21	23	8	7	38
22	41	157	40	22	25	163	20	173	38	186	222
23	157	49	25	1	40	171	64	199	91	223	10
24	56	20	211	41	1	49	222	65	122	21	56
25	171	51	149	16	22	41	1	209	17	20	24

Bibliography

[1] *Jacobian 3.0*. Numerica Technology, LLC, Cambridge, MA, 2007.

[2] M. Akashi, T. Ichise, T. Mamine, and T. Takumi. Molecular mechanism of cell-autonomous circadian gene expression of Period2, a crucial regulator of the mammalian circadian clock. *Mol. Biol. Cell*, 17:555–565, 2006.

[3] M. Akashi, Y. Tsuchiya, T. Yoshino, and E. Nishida. Control of intracellular dynamics of mammalian period proteins by casein kinase I ϵ and CKIδ in cultured cells. *Mol. Cell. Biol.*, 22:1693 –1703, 2002.

[4] U. Albrecht, Z.S. Sun, G. Eichele, and C. C. Lee. A differential response of two putative mammalian circadian regulators, *mper1* and *mper2* to light. *Cell*, 91:1055–1064, 1997.

[5] A. A. Andronov, A. A. Vitt, and S. E. Khaikin. *Theory of Oscillators*. Addison-Wesley Publishing Co., Inc., Reading, MA, 1966.

[6] S. Audoly, G. Bellu, L. D'Angio, M. P. Saccomani, and C. Cobelli. Global identifiability of nonlinear models of biological systems. *IEEE Trans. Biomed. Eng.*, 48:55–65, 2001.

[7] S. P. Ausprey and S. Macchietto. Statistical tools for optimal dynamic model building. *Comput. Chem. Eng.*, 24:1261–1267, 2000.

[8] K. Bae, X. Jin, E. S. Maywood, M. H. Hastings, S. M. Reppert, and D. R. Weaver. Differential functions of *mPer1*, *mPer2* and *mPer3* in the SCN circadian clock. *Neuron*, 30:525–536, 2001.

[9] N. Bagheri, J. Stelling, and F. J. Doyle III. Circadian phase entrainment via nonlinear model predictive control. *Int. J. Robust Nonlinear Control*, 17:1555–1571, 2007.

[10] N. Bagheri, J. Stelling, and F. J. Doyle III. Quantitative performance metrics for robustness in circadian rhythms. *Bioinformatics*, 23:358–364, 2007.

[11] Y. Bard. *Nonlinear parameter estimation*. Academic Press, New York, NY, 1974.

[12] S. Becker-Weimann, J. Wolf, H. Herzel, and A. Kramer. Modeling feedback loops of the mammalian circadian oscillator. *Biophys. J.*, 87:3023–3034, 2004.

[13] S. Becker-Weimann, J. Wolf, A. Kramer, and H. Herzel. A model of the mammalian circadian oscillator including the REV-ERBα module. *Genome Inf.*, 15:3–12, 2004.

[14] R. Bellman and K. J. Astrom. On structural identifiability. *Math. Biosci.*, 7:329–339, 1970.

[15] K. Bernaerts and J. F. Van Impe. Data-driven approaches to the modelling of bioprocesses. *T. I. Meas. Control*, 26:349–372, 2004.

[16] C. A. Bever. *Selecting high-confidence predictions from ordinary differential equation models of biological networks.* PhD thesis, Massachussetts Institute of Technology, 2008.

[17] K. S. Brown, C. C. Hill, G. A. Calero, C. R. Myers, K. H. Lee, J. P. Sethna, and R. A. Cerione. The statistical mechanics of complex signaling networks: nerve growth factor signaling. *Phys. Biol.*, 1:184–195, 2004.

[18] E. G. Bure and E. Rosenwasser. The study of the sensitivity of oscillatory systems. *Autom. Remote Control*, 7:1045–1052, 1974.

[19] L. Busino, F. Bassermann, A. Maiolica, C. Lee, and P. M. Nolan et al. Scf^{Fbx13} controls the oscillation of the circadian clock by directing the degradation of cryptochrome proteins. *Science*, 316:900–904, 2007.

[20] C. A. Czeisler, J. F. Duffy, T. L. Shanahan, E. N. Brown, J. F. Mitchell, D. W. Rimmer, J. F. Ronda, E. J. Silva, J. S. Allan, J. S. Emens, D.-J. Dijk, and R. E. Kronauer. Stability, precision, and the near-24-hour period of the human circadian pacemaker. *Science*, 284:2177–2181, 1999.

[21] A. Demir. Floquet theory and non-linear perturbation analysis for oscillators with differential-algebraic equations. *Int. J. Circ. Theor. Appl.*, 28:163–185, 2000.

[22] A. Demir, A. Mehrotra, and J. Roychowdhury. Phase noise in oscillators: A unifying theory and numerical methods for characterization. *IEEE Trans. Circuits Syst.*, 47:655–674, 2000.

[23] A. Demir and J. Roychowdhury. A reliable and efficient procedure for oscillator PPV computation, with phase noise macromodeling applications. *IEEE Trans. Circuits Syst.*, 22:188–197, 2003.

[24] E. J. Doedel, W. Govaerts, and YU. A. Kuznetsov. Computation of periodic solution bifurcations in ODEs using bordered systems. *SIAM J. Numer. Anal.*, 41:401–435, 2003.

[25] J. C. Dunlap. Molecular bases for circadian clocks. *Cell*, 96:271–290, 1999.

[26] J. C. Dunlap. *Chronobiology - Biological Timekeeping.* Sinauer Associates, Inc., Sunderland, MA, 2004.

[27] D. Edelson and V. M. Thomas. Sensitivity analysis of oscillating reaction. 1. The period of the oregonator. *J. Phys. Chem.*, 85:1555–1558, 1981.

[28] W. F. Feehery, J. E. Tolsma, and P. I. Barton. Efficient sensitivity analysis of large-scale differential-algebraic systems. *Appl. Numer. Math.*, 25:41–54, 1997.

[29] D. B. Forger and C. S. Peskin. A detailed predictive model of the mammalian circadian clock. *Proc. Natl. Acad. Sci. U.S.A.*, 100:14806–14811, 2003.

[30] K. G. Gadkar, R. Gunawan, and F. J. Doyle III. Iterative approach to model identification of biological networks. *BMC Bioinformatics*, 6:155, 2005.

[31] M. Gallego, E. J. Eide, M. F. Woolf, D. M. Virshup, and D. B. Forger. An opposite role for *tau* in circadian rhythms revealed by mathematical modeling. *Proc. Natl. Acad. Sci. U.S.A.*, 103:10618–10623, 2006.

[32] M. Gallego, H. Kang, and D.M. Virshup. Protein phosphatase 1 regulates the stability of the circadian protein PER2. *Biochem. J.*, 399:169–175, 2006.

[33] M. Gallego and D. M. Virshup. Post-translational modifications regulate the ticking of the circadian clock. *Nature Reviews*, 8:139–148, 2007.

[34] P. E. Gill, W. Murray, and M. A. Saunders. SNOPT: An SQP algorithm for large-scale constrained optimization. *SIAM J. Optimiz.*, 12:979–1006, 2002.

[35] A. Goldbeter. A model for circadian oscillations in the *Drosophila* period protein (PER). *Proc. R. Soc. London Ser. B*, 261:319–324, 1995.

[36] F. Guillaumond, H. Derdente, V. Giguere, and N. Cermakian. Differential control of Bmal1 circadian transcription by Rev-Erb and ROR nuclear receptors. *J. Biol. Rhythms*, 41:401–435, 2003.

[37] R. Gunwan and F. J. Doyle III. Isochron-based phase response analysis of circadian rhythms. *Biophys. J.*, 91:2131–2141, 2006.

[38] R. Gunwan and F. J. Doyle III. Phase sensitivity analysis of circadian rhythm entrainment. *J. Biol. Rhythms*, 22:180–194, 2007.

[39] R. N. Gutenkunst, J. J. Waterfall, F. P. Casey, K. S. Brown, C. R. Myers, and J. P. Sethna. Universally sloppy parameter sensitivities in systems biology models. *PLoS Comput. Biol.*, 3:1871–1878, 2007.

[40] H. Hamaguchi, K. Fujimoto, T. Kawamoto, M. Noshiro, K. Maemura, N. Takeda, R. Nagai, M. Furukawa, S. Honma, K. Honma, H. Kurihara, and Y. Kato. Expression of the gene for Dec2, a bsaic helix-loop-helix transcription factor, is regulated by a molecular clock. *Biochem. J.*, 382:43–50, 2004.

[41] P. Hartman. *Ordinary Differential Equations*. SIAM, Philadelphia, PA, 2nd edition, 2002.

[42] M. Hastings, J. S. O'Neill, and E. S. Maywood. Circadian clocks: regulators of endocrine and metabolic rhythms. *J. Endocrinol.*, 195:187–198, 2007.

[43] A. C. Hindmarsh and R. Serban. *User documentation for CVODES, an ODE solver with sensitivity analysis capabilities*. Lawrence Livermore National Library, 2002.

[44] C. I. Hong, E. D. Conrad, and J. J. Tyson. A proposal for robust temperature compensation of circadian rhythms. *Proc. Natl. Acad. Sci. U.S.A.*, 104:1195–1200, 2007.

[45] S. Honma, T. Kawamoto, Y takagi, K. Fujimoto, F. Sato, M. Noshiro, Y. Kato, and K.-I. Honma. Dec1 and Dec2 are regulators of the mammalian circadian clock. *Nature*, 419:841–844, 2002.

[46] A. E. C. Ihekwaba, D. S. Broomhead, R. L. Grimley, N. Benson, and D. B. Kell. Sensitivity analysis of parameters controlling oscillatory signalling in the NF-κB pathway: the roles of IKK and IκBα. *Syst. Biol.*, 1:93–103, 2004.

[47] F. J. Doyle III, R. Gunawan, N. Bagheri, H. Mirsky, and T. L. To. Circadian rhythm: A natural, robust, multi-scale control system. *Comput. Chem. Eng.*, 30:1700–1711, 2006.

[48] B. P. Ingalls. Autonomously oscillating biochemical systems: Parametric sensitivities of extrema and period. *IEE Systems Biology*, 1:62–70, 2004.

[49] B. P. Ingalls and H. M. Sauro. Sensitivity analysis of stoichiometric networks: An extension of metabolic control analysis to non-steady state trajectories. *J. Theor. Biol.*, 222:23–36, 2003.

[50] J. A. Jacquez and T. Perry. Parameter estimation: local identifiability of parameters. *Am. J. Physiol. Endocrinol. Metab.*, 258:E727–E736, 1990.

[51] K. Jaqaman and G. Danuser. Linking data to models: data regression. *Nat. Rev. Mol. Cell. Biol.*, 7:813–819, 2006.

[52] K. P. Wright Jr., R. J. Hughes, R. E. Kronauer, D.-J. Dijk, and C. A. Czeisler. Intrinsic near-24-h pacemaker period determies limits of circadian entrainment to a weak synchronizer in humans. *Proc. Natl. Acad. Sci. U.S.A.*, 98:14027–14032, 2001.

[53] F. X. Kaertner. Analysis of white and $f^{-\alpha}$ noise in oscillators. *Int. J. Circ. Theor. App.*, 18:485–519, 1990.

[54] T. Kawamoto, M. Noshiro, F. Sato, K. Maemura, N. Takeda, R. Nagai, T. Iwata, K. Fijimoto, M. Furukawa, K. Miyazaki, S. Honma, K. Honma, and Y. Kato. A novel autofeedback loop of Dec1 transcription involved in circadian rhythm regulation. *Biochem. Biophys. Res. Commun.*, 313:117–124, 2004.

[55] U. Knippschild, A. Gocht, S. Wolff, N. Huber, J. Lohler, and M. Stoter. The casein kinase 1 family: Participation in multiple cellular processes in eukaryotes. *Cell. Signal.*, 17:675–689, 2005.

[56] M. A. Kramer, H. Rabitz, and J. M. Calo. Sensitivity analysis of oscillatory systems. *Appl. Math. Modelling*, 8:328–340, 1984.

[57] A. Kremling and J. Saez-Rodriguez. Systems biology – an engineering perspective. *J. Biotechnol.*, 129:329–351, 2007.

[58] K. Kume, M. J. Zylka, S. Sriram, L. P. Shearman, D. R. Weaver, X. Jin, E. S. Maywood, M. H. Hastings, and S. M. Reppert. mCRY1 and mCRY2 are essential components of the negative limb of the circadian clock feedback loop. *Cell*, 98:193–205, 1999.

[59] G. Kurosawa and Y. Iwasa. Temperature compensation in circadian clock models. *J. Theor. Biol.*, 233:453–468, 2005.

[60] I. Kwon, J. Lee, S. H. Chang, N. C. Jung, B. J.Lee, G. H. Son, K. Kim, and K. H. Lee. BMAL1 shuttling controls transactivation and degradation of the CLOCK/BMAL1 heterodimer. *Mol. Cell. Biol.*, 26:7318–7330, 2006.

[61] P. Lakin-Thomas and S. Brody. Circadian rhythms in microorganisms: New complexities. *Annu. Rev. Microbiol.*, 58:489–519, 2004.

[62] R. Lamour. Oscillations in differential-algebraic equations. In E. Griepentrog, M. Klarke, and R. Maerz, editors, *Berliner Seminar on Differential Algebraic Equations*. Berlin, Germany, 1992.

[63] R. Larter. Sensitivity analysis of autonomous oscillators. Separation of secular terms and determination of structural stability. *J. Phys. Chem.*, 87:3114–3121, 1983.

[64] R. Larter, H. Rabitz, and M. A. Kramer. Sensitivity analysis of limit cycles with application to the Brusselator. *J. Chem. Phys.*, 80:4210–4128, 1984.

[65] C. Lee, J.-P. Etchegaray, F. R. A. Cagampang, A. S. I. Loudon, and S.M. Reppert. Posttranslational mechanisms regulate the mammalian circadian clock. *Cell*, 107:855–867, 2001.

[66] J.-C. Leloup and A. Goldbeter. Temperature compensation of circadian rhtythms: Control of the period in a model for circadian oscillations of the PER protein in *Drosophila*. *Chronobiol. Int.*, 14(5):511–520, 1997.

[67] J.-C. Leloup and A. Goldbeter. A model for circadian rhythms in Drosophila incorporating the formation of a complex between the per and tim proteins. *J. Biol. Rhythms*, 13:70–87, 1998.

[68] J.-C. Leloup and A. Goldbeter. Toward a detailed computational model for the mammalian circadian clock. *Proc. Natl. Acad. Sci. U.S.A.*, 100:7051–7056, 2003.

[69] J.-C. Leloup and A. Goldbeter. Modeling the mammmalian circadian clock: Sensitivity analysis and multiplicity of oscillatory mechanisms. *J. Theor. Biol.*, 230:541–562, 2004.

[70] A. J. Lewy, B. J. Lefler, J. S. Emens, and V. K. Bauer. The circadian basis of winter depression. *Proc. Natl. Acad. Sci. U.S.A.*, 19:7415–7419, 2006.

[71] P.L. Lowrey, K. Shimomura, M. P. Antoch, S. Yamazaki, and P. D. et al. Zemenides. Positional systematic cloning and functional characterization of the mammalian circadian mutation *tau*. *Science*, 288:483–492, 2000.

[72] T. Maly and L. R. Petzold. Efficient sensitivity analysis of large-scale differential-algebraic systems. *Appl. Numer. Math.*, 20:57–79, 1996.

[73] M. Merrow, G. Mazzotta, Z. Chen, and T. Roenneberg. The right place at the right time: Regulation of daily timing by phosphorylation. *Genes Dev.*, 20:2629–2633, 2006.

[74] R. Y. Moore. Circadian rhythms: Basic neurobiology and clinical applications. *Annu. Rev. Med*, 48:253–266, 1997.

[75] M. Nakajima, K. Imai, H. Ito, T. Nishiwaki, Y. Murayama, H. Iwasaki, T. Oyama, and T. Kondo. Reconstitution of circadian oscillation of cyanobacterial KaiC phosphorylation in vitro. *Science*, 308:414–415, 2005.

[76] E. V. Nikolaev, J. C. Atlas, and M. L. Shuler. Sensitivity and control analysis of periodically forced reaction networks using the green's function method. *J. Theor. Biol.*, 247:442–461, 2007.

[77] H. Okamura, S. Miyake, Y. Sumi, S. Yamaguchi, A. Yasui, M. Muitjens, J. H. J. Hoeijmakers, and G. T. J. van der Horst. Photic induction of mPer1 and mPer2 in Cry-deficient mice lacking a biological clock. *Science*, 286:2531–2534, 1999.

[78] D. B. Ozyurt and P. I. Barton. Cheap second order directional derivatives of stiff ODE embedded functionals. *SIAM J. Sci. Comput.*, 26:1725–1743, 2005.

[79] J. D. Palmer. *The Living Clock: The Orchestrator of Biological Rhythms*. Oxford University Press, New York, NY, 2002.

[80] C. L. Partch, K. F. Shields, C. L. Thompson, C. P. Selby, and A. Sancar. Posttranslational regulation of the mammalian circadian clock by chryptochrome and protein phosphatase 5. *Proc. Natl. Acad. Sci. U.S.A.*, 103:1067–1072, 2006.

[81] M. Pernice and H. F. Walker. NITSOL: A Newton iterative solver for nonlinear systems. *SIAM J. Sci. Comput.*, 19:302–318, 1998.

[82] C. S. Pittendrigh and S. Daan. A functional analysis of circadian pacemakers in nocturnal rodents: 1. The stability and lability of spontaneous frequency. *J. comp. Physiol.*, 106:223–252, 1976.

[83] N. Preitner, F. Damiola, L.-L. Molina, J. Zakany, D. Doboule, U. Albrecht, and U. Schibler. The orphan nuclear receptor Rev-Erbα controls circadian transcription within the positive limb of the mammalian circadian oscillator. *Cell*, 110:251–260, 2002.

[84] M. A. Price. CKI, there's more than one: Casein kinase I family members in Wnt and Hedgehog signaling. *Genes Dev.*, 20:399–410, 2006.

[85] D. A. Rand, B. V. Shulgin, D. Salazar, and A. J. Millar. Design principles underlying circadian clocks. *J. R. Soc. Interface*, 1:119–130, 2004.

[86] A. B. Reddy, M. D. Field, E. S. Maywood, and M. H. Hastings. Differential resynchronization of circadian clock gene expression within the suprachiasmatic nuclei of mice subjected to experimental jet lag. *J. Neurosci.*, 22:7326–7330, 2002.

[87] S. M. Reppert and D. R. Weaver. Molecular analysis of mammalian circadian rhythms. *Annu. Rev. Physiol.*, 63:647–676, 2001.

[88] S. M. Reppert and D. R Weaver. Coordination of circadian timing in mammals. *Nature*, 418:935–941, 2002.

[89] E. Rosenwasser and R. Yusupov. *Sensitivity of Automatic Control Systems*. CRC Press, Boca Raton, Florida, 2002.

[90] P. Ruoff and L. Rensing. The temperature-compensated Goodwin model simulates many circadian clock properties. *J. Theor. Biol.*, 179:275–285, 1996.

[91] T.K. Sato, S. Panda, L. J. Miraglia, T. M. Reyes, R. D. Rudic, P. McNamara, K. A. Naik, G. A. FithGerald, S. A. Kay, and J. B. Hogenesch. A functional genomics strategy reveals rora as a component of the mammalian circadian clock. *Neuron*, 43:527–537, 2004.

[92] R. Seydel. *Practical Bifurcation and Stability Analysis - From Equilibrium to Chaos*. Springer-Verlag, New York, N.Y., 1994.

[93] L. P. Shearman, S. Sriram, D. R. Weaver, E. S. Maywood, I. Chaves, B. Zheng, K. Kume, C. C. Lee, G. T. J. van der Horst, M. H. Hastings, and S. M. Reppert. Interacting molecular loops in the mammalian circadian clock. *Science*, 288:1013–1019, 2000.

[94] J. Stelling, E. D. Gilles, and F. J. Doyle III. Robustness properties of the circadian clock architectures. *Proc. Natl. Acad. Sci. U.S.A.*, 101(36):13210–13215, 2004.

[95] G. Strang. *Linear Algebra and its Applications*. Brooks Cole, 1988.

[96] S. H. Strogatz. *Nonlinear Dynamics and Chaos*. Perseus Books Publishing, LLC, Cambridge, MA, 1994.

[97] K. L. Toh, C. R. Jones, Y. He, E. J. Eide, W. A. Hinz, D. M. Virshup, L. J. Ptacek, and Y.-H. Fu. An h*Per2* phosphorylation site mutation in Familial Advanced Sleep Phase Syndrome. *Science*, 291:1040–1043, 2001.

[98] J. Tolsma and P. I. Barton. DAEPACK: An open modeling environment for legacy models. *Ind. Eng. Chem. Res.*, 39:1826–1839, 2000.

[99] R. Tomovic and M. Vukubratovic. *General Sensitivity Theory*. American Elsevier Publishing Company, Inc., New York, NY, 1972.

[100] J. J. Tyson, C. I. Hong, C. D. Thron, and B. Novak. A simple model of circadian rhythm based on dimerization and proetolysis of PER and TIM. *Biophys. J.*, 77:2411–2417, 1999.

[101] H. R. Ueda, M. Hagiwara, and H. Kitano. Robust oscillations within the interlocked feedback model of *Drosophila* circadian rhythm. *J. Theor. Biol*, 210:401–406, 2001.

[102] G. T. J. van der Horst, M. Muitjens, K. Kobayashi, R. Takano, S. Kanno, M. Takao, J. de Wit, A. Verkerk, A. P. M. Eker, D. van Leenen, R. Buijs, D. Bootsma, J. H. J. Hoeijmakers, and A. Yasui. Mammalian Cry1 and Cry2 are essential for maintenance of circadian rhythm. *Nature*, 398:627–630, 1999.

[103] K. Vanselow, J. T. Vanselow, P. O. Westermark, S. Reischl, B. Maier, T. Korte, A. Herrmann, H. Herzel, A. Schlosser, and A. Kramer. Differential effects of PER2 phosphorylation: molecular basis for the human familial advanced sleep phase syndrome (FASPS). *Genes Dev.*, 107:2216–2238, 2003.

[104] A. Varma, M. Morbidelli, and H. Wu. *Parametric Sensitivity in Chemical Systems*. Cambridge University Press, Cambridge, UK, 1999.

[105] F. Weber, H.-C. Hu, C. Maurer, and S. A. Kay. Second messenger and ras/MAPK signalling pathways regulate CLOCK/CYCLE-dependent transcription. *J. Neurochem.*, 98:248–257, 2006.

[106] A. K. Wilkins, P. I. Barton, and B. Tidor. The Per2 negative feedback loop sets the period in the mammalian circadian clock mechanism. *PLoS Comput. Biol.*, 3:e242. doi:10.1371/journal.pcbi.0030242, 2007.

[107] A. K. Wilkins, B. Tidor, J. K. White, and P. I. Barton. Sensitivity analysis of oscillating dynamical systems. *SIAM J. Sci. Comp.*, submitted.

[108] J. Wolf, S. Becker-Weimann, and R. Heinrich. Analysing the robustness of cellular rhythms. *Syst. Biol.*, 2:35–41, 2005.

[109] Y. Xu, Q. S. Padiath, R. E. Shapiro, C. R. Jones, and S. C. Wu et al. Functional consequences of a ck1δ mutation causing familial advanced sleep phase syndrome. *Nature*, 434:644–644, 2005.

[110] B.-B. Youan. Chronopharmaceutics: Gimmick or clinically relevant approach to drug delivery? *J. Control. Release*, 98:337–353, 2004.

[111] D. E. Zak, J. Stelling, and F. J. Doyle III. Sensitivity analysis of oscillatory (bio)chemical systems. *Comput. Chem. Eng.*, 29:663–673, 2005.

[112] B. Zheng, U. Albrecht, K. Kaasik, M. Sage, S. Vaishnav, Q. Li, Z. S. Sun, G. Eichele, A. Bradley, and C. Lee. Nonredundant roles of the mPer1 and mPer2 genes in the mammalian circadian clock. *Cell*, 105:683–694, 2001.

[113] B. Zheng, D. W. Larkin, U. Albrecht, Z. S. Sun, M. Sage, G. Eichele, C. Lee, and A. Bradley. The mPer2 gene encodes a functional component of the mammalian circadian clock. *Nature*, 400:169–173, 1999.

[114] I. GY. Zsely, J. Zador, and T. Turanyi. Similarity of sensitivity functions of reaction kinetic models. *J. Phys. Chem.*, 107:2216–2238, 2003.